# Microbial activity and transport processes in near-shore, permeable sediments

**Dissertation zur Erlangung des Doktorgrades der Naturwissenschaften**

**Dem Fachbereich Biologie/Chemie der Universität Bremen vorgelegt von**

**Ursula Werner**

**Bremen**
**September 2005**

Die vorliegende Arbeit wurde in der Zeit von Juni 2001 bis September 2005 am Max-Planck-Institut für marine Mikrobiologie in Bremen angefertigt.

*Gutachter*

Prof. Dr. Gunter Kirst (Erstgutachter)
Prof. Dr. Bo Barker Jørgensen (Zweitgutachter)

*Prüfer*

Dr. Dirk de Beer
Prof. Dr. Matthias Wolff

*Weitere Mitglieder des Prüfungsausschusses*

Susanne Hinck (Studentin)
Angela Scharfbillig (Studentin)

Datum des Promotionskolloquiums: 14. Oktober 2005

## Table of contents

**Summary**

High organic carbon turnover in permeable sands is considered to be fueled by the efficient supply of solutes (e.g., oxygen) and organic matter from the overlying water by pore water advection. In situ quantifications of microbial activity in the presence of pore water advection are still rare. In this thesis, microbial activity and transport processes were investigated in near-shore, permeable sediments.

A novel method for the measurement of volumetric oxygen consumption rate (OCR) profiles with high depth resolution in permeable sediments was evaluated in chapter 2. Three technical approaches were presented using either oxygen micro-sensors or planar optodes. For the calculation of areal OCR, the volumetric OCR can be integrated over the oxygen penetration depths measured in situ over extended time periods. These areal OCR reflect the influence of hydrodynamics on oxygen distribution. The method was consistent with established methods (interfacial gradients combined with Fick's first law of diffusion, benthic-chambers).

The importance of pore water advection for sediment oxygenation and benthic mineralization was shown at the intertidal sand flat Hausstrand (Sylt/Germany) (chapter 3). Three stations were chosen on a transect from the low - to the high water line. Due to pore water advection, oxygen penetrated deeper and more dynamically during inundation than during exposure of the flat. The oxygen penetration depths were closely coupled to bottom water current velocities, proving the impact of pore water advection on sediment oxygenation. Driven by the advective oxygen supply, benthic OCR were high: 71 - 90% of oxygen consumption took place during inundation and aerobic mineralization was the dominant mineralization process at all stations. Mineralization rates were linked to the inundation time of the stations: Oxygen consumption rates were elevated at the lower flat, sulfate reduction rates decreased sharply from the low- to the high-waterline.

At two stations (upper- and lower flat) at the intertidal sand flat Janssand near the island of Spiekeroog (German Wadden Sea), also a deeper oxygen penetration was found during inundation (chapter 4). Similar to the Hausstrand, OCR were high and highest during inundation, and sulfate reduction contributed only between 3 - 25% to

total mineralization. However, at the two stations, similar surface mineralization rates were measured. In contrast to this, the concentrations of mineralization end products in the pore water at the low water flat were up to 15 times higher than at the upper flat, and the solute concentrations varied independent of season at this station. It was concluded that two filtration processes influence the distribution of metabolic products: (1) a rapid “skin filtration” in the upper sediment layer during inundation driven by pore water advection and (2) a slow “body filtration” through deeper sediment layers during exposure driven by drainage.

In the coral reef sediments of Heron Reef (Australia), four sites exhibiting different hydrodynamic regimes were investigated (chapter 5). Oxygen penetration and dynamics as well as oxygen consumption, aerobic mineralization and sulfate reduction rates were highly variable between these sites. The supply of oxygen by pore water advection stimulated aerobic mineralization. A simple estimate of the organic matter supplied to the sediments by pore water advection only explained a fraction of the mineralization rates, indicating the importance of other organic carbon sources like benthic primary production.

The microphytobenthos at Heron Reef was dominated by diatoms, dinoflagellates and cyanobacteria (chapter 6). Episammic colonies were highly diverse with respect to cyanobacterial 16S rDNA sequences. Photosynthesis was high per unit chlorophyll-*a*, indicating an active microphytobenthic community. Estimates on the microphytobenthic photosynthetic production in the entire reef were in the order of magnitude as the estimated production by corals. Photosynthesis stimulated calcification at the four investigated sites. The sediments of at least three stations were net calcifying. Sedimentary $N_2$-fixation (acetylene reduction) was highest in the light, indicating the importance of heterocystous cyanobacteria. In coral fingers no $N_2$-fixation was measurable, which stresses the importance of the sediment compartment for reef nitrogen cycling.

**Zusammenfassung**

In permeablen Sanden wird ein hoher Umsatz von organischen Kohlenstoff durch Porenwasser-Advektion erreicht, durch die es zu einem effektiven Eintrag von gelösten Substanzen (z.B. Sauerstoff) und partikulärem organischen Material aus dem überliegenden Wasser in das Sediment kommt. In situ Untersuchungen zur mikrobiellen Aktivität in advektions-dominierten Sanden sind jedoch bisher selten durchgeführt worden. In dieser Arbeit wurden mikrobielle Aktivität und Transportprozesse in küstennahen, permeablen Sedimenten untersucht.

Kaptitel 2 befasst sich mit einer neuen Methode zur Messung volumetrischer Sauerstoffzehrungsraten in permeablen Sedimenten mit einer hohen räumlichen Auflösung. Es wurden drei technische Ansätze vorgestellt, bei denen entweder Sauerstoff-Mikrosensoren oder planare Optoden verwendet werden. Zur Berechnung von flächenbezogenen Sauerstoffzehrungsraten können die volumetrischen Sauerstoff-Zehrungsraten über in situ Langzeitmessungen der Sauerstoffeindringtiefe integriert werden. Die so ermittelten flächenintegrierten Sauerstoffzehrungsraten spiegeln den Einfluß der Hydrodynamik auf die Sauerstoffverteilung wider. Die vorgestellte Methode war konsistent zu etablierten Methoden (Diffusion über Grenzschichten (erstes Fick´sche Gesetz); benthische Kammern).

Die Bedeutung der Porenwasseradvektion für die Sauerstoffverteilung im Sediment und benthische Mineralizierungsprozcesse konnte im Gezeitenbereich des Hausstrandes (Sylt/Deutschland) gezeigt werden (Kapitel 3). Drei Stationen wurden entlang eines Transektes von der Niedrig- zur Hochwasserlinie untersucht. Durch Porenwasseradvektion wurde Sauerstoff während der Wasserbedeckung tiefer und zeitlich variabler ins Sediment eingetragen als zu Zeiten des Freifalls des Gezeitenbereichs. Die Sauerstoffeindringtiefen waren eng mit bodennahen Strömungsgeschwindigkeiten korreliert, was den Einfluß von Porenwasser-Advektion auf die Sediment-Oxygenierung verdeutlichte. Aufgrund des advektiven Sauerstoffeintrages waren die benthischen Sauerstoffzehrungsraten hoch. Während der Wasserbedeckung der Sedimente fand 71 – 90% der Gesamtmineralisierung statt, und aerobe Mineralisierung war der dominierende Mineralisierungsprozess an allen drei Stationen. Die Mineralisierungsraten korrelierten mit den Überflutungszeiten der Stationen: Die

Sauerstoffzehrungsraten waren nahe der Niedrigwasserlinie erhöht und die Sulfatreduktionsraten nahmen stark von der Niedrig- zur Hochwasserlinie ab.

An zwei Stationen (nahe Niedrigwasserlinie und höhergelegene Plate) an der Sandplate Janssand nahe der Insel Spiekeroog (Deutsches Wattenmeer) drang Sauerstoff ebenfalls am tiefsten während der Wasserbedeckung in das Sediment ein (Kapitel 4). Ähnlich wie am Sylter Hausstrand, waren die Sauerstoffzehrungsraten hoch und am höchsten während der Zeiten derWasserbedeckung. Sulfatreduktion trug nur zwischen 3 – 25 % zur gesamten Mineralisation bei. An beiden Stationen wurden jedoch ähnliche Mineralisierungsraten an der Sediment-Oberfläche gemessen. Im Gegensatz dazu waren die Konzentrationen von Endprodukten der Mineralisierung im Porenwasser an der Niedrigwasserlinie bis zu 15-fach erhöht gegenüber der oberen Sandplate. Die Porenwasserkonzentrationen an der Niedrigwasserlinie variierten zudem unabhängig von den Jahreszeiten. Zwei Filtrationsprozesse beeinflussten die Verteilung metabolischer Endprodukte auf dieser Sandplate: (1) eine schnelle „skin filtration“ in der oberen Sedimentschicht angetrieben durch Porenwasser-Advektion während Wasserbedeckung und (2) eine langsame „body filtration“ in den tieferen Sedimentschichten angetrieben durch Drainage-Prozesse während des Freifalls der Plate.

In den Sedimenten des Koralriffs *Heron Reef* (Australien) wurden vier Stationen mit stark unterschiedlichem hydrodynamischem Regime untersucht (Kapitel 5). Die Sauerstoffeindringtiefe und deren Dynamik sowie Sauerstoffzehrungsraten, aerobe Mineralisierung und Sulfatreduktion variierten stark zwischen diesen Stationen. Die Zufuhr von Sauerstoff durch Porenwasseradvektion stimulierte die aerobe Mineralisierung. Eine Abschätzung des durch Porenwasseradvektion filtrierten organischen Materials konnte nur einen Teil der ermittelten Mineralisierungsraten erklären. Es muss angenommen werden, dass andere organische Kohlenstoff Quellen für die benthische Mineralisierung wichtig waren, wie z.B. die benthische Primärproduktion.

Das Mikrophytobenthos im *Heron Reef* wurde von Diatomeen, Dinoflagellaten und Cyanobakterien dominiert (Kapitel 6). Episammische Kolonien waren hoch divers bezüglich der 16S rDNA Sequenzen von Cyanobakterien. Die Photosynthese pro Einheit Chlorophyll-*a* war hoch, was auf eine aktive mikrophytobenthische Gemeinschaft hinwies. Abschätzungen der photosynthetischen Produktion des Mikrophytobenthos für

das gesamte Riff waren in der gleichen Größenordnung wie eine Abschätzung der Produktion durch die Korallen. Photosynthese stimulierte Kalzifizierung an allen untersuchten Standorten des Riffs. Das Sediment von wenigstens drei Stationen war netto-kalzifizierend. Sedimentäre $N_2$-Fixierung (Acetylen Reduktion) war am höchsten im Licht, was auf die Bedeutung von Cyanobacterien mit Heterocysten hinweißt. In Korallenbruchstücken war keine $N_2$-Fixierung meßbar, was die Wichtigkeit der Riffsedimente für den Stickstoff-Kreislaufs des Riffs aufzeigt.

# Introduction

## Introduction

In this thesis, microbial processes and the role of pore water advection for benthic processes are investigated in permeable sediments using a set of in situ and laboratory techniques. The core of this work focuses on benthic aerobic and anaerobic mineralization and the impact of pore water advection on benthic mineralization in permeable sediments. The sands of three sites were investigated, two intertidal sand flats in the German Wadden Sea and subtidal carbonate sediments in a coral reef (Heron Reef, Australia). Additionally, microphytobenthic photosynthesis in coral reef sediments was investigated.

## The shelf seas

*The role of shelf seas in the global oceans:* The global oceans cover around 70% of the Earth's surface and play a fundamental role in the global bio-geochemical cycles. The oceans harbor an enormous species diversity, form an essential buffer for the global climate and water balance and are of substantial (e.g. economic) value for mankind. About 40000 Gt of the global carbon is allocated to the oceans. By taking up $CO_2$ from the atmosphere, nowadays oceans function as a carbon sink. They are thus acting antagonistically to the anthropogenic $CO_2$ release into the atmosphere, a major cause for global warming.

The shelf seas are the sites where land, oceans and atmosphere interact. They comprise a large variety of ecosystems, such as intertidal flats, estuaries, macrophyte communities, mangroves and coral reefs. Shelf seas cover only 7 - 8% ($26 \times 10^6$ $km^2$) of the global oceans area and contribute to 0.5% of the global oceans volume, due to their shallow water depths. The shelves are part of the continental crusts and extend from the shore to the shelf break, where the seabed steeply descends towards the deep sea. The average water depth on the shelves is 75 m, varying from zero at the shoreline to about 150 m near the shelf break (down to 400 m depths in the polar regions). The continental shelves are on average 80 km wide, however, some areas have virtually no shelf whereas the largest shelf (the Siberian shelf in the Arctic Ocean) stretches across up to 1500 km.

Although shelves cover only a small area within the global oceans, they are among the most active biological and geochemical areas in the world, due to the following reasons (Walsh 1991; Wollast 1991; Gattuso et al. 1998; Herbert 1999):

- They receive considerable input of terrestrial organic matter and nutrients through run-off and groundwater discharge.
- The shallow water depths allow an efficient cycling of matter, thus, the shelf benthic and pelagic systems are closely coupled.
- The shelf seas import nutrients from upwelling areas at the continental shelf edges and export organic carbon to the open sea.

Thus, shelf seas account for 14 - 33% of total oceanic primary production (Martin et al. 1987; Wollast 1991; Gattuso et al. 1998), and at least 90% of global fish catch (Holligan and Reiners 1992).

In the shelf seas, around 20 - 60% of the local net primary production is deposited on the sediments (Wollast 1991). Additionally, most areas of the continental shelf sediments receive enough light for benthic photosynthesis; coral reef ecosystems are an impressive example for benthic primary productivity. The shelf sediments account for 90% of the oceanic sedimentary mineralization and are thus a vital part within the global carbon and nutrient cycles (Gattuso et al. 1998).

*Shelf sea sediments:* Shelf sediments are composed of particles derived from the land and transported to the sea primarily by rivers or ice (Jaeger et al. 1998) and are dominated by sands. Approximately 50% of the continental shelf area is covered by coarse, relict sands (Johnson and Bladwin 1986). Relict sands are sediments that were deposited on the continental shelves during or after glacial epochs. Their distribution, origin and composition is thus mainly unrelated to their present environment.

Up to 90% of the worldwide sedimentation takes place on today's continental shelves (Gattuso et al. 1998). In contrast to the relict sands, recent sands and muds are transported to the shelves mainly by rivers that discharge at deltas. Thus, a second reason for the dominance of sands on shelves is that the hydrodynamic forcing in the shelf seas leads to a sorting of sediments. Recent coarse sands are deposited preferably in areas with shallow water depths and intense hydrodynamics. Fine grained deposits can often be found in distinct mud

belts close to the river mouths (McCave 1972; de Haas et al. 2002; Crockett and Nittrouer 2004), in zones of increased water depth and reduced hydrodynamics or, are transported to the shelf edges and beyond (Harris and Wiberg 2002; Huthnance et al. 2002). On a global scale, shelves are dominated by lithogenous sand and silt, but locally biogenic components can be dominant. Shallow water coral reef sediments can be dominated by carbonate sands originating from calcifying organisms.

*Shelf sea hydrodynamics:* Sediment distribution and seabed topography are strongly influenced by the hydrodynamic forcing within the water. If the hydrodynamical forcing causes a high enough shear stress, it can lead to erosion and transport of particles from the sea bed (Nittrouer and Wright 1994). Ripple marks, the undulated sediment surface consisting of ripples crests and troughs (Fig. 1), are produced by an interaction of currents with the sediment surface. Hydrodynamic forcing is also of major importance for the productivity of the water column and the sediments as it determines the transport of solutes and particles in the water column and to the sediment/water interface.

Figure 1: Ripple marks at the Haustrand (Sylt)

Hydrodynamic forcing within shelf sea waters is more complex and much more affected by turbulence than in the open ocean due to the presence of the sea bottom in the depth range of moderate or strong water movement. Especially in the immediate vicinity of the coastline, water- and sediment movement are pronounced (Bearman 1989; Nittrouer and Wright 1994). Within the shelf seas, hydrodynamics are mainly tidal, wind- and density driven. The tidal motion and amplitude can be increased by shallow water depths and seafloor morphology. Wind energy is transferred to the oceans at the atmosphere-water interface where it creates currents and surface gravity waves. Density driven currents are generated by horizontal and vertical density gradients (from salinity and/or temperature differences in the

water). Shallow water depths enhance the seasonal cycles with respect to temperature, as the water volume available for mixing is limited. The effect of fresh water input can also be substantial in a small water body and the combined effects can lead to a strong seasonal thermocline.

Furthermore, the presence of the coast has influences on hydrodynamics: Surface water that is forced away from the coast can only be replaced by upwelling waters from deep water layers. These upwelling zones constitute a major process for nutrient regeneration in the surface waters.

*Role of sands in shelf seas organic carbon cycling:* The primary production in shelf seas is high (pelagic net production is ca. 220 – 250 g C $m^{-2}$ $y^{-1}$), and additionally organic carbon is imported from land (Wollast 1991; Gattuso et al. 1998). Still, the fate of the organic matter in shelf waters is poorly understood and is one of the major uncertainties in the global carbon cycle (Gattuso et al. 1998).

The organic material in the coastal oceans can either accumulate in the sediments, can be exported from the shelves to the open ocean, or can be mineralized to $CO_2$, which may be partially released to the atmosphere (Wollast 1991; Gattuso et al. 1998).

There is an ongoing debate about the burial of organic carbon in present day's oceans. It seems that burial of organic carbon in shelf sediments is low (Walsh et al. 1981; De Haas et al. 2002, but see Hedges and Keil 1995). Additionally, the amounts of shelf sea carbon that is exported to the continental slope is considered to be relatively small (5%, or ca. 1 x $10^{15}$ g C $y^{-1}$) (Wollast 1991; De Haas et al. 2002). Thus, mineralization within the shelf seas must play a vital role in the fate of the organic carbon.

As large amounts of organic carbon are deposited on the seafloor and as large areas within the shelf seas are occupied by sands, they must be important sites of organic matter mineralization. The organic matter content in sediments is usually strongly correlated with the silt and clay fraction, due to sorption of organic matter to the grain surfaces and, possibly, a capture in the small sedimentary pore spaces.

Sands are characterized by very low contents of organic carbon and were for long times judged as biological deserts and neglected in marine research (Huettel and Gust 1992a; Shum and Sundby 1996; Boudreau et al. 2001). In the

1960s (Webb and Theodor 1968) proposed that it is the hydrodynamic forcing which promotes mineralization in sandy sediments. They argued that water flowing through permeable sediments transports oxygen and organic carbon from the water column to the sands and that the low organic content indicates a high carbon turnover. Indeed, it was found that the organic matter mineralization in sands can be equivalent to silty or muddy sites (Andersen and Helder 1987; Rowe et al. 1988; Cammen 1991). Isotope measurements of $^{210}$Pb in the relict sands indicated that shelf sea organic matter undergoes several deposition - mineralization and resuspension cycles in these sands before it is transported over the shelf edge, becoming highly refractory by this cycling (Bacon et al. 1994)[1].

[1] The $^{210}$Pb isotope is imported by the oceanic waters from atmosphere, where it attaches to organic material. In sediments the $^{210}$Pb can be found in the organic carbon coating of the sediments and can be used as a marker for transport rates to the sediments and of sedimentary turnover Bacon, M. P., R. A. Belastock, and M. H. Bothner. 1994. Pb-210 Balance and Implications for Particle-Transport on the Continental-Shelf, US Middle Atlantic Bight. Deep-Sea Res. Part II-Top. Stud. Oceanogr. **41:** 511-535..

## Carbon cycling in marine sediments

*Organic carbon synthesis*: Autotrophic organisms are able to build up their biomass from $CO_2$. Organic carbon is synthesized by photosynthesis using light energy, or by chemosynthesis using energy from chemical reactions (oxidation of inorganic compounds). For the production of organic carbon oxygenic photosynthesis is most important. In the shelf seas planktonic primary production is high, but also benthic primary production by microphytobenthos (MPB) is recognized to contribute significantly to ecosystem productivity (Colijn and Dejonge 1984; MacIntyre et al. 1996). The major benthic primary producers are the microscopic small eukaryotic diatoms and dinoflagellates and the prokaryotic cyanobacteria that grow within the upper several millimeters of illuminated sediments (MacIntyre et al. 1996; Brotas and Plante-Cuny 2003). Locally, macroalgae (e.g., diverse macroalgae communities at rocky shores) and higher plants (e.g, seagrasses) can also be important. A simplified reaction of oxygenic photosynthesis is given in the following, with $H_2O$ as the electron donor and $CO_2$ as electron acceptor:

$$CO_2 + H_2O \rightarrow CH_2O + O_2 \qquad (1)$$

By taking up nutrients the MPB has a significant impact on pore water nutrients concentrations and nutrient fluxes, the nitrogen cycle may additionally be affected by atmospheric $N_2$-fixation (Larkum et al. 1988; Herbert 1999; Dalsgaard 2003). $N_2$-fixation can be of major importance for the productivity of coastal ecosystems where $N_2$ is limiting primary production (Larkum et al. 1988; Charpy-Roubaud et al. 2001). $N_2$-fixation is a purely prokaryotic process carried out by cyanobacteria and a range of heterotrophs, the highest rates are, however, found in photoautotrophs because of the high metabolic cost of $N_2$-fixation (Herbert 1999). $N_2$-fixing (diazotrophic) cyanobacteria can be broadly grouped as heterocystous and non-heterocystous forms. All heterocystous cyanobacteria can fix $N_2$, in the heterocysts the $N_2$-fixing enzyme nitrogenase is protected from oxygen. Only a few non-heterocystous cyanobacteria can fix $N_2$ in the presence of oxygen.

There are many inorganic electron donors used by a large and diverse group of chemotrophic prokaryots. Many sulfur compounds (like $H_2S$, $S^0$, $S_2O_3^{2-}$) can be used for chemosynthesis (sulfide oxidation processes), for example by the aerobic

colorless sulfur bacteria *Beggiatoa spp*. $NH_4^+$, $NO_2^-$, $Fe^{2+}$ and $Mn^{2+}$ are also used as electron donors (e.g., in the processes of anaerobic ammonium oxidation and nitrification). Chemotrophic organisms play an important role for chemistry and mineral cycling in sediments by re-oxidizing reduced electron acceptors from anaerobic mineralization processes (see below).

*Organic matter degradation*: Organic carbon is used by heterotrophic organisms as an electron donor to obtain energy and as carbon source for the build up of biomass. The organic matter in marine sediments is mineralized via aerobic or anaerobic processes or by fermentation, the rates depend largely on the quality of the organic material (Herbert 1999). Organic matter mineralization is performed by a diverse community of organisms, however, prokaryotes have a special role as they can use a large variety of electron acceptors for the oxidation processes (Table 1). Up to $4 \times 10^9$ bacteria per cubic centimeter were found in German Wadden Sea sediments, indicating that prokaryotes can be abundant in marine sediments (Llobet-Brossa et al. 1998).

The sediments can be divided into two zones for benthic mineralization: the oxic zone, where oxygen is used as a terminal electron acceptor, and the anoxic zone, where various electron acceptors such as sulfate, nitrate and iron are used. Aerobic heterotrophic respiration is performed by eukaryotes like benthic algae and fauna and a wide array of bacteria. With oxygen as an electron acceptor, complex organic matter can be degraded to $CO_2$ by a single organism (Table 1, reaction a). However, prokaryotes are unable to take up organic matter of high molecular weight. Therefore, the extracellular hydrolysis of organic matter by exo-enzymes originating from heterotrophic bacteria is a critical (and often rate limiting) initial step preluding prokaryotic metabolism (Jørgensen 2000). Members of the Cytophaga-Flavobacterium group were the dominant group of prokaryotes (15 - 20% of detectable bacteria) in Wadden Sea sediments (Llobet-Brossa et al. 1998). These are mainly aerobic bacteria that are specialized in the degradation of complex molecules. Only a few aerobic bacteria are obligate aerobes, facultative aerobes are able to use other metabolic pathways in the absence of oxygen.

Oxygen is supplied to the sediments from the above water column or by benthic primary production in the upper sediment layers. The saturation concentration of oxygen in seawater is typically around $200 - 400\ \mu mol\ L^{-1}$

(depending on water temperature and salinity), thus, oxygen concentrations are rather low. In the presence of organic carbon that can be aerobically respired, undisturbed sediments, therefore, become quickly anoxic with depth and anaerobic organic matter oxidation pathways become important. In the anoxic zone, several microorganisms jointly degrade organic compounds, forming the anaerobic food web. The products of hydrolysis are taken up by fermenting bacteria. During fermentation the used organic compound serves as both, electron donor and electron acceptor. There are a large variety of fermentative pathways (e.g., reaction g, Table 1) and a large variety of organic compounds used (e.g. sugars, amino acids, fatty acids and glucose), and the endproducts are, for example, alcohols, $CO_2$, $H_2$ or acetate. The end products of fermentation are used as substrates during terminal anaerobic oxidation.

Electron acceptors other than $CO_2$ are usually supplied to the sediments from the overlying water. Thus, in undisturbed, diffusion dominated sediments, rather stable horizontal gradients develop in which various electron acceptors are consumed, usually in the order of decreasing redox potentials (Froelich et al. 1979; Reeburgh 1983).

In the suboxic layer, nitrate is an important electron acceptor. In the strictly anaerobic process of nitrate reduction (or denitrification; reaction b, Table 1) nitrate is sequentially reduced to nitrogen gas via nitrite, nitrous oxide and dinitrogen oxide. The gaseous components can be lost from the benthic environment. In the presence of oxygen, denitrifying organisms perform aerobic mineralization. Manganese and iron oxides are electron acceptors for manganese (IV) and iron (III) reducing bacteria (exemplary reactions c and d, Table 1). As reduced manganese and reduced iron diffuse upward the reduced sediments they are deposited as metal oxides already in the presence of low oxygen concentrations.

Table 1: Examples of organic matter oxidation, hydrogen transformation and fermentation pathways and their standard free energy yields, ΔG°, per mol organic carbon (modified from Jørgensen 2000). Underlined are the reduced substances that can be re-oxidized by chemotrophic organisms.

| Reaction | | ΔG° (kJ $mol^{-1}$) |
|---|---|---|
| Oxic respiration | | |
| a) | $CH_2O + O_2 \rightarrow CO_2 + H_2O$ | -479 |
| Nitrate reduction | | |
| b) | $5CH_2O + 4NO_3^- \rightarrow 2N_2 + 4HCO_3^- + CO_2 + 3H_2O$ | -453 |
| Manganese (IV) reduction | | |
| c) | $CH_2O + 3CO_2 + H_2O + 2MnO_2 \rightarrow \underline{2Mn}^{2+} + 4HCO_3^-$ | -349 |
| Iron (III) reduction | | |
| d) | $CH_2O + 7CO_2 + 4Fe(OH)_3 \rightarrow \underline{4Fe}^{2+} + 8HCO_3^- + 3H_2O$ | -114 |
| Sulfate reduction | | |
| e) | $2CH_2O + SO_4^{2-} \rightarrow \underline{H_2S} + 2HCO_3^-$ | -77 |
| | $H_2 + SO_4^{2-} + H^+ \rightarrow \underline{HS}^- + 4H_2O$ | -152 |
| | $CH_3COO^- + SO_4^{2-} + 2H^+ \rightarrow 2CO_2 + \underline{HS}^- + 2H_2O$ | -41 |
| Methanogenesis | | |
| f) | $CH_3COO^- + H^+ \rightarrow CH_4 + CO_2$ | -28 |
| Fermentation | | |
| g) | $CH_3CH_2OH + H_2O \rightarrow CH_3COO^- + \underline{4H_2} + H^+$ | 77 |

When other energetically more favorable electron acceptors are depleted, sulfate is used as electron acceptor by sulfate reducing bacteria (SRB). Because of the high sulfate concentrations in the marine environment (25 - 28 mmol $L^{-1}$), dissimilatory sulfate reduction (exemplary reactions e, Table 1) is often found to be the most important anaerobic mineralization pathway (Jørgensen 1982; Canfield et al. 1993a; Canfield et al. 1993b). SRB have variable morphologies (Llobet-Brossa et al. 1998) and are polyphyletic, however, most cultivated SRB belong to the δ-subclass of Proteobacteria. SRB of the δ-subclass of Proteobacteria made up the second largest group (6.5%) of detectable bacteria in the Wadden Sea sediments (Llobet-Brossa et al. 1998). Sulfate reducing bacteria are physiological diverse (e.g., Widdel and Pfennig 1982; Coleman et al. 1993) and seem to have the broadest spectrum of potential electron acceptors of mineralizing bacteria. They also use a large varied of organic compounds and $H_2$ as electron donors. Like some cyanobacteria, a few SRB able to fix $N_2$ in the absence of oxygen.

In sediment zones and habitats (e.g., fresh water habitats) where sulfate is depleted or low, methanogenesis by Archaea (reaction f, Table1) is an important process (e.g., Winfrey and Ward 1983; Purdy et al. 2003). Methanogens can use formiate, acetate and $H_2$ as electron donors. Sulfate reducing bacteria are thought to outcompete methanogens when sulfate is available (e.g., Winfrey and Ward 1983), as cultured strains had a higher specific affinity for the main substrates used by both groups (Lovley et al. 1982). Methane produced in anoxic habitats can be oxidized in the process of anaerobic methane oxidation using sulfate as an electron acceptor, or it transported to oxic layers where it is oxidized to $CO_2$ by methanotrophs.

*Calcification/decalcification*: The carbon cycling in the marine environment is influenced by calcification and decalcification reactions that are often driven by biological activities. In the ocean carbon dioxide combines with water and generates carbonic acid, bicarbonates and carbonates ions (forming together the total dissolved inorganic carbon (DIC)) that are related by the following equilibria:

$$H_2O + CO_2 \leftrightarrow H_2CO_3 \leftrightarrow H^+ + HCO_3^- \leftrightarrow 2H^+ + CO_3^{2-} \quad (2)$$

The concentrations of the species depend on equilibrium constants that are controlled by temperature, salinity and pressure. The relative proportions of $CO_2$, $HCO_3^-$ and $CO_3^{2-}$ and the seawater alkalinity control the pH of the water (Fig. 2).

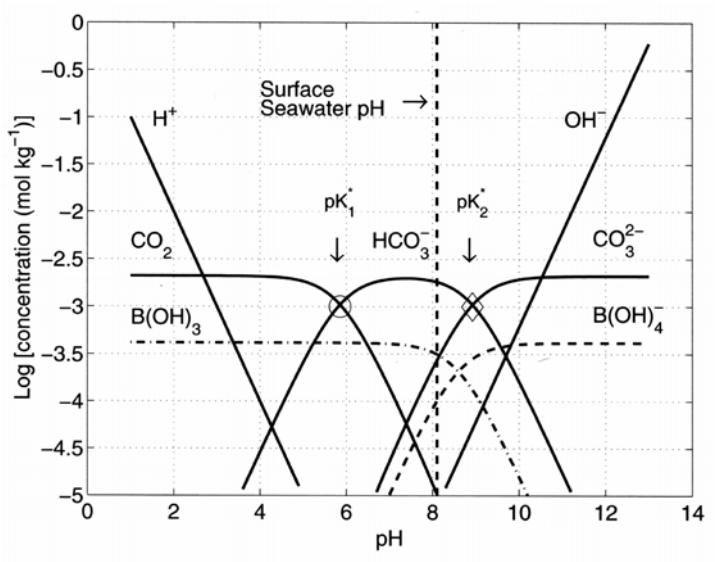


Figure 2: Relation of $CO_2$, $HCO_3^-$ and $CO_3^{2-}$ concentrations and pH in seawater (from Zeebe and Gladrow 2005).

Calcification (or, from right to left the dissolution of $CaCO_3$) at circumneutral pH can be written as

$$Ca^{2+} + 2HCO_3^- \leftrightarrow CaCO_3 + CO_2 + H_2O \quad (3)$$

Whether $CaCO_3$ precipitates or dissolves depend to a large extend on the saturation state of the solution with respect to $Ca^{2+}$ and $CO_3^{2-}$. Surface seawater is mostly highly supersaturated with respect to $CaCO_3$ (e.g., 4 times with respect to aragonite). However, oversaturation does not necessary lead to precipitation as the presence of inhibitors such as magnesium and certain organic compounds may prevent a nucleation (Canfield and Raiswell 1991).

Photosynthesis removes $CO_2$ from seawater (formula 1), thereby reducing DIC and increasing the pH (up to values above pH 9), photosynthesis also slightly increases the total alkalinity (TA) by the uptake of nutrients (see Fig. 3). By increasing the saturation state of the solution with respect to $CO_3^{2-}$, photosynthesis stimulates calcification. By buffering the pH, calcification is acting beneficial for photosynthetic organisms, as most of them preferentially take up $CO_2$, which is more abundant at lower pH (Fig. 2). Calcifying corals are an example for the beneficial coupling of calcification and photosynthesis.

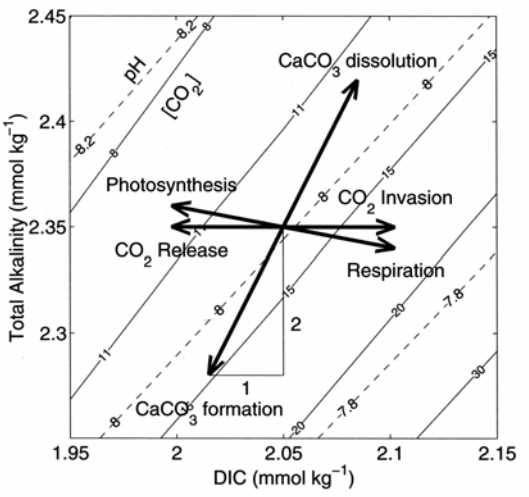


Figure 3: Influence of photosynthesis, aerobic respiration, calcification and decalcification on DIC, TA and pH (from Zeebe and Gladrow 2005).

The aerobic oxidation of organic matter may promote decalcification (reaction a, Table 1) by increasing the DIC, lowering pH and TA (Tribble 1993; Sanders 2003). Benthic mineralization in the anoxic sediment layers (see Table 1) may lead to $CaCO_3$ dissolution, as for example some pathways of sulfate reduction and the (anaerobic) oxidation of the end product $H_2S$ can induce a drop in pH

(Morse et al. 1985; Tribble 1993; Sanders 2003). At high sulfate reduction rates, the substantial bicarbonate production and the resulting alkalinity rise may outweigh the drop in pH and lead to carbonate precipitation (Tribble 1993; Visscher et al. 1998; Sanders 2003).

The marine carbonate system plays an important role in the world oceans as it affects the $CO_2$ concentrations in seawater and atmosphere, it determines the extend of burial of $CaCO_3$ in marine sediments and is the natural buffer for seawater pH.

**Transport mechanisms in marine sediments**

By exchanging and distributing electron donors, electron acceptors and nutrients, transport mechanisms between sediments and water column are important for biogeochemical processes in both compartments. Transport mechanisms via the sediment/water interface and within sediments can be divided into diffusion and mass flow processes (bioirrigation, bioturbation, pore water advection). Diffusion is driven by concentration gradients and only solutes are transported. Mass flow processes are independent of concentration gradients and solutes and particles are transported. Which transport process is dominant, depends to a large extend on sediment composition and benthic faunal activity (Huettel et al. 1998).

*Diffusion:* In cohesive sediments (or "muds", grain size ≤ 63µm) the physical solute transport is mainly restricted to diffusion. During diffusion the net transport is driven by thermally-induced random movements of molecules along solute concentration gradients from sites of high- to sites of low concentrations. The flux (J) of a solute is proportional to the magnitude of the vertical concentration gradient (dC/dz) as it is described in Fick´s first law:

$$J = - D_0 (dC/dz) \quad (4)$$

with $D_0$ being the substrate-dependent diffusion coefficient in water at a given temperature and salinity.

In the pore spaces of sediment, the effective diffusion is lower compared to water as the sediment particles prolong the actual distance the diffusing solute must travel[1] (Ullman and Aller 1982; Iversen and Jørgensen 1993; Boudreau 1996). Thus, a modification of Fick`s first law is used for sediments:

$$J = - \phi \, Ds \, (dC/dz) \qquad (5)$$

where $\phi$ is the sediment porosity and Ds is the effective diffusion coefficient in the pore water. The relation between $\phi$ and Ds can be found in the literature for different types of sediments (Ullman and Aller 1982; Iversen and Jørgensen 1993). Gradients are relatively stable in cohesive sediments, as diffusion is only efficient over small distances: the time a molecule needs to travel a certain distance increases with the square of the distance (at 10°C oxygen travels ca. 3-4 mm in 1 hour; 2 cm in 1 day and 10 m in 1000 years (from Jørgensen 2000).

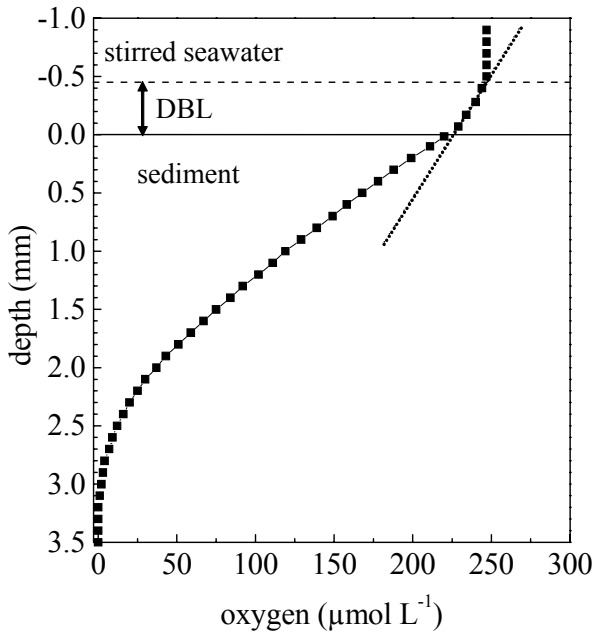


Figure 4 shows a typical oxygen profile measured in a cohesive sediment with the stirred seawater overlying the DBL and the sediment. The oxygen decreases linearly in the DBL (dotted line) and the sediment the profile shape is rather parabolic (from U. Franke).

The water column above sediments is usually well mixed by turbulent water motion. When the moving water encounters the stationary sediment surface, frictional forces lead to the development of the diffusive benthic boundary layer (DBL; usually 0.2 - 1.2 mm thick) above the surface of cohesive sediments (Fig. 4).

[1] geometric tortuosity = actual distance the ion must travel through a porous media relative to the length of the straight path

In the DBL transport is restricted to diffusion. This has important implications for benthic processes. Although in zones of weak currents organic rich material preferably settles at the sediment surface, its degradation in the sediments is largely determined by the diffusive transport of electron acceptors to the sediment and, thus, by the solute uptake rate in the sediments and the solute concentration in the overlying water. If, for example, oxygen consumption in the sediments is high, steep oxygen gradients develop between the sediment and the overlying water and the transport through the DBL may completely limit sedimentary oxygen consumption rates (Jørgensen and Revsbech 1985).

*Transport by faunal activity:* The transport of solutes may be greatly enhanced by benthic meio- and macrofauna via bioirrigation or bioturbation (Krantzberg 1985; Aller 1988; Aller 2001). The biogenic transport is most intense in the upper sediment layers and depends on abundance and activity of the organisms.

Bioirrigating fauna pumps oxygen rich surface water into deep sediment layers in requirement of, for example, oxygen and organic matter. Physical reworking of sediments due to bioturbation results in mass transport of solutes and particles (Aller 1994; Graf and Rosenberg 1997).

The burrow walls of bioirrigating fauna increase the effective exchange area of the sediment surface for solutes (Aller 1988; Kristensen 2000; Wenzhöfer and Glud 2004). Faunal activity disturbs the hypothetical vertical distribution pattern of solutes in diffusion dominated systems. Due to faunal activity, horizontal gradients establish and solute distribution patterns may change on short time scales. Experimental evidence and theoretical considerations indicated that periodic, even brief, exposure to oxygen results in more complete and sometimes more rapid decomposition of organic matter in sediments as it is possible under constant conditions or unidirectional redox changes (Aller 1994; Aller and Aller 1998).

*Transport in permeable sediments – pore water advection:* Sandy sediments are porous and therefore permit the flow of fluids through their interstices. Permeability is a measure of the ease with which fluids can flow through porous media. The permeability of sediments depends on sediment properties, with median grain size, sediment sorting and porosity being the most important determinants.

The physically induced mass flow of pore water and the exchange of pore- and overlying water in these sediments is referred to as pore water advection. This is an important mass transport mechanism in permeable sediments, additionally to diffusion and transport by fauna (Webb and Theodor 1968; Riedl et al. 1972; Huettel and Gust 1992a; Shum 1992). Pore water advection can exceed diffusive solute transport by orders of magnitude (Huettel et al. 2003).

Pore water advection is driven by pressure gradients along the sediment. The flow rates are reduced by frictional forces in the pore spaces that depend on the viscosity of the fluid medium and the permeability of sediment. The relation between pore water flow velocity (u), the sediment permeability (k), porosity ($\varphi$), the pore water viscosity ($\mu$) and the spatial pressure gradient ($\nabla p$) is described in Darcys law (Darcy 1856)

$$u = \frac{k}{\varphi \mu} \nabla p \qquad (6)$$

Pore water advection is significant in sediments that have a permeability > $10^{-12}$ $m^2$ (Huettel and Gust 1992a). At such permeabilities a natural pressure differential of less than 1 Pa is sufficient to induce pore water flow through the upper sediment layer (Huettel and Gust 1992a). Pressure gradients in laboratory studies were mostly in the range of a few Pascal (Thibodeaux and Boyle 1987; Huettel and Gust 1992a; Huettel et al. 1996), in situ measurements of pressure gradients are still lacking. Pressure gradients across the sediment may result from waves, currents and density changes.

*Pore water advection induced by waves:* The interaction of waves and subtidal sediments was amongst the earliest foci of work in permeable sediments. During their pioneering work in the late sixties, Webb and Theodor (1968) investigated in a field study the effect of surface gravity waves on pore water flow. The quick relocation of dye within and out of rippled sandy sediments was attributed to wave action. The pore water circulation pattern found was symmetric, with pore water leaving the sediment at the ripple crest and overlying water forced into the sediment at the ripple flanks and troughs (Webb and Theodor 1968; Webb and Theodor 1972).

Although the work of Webb and Theodor (1968) initiated studies on permeable sediments, many of the early investigations and models focused on the

wave induced transport in permeable sediments with a flat sediment surface (Riedl et al. 1972; Vanderloeff 1981; Harrison et al. 1983; Webster and Taylor 1992). In the early 1970s, Riedl et al. (1972) introduced the term “subtidal pump” for wave induced water transport in flat sediments. The assumed mechanism was the difference in hydrostatic pressure between wave crest and the wave troughs that travel with the wave propagation. These temporally changing pressure gradients at the sediment surface can lead to pulsing pore water flow. The importance of this process was stressed by their estimation that sandy shelf sediments could filter the total volume of the global oceans within 14.000 years.

When the water depth is lower than half of the wave length, surface gravity waves generate oscillatory bottom water currents at the sediment surface (Denny 1988). Flow above the sediment may also produce sediment ripples. Recent investigations showed that pore water advection rates induced by oscillating currents from waves above sediment topography are much higher than when induced by hydrostatic wave pumping (Shum 1992; Precht and Huettel 2003; Precht and Huettel 2004). Experiments and models showed that the pore water flow patterns induced by oscillating currents is similar to those observed in situ (Webb and Theodor 1968; Webb and Theodor 1972), and that the total exchange rate increased with increasing ripple slope and strength of wave motion.

*Pore water advection driven by unidirectional bottom currents:* Similarly to oscillating currents, unidirectional bottom flow generates pressure gradients over sediments with uneven topography (Thibodeaux and Boyle 1987; Huettel and Gust 1992a; Ziebis et al. 1996b). Unidirectional currents result from wind and tides.

Figure 5 shows the pressure distribution along a sediment mound and the resulting water flow field in the presence of a unidirectional current (Huettel et al. 1996). As the flow encounters the obstacle it is deflected from the surface, resulting in a high pressure zone at the upstream flank of the ripple. Downstream behind the ripple crest the flow accelerates and separates from the surface, resulting in a zone of low pressure. Where the flow reattaches to the surface, a second zone of high pressure can be found. Due to this pressure distribution, the water enters the sediments at the ripple troughs whereas the water is released at the low pressure zone close to the crest. The pore water flow pattern resulting from unidirectional flow is, thus, very similar to the pattern observed under oscillating currents, with

the difference that the pore water leaves the sediments not directly at the crest but on the leeward side of the crest (Thibodeaux and Boyle 1987; Huettel and Gust 1992a). As can also be derived from Figure 5 the pore water flow velocities are highest at the outflow area at the ripple crest, as the area of pore water emergence is smaller than the area of bottom water intrusion.

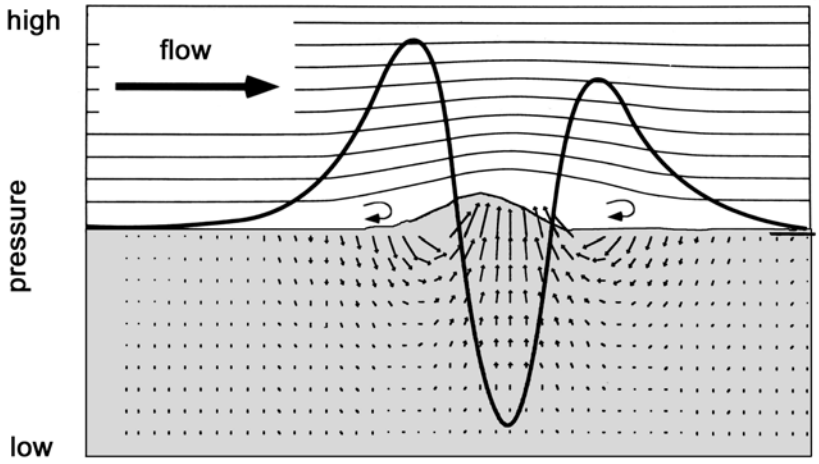


Figure 5. Pressure field created by unidirectional currents over sediment topography. Direction and magnitude of pore water flow in the sediment is indicated by the arrows (modified from Huettel et al. 1996)

In laboratory studies, it was found that significant pore water advection can be generated by water flowing over small obstruction, mounds, animals and depression on the sediment surface (Thibodeaux and Boyle 1987; Huettel and Gust 1992a). The pressure gradients measured grew with obstacle size and increasing flow velocities (Huettel and Gust 1992a). Already at water flow velocities of 10 cm $s^{-1}$ a mound of 2.4 cm height could force the overlying water as deep as 5 cm into the sediment and the interfacial solute exchange was up to 3 orders of magnitude higher than compared to molecular diffusion (Huettel and Gust 1992a).

*Pore water advection driven by density differences*: Pressure gradients also develop where density differences exist between the pore- and the overlying water (haline and thermal convection) (Webster et al. 1996). These density differences may, for example, be important in estuaries or on intertidal flats. Thermal convection after initial inundation of a heated-up intertidal sand resulted in solute

exchange rates that were three orders of magnitude higher as compared to diffusion (Rocha 1998).

*Pore water advection via groundwater discharge:* The submarine discharge of groundwater through aquifers (derived from land or composed of re-circulated seawater) may also drive advective transport processes in coastal regions, and especially in permeable sands. Although, on a global scale, submarine groundwater discharge is less important than river run-off, in some areas it is an important process coupling sediments and overlying water (Johannes 1980; Simmons 1992; Burnett et al. 2003).

*Special types of pore water advection on intertidal flats:* The morphology and nature of shorelines varies greatly in relation to wave- and tidal energy and to sediment properties. Shorelines range from high-energy coarse sandy beaches to low energy sand- and mudflats, where physical forces are less dominant (McLachlan and Turner 1994). Reflective beaches have coarse sands, steep slopes, flat waves and small tidal ranges and the wave energy is reflected out to the sea. Dissipative beaches (or intertidal flats) have fine sands, steep waves and large tidal ranges. They are characterized by flat slopes where waves gradually dissipate their energy (McLachlan and Turner 1994).

As waves break on coarse gravel- and shingle beaches during transition to exposure or inundation, swashes percolate into unsaturated sediments (Riedl and Machan 1972; McLachlan 1989). Significant volumes of water circulates back through the sediments, thus, reflective beaches filter large water volumes with short residence times (McLachlan and Turner 1994). This can lead to a sediment oxygenation down to the depths of meters (Riedl and Machan 1972). In contrast, large areas of finer grained intertidal sediments stay water saturated due to capillary forces and net swash infiltration is negligible (McLachlan and Turner 1994; Turner and Nielsen 1997; Turner and Masselink 1998).

During exposure of intertidal flats pressure gradient develop between the sea water level and the slower dropping pore water table (Nielsen 1990). The resulting pressure gradient drives drainage flow of pore water through the sediments towards the seawater.

*Special types of pore water advection in coral reef sediments:* Coral reef sediments and the reef framework are highly permeable, reaching permeablities of

$10^{-9}$ $m^2$ (Enos and Sawatsky 1981; Wheatcraft and Buddemeier 1981; Rasheed et al. 2003b). A significant water flow through reef sediments and framework can be generated by pressure gradients that develop across the reef crest when the crest act as a barrier for tidal water motion, thereby resulting in sea water level differences between the outside and the inside of the reef (Oberdorfer and Buddemeier 1986; Parnell 1986).

**Impact of pore water advection on sediment biogeochemistry**

*Transport of solutes by pore water advection*: Pore water advection efficiently transports solutes such as oxygen and sulfate from the water column to deep sediment layers and pore water solutes to the top sediment layers or to the overlying water column. Oxygen is a key element in sediments and its distribution has major implications for benthic metabolism. Oxygen concentrations vary along a ripple bed in the presence of pore water advection. The oxygen penetrates deeper below a trough, and less below the crest, and, due to the rather u-shaped flow path of solutes through the sediments, horizontal gradients can be in the same order as vertical gradients (Shum 1993; Precht et al. 2004).

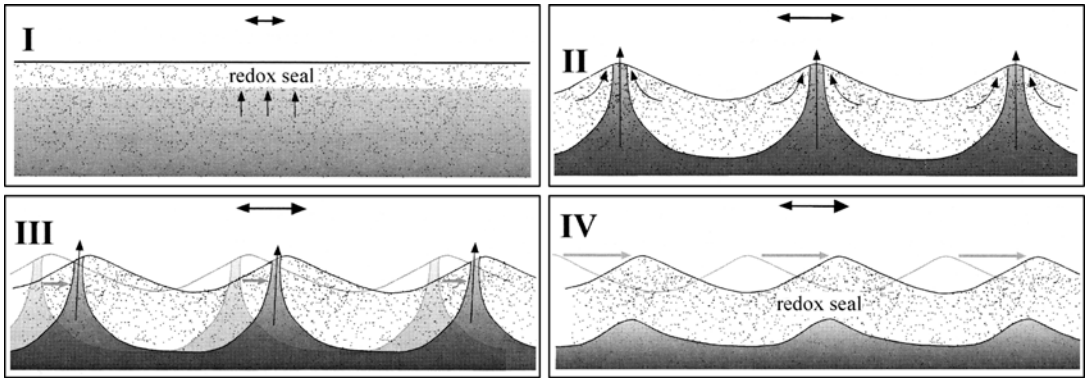


Figure 6: Dependency of sediment redox conditions on oscillating current velocity (black arrows) and ripple migration (grey arrows). I) no topography, low current velocity, a redox seal establishes II) stationary ripples, the anoxic pore water is transported to the upper sediment layers II) ripples moving slower than the pore water and IV) ripples moving faster than the pore water which is leading also to a redox seal. Figure modified from Precht et al. (2004).

The depth distribution of oxygen depends on the magnitude of pore water advection and on oxygen consumption processes in the sediments (Shum 1993). If oxygen consumption processes are high, oxygen penetration depth is shallow and

the concentration decrease is most pronounced below the outflow area at the crest. In case of low oxygen consumption rates, a fairly uniform distribution establishes along the ripple field. The dynamic nature and pore water distribution patterns of permeable sediment are summarized in Figure 6 (Precht et al. 2004).

In situ oxygen was found to penetrate several centimetre into permeable sediments. In an intertidal flat oxygen penetration significantly increased during inundation of the flat, being around 1 – 3 cm in warm months and around 4 – 8 cm in cooler months (de Beer et al. 2005). An oxygen penetration depth down to 25 cm was found at an intertidal sand flat with high abundances of macrofauna (D'Andrea et al. 2002; D'Andrea et al. 2004). In coral reefs sediments oxygen penetration depths of 0.5 – 1 cm were found (King et al. 1990), but also extreme oxygen penetration depths of 15 – 50 cm (Falter and Sansone 2000).

Pore water advection is visible in oxygen profiles, as oxygen profiles with enhanced transport in the upper sediment layer are rather sigmoidal (Fig. 7) whereas diffusion dominated profiles have a nearly parabolic shape (Fig. 4) (Revsbech et al. 1980a; Forster et al. 1996; Lohse et al. 1996).

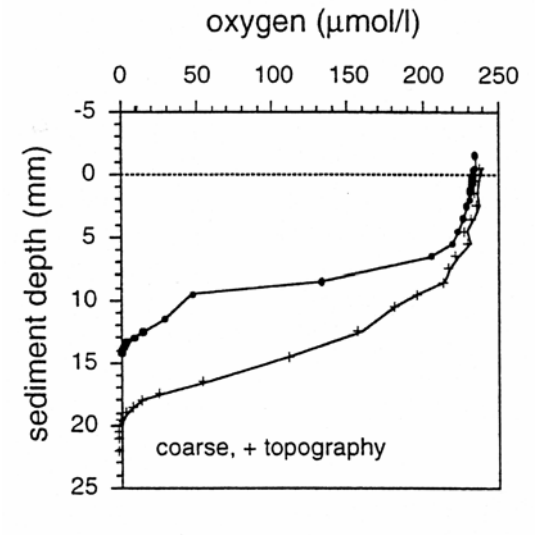


Figure 7: Oxygen profiles measured in coarse (even surface and with topography) sediments under unidirectional flow (from Forster et al. 1996)

Oxygen is consumed in sediments by aerobic heterotrophic organisms and by the oxidation of reduced substances from anaerobic decay. Oxygen consumption rates are thus considered to represent an integrated signal over total benthic metabolism. Oxygen consumption rates in permeable sediments are enhanced by the deep supply of oxygen: the sedimentary oxygen consumption was a function of flow velocity in a flume experiment (Forster et al. 1996), as higher flow velocities

increased the oxic volume of the sediment. In the presence of mounds from the shrimp *Callianassa truncata* oxygen penetration increased 10 fold, the oxic sediment volume increased 1.5 fold and oxygen consumption rates 1.7 fold (Ziebis et al. 1996a). Higher oxygen consumption rates due to hydrostatic wave pumping were measured in situ in benthic chambers with flexible tops compared to chambers with solid tops (Malan and McLachlan 1991).

The advective removal of dissolved inorganic nitrogen species, silicate and phosphate by pore water advection may be derived from low pore water concentrations as well as from the shape of pore water concentration profiles (Marinelli et al. 1998; D'Andrea et al. 2002; Ehrenhauss et al. 2004). Through the upwards transport of anoxic pore water, potentially inhibitory products for sedimentary metabolism such as ammonium and hydrogen sulfide may effectively be removed from the sediments or be oxidized (Ziebis et al. 1996a; Huettel et al. 1998).

As found for bioturbated sediments, fluctuating anoxic-oxic boundaries and redox conditions may be beneficial for organic matter processing in sediments (Aller and Aller 1998; Huettel et al. 1998). For example, the temporal dispersions of oxygen into ammonium rich sediment layers can stimulated nitrification, which in turn can stimulate denitrification (Lohse et al. 1993). Fluid flow may be beneficial for bacteria attached to sand grains by increasing the supply of electron acceptors, nutrients or dissolved organic carbon (Van Loosdrecht et al. 1990; Logan and Kirchman 1991).

*Transport of particles by pore water advection:* Particles (bacteria, microalgae, detritus) can be transported several centimeter deep into sediments by pore water advection. This is of major importance for benthic minerlization rates as settling of particles is low in sandy areas due to the intense hydrodynamics. Particle transport is most efficient in the upper sediment layers, as the pore water flow decreases with depths, thus, the existence of an upper decomposition layer was proposed (Huettel and Rusch 2000; Rusch and Huettel 2000). In an experiment using sediments with small topography, it was shown that water penetrated 5.5 cm into the sediments and particles from the sediment surface were co-transported down halfway into the sediment (Huettel et al. 1996). The transport of particles

stops where fluid velocity drops below the threshold necessary to overcome the retention forces acting against the particle movement (Huettel et al. 1996). The transport efficiency depends on the size of the particles, the surface of the particles and grain size and permeability of the medium (Huettel et al. 1996; Huettel and Rusch 2000; Rusch and Huettel 2000; Rusch et al. 2001). However, even chain forming diatoms were transported down to 5 cm depths (Ehrenhauss and Huettel 2004).

Diatoms trapped by pore water advection significantly enhanced mineralization rates in permeable sediments (Forster et al. 1996; Huettel and Rusch 2000; Ehrenhauss and Huettel 2004). High sedimentary mineralization may be supported by the mechanical breakage of cells by moving sediment grains (Huettel and Rusch 2000).

**Special role of carbonate sediments**

In shallow coral reef systems, the highly permeable carbonate sediments are important sites of organic matter turnover and a source of nutrients to the overlying water (Boucher et al. 1994; Clavier and Garrigue 1999; Rasheed et al. 2003b; Rasheed et al. 2004; Wild et al. 2004b; Wild et al. 2004c) and may thus be an important compartment for the energy and matter cycling within the entire system. Coral reefs sediments mainly result from the biological and mechanical destruction of reef structures and coral heads and calcareous algae and, additionally, molluscs and foraminifers biofacies can be abundant (Boucher et al. 1998). A two fold higher permeability of carbonate sediments was measured compared to silicate sediments with the same grain size (Rasheed et al. 2003b), which is thus permitting high pore water advection rates. Due to their porous structure carbonate grains have a relatively large surface area (Rasheed et al. 2003a), and provide space for dense populations of bacteria (Wild personal communication). These factors, together with the high water temperatures, can promote high benthic turnover rates in coral reef sediments. Oxygen consumption rates were higher in carbonate sediments when compared to silicate sediments of the same grain size from nearby stations (Rasheed et al. 2003a). Another factor promoting high benthic turnover in coral reef sediments is that the $CaCO_3$ grains are reactive and can buffer the pore water pH (in contrast to silicate grains).

**In situ measurements –methodological problems**

Major findings on transport and mineralization processes in permeable sediments result from flume, wave tank, and other type of laboratory studies or modeling. As sands only gained intensive consideration in the last decade, in situ work is still not abundant. The investigations available showed that pore water advection is of paramount importance for the magnitude of benthic mineralization in temperate coastal sands (Jahnke et al. 2000; D'Andrea et al. 2002; Ehrenhauss et al. 2004; de Beer et al. 2005; Janssen et al. 2005), or for coral reef sediments (Buddemeier and Oberdorfer 1988; Rasheed et al. 2004; Wild et al. 2004a; Wild et al. 2004b; Wild et al. 2004c). As stated above, in situ oxygen penetration was found to be deep and dynamic (King et al. 1990; Lohse et al. 1996; D'Andrea et al. 2002; De Beer et al. 2005). Due to deep oxygen penetration, aerobic mineralization was found to be dominant (D'Andrea et al. 2002; de Beer et al. 2005).

As the magnitude of mineralization rates in permeable sediments depends on the transport of the electron acceptors and organic carbon, the choice of methods to obtain in situ investigations is critical (Buddemeier and Oberdorfer 1988; Reimers et al. 2004).

Flux estimates in cores where diffusion is dominant lead to underestimation of solute supply and benthic mineralization rates. Flux calculations on concentration profiles influenced by pore water advection do not give reliable results (Jahnke et al. 2000).

Benthic chambers that allow stirring or pumping of the enclosed water body are useful tools for areal exchange measurements of solutes in permeable sediments using defined flow conditions. The stirring can be adjusted to local hydrodynamic conditions and fluxes and transport rates can be quantified (Huettel and Gust 1992b). Benthic chambers with flexible tops (Malan and McLachlan 1991) are used to assess the effect of hydrostatic wave pumping on benthic fluxes. However, during an in situ study on an intertidal sand flat, it was found that oxygen fluxes measured with chambers were only half of those derived from a novel method (see below) (de Beer et al. 2005). This is due to a major drawback of benthic chambers: it is very difficult to mimic natural hydrodynamics.

The method introduced by de Beer et al. (2005) combines in situ measurements of oxygen dynamics with laboratory measurements of volumetric oxygen consumption rates. For in situ oxygen distribution and dynamics, oxygen profiles are continuously measured in short time intervals over long time periods like a day or a tidal cycle by the use of microsensors (Fig. 8). The oxygen penetration depths thus obtained vary in relation to in situ hydrodynamics and sediment topography and should reflect an averaged oxygen penetration within the pore water flow field. Volumetric, potential oxygen consumption rates are obtained by first percolating oxygen rich water through the sediments. Upon stopping the percolation the decrease of oxygen is monitored at various depths by either microsensors or planar oxygen optodes. To obtain areal oxygen consumption rates the volumetric oxygen consumption rates are integrated over the varying depths of oxygen penetration from the field. The areal oxygen consumption rates, thus, include the impact of in situ hydrodynamics on sedimentary oxygen distribution.

Another promising method is the in situ measurement of net benthic fluxes above undisturbed sediment by the eddy correlation technique that is based on the simultaneous measurements of flow and solute concentration in the benthic boundary layer (Berg et al. 2003).

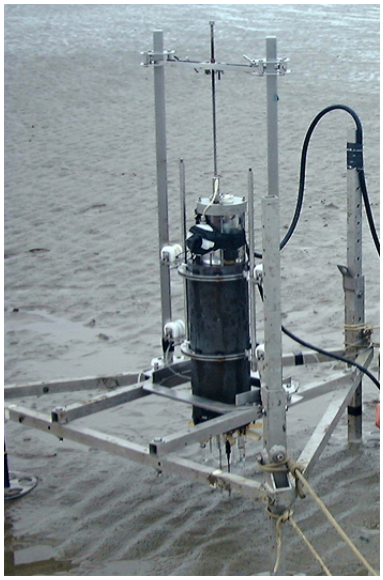

Figure 8: Microsensors attached to a Profiler (at Janssand). This measuring device can automatically measure consecutive solute profiles.

**The aim of the thesis**

Sands may play an important role in coastal carbon and nutrient cycling. Research in permeable sediments is often constrained to laboratory measurements. In situ investigations on carbon turnover in these sediments and on the role of pore water advection for benthic metabolism are rather scarce. In this thesis, microbial processes and the role of pore water advection for benthic metabolism are investigated on natural sediments, by a combination of in situ and laboratory methods. Two intertidal flats in the German Wadden Sea and subtidal carbonate sediments in a coral reef (Heron Reef, Australia) were investigated.

The overall aim of the study is to improve to the understanding of the role of permeable sediments in coastal ecosystems. The specific objectives are to:

- measure in situ distribution and dynamics of the electron acceptor oxygen in permeable coastal sediments
- evaluate the role of pore water advection for sediment oxygenation in natural sediments
- quantify benthic mineralization processes in permeable coastal sediments
- evaluate the role of oxygen and organic carbon supply by pore water advection on mineralization rates
- determine the relative contribution of aerobic and anaerobic mineralization
- evaluate pore water nutrient dynamics and the driving forces
- give a structural and functional analysis of the microphytobenthos in porous reef sediments

The first manuscript (chapter 2) characterizes the percolation method for the determination of potential oxygen consumption rates and areal oxygen consumption rates in permeable sediments. The method compared to other methods (like flux calculations and benthic chambers) and its applications and potential limitations are described in detail.

***Investigations in intertidal temperate sands***

The second manuscript (chapter 3) presents the results of a seasonal in situ study on transport and mineralization in an intertidal sand flat (Sylt/Germany). We hypothesized that oxygen distribution and dynamics are linked to pore water

advection and that magnitude and relative importance of oxygen consumption, aerobic mineralization and sulfate reduction rates depended on inundation time (i.e., period of pore water advection) at the intertidal flat. Therefore, we chose three stations in a transect stretching from the low- towards the high water line. The dynamics of pore water solutes over the tidal cycle and pore water drainage during exposure of the flat were examined.

The third manuscript (chapter 4) presents the results of a seasonal in situ study on transport and mineralization in a sloping intertidal sandflat (Janssand/Germany). Pore water nutrients and surface mineralization rates (oxygen consumption, sulfate reduction) were investigated on the upper and the lower flat on a tidal and seasonal basis to assess the temporal and spatial scales of mineralization. At the lower flat, pore water drained out of the sediments during exposure to air. The specific question formulated on this observation, was, whether the recycling of sedimentary mineralization products is governed by two main pore water circulation patterns operating on distinctly different temporal and spatial scales.

***Investigations in coral reef sands***

Chapter 5 presents the results of an in situ study on transport and mineralization on four stations in carbonate coral reef sediment (Heron Reef, Australia). Four study sites were selected with different hydrodynamic regimes, to examine whether pore water advection is the main controlling parameter for benthic mineralization rates and to examine the ratio between aerobic and anaerobic mineralization.

The fifth manuscript (chapter 6) is a laboratory study with special emphasis on structural and functional analysis of the microphytobenthos in the sediments of Heron Reef. The heterogeneity of the microphytobenthos, microphytobenthic photosynthesis and associated processes are investigated.

**Introduction to the study sites**

*The Wadden Sea:* Tidal flats are among the most productive ecosystems of the world and are strongly influenced by interactions of physicochemical and biological processes (Grossart et al. 2004). The largest tidal flat ecosystem, globally, is the Wadden Sea in the North Sea (Grossart et al. 2004). The Wadden Sea comprises a shallow water body (average water depths of ca. 2 - 3 m) and coastal wetlands. It stretches from Den Helder in the Netherlands to Esbjerg in Denmark in the north (length of coastline is ca. 500 km, widths is on average 10 km and total area is about 10.000 km²). In the southwest the Wadden Sea is influenced by large river estuaries. Intertidal areas (covering ca. 50% of the area) are characteristic for the Wadden Sea, also sandbanks and islands that present a barrier against the North Sea.

The sediments of the Wadden Sea are dominated by medium to fine sands, the median grain size generally becoming progressively finer towards the mainland coasts (Figge 1981; Flemming and Ziegler 1995). For the backbarrier region of Spiekeroog it was shown that the construction of dikes led to the removal of muds, as fine particles can not settle because of high hydrodynamic energy in the vicinity of the dikes (Flemming and Ziegler 1995). Strong hydrodynamic forcing by wind, tides and turbulent water motion make the Wadden Sea a very dynamic ecosystem, leading to the formation and erosion of the flats, banks and islands. The strong hydrodynamic regime results in fast transport, dispersion and mixing of dissolved and particulate matter from various sources (Flemming and Ziegler 1995; Grossart et al. 2004).

In the Wadden Sea, labile organic matter is mainly supplied to the ecosystem via the primary production of phytoplankton and phytobenthos. The contribution of phytobenthos to total primary production is high and in many areas nearly equivalent to the production of pelagic phytoplankton (van Beusekom et al. 1999). Due to the high nutrient availability primary production is mainly light limited over the whole year due to the high water turbidity (Colijn and Cadee 2003). Primary production rates in the Wadden Sea ranges between 210 - 309 g C $m^{-2}$ $y^{-1}$, remineralization rates between 290 – 450 g C $m^{-2}$ $y^{-1}$, thus, in general the Wadden Sea can be regarded as net-heterotrophic (van Beusekom et al. 1999).

Organic matter is imported (80 - 152 g C $m^{-2}$ $y^{-1}$) to the Wadden Sea from the coastal zone (van Beusekom et al. 1999). In the Wadden Sea, 42 - 72% of the mineralization occurs in the sediments, and the organic matter has to be turned over two to three times to explain the annual primary production rates (van Beusekom et al. 1999).

As a result of its vicinity to densely populated countries and due to the large discharge water volume of rivers, the Wadden Sea is at present 5 times more eutrophic than before industrialisation, with eutrophication being most pronounced in the southern Wadden Sea (Lotze et al. 2005; van Beusekom 2005). The increased nutrient loadings lead e.g., to *Phaeocystis*-blooms, blooms of green macroalgae and the formation of "black spots" in sediments (anoxic sediments up to the surface).

In this study, two intertidal sand flats were investigated within the German Wadden Sea, the Hausstrand on Sylt, and the (sandbank) Janssand in the backbarrier region of Spiekeroog (Fig. 9). The Hausstrand is characterized by medium sands (median grain size: 380 µm) and a level intertidal zone, the steeper sloping Janssand is composed of fine sands (median grain size: 176 µm).

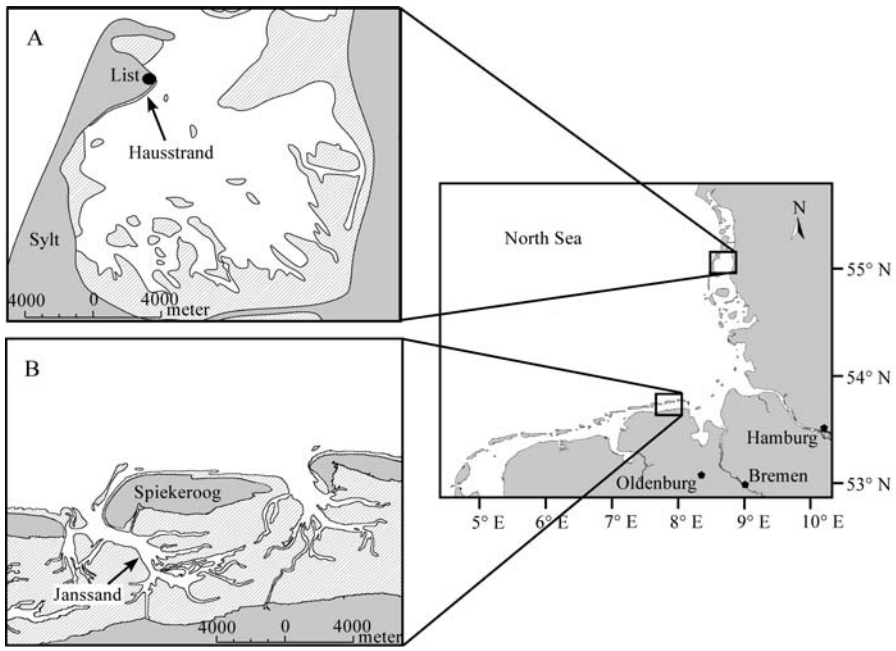


Figure 9: Study sites in the Wadden Sea (from M. Billerbeck)

Intertidal flats are highly dynamic systems with short-term and long-term changes in physical, chemical and biological properties. Over the tidal cycle, intertidal flats may be exposed to air or during inundation exposed to intense hydrodynamics. During a tidal cycle the abundance of predators, insolation, temperature and salinity may undergo extreme changes. Also seasonal changes are pronounced, with temperatures below zero in winter and temperature above 30°C in summer.

*Coral Reefs:* Warm water coral reefs are calcium carbonate structures, which mostly occur in the tropical oceans (Gattuso et al. 1998) and cover about 6 x $10^5$ $km^2$ of the global surface area (Smith 1978). These reef are restricted to shallow areas (usually less than 100 m water depth) with winter water temperatures of at least 18°C and a low water turbidity. Shallow coral reefs harbor a great diversity of organisms. They are dominated by scleractinian corals and calcareous algae that both display high rates of calcification and, thus, contribute to reef building processes.

Shallow water coral reefs are characterized by high biomass, high community gross primary production rates (300 - 7000 g C $m^{-2}$ $y^{-1}$) and similarly high respiration rates (Crossland and Barnes 1983; Kinsey 1985; Crossland et al. 1991; Gattuso et al. 1998), although they are situated in oligotrophic waters. This means that essential nutrients need to be efficiently recycled within the ecosystem. The reef metabolism is dominated by benthic processes (Gattuso et al. 1996), and benthic photosynthesis is responsible for 70 - 90% of reefal carbon fixation: The remainder is covered by calcification (Kinsey 1985) and is clearly coupled to photosynthesis. Recent work estimates the worldwide carbonate production of coral reefs to be 0.65-0.83 Gt $CaCO_3$ $y^{-1}$ (Vecsei 2004).

An important compartment for energy and matter recycling within the reef ecosystem are the coral reef sediments that often cover large areas within the reef (Boucher et al. 1998). Coral reef sediments are typically sands of biogenic origin. Coral reef sands (and also the reef framework) are highly permeable, reaching permeabilities of $10^{-9}$ $m^2$ (Enos and Sawatsky 1981; Wheatcraft and Buddemeier 1981; Rasheed et al. 2003b). In addition, wind and tide driven currents can be strong (Buddemeier and Oberdorfer 1988; Hamner and Wolanski 1988; Hearn and

Parker 1988; Tribble et al. 1992; Falter and Sansone 2000) and induce an intensive bentho-pelagic coupling between reef sands and water column in these shallow-water environments..

Past research has shown that the reef sediments can be very active, with microphytobenthos contributing significantly to reef primary production (Kinsey 1985; Boucher et al. 1998; Clavier and Garrigue 1999), and with high rates of carbon mineralization and nutrient release (Alongi et al. 1996; Rasheed et al. 2003b; Rasheed et al. 2004; Wild et al. 2004b; Wild et al. 2004c).

The investigations on coral reef sediments during this thesis were conducted at the platform reef system Heron Reef at the southern end of the Great Barrier Reef (Fig. 10). The Great Barrier Reef stretches along the North-East coast of Australia and represents, with an overall length of more than 2000 km, the world's largest coral reef.

Figure 10: Heron Reef, with Heron Island (from http://visibleearth.nasa.gov )

**Microsensors**

Microsensors were key tools in this thesis and are introduced in the following section. Microsensors allow the measurement of physical and chemical gradients with high spatial resolution in environments such as sediments and microbial mats (Kuehl and Revsbech 2001). Due to their small tip-sizes, the disturbance of samples with needle-type microsensors is negligible. Microsensors used in environmental studies can be broadly divided into three groups: 1) Electrochemical microsensors (microelectrodes) which convert a chemical into an electrical signal, 2) optical sensors (optodes) which are based on measuring optical property changes (light signals) when the analyte interacts with an indicator and 3) bio-microsensors where cultures of microorganisms or enzymes are immobilized behind a membrane and convert the analyte into a product that can be measured by an associated electrochemical sensor (Glud et al. 1999; Kuehl and Revsbech 2001). A large variety of sensors and detection principles exist. Among the analytes, the following parameters can be measured: $O_2$, $H_2$, $H_2S$, $CO_2$, $Ca^{2+}$, pH, $NO_2^-$, $NO_x$, $Fe^{2+}$, temperature, glucose, diffusivity, DOC, $CH_4$ and irradiance (for more information the reader is referred to Kuehl and Revsbech (2001).

The main sensors used in this study were needle-type microsensors (small sensor tip) for the measurement of $O_2$, pH and $Ca^{2+}$ and planar optodes for the measurement of $O_2$ in two-dimensions. Needle-type microsensors measure the analyte at single points or in one-dimensional profiles. Planar optodes allow the determination of e.g., oxygen in two-dimensions.

The most frequently used $O_2$ microsensor is the Clarke-type sensor with a guard cathode (Revsbech 1989). It consists of a gold-coated cathode and an Ag/AgCl reference that are immersed in an alkaline electrolyte solution within a glass casing behind an ion-impermeable, but gas-permeable silicone membrane (Fig. 11). The partial pressure of oxygen is measured (gas microsensor). Oxygen is reduced at the cathode by polarizing voltage and the current resulting from this reaction is read by a sensitive pico-amperemeter. The guard cathode consumes oxygen in the electrolyte and thus prevents oxygen from diffusing towards the sensor tip. Tip-sizes of the oxygen sensors can vary between 1 – 100 µm, the detection limit is around 0.1 µmol $L^{-1}$, the response time is short (< 0.5 s), the

stirring sensitivities is small (1 – 2 %) and the output signal changes linearly with changing oxygen concentrations (Kuehl and Revsbech 2001). The oxygen sensor is stable for months. The $O_2$ microsensor was used in this study for in situ oxygen distribution measurements, for the assessment of oxygen consumption rates and for the measurement of microphytobenthic photosynthesis.

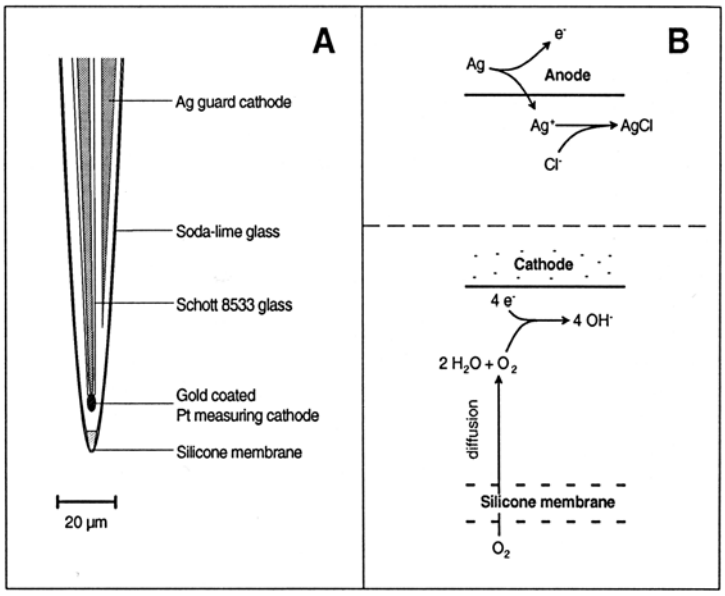


Figure 11: A) Detailed drawing of $O_2$ microsensor tip. B) Measuring principle and reactions (from Kühl and Revsbech 2001)

For the measurement of pH and $Ca^{2+}$, ion-exchange-based microsensors were used. In these types of sensors, a potential is build-up across a solid or liquid ion-exchanger membrane (LIX) that are selective for the analyte. The potential is read by a high impedance voltameter. We used microsensors with liquid ion-exchanger membrane (LIX-microsensors). The LIX is positioned in the capillary tip of the sensor, its hydrophobic nature prevent a displacement in water. pH-LIX sensors have a tip diameter between 1 – 20 µm and a detection limit between 3 – 11 pH (De Beer et al. 1997). $Ca^{2+}$-Lix sensors also have a tip sizes of 1 – 20 µm, the detection limit is < 0.1µmol $L^{-1}$ in freshwater and < 10 µmol $L^{-1}$ in seawater (Amman 1986). pH sensors were used for the pH measurements in the sediments, the $Ca^{2+}$ sensors were sued for the assessment of calcification and decalcification rates.

The $O_2$ optodes used in this study belong to the group of optical sensors that measure physicochemical variables by changes in fluorescence of an indicator dye

immobilized in the sensor matrix (Liebsch et al. 2000; Holst and Grunwald 2001). They are very stable, easy to make and do not consume oxygen, thus, they are not sensitive to stirring.

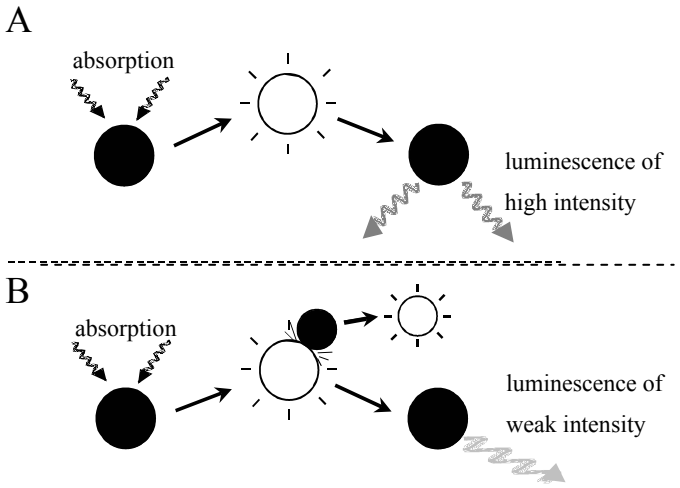


Figure 12: Reactions of the fluorophore in the absence of oxygen (A) and in the presence of oxygen (B). (A) The excited fluorophore returns to its ground state by emitting luminescence of high intensity and long lifetime. (B) The luminescence is quenched by oxygen, resulting in a weaker intensity and shorter life time (from Franke 2005).

The measuring principle of the used $O_2$ optodes is the dynamic quenching of a fluorophore (e.g., ruthenium-diimine or platinum-porphyrin complexes) by oxygen. When light is absorbed by the dye, the fluorophores are excited above their ground energy level and upon returning to this energy level they emit fluorescent light. This emission is altered by the presence of oxygen molecules. Collision of oxygen with the excited dye results in a decrease of the intensity and/or lifetime of the emitted fluorescence (Fig. 12) (Luebbers 1995). Both, the fluorescence intensity and the lifetime can be used to measure the analyte, whereby lifetime is less effected by analytical errors and other difficulties (e.g. background luminescence can be effectively suppressed (Holst and Grunwald 2001)). Lifetime is defined as the time-interval after which the luminescence intensity decreases to 1/e times the initial intensity.

In this study, planar $O_2$ optodes were used enabling the measurement of two-dimensional oxygen distribution and oxygen consumption rates. The fluorescence lifetime was evaluated with the MOLLI system (Holst and Grunwald 2001). The planar optodes are excited by LEDs and a camera system detects and

monitors the luminescence signal. For extensive description and review of $O_2$ optodes see Franke (2005).

Fiber-optic microprobes that measure an inherent light field (here fluorescence) from the tip surrounding were used to monitor the flow path of a dye in the pore spaces of the sediments. They consist of a simple optical fiber that emits light and subsequently monitors collecting the backscattered light.

*Information derived from microsensor measurements:* Microsensors are a useful tool for the measurement of microbial activity. The linear concentration gradient of a solute in the DBL can be used to calculate diffusive solute production or uptake rates in diffusion dominated sediment (Jørgensen and Revsbech 1985; Rasmussen and Jørgensen 1992; Kuehl et al. 1996) using Fick´s law (see formula 4). Conversion rates can be measured by measuring concentration changes of chemicals involved in the reactions. From oxygen profiles in the light, the net oxygen production can be evaluated by calculating downward and upward fluxes from the photosynthetic active layer. With fast $O_2$ microsensors ($t_{90} < 0.2$ s) photo-synthetic gross production can be measured by the light- dark-shift method (Revsbech and Jørgensen 1983; Glud et al. 1992). In this method, the environmental sample is illuminated until a steady state is achieved for oxygen production, diffusive oxygen fluxes and oxygen consumption. Upon darkening, the diffusive fluxes and the respiration are assumed to stay similar for the first few seconds and thus the initial oxygen concentration decrease is considered to equal the former oxygen production.

Microsensors are used to measure the in situ distribution of the analytes. The measurements of $O_2$ in sediments in the 1980s revealed that the oxic sediment layers are much narrower as assumed earlier when judged from the color of the sediment layers (Revsbech et al. 1980a; Revsbech et al. 1980b). Previously, the brown sediment layer (several millimeters deep), overlying grey (rich in $FeS_2$) and black (rich in FeS) sediment, was assumed to be oxic. Microsensors attached to electronic measuring devices such as the profiler (Fig. 8) allow the continuous monitoring of profiles over extended time periods (Glud et al. 1999; Wenzhöfer et al. 2000).

## References

Aller, R. C. 1988. Benthic fauna and biogeochemical processes in marine sediments: the role of burrow structures, p. 301-338. In T.H. Blackburn and J. Sørensen [eds.]: Nitrogen cycling in coastal marine environments, John Wiley.

---. 1994. Bioturbation and remineralization of sedimentary organic-matter - effects of redox oscillation. Chem. Geol. **114:** 331-345.

---. 2001. Transport and reactions in the bioirrgated zone, p. 269-301. *In* B. P. Boudreau andB. B. Jørgensen [eds.], The Benthic Boundary Layer. Oxford University Press.

Aller, R. C., and J. Y. Aller. 1998. The effect of biogenic irrigation intensity and solute exchange on diagenetic reaction rates in marine sediments. J. Mar. Res. **56:** 905-936.

Alongi, D. M., F. Tirendi, and A. Goldrick. 1996. Organic matter oxidation and sediment chemistry in mixed terrigenous-carbonate sands of Ningaloo Reef, Western Australia. Mar. Chem. **54:** 203-219.

Amman, D. 1986. Ion-selective microelectrodes: principles, design and applications. Springer Verlag, Heidelberg.

Andersen, F. O., and W. Helder. 1987. Comparison of oxygen microgradients, oxygen flux rates and electron-transport system activity in coastal marine-sediments. Mar. Ecol.-Prog. Ser. **37:** 259-264.

Bacon, M. P., R. A. Belastock, and M. H. Bothner. 1994. Pb-210 Balance and implications for particle-transport on the continental-shelf, US Middle Atlantic Bight. Deep-Sea Res. Part II-Top. Stud. Oceanogr. **41:** 511-535.

Bearman, G. 1989. Waves, tides and shallow-water processes. Pergamon Press, Oxford (Open Univ.).

Berg, P., H. Røy, F. Janssen, V. Meyer, B. B. Jørgensen, M. Huettel, and D. de Beer. 2003. Oxygen uptake by aquatic sediments measured with a novel non-invasive eddy-correlation technique. Mar. Ecol. Prog. Ser. **261:** 75-83.

Boucher, G., J. Clavier, and C. Garrigue. 1994. Oxygen and carbon-dioxide fluxes at the water-sediment interface of a tropical lagoon. Mar. Ecol. Prog. Ser. **107:** 185-193.

Boucher, G., J. Clavier, C. Hily, and J. P. Gattuso. 1998. Contribution of soft-bottoms to the community metabolism (primary production and calcification) of a barrier reef flat (Moorea, French Polynesia). J. Exp. Mar. Biol. Ecol. **225:** 269-283.

Boudreau, B., M. Huettel, R. Forster, A. Jahnke, J. McLachlan, J. Middelburg, P. Nielsen, F. Sansone, G. Taghon, W. Van Raaphorst, I. Webster, J. Weslawski, P. Wiberg, and B. Sundby. 2001. Permeable marine sediments: Overturning an old paradigm. EOS,TransAGU **82:** 133-136.

Boudreau, B. P. 1996. The diffusive tortuosity of fine-grained unlithified sediments. Geochim. Cosmochim. Acta **60:** 3139-3142.

Brotas, V., and M. R. Plante-Cuny. 2003. The use of HPLC pigment analysis to study microphytobenthos communities. Acta Oecol.-Int. J. Ecol. **24:** 109 -115.

Buddemeier, R., and J. Oberdorfer. 1988. Hydrogeology and hydrodynamics of coral reef pore waters. Proc. Sixth Internat. Coral Reef Symp. **2:** 485-490.

Burnett, W. C., H. Bokuniewicz, M. Huettel, W. S. Moore, and M. Taniguchi. 2003. Groundwater and pore water inputs to the coastal zone. Biogeochemistry **66:** 3-33.

Cammen, L. M. 1991. Annual bacterial production in relation to benthic microalgal production and sediment oxygen-uptake in an intertidal sandflat and an intertidal mudflat. Mar. Ecol. Prog. Ser. **71:** 13-25.

Canfield, D. E., B. B. Jørgensen, H. Fossing, R. Glud, J. Gundersen, N. B. Ramsing, B. Thamdrup, J. W. Hansen, L. P. Nielsen, and P. O. J. Hall. 1993a. Pathways of organic-carbon oxidation in three continental-margin sediments. Mar Geol **113:** 27-40.

Canfield, D. E., and R. Raiswell. 1991. Carbonate precipitation and dissolution: Its relevance to fossil preservation. Plenum Press.

Canfield, D. E., B. Thamdrup, and J. W. Hansen. 1993b. The anaerobic degradation of organic-matter in danish coastal sediments - Iron reduction, manganese reduction, and sulfate reduction. Geochim. Cosmochim. Acta **57:** 3867-3883.

Charpy-Roubaud, C., L. Charpy, and A. W. D. Larkum. 2001. Atmospheric dinitrogen fixation by benthic communities of Tikehau Lagoon (Tuamotu Archipelago, French Polynesia) and its contribution to benthic primary production. Mar Biol **139:** 991-997.

Clavier, J., and C. Garrigue. 1999. Annual sediment primary production and respiration in a large coral reef lagoon (SW New Caledonia). Mar. Ecol. Prog. Ser. **191:** 79-89.

Coleman, M. L., D. B. Hedrick, D. R. Lovley, D. C. White, and K. Pye. 1993. Reduction of Fe(III) in sediments by sulfate-reducing bacteria. Nature **361:** 436-438.

Colijn, F., and G. C. Cadee. 2003. Is phytoplankton growth in the Wadden Sea light or nitrogen limited? J. Sea Res. **49:** 83-93.

Colijn, F., and V. N. Dejonge. 1984. Primary production of microphytobenthos in the Ems-Dollard estuary. Mar. Ecol. Prog. Ser. **14:** 185-196.

Crockett, J. S., and C. A. Nittrouer. 2004. The sandy inner shelf as a repository for muddy sediment: an example from Northern California. Cont. Shelf Res. **24:** 55-73.

Crossland, C. J., and D. J. Barnes. 1983. Dissolved nutrients and organic particulates in water flowing over coral reefs at Lizard-Island. Aust. J. Mar. Freshw. Res. **34:** 835-844.

Crossland, C. J., B. G. Hatcher, and S. V. Smith. 1991. Role of coral reefs in global ocean production. Coral Reefs **10:** 55-64.

Dalsgaard, T. 2003. Benthic primary production and nutrient cycling in sediments with benthic microalgae and transient accumulation of macroalgae. Limnol. Oceanogr. **48:** 2138-2150.

D'Andrea, A. F., R. C. Aller, and G. R. Lopez. 2002. Organic matter flux and reactivity on a South Carolina sandflat: The impacts of porewater advection and macrobiological structures. Limnol. Oceanogr. **47:** 1056-1070.

D'Andrea, A. F., G. R. Lopez, and R. C. Aller. 2004. Rapid physical and biological particle mixing on an intertidal sandflat. J. Mar. Res. **62:** 67-92.

Darcy, H. 1856. Les Fontaines Publiques de la Ville de Dijon. Dalmont.

de Beer, D., A. Glud, E. Epping, and M. Kuhl. 1997. A fast-responding CO2 microelectrode for profiling sediments, microbial mats, and biofilms. Limnol. Oceanogr. **42:** 1590-1600.

de Beer, D., F. Wenzhöfer, T. G. Ferdelman, S. E. Boehme, M. Huettel, J. E. E. van Beusekom, M. E. Boettcher, N. Musat, and N. Dubillier. 2005. Transport and mineralization rates in North Sea sandy intertidal sediments, Sylt-Rømø Basin, Wadden Sea. Limnol. Oceanogr. **50:** 113-127.

de Haas, H., T. C. E. van Weering, and H. de Stieger. 2002. Organic carbon in shelf seas: sinks or sources, processes and products. Cont. Shelf Res. **22:** 691-717.

Denny, M. W. 1988. Biology and the mechanics of the wave-swept environment. Princeton University Press.

Ehrenhauss, S., and M. Huettel. 2004. Advective transport and decomposition of chain-forming planktonic diatoms in permeable sediments. J. Sea Res. **52:** 179-197.

Ehrenhauss, S., U. Witte, F. Janssen, and M. Huettel. 2004. Decomposition of diatoms and nutrient dynamics in permeable North Sea sediments. Cont. Shelf Res. **24:** 721-737.

Enos, P., and L. H. Sawatsky. 1981. Pore networks in holocene carbonate sediments. J Sediment Petrol **51:** 961-985.

Falter, J. L., and F. J. Sansone. 2000. Hydraulic control of pore water geochemistry within the oxic-suboxic zone of a permeable sediment. Limnol. Oceanogr. **45:** 550-557.

Figge, K. 1981. Sedimentverteilung in der Deutschen Bucht. Deutsches Hydrographisches Institut.

Flemming, B., and K. Ziegler. 1995. High-resolution grain size distribution patterns and textural trends in the backbarrier environment of Spiekeroog Island (Southern North Sea). Senckenbergiana maritima **26:** 1-24.

Forster, S., M. Huettel, and W. Ziebis. 1996. Impact of boundary layer flow velocity on oxygen utilisation in coastal sediments. Mar. Ecol. Prog. Ser. **143:** 173-185.

Franke, U. 2005. Applications of planar oxygen optodes in biological aquatic systems. Thesis, University of Bremen.

Froelich, P. N., G. P. Klinkhammer, M. L. Bender, N. A. Luedtke, G. R. Heath, D. Cullen, P. Dauphin, D. Hammond, B. Hartman, and V. Maynard. 1979. Early oxidation of organic-matter in pelagic sediments of the Eastern Equatorial Atlantic - Suboxic diagenesis. Geochim. Cosmochim. Acta **43:** 1075-1090.

Gattuso, J. P., M. Frankignoulle, S. V. Smith, J. R. Ware, and R. Wollast. 1996. Coral reefs and carbon dioxide. Science **271:** 1298-1298.

Gattuso, J. P., M. Frankignoulle, and R. Wollast. 1998. Carbon and carbonate metabolism in coastal aquatic ecosystems. Annu. Rev. Ecol. Syst. **29:** 405-434.

Glud, R. N., I. Klimant, G. Holst, O. Kohls, V. Meyer, M. Kuhl, and J. K. Gundersen. 1999. Adaptation, test and in situ measurements with O-2 microopt(r)odes on benthic landers. Deep-Sea Res. Part I-Oceanogr. Res. Pap. **46:** 171-183.

Glud, R. N., N. B. Ramsing, and N. P. Revsbech. 1992. Photosynthesis and photosynthesis-coupled respiration in natural biofilms quantified with oxygen microsensors. J. Phycol. **28:** 51-60.

Graf, G., and R. Rosenberg. 1997. Bioresuspension and biodeposition: A review. J. Mar. Syst. **11:** 269-278.

Grossart, H. P., T. Brinkhoff, T. Martens, C. Duerselen, G. Liebezeit, and M. Simon. 2004. Tidal dynamics of dissolved and particulate matter and bacteria in a tidal flat ecosystem in spring and fall. Limnol. Oceanogr. **49:** 2212-2222.

Hamner, W., and E. Wolanski. 1988. Hydrodynamic forcing functions and biological processes on coral reefs: a status review. Proc. Sixth Internat. Coral Reef Symp. **1:** 103-113.

Harris, C. K., and P. Wiberg. 2002. Across-shelf sediment transport: Interactions between suspended sediment and bed sediment. J. Geophys. Res.-Oceans **107**.

Harrison, W. D., D. Musgrave, and W. S. Reeburgh. 1983. A wave-induced transport process in marine-sediments. Journal of Geophysical Research-Oceans and Atmospheres **88:** 7617-7622.

Hearn, C., and I. Parker. 1988. Hydrodynamic processes on the Ningaloo Coral Reef, Western Australia. Proc. Sixth Internat. Coral Reef Symp. **2:** 497-502.

Hedges, J. I., and R. G. Keil. 1995. Sedimentary organic-matter preservation - an assessment and speculative synthesis. Mar. Chem. 49: 81-115.

Herbert, R. A. 1999. Nitrogen cycling in coastal marine ecosystems. Fems Microbiol. Rev. **23:** 563-590.

Holligan, P. M., and W. A. Reiners. 1992. Predicting the responses of the coastal zone to global change. Adv. Ecol. Res. **22:** 211-255.

Holst, G., and B. Grunwald. 2001. Luminescence lifetime imaging with transparent oxygen optodes. Sens. Actuator B-Chem. **74:** 78-90.

Huettel, M., and G. Gust. 1992a. Impact of bioroughness on interfacial solute exchange in permeable sediments. Mar. Ecol. Prog. Ser. **89:** 253-267.

---. 1992b. Solute release mechanisms from confined sediment cores in stirred benthic chambers and flume flows. Mar. Ecol. Prog. Ser. **82:** 187-197.

Huettel, M., H. Røy, E. Precht, and S. Ehrenhauss. 2003. Hydrodynamical impact on biogeochemical processes in aquatic sediments. Hydrobiologia **494:** 231-236.

Huettel, M., and A. Rusch. 2000. Transport and degradation of phytoplankton in permeable sediment. Limnol. Oceanogr. **45:** 534-549.

Huettel, M., W. Ziebis, and S. Forster. 1996. Flow-induced uptake of particulate matter in permeable sediments. Limnol. Oceanogr. **41:** 309-322.

Huettel, M., W. Ziebis, S. Forster, and G. W. Luther. 1998. Advective transport affecting metal and nutrient distributions and interfacial fluxes in permeable sediments. Geochim. Cosmochim. Acta **62:** 613-631.

Huthnance, J. M., J. D. Humphery, P. J. Knight, P. G. Chatwin, L. Thomsen, and M. White. 2002. Near-bed turbulence measurements, stress estimates and sediment mobility at the continental shelf edge. Prog. Oceanogr. **52:** 171-194.

Iversen, N., and B. B. Jørgensen. 1993. Diffusion-coefficients of sulfate and methane in marine-sediments - Influence of porosity. Geochim. Cosmochim. Acta **57:** 571-578.

Jaeger, J. M., C. A. Nittrouer, N. D. Scott, and J. D. Milliman. 1998. Sediment accumulation along a glacially impacted mountainous coastline: North-east Gulf of Alaska. Basin Res. **10:** 155-173.

Jahnke, R. A., J. R. Nelson, R. L. Marinelli, and J. E. Eckman. 2000. Benthic flux of biogenic elements on the Southeastern US continental shelf: influence of pore water advective transport and benthic microalgae. Cont. Shelf Res. **20:** 109-127.

Janssen, F., M. Huettel, and U. Witte. 2005. Pore-water advection and solute fluxes in permeable marine sediments (II): Benthic respiration at three sandy sites with different permeabilities (German Bight, North Sea). Limnol. Oceanogr. **50:** 779-792.

Johannes, R. E. 1980. The ecological significance of the submarine discharge of groundwater. Mar. Ecol. Prog. Ser. **3:** 365-373.

Johnson, H. D., and C. T. Bladwin. 1986. Shallow siliclastic seas. p. 229-282. In H.G. Reading [ed]: Sedimentary environments and Facies, Blackwell Scientific Publications.

Jørgensen, B. B. 1982. Mineralization of organic-matter in the sea bed - the role of sulfate reduction. Nature **296:** 643-645.

---. 2000. Bacteria and marine biogeochemistry. p.173-208. In H.D.Schulz and M. Zabel [eds]: Marine Geochemistry, Springer Verlag. Berlin/Heidelberg

Jørgensen, B. B., and N. P. Revsbech. 1985. Diffusive boundary-layers and the oxygen-uptake of sediments and detritus. Limnol. Oceanogr. **30:** 111-122.

King, G. M., R. G. Carlton, and T. E. Sawyer. 1990. Anaerobic metabolism and oxygen distribution in the carbonate sediments of a submarine-canyon. Mar. Ecol. Prog. Ser. **58:** 275-285.

Kinsey, D. 1985. Metabolism, calcification and carbon production, I, system level studies. Proc. **4:** 506-526.

Krantzberg, G. 1985. The influence of bioturbation on physical, chemical and biological parameters in aquatic environments - a review. Environmental Pollution Series a-Ecological and Biological **39:** 99-122.

Kristensen, E. 2000. Organic matter diagenesis at the oxic/anoxic interface in coastal marine sediments, with emphasis on the role of burrowing animals. Hydrobiologia **426:** 1-24.

Kuehl, M., R. N. Glud, H. Ploug, and N. B. Ramsing. 1996. Microenvironmental control of photosynthesis and photosynthesis-coupled respiration in an epilithic cyanobacterial biofilm. J. Phycol. **32:** 799-812.

Kuehl, M., and N. P. Revsbech. 2001. Biogeochemical microsensors for boundary layer studies. p. 180-210. In B. P. Boudreau and B.B. Jørgensen [eds]: The benthic boundary layer, Oxford University Press.

Larkum, A. W. D., I. R. Kennedy, and W. J. Muller. 1988. Nitrogen-fixation on a coral-reef. Mar. Biol. **98:** 143-155.

Liebsch, G., I. Klimant, B. Frank, G. Holst, and O. S. Wolfbeis. 2000. Luminescence lifetime imaging of oxygen, pH, and carbon dioxide distribution using optical sensors. Appl. Spectrosc. **54:** 548-559.

Llobet-Brossa, E., R. Rossello-Mora, and R. Amann. 1998. Microbial community composition of Wadden Sea sediments as revealed by fluorescence in situ hybridization. Appl. Environ. Microbiol. **64:** 2691-2696.

Logan, B. E., and D. L. Kirchman. 1991. Uptake of dissolved organics by marine-bacteria as a function of fluid motion. Mar Biol **111:** 175-181.

Lohse, L., E. H. G. Epping, W. Helder, and W. van Raaphorst. 1996. Oxygen pore water profiles in continental shelf sediments of the North Sea: Turbulent versus molecular diffusion. Mar. Ecol. Prog. Ser. **145:** 63-75.

Lohse, L., J. F. P. Malschaert, C. P. Slomp, W. Helder, and W. Van Raaphorst. 1993. Nitrogen cycling in North-Sea sediments - Interaction of denitrification and nitrification in offshore and coastal areas. Mar. Ecol.-Prog. Ser. **101:** 283-296.

Lotze, H. K., K. Reise, B. Worm, J. van Beusekom, M. Busch, A. Ehlers, D. Heinrich, R. C. Hoffmann, P. Holm, C. Jensen, O. S. Knottnerus, N. Langhanki, W. Prummel, M. Vollmer, and W. J. Wolff. 2005. Human transformations of the Wadden Sea ecosystem through time: a synthesis. Helgoland Mar. Res. **59:** 84-95.

Lovley, D. R., D. F. Dwyer, and M. J. Klug. 1982. Kinetic-analysis of competition between sulfate reducers and methanogens for hydrogen in sediments. Appl. Environ. Microbiol. **43:** 1373-1379.

Luebbers, D. W. 1995. Optical sensors for clinical monitoring. Acta Anaesthesiol. Scand. **39:** 37-54.

MacIntyre, H. L., R. J. Geider, and D. C. Miller. 1996. Microphytobenthos: The ecological role of the "secret garden" of unvegetated, shallow-water marine habitats. 1. Distribution, abundance and primary production. Estuaries **19:** 186-201.

Malan, D. E., and A. McLachlan. 1991. In situ benthic oxygen fluxes in a nearshore coastal marine system - a new approach to quantify the effect of wave action. Mar. Ecol. Prog. Ser. **73:** 69-81.

Marinelli, R. L., R. A. Jahnke, D. B. Craven, J. R. Nelson, and J. E. Eckman. 1998. Sediment nutrient dynamics on the South Atlantic Bight continental shelf. Limnol. Oceanogr. **43:** 1305-1320.

Martin, J. H., G. A. Knauer, D. M. Karl, and W. W. Broenkow. 1987. Vertex - carbon cycling in the Northeast Pacific. Deep-Sea Research Part a-Oceanographic Research Papers **34:** 267-285.

McCave, I. N. 1972. Transport and escape of fine-grained sediment from shelf areas. In D. Swift, D. Duane and O. Pilke [eds]: Shelf sediments and transport: process and pattern, Hutchinson & Ross.

McLachlan, A. 1989. Water filtration by dissipative beaches. Limnol. Oceanogr. **34:** 774-780.

McLachlan, A., and I. Turner. 1994. The interstitial environment of sandy beaches. Mar. Ecol.-Pubbl. Stn. Zool. Napoli **15:** 177-211.

Morse, J. W., J. J. Zullig, L. D. Bernstein, F. J. Millero, P. Milne, A. Mucci, and G. R. Choppin. 1985. Chemistry of calcium carbonate rich shallow-water sediments in the Bahamas. Am. J. Sci. **285:** 147-185.

Nielsen, P. 1990. Tidal dynamics of the water-table in beaches. Water Resour. Res. **26:** 2127-2134.

Nittrouer, C. A., and L. D. Wright. 1994. Transport of particles across continental shelves. Rev. Geophys. **32:** 85-113.

Oberdorfer, J. A., and R. W. Buddemeier. 1986. Coral-reef hydrology - field studies of water-movement within a barrier-reef. Coral Reefs **5:** 7-12.

Parnell, K. E. 1986. Water-movement within a fringing-reef flat, Orpheus-Island, North-Queensland, Australia. Coral Reefs **5:** 1-6.

Precht, E., U. Franke, L. Polerecky, and M. Huettel. 2004. Oxygen dynamics in permeable sediments with wave-driven pore water exchange. Limnol. Oceanogr. **49:** 693-705.

Precht, E., and M. Huettel. 2003. Advective pore-water exchange driven by surface gravity waves and its ecological implications. Limnol. Oceanogr. **48:** 1674-1684.

---. 2004. Rapid wave-driven advective pore water exchange in a permeable coastal sediment. J. Sea Res. **51:** 93-107.

Purdy, K. J., D. B. Nedwell, and T. M. Embley. 2003. Analysis of the sulfate-reducing bacterial and methanogenic archaeal populations in contrasting Antarctic sediments. Appl. Environ. Microbiol. **69:** 3181-3191.

Rasheed, M., M. I. Badran, and M. Huettel. 2003a. Influence of sediment permeability and mineral composition on organic matter degradation in three sediments from the Gulf of Aqaba, Red Sea. Est. Coast. Shelf. Sci. **57:** 369-384.

---. 2003b. Particulate matter filtration and seasonal nutrient dynamics in permeable carbonate and silicate sands of the Gulf of Aqaba, Red Sea. Coral Reefs **22:** 167-177.

Rasheed, M., C. Wild, U. Franke, and M. Huettel. 2004. Benthic photosynthesis and oxygen consumption in permeable carbonate sediments at Heron Island, Great Barrier Reef, Australia. Est Coast Shelf Sci **59:** 139-150.

Rasmussen, H., and B. B. Jørgensen. 1992. Microelectrode studies of seasonal oxygen-uptake in a coastal sediment - Role of molecular-diffusion. Mar. Ecol.-Prog. Ser. **81:** 289-303.

Reeburgh, W. S. 1983. Rates of biogeochemical processes in anoxic sediments. Annu. Rev. Earth Planet. Sci. **11:** 269-298.

Reimers, C. E., H. A. Stecher, G. L. Taghon, C. M. Fuller, M. Huettel, A. Rusch, N. Ryckelynck, and C. Wild. 2004. In situ measurements of advective solute transport in permeable shelf sands. Cont. Shelf Res. 24: 183-201.

Revsbech, N. P. 1989. An oxygen microsensor with a guard cathode. Limnol. Oceanogr. **34:** 474-478.

Revsbech, N. P., and B. B. Jørgensen. 1983. Photosynthesis of benthic microflora measured with high spatial-resolution by the oxygen microprofile method - capabilities and limitations of the method. Limnol. Oceanogr. **28:** 749-756.

Revsbech, N. P., B. B. Jørgensen, and T. H. Blackburn. 1980a. Oxygen in the sea bottom measured with a microelectrode. Science **207:** 1355-1356.

Revsbech, N. P., J. Sørensen, T. H. Blackburn, and J. P. Lomholt. 1980b. Distribution of oxygen in marine-sediments measured with microelectrodes. Limnol. Oceanogr. **25:** 403-411.

Riedl, R. J., and R. Machan. 1972. Hydrodynamic patterns in lotic intertidal sands and their bioclimatological implications. Mar. Biol. **13:** 179-&.

Riedl, R. J., R. Machan, and N. Huang. 1972. Subtidal pump - mechanism of interstitial water exchange by wave action. Mar. Biol. **13:** 210-&.

Rocha, C. 1998. Rhythmic ammonium regeneration and flushing in intertidal sediments of the Sado estuary. Limnol. Oceanogr. **43:** 823-831.

Rowe, G. T., R. Theroux, W. Phoel, H. Quinby, R. Wilke, D. Koschoreck, T. E. Whitledge, P. G. Falowski, and C. Fray. 1988. Benthic carbon budgets for the continental-shelf south of New-England. Cont. Shelf Res. **8:** 511-527.

Rusch, A., S. Forster, and M. Huettel. 2001. Bacteria, diatoms and detritus in an intertidal sandflat subject to advective transport across the water-sediment interface. Biogeochemistry **55:** 1-27.

Rusch, A., and M. Huettel. 2000. Advective particle transport into permeable sediments - evidence from experiments in an intertidal sandflat. Limnol. Oceanogr. **45:** 525-533.

Sanders, D. 2003. Syndepositional dissolution of calcium carbonate in neritic carbonate environments: geological recognition, processes, potential significance. J. Afr. Earth Sci. **36:** 99-134.

Shum, K. T. 1992. Wave-induced advective transport below a rippled water-sediment interface. J. Geophys. Res.-Oceans **97:** 789-808.

---. 1993. The effects of wave-induced pore-water circulation on the transport of reactive solutes below a rippled sediment bed. J. Geophys. Res.-Oceans **98:** 10289-10301.

Shum, K. T., and B. Sundby. 1996. Organic matter processing in continental shelf sediments - The subtidal pump revisited. Mar. Chem. **53:** 81-87.

Simmons, G. M. 1992. Importance of submarine groundwater discharge (SGDW) and seawater cycling to material flux across sediment water interfaces in marine environments. Mar. Ecol. Prog. Ser. **84:** 173-184.

Smith, S. V. 1978. Coral-reef area and contributions of reefs to processes and resources of worlds oceans. Nature **273:** 225-226.

Thibodeaux, L. J., and J. D. Boyle. 1987. Bedform-generated convective-transport in bottom sediment. Nature **325:** 341-343.

Tribble, G. W. 1993. Organic-matter oxidation and aragonite diagenesis in a coral-reef. J. Sediment Petrol. **63:** 523-527.

Tribble, G. W., F. J. Sansone, R. W. Buddemeier, and Y. H. Li. 1992. Hydraulic exchange between a coral-reef and surface sea-water. Geol. Soc. Am. Bull. **104:** 1280-1291.

Turner, I. L., and G. Masselink. 1998. Swash infiltration-exfiltration and sediment transport. J. Geophys. Res.-Oceans **103:** 30813-30824.

Turner, I. L., and P. Nielsen. 1997. Rapid water table fluctuations within the beach face: Implications for swash zone sediment mobility? Coast. Eng. **32:** 45-59.

Ullman, W. J., and R. C. Aller. 1982. Diffusion-coefficients in nearshore marine-sediments. Limnol. Oceanogr. **27:** 552-556.

van Beusekom, J. E. E. 2005. A historic perspective on Wadden Sea eutrophication. Helgoland Mar. Res. **59:** 45-54.

van Beusekom, J. E. E., U. H. Brockmann, K. J. Hesse, W. Hickel, K. Poremba, and U. Tillmann. 1999. The importance of sediments in the transformation and turnover of nutrients and organic matter in the Wadden Sea and German Bight. Deutsche Hydrographische Zeitschrift **51:** 245-266.

van Loosdrecht, M. C. M., J. Lyklema, W. Norde, and A. J. B. Zehnder. 1990. Influence of interfaces on microbial activity. Microbiol. Rev. **54:** 75-87.

Vanderloeff, M. M. R. 1981. Wave effects on sediment water exchange in a submerged sand bed. Neth. J. Sea Res. **15:** 100-112.

Vecsei, A. 2004. A new estimate of global reefal carbonate production including the fore-reefs. Glob. Planet. Change **43:** 1-18.

Visscher, P. T., R. P. Reid, B. M. Bebout, S. E. Hoeft, I. G. MacIntyre, and J. A. Thompson. 1998. Formation of lithified micritic laminae in modern marine stromatolites (Bahamas): The role of sulfur cycling. American Mineralogist **83:** 1482-1493.

Walsh, J. J. 1991. Importance of continental margins in the marine biogeochemical cycling of carbon and nitrogen. Nature **350:** 53-55.

Walsh, J. J., G. T. Rowe, R. L. Iverson, and C. P. McRoy. 1981. Biological export of shelf carbon is a sink of the global CO2 cycle. Nature **291:** 196-201.

Webb, J. E., and J. Theodor. 1968. Irrigation of submerged marine sands through wave action. Nature **220:** 682-683.

Webb, J. E., and J. L. Theodor. 1972. Wave-induced circulation in submerged sands. J. Mar. Biol. Assoc. U.K. **52:** 903-&.

Webster, I. T., S. J. Norquay, F. C. Ross, and R. A. Wooding. 1996. Solute exchange by convection within estuarine sediments. Est. Coast. Shelf Sci. **42:** 171-183.

Webster, I. T., and J. H. Taylor. 1992. Rotational dispersion in porous-media due to fluctuating flows. Water Resour. Res. **28:** 109-119.

Wenzhöfer, F., and R. N. Glud. 2004. Small-scale spatial and temporal variability in coastal benthic O-2 dynamics: Effects of fauna activity. Limnol. Oceanogr. **49:** 1471-1481.

Wenzhöfer, F., O. Holby, R. N. Glud, H. K. Nielsen, and J. K. Gundersen. 2000. In situ microsensor studies of a shallow water hydrothermal vent at Milos, Greece. Mar. Chem. **69:** 43-54.

Wheatcraft, S. W., and R. W. Buddemeier. 1981. Atoll-island hydrology. Ground Water **19:** 311-320.

Widdel, F., and N. Pfennig. 1982. Studies on dissimilatory sulfate-reducing bacteria that decompose fatty-acids. 2. Incomplete oxidation of propionate by Desulfobulbus-Propionicus Gen-Nov, Sp-Nov. Arch. Microbiol. **131:** 360-365.

Wild, C., M. Huettel, A. Klueter, S. G. Kremb, M. Y. M. Rasheed, and B. B. Jørgensen. 2004a. Coral mucus functions as an energy carrier and particle trap in the reef ecosystem. Nature **428:** 66-70.

Wild, C., M. Rasheed, U. Werner, U. Franke, R. Johnstone, and M. Huettel. 2004b. Degradation and mineralization of coral mucus in reef environments. Mar. Ecol. Prog. Ser. **267:** 159-171.

Wild, C., R. Tollrian, and M. Huettel. 2004c. Rapid recycling of coral mass-spawning products in permeable reef sediments. Mar. Ecol. Prog. Ser. **271:** 159-166.

Winfrey, M. R., and D. M. Ward. 1983. Substrates for sulfate reduction and methane production in intertidal sediments. Appl. Environ. Microbiol. **45:** 193-199.

Wollast, R. 1991. The coastal organic carbon cycle: fluxes, sources, and sinks. pp. 365-382. In: M. R.F.C. Mantoura, J.M. Martin and R. Wollast [eds].Ocean margin processes in global change (Ed. by),. John Wiley & Sons, London. John Wiley & Sons.

Zeebe, R. E., and D. A. Gladrow. 2005. CO2 in seawater: equilibrium, kinetics, isotopes. **65**, pp. 346. Elsevier Oceanography Series. Amsterdam.

Ziebis, W., S. Forster, M. Huettel, and B. B. Jørgensen. 1996a. Complex burrows of the mud shrimp *Callianassa truncata* and their geochemical impact in the sea bed. Nature **383:** 457-457.

Ziebis, W., M. Huettel, and S. Forster. 1996b. Impact of biogenic sediment topography on oxygen fluxes in permeable seabeds. Mar. Ecol. Prog. Ser. **140:** 227-237.

## Overview over enclosed manuscripts

The thesis comprises five manuscripts, presented here as chapters.

**Chapter 2: High spatial resolution measurement of oxygen consumption rates in permeable sediments**

by Lubos Polerecky, Ulrich Franke, Ursula Werner, Björn Grunwald and Dirk de Beer

The concept was developed by D. de B., U. F., L. P. with contribution of U. W.. L. P., U. F. and U. W. conducted the experiments and evaluated the data. L. P. and U. F. and wrote the manuscript with editorial help and input of U. W. and D. de B..

This manuscript is published in Limnology and Oceanography: Methods 

**Chapter 3: Spatial and temporal patterns of mineralization rates and oxygen distribution in a permeable intertidal sand flat (Sylt, Germany)**

by Ursula Werner, Markus Billerbeck, Lubos Polerecky, Ulrich Franke, Markus Huettel, Justus van Beusekom and Dirk de Beer

The concept of the study was developed by U. W., M. B. and D. de B..

U. W. M.B. L.P. and U. F. carried out the experiments. U.W. measured and evaluated all data except the following: M. B. and M. H. initiated the study on pore- and bottom water flow velocity measurements, M. B. carried out the measurements, and evaluated the data. L. P. and U. F. measured the oxygen consumption rates with planar optodes. J. v. B. provided the water column chl-*a* values.

U. W. wrote the manuscript with editorial help of all co-authors.

This manuscript has been submitted to Limnology and Oceanography.

**Chapter 4: Surficial and deep pore water circulation governs spatial and temporal scales of nutrient recycling in intertidal sand flat sediment**

by Markus Billerbeck, Ursula Werner, Lubos Polerecky, Eva Walpersdorf , Dirk de Beer, Markus Huettel

The study was initiated by M. B., U. W., M. H., and D. de B..

Experiments were carried out by M. B., U. W., E. W. and L. P.. The data were analyzed by M.B. U. W. measured and evaluated the microbial rates in the surface layer, with contribution of L.P.. The oxygen penetration depths were evaluated by E.W..

M. B. wrote the manuscript with editorial help of all co-authors.

This manuscript has been submitted to Marine Ecology Progress Series.

**Chapter 5: Spatial patterns of aerobic and anaerobic mineralization rates and oxygen penetration dynamics in coral reef sediments (Heron Island, Australia)**

by Ursula Werner, Paul Bird, Christian Wild, Timothy Ferdelman, Lubos Polerecky, Gabriele Eikert, Ron Jonstone, Ove Hoegh-Guldberg, and Dirk de Beer

The concept of the study was developed by U. W. and D. de B.. U. W. measured and evaluated the microbial rates and evaluated the oxygen profile data. The in situ oxygen measurements were performed by P. B,, D. de. B., G. E. and U. W.. L. P. designed a computer program that simplified the evaluation of large profile data sets.

U. Werner wrote the manuscript with editorial help of all co-authors.

This manuscript was submitted to Marine Ecology Progress Series.

**Chapter 6: Photosynthesis in coral reef sediments (Heron Reef, Australia)**

by Ursula Werner, Anna Blazejak, Paul Bird, Gabriele Eickert and Dirk de Beer

D. de B. developed the concept, with contribution of U. W.. Experiments were carried out by D. de B., U. W., A. B., G. E. and P. B.. U. W. evaluated all data, except the following: The cyanobacterial 16s DNA sequences were provided by A. B., P. B. measured the $^{14}C$ measurements. U. W. wrote the manuscript with editorial help by D. de Beer and A. Blazejak.

This manuscript is in preparation for submission.

# High spatial resolution measurement of oxygen consumption rates in permeable sediments

Lubos Polerecky, Ulrich Franke, Ursula Werner, Björn Grunwald
and Dirk de Beer

published in Limnology and Oceanography: Methods
vol. 3, 2005, p. 75-85

**Abstract**

A method is presented for the measurement of depth profiles of volumetric oxygen consumption rates in permeable sediments with high spatial resolution. When combined with in situ oxygen microprofiles measured by microsensors, areal rates of aerobic respiration in sediments can be calculated. The method is useful for characterizing sediments exposed to highly dynamic advective water exchange, such as intertidal sandy sediments. The method is based on percolating the sediment in a sampling core with aerated water and monitoring oxygen in the sediment using either an oxygen microelectrode or a planar oxygen optode. The oxygen consumption rates are determined using three approaches: (1) as the initial rate of oxygen decrease measured at discrete points after the percolation is stopped, (2) from oxygen microprofiles measured sequentially after the percolation is stopped, (3) as a derivative of steady-state oxygen microprofiles measured during a constant percolation of the sediment. The spatial resolution of a typical 3–4 cm profile within a measurement time of 1–2 h is better with planar optodes (≈0.3 mm) then with microelectrodes (2–5 mm), whereas the precision of oxygen consumption rate measurements at individual points is similar (0.1–0.5 μmol $L^{-1}$ $min^{-1}$) for both sensing methods. The method is consistent with the established methods (interfacial gradients combined with Fick's law of diffusion, benthic-chambers), when tested on the same sediment sample under identical, diffusion-controlled conditions.

Keywords: oxygen consumption rate, permeable sediment, advection, planar optode

## Introduction

Aerobic respiration plays an important role in the degradation of carbon and is typically estimated to account for 25–50 % of carbon mineralisation in coastal sediments. Two established methods have been used for the determination of areal oxygen consumption rates (OCR) in sediments, namely the diffusive oxygen uptake and the benthic-chamber total oxygen uptake methods. The first method, which will be referred to as the flux method, exploits the possibility provided by oxygen microelectrodes to measure diffusive oxygen microprofiles across the sediment-water interface (e.g., Revsbech et al. 1980; Glud et al. 1994). Using Fick's law of diffusion and a measured oxygen microprofile, one can calculate an areal diffusive oxygen uptake rate. However, to obtain an estimation of the possible lateral heterogeneity of areal rates, it is necessary to measure multiple microprofiles, which can be time consuming and requires constant conditions of the system during the measurements. The second method uses a sealed benthic chamber positioned at the surface of the sediment, enclosing a known area of the sediment surface and a known volume of the bottom water (e.g., Pamatmat 1971; Smith 1978; Glud et al. 1994). The areal OCR is evaluated from the temporal decrease of oxygen content in the overlying water in the chamber, which is determined either continuously by, e.g., an oxygen electrode or an oxygen microoptode present in the chamber (Glud et al. 1994; Tengberg et al. 1995; Glud et al. 1996) or by sampling the water from the chamber and analysing its oxygen content using the Winkler titration technique.

A known problem associated with the flux method is that the obtained areal OCR values can often underestimate the true uptake rates by not including the bio-irrigation activity of macrofauna living in the sediment (for citations, see Viollier et al. 2003). This problem is overcome by the benthic-chamber technique, where the measured decrease of oxygen reflects the respiratory activity of all organisms living in the sediment, including bio-irrigating macrofauna. However, the use of a benthic chamber may significantly alter the hydrodynamic conditions to which the measured sediment is exposed. The diffusive uptake of oxygen by the sediment depends considerably on the thickness of the diffusive boundary layer (DBL), which depends strongly on hydrodynamic conditions above the sediment surface.

The water inside the chamber is therefore stirred so that the hydrodynamic conditions in the chamber resemble the natural situation as closely as possible.

Advection can be a highly effective transport process across the sediment-water interface (Huettel and Gust 1992; Huettel et al. 1996; Precht and Huettel 2003; Precht et al. 2004), particularly in permeable sediments, which are common in coastal environments (Emery 1968; de Haas et al. 2002). Due to tidal pumping, waves or the interaction of the water flow with the surface topography (e.g., ripples), the sediments are flushed with oxygen-rich water, thus significantly enhancing rates of carbon mineralisation due to aerobic respiration. In advection-driven systems, the state of oxygenation of the sediment is often very dynamic, making the flux method, based on the measurement of steady-state diffusive microprofiles, unsuitable. Efforts have been made to mimic advective water exchange through the sediment-water interface inside benthic chambers. Cylindrical benthic chambers with stirring-induced radial pressure gradients, as a substitute for horizontal pressure gradients, served as model systems (Glud et al. 1996). Chambers with flexible walls were deployed to allow pressure variations driven by waves to propagate into the chambers (Malan and McLachlan 1991). However, these modifications cannot always mimic the highly dynamic conditions in the systems where advection is the dominant process of oxygen transport, thus limiting the use of benthic chambers under such circumstances.

Recently, an adaptation of eddy correlation to mass flow in aquatic systems was reported (Berg et al. 2003). The method is non-invasive and independent of the transfer mechanism of solutes through the sediment-water interface, which makes it suitable for the study of advective systems. Eddy correlation measures area-integrated fluxes of solutes such as oxygen. The footprint of the method is several square meters, which makes it an attractive tool for the assessment of total solute exchange. The measurement, however, cannot provide the functional information nor the small scale variability of the processes governing the solute uptake.

The dynamics of oxygen supply in advection-driven systems can be assessed by in-situ microprofiling using microelectrodes or planar optodes attached to autonomous profilers (Glud et al. 1994; Glud et al. 1999a; Glud et al. 2001; Wenzhöfer and Glud 2002). The variability of oxygen penetration can be

determined with high temporal (ranging from a couple of seconds with an optode-based to 10–30 min with a microelectrode-based in situ profiler) and spatial (in the sub-millimeter range) resolutions. To estimate the rate of aerobic degradation of organic matter in such sediments, a method is needed for the determination of a depth profile of volumetric OCR with a comparably high spatial resolution. Once a depth profile of volumetric OCR is known, it can be integrated over the depth of oxygen penetration to obtain areal oxygen uptake rates of the sediment. Such a method was recently introduced by de Beer et al. (2005). It is based on percolating the sediment in a sample core with air saturated water and observing the decrease of oxygen in the sediment after the percolation is stopped.

In this article four variations of the basic method introduced by de Beer et al. (2005) are described in detail. The first exploits alternating between the on and off periods of water flow through a sediment column and monitoring with a microelectrode the decrease of oxygen at distinct locations. The second procedure employs oxygen microprofiles measured repeatedly during a single flow-off period. In the third variation, planar oxygen optodes are used to monitor oxygen dynamics in the sediment, allowing a time-efficient determination of a two-dimensional map of OCR with a sub-millimeter spatial resolution. The fourth approach is based on the measurement of steady-state $O_2$ microprofiles during steady percolation of the sediment. Each of the method variations was tried using cores of permeable sandy sediment and compared with the flux and benthic-chamber methods under rigorously controlled conditions. Furthermore, the applicability and limitations of the method are critically assessed and discussed.

## Materials and Procedures

*Materials*: The method was applied to permeable sandy sediments collected from an intertidal sandflat in the Wadden Sea (Janssand, near Neuharlingersiel, Germany). The sediment was collected from areas where flushing with oxygen-rich water was, due to waves and tidal pumping, intense and dynamic (the field data obtained by an autonomous microsensor profiler will be published elsewhere). The porosity of the sediment was $\phi$=0.45, and the measurements were conducted using

sea water (salinity 30) from the study site that was saturated with air at a temperature of 12° C (oxygen concentration 280 µmol $L^{-1}$).

The flow-through method is assembled as schematically shown in Fig. 1. A core with the sediment sample collected from an area of investigation is first fixed onto a stand so as to allow a flow of water through the sediment in the downward direction. Two types of sediment cores were used for the demonstration of the method reported here: a cylindrical plexiglass core (inner diameter 36 mm, height 200 mm, wall thickness 3 mm) and a rectangular stainless steel core (inner dimensions 70×75 mm, height 250 mm, wall thickness 2 mm). The plexiglass core was equipped with a rubber stopper into which a valve was incorporated. The removable bottom of the steel core, also equipped with a valve, contained a depression (3mm wide, 1mm deep) with the dimensions fitting the dimensions of the core. The depression was filled with silicone which enabled water-tight enclosure immediately after the collection of the sediment sample.

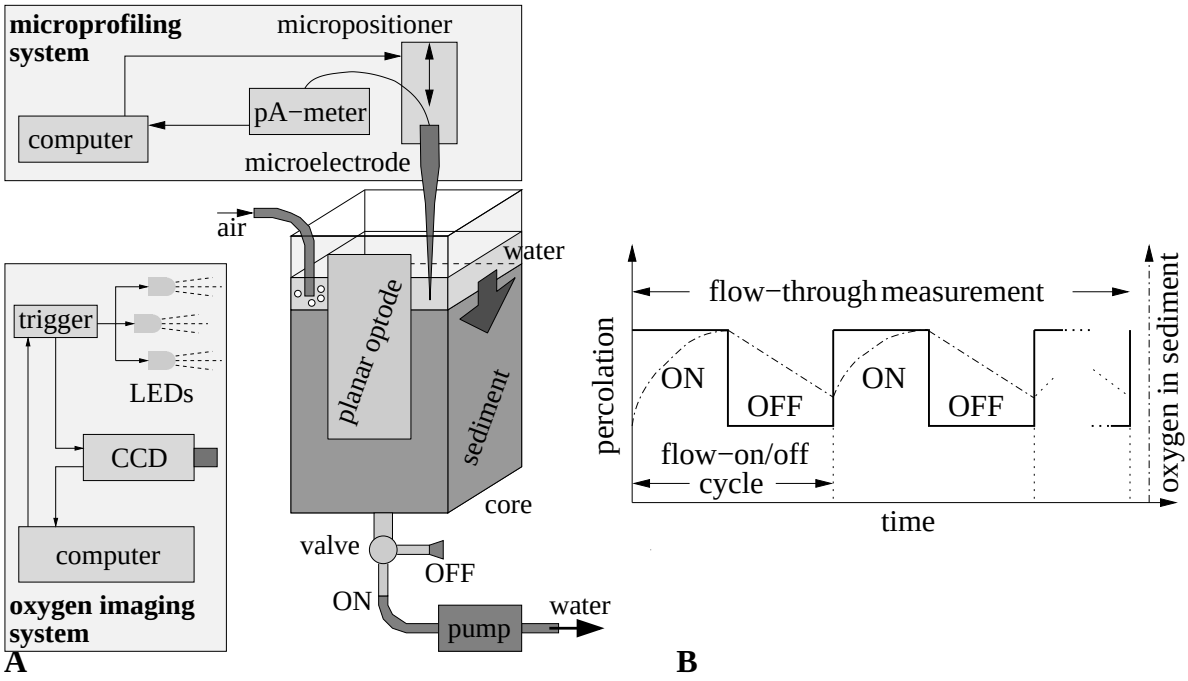


**Figure 1:** Schematic diagram of the (A) experimental configuration and (B) timing protocol of the flow-through method.

One side of the steel core contained a polycarbonate window (dimensions 50×150×4 mm) glued to the steel by silicone. A semi-transparent planar oxygen optode was glued onto the polycarbonate plate by silicone grease (Elastosil, E4, Wacker) and the firm and water-resistant attachment was reinforced with tape at the foil edges. The foil was inside the core, enabling the measurement of oxygen in the water and sediment in direct contact with the wall. Details of the employed planar optode are given elsewhere (Precht et al. 2004).

The optode measurements were carried out using the MOLLI system (Holst et al. 1998; Holst and Grunwald 2001). The system consisted of a fast gateable CCD camera (SensiCam; PCO, Kelheim, Germany), a self-made triggering device, an array of blue LEDs (LXHL-LB5C, $\lambda_{max}$ = 470 nm; Lumileds Lighting, San Jose, CA, USA) with a power supply and a red filter (Amber red; Lee Filters, Hampshire, UK). The measuring software enabled computer-controlled acquisition of images with high spatial resolution and desired timing protocol. Oxygen images were calculated using the rapid lifetime determination method in combination with Stern-Volmer equation describing lifetime quenching by oxygen (Holst et al. 1998).

High spatial resolution oxygen microprofiles were measured with an oxygen microelectrode (Revsbech 1989), which was attached to a micromanipulator placed above the core. The micromanipulator was fixed onto a motorized stage (VT-80; Micos, Eschbach, Germany), enabling reproducible positioning of the sensor tip with 1 μm precision. The microelectrode was connected to a high-precision picoammeter, and the meter output was collected by a data-acquisition card (AI-16XE-50, data box CB68-LP; National Instruments, Austin, TX, USA). The microprofiling was facilitated by a computer program.

During the measurements, a constant water level above the sediment surface was maintained by a pump regulated by a float lever connected to an electrical switch. The overlying water was kept air-saturated by continuous bubbling with air.

When the permeability of the studied sediment permitted the flow of water solely due to gravity, a valve was used to regulate the speed of water percolation. When the sediment was less permeable, the valve was opened fully and a pump was used to suck the water through the sediment.

*Basic theory:* Each measurement of OCR consisted of two stages. In the first stage, referred to as the "flow-on" period, the sediment was percolated with air-saturated water. Subsequently, the percolation was stopped (this period is referred to as the "flow-off" period) and the decrease of oxygen in the sediment was recorded (Fig. 1B).

According to the diffusion equation, the rate of decrease of oxygen in the sediment during the flow-off period is determined by (i) the local oxygen consumption rate, denoted as $R$, and (ii) the local concentration variations, mathematically expressed by the diffusion term $D_s \Delta c$, $\Delta$ denoting the Laplacian operator and $D_s$ being the diffusion coefficient of oxygen in the sediment (Crank 1975). The percolation speed and the duration of the flow-on period of the measurement are selected so that a steady and approximately homogeneous distribution of oxygen is reached in the sediment. This is an important experimental condition, as it guarantees that the diffusive term $D_s \Delta c$ is zero or negligible in comparison with the local consumption rate $R$ at the time when the flow-off period starts. If $R$ is distributed inhomogeneously, local concentration gradients will develop, leading to the measured decrease of oxygen being influenced by the diffusion. Therefore, the local OCR was evaluated as the initial slope of the measured decrease of oxygen concentration.

An alternative approach for determining the depth profile of OCR is based on the theoretical description of the oxygen transport in permeable sediments driven mainly by advection. Under steady flow during the flow-on period, oxygen dissolved in the percolating water is respired on the way through the sediment. In a region of thickness $\Delta z$ located at depth $z$ of the sediment, the balance of the dissolved oxygen concentration, $c$, can be written as

$$v_f c(z + \Delta z) - v_f c(z) = -\phi A \Delta z R(z) \qquad (1)$$

where $v_f$ is the flow rate in $m^3\ s^{-1}$, $R(z)$ is the local OCR[1] in $mol\ m^{-3}\ s^{-1}$, $\phi$ is the porosity and $A$ is the area of the horizontal cross-section in $m^2$. This equation formulates that the amount of oxygen being transported by water flow at depth

[1]Note that $R>0$ refers to oxygen consumption, while $R<0$ would represent oxygen production.

$z+\Delta z$ is reduced in comparison to that transported at depth $z$ by an amount consumed in the volume $\Delta V=\phi A\Delta z$ with the consumption rate $R(z)$, which is assumed to be constant in the depth interval between $z$ and $z+\Delta z$.

Considering that the depth difference, $\Delta z$, is infinitesimal and $v_f$ is constant with depth, equation (1) can be rewritten in the form of a differential equation

$$-\frac{v_f}{\phi A}\frac{\partial c(z)}{\partial z}=R(z) \qquad (2)$$

which is a one-dimensional equation describing the variation of an oxygen concentration profile in the sediment in a stationary situation, i.e., $\partial c(z)/\partial t=0$, where constant advection is the dominant transport mechanism, i.e., $D_s\partial c/\partial z << v_f c(z)/A$. From this equation it follows that the depth profile of OCR can be determined from the derivative of a stationary oxygen profile during the flow-on period.

*Measurement procedure*: The measurement of the OCR profile was realised by four different approaches.

(a) *$O_2(t)$ measured at discrete depths by microelectrode* — An oxygen microelectrode was positioned at a specific depth in the sediment and the decrease of oxygen during the flow-off period was recorded. The duration of this period depended on the local oxygen consumption activity of the sediment, and was dynamically selected so that the observed decrease of oxygen was sufficient for precise determination of the slope (typically a couple of minutes). The local OCR was determined as an initial slope of the observed oxygen decrease, obtained by regression analysis. The microelectrode was then repositioned and the procedure was repeated until a complete OCR profile was measured.

(b) *Continuous $O_2$ profiling by microelectrode* — Oxygen microprofiles were measured continuously by a microelectrode during the flow-off period (Epping et al. 1999). The OCR profile was determined by subtracting oxygen concentrations measured at different times at individual depths and dividing each value of $\Delta c(z)$ by the time interval between the subsequent oxygen readings. This subtraction was carried out only for nonzero oxygen readings.

(c) *Continuous $O_2$ imaging by planar optode* — Continuous oxygen imaging was facilitated by the MOLLI system. During the flow-off period, oxygen images were recorded until a significant decrease of oxygen was observed in each pixel (typically for a couple of minutes up to an hour, if the consumption was very slow). The local OCR was determined by evaluating the initial slope of the oxygen decrease in each pixel, resulting in a two-dimensional (2D) map of OCR (see below).

(d) *$O_2$ profiling by microelectrode during steady-state flow-on period* — Oxygen microprofiles were measured during the flow-on period at different lateral positions. The depth profile of OCR was calculated from the steady state oxygen profiles using Eq. (2) and the known values of the flow speed, porosity and the cross-section of the sediment core.

Oxygen images were usually superposed with noise, which, depending on the optodes used, was up to ±5 % of air saturation. The noise originated from the acquisition of fluorescence images by the CCD camera used and the way the oxygen images were calculated from the raw data (Holst and Grunwald 2001). Such noise levels introduced a complication when determining the initial slope of the oxygen decrease. In particular, when the oxygen images were recorded over sufficient time to ensure that the decrease in oxygen was greater than the noise level in all pixels, the observed oxygen dynamics could be already influenced by the diffusion in some pixels while it was still unaltered in others. This was manifested by the increase or decrease of the observed slope of the oxygen signal in the 'diffusion-affected' pixels (depending on whether the pixel is surrounded by a region of a higher or lower consumption activity, respectively), while the linear decrease of oxygen remained unaltered in the 'diffusion-unaffected' pixels.

To distinguish between these types of behaviour with a statistical measure of significance, the following strategy was implemented in the pixelwise determination of the initial slope. The time evolution of oxygen in a pixel *i* of the image, denoted as $O_2(i;t)$, was fitted with polynomials between the 0th and 4th orders, i.e., $O_2(i;t) \doteq P_0(i;t)$, or $O_2(i;t) \doteq P_1(i;t)$, …, or $O_2(i;t) \doteq P_4(i;t)$, where $P_k(t)=a_0+a_1t+\cdots+a_kt^k$ and each coefficient $a_k \equiv a_k(i)$ is a function of the pixel

position. The parameters of the fitting polynomial were obtained by the procedure of minimising the sum of residues (Kleinbaum and Kupper 1978), i.e., by minimising the function $\chi_k^2(i) = \Sigma_{n=1}^{N}[O_2(i;t_n) - P_k(i;t_n)]^2$, $N$ being the number of oxygen images considered in the fitting procedure.

The higher the order of the fitting polynomial, the better the quality of the fit, i.e., $\chi_0^2 \geq \chi_1^2 \geq ... \geq \chi_4^2$. However, even though the fit with a higher order polynomial is better than that with the lower order polynomial, it may not be significantly better. This consideration of a significant improvement of the fit was used to decide by which polynomial the observed evolution $O_2(i;t)$ was eventually fitted. The order of the fitting polynomial was selected as the maximum order $K$, such that the fit by a polynomial of any higher order, i.e., $P_{K+1},...,P_{k=4}$, was not significantly better than the fit by the polynomial $P_K$. The significant improvement was determined by a statistical hypothesis testing described in textbooks (Sokal and Rohlf 1995), using the statistical significance level of 0.95. The OCR in the pixel $i$ was then taken as the initial slope of the fitting polynomial (we refer to it as the most suitable polynomial), i.e., equal to the coefficient $a_1(i)$ when $K \geq 1$ or to zero when $K$=0. This procedure was implemented in a program written in Matlab, enabling the calculation of an OCR image within seconds.

**Assessment**

*$O_2$(t) measured at discrete depths by microelectrode*: The speed of the air-saturated water flow through the sediment was adjusted by the valve to $v_f$=33 cm$^3$ min$^{-1}$ and the sediment was percolated for 10 min. The flow-off periods were between 4 and 11 minutes long and the corresponding time evolutions of oxygen were recorded at six depths between 5 and 30 mm (Fig. 2A).

The linear decrease of oxygen at each measured depth suggested that the measurements were not influenced by diffusion during the measuring time. The values of OCR, determined from the slope of $O_2(i;t)$ and shown in Fig. 2B, were expressed per unit of the sediment volume.

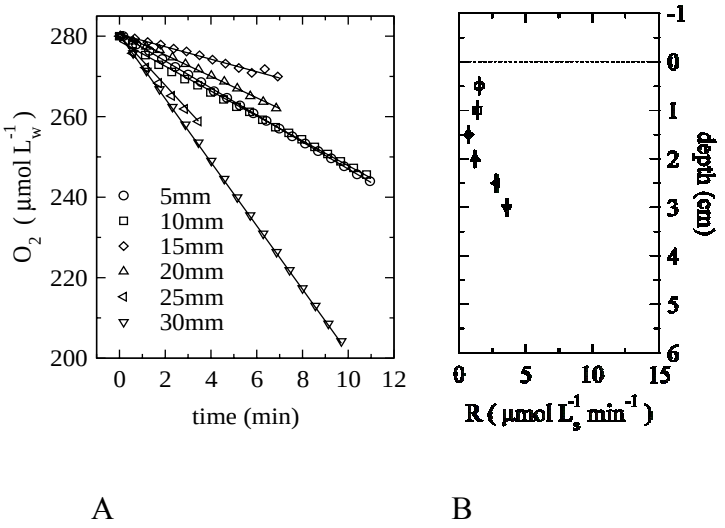


**Figure 2:** (A) Time evolution of the oxygen concentration measured at different sediment depths during the flow-off period of the flow-through experiment. (B) Corresponding oxygen consumption rates calculated as the initial slope of the oxygen decrease, corrected for the sediment porosity. The subscripts *w* and *s* refer to the volume of pore-water and sediment, respectively.

One pump-on/off cycle lasted between approximately 15 and 20 minutes, resulting in the total time necessary to determine a single OCR profile of just under 2 hours. The precision of the determined OCR values, taken as the standard error of the slope of the measured $O_2(t)$ at each position, was 0.01–0.1 $\mu molL_s^{-1}\,\mathrm{min}^{-1}$. Multiple flow-on/off cycles performed at each position showed that the measurements were reproducible with the same or lower variability. The spatial resolution was rather coarse (5 mm) and the profile was measured only at a single horizontal location (due to time constrains). A statistically representative determination of high resolution depth profiles of OCR would take several days to complete by this approach, unless multiple sensors are used simultaneously.

*Continuous $O_2$ profiling by microelectrode:* The approach based on continuous $O_2$ profiling by a microelectrode during the flow-off period was repeated on the same sediment core, however, at another horizontal position. Line #1 in Fig. 3A shows that initially, during the flow-on period (flow rate $v_f$=33 $\mathrm{cm}^3\,\mathrm{min}^{-1}$), oxygen was almost homogeneously distributed in the sediment. During the subsequent flow-off period, oxygen microprofiles were measured in time intervals of 15–30 min with a step-size of 2 mm (lines #2 to #6 in Fig. 3A).

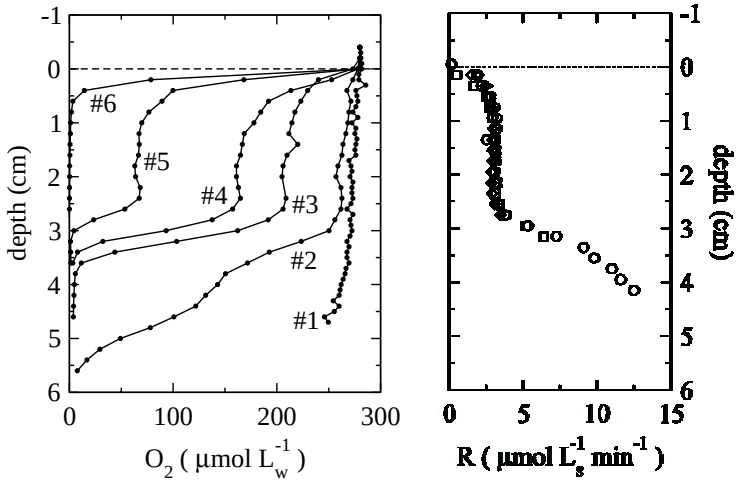


**Figure 3:** (A) Oxygen profiles measured during the flow-on (line #1) and flow-off (lines #2 to #6) periods of the flow-through measurement. Time differences between the starting points of profiles #2–#3, #3–#4, #4–#5 and #5–#6 were 17, 14, 30 and 34 min, respectively. (B) Corresponding profiles of oxygen consumption rates. Different symbols correspond to different profile pairs. The subscripts *w* and *s* refer to the volume of water and sediment, respectively.

The procedure described above resulted in OCR profiles shown in Fig. 3B. The OCR profiles obtained by the subtraction of different pairs of microprofiles were almost identical. The same procedure was conducted at another horizontal location, with similar results (data not shown).

The measured OCR profile is very close to that obtained by the approach employing the measurement of $O_2(t)$ at discrete depths, while the spatial resolution was improved (2 mm). However, since the sediment could be profiled at best every ≈15 min, the individual OCR determinations may include diffusion artifacts. For example, figure 3B shows that the measured OCR rapidly increases at depths immediately below 3cm. This means that local concentration gradients developed during the measurement, leading to a possibly overestimated value of the measured OCR. A similar artifact may be observed near the sediment-water interface where oxygen may be renewed by diffusion from the overlying water, thus resulting in a possibly underestimated value of OCR.

The degree of under or overestimation can be estimated. This is done by approximating the diffusion contribution

as $D_s \partial^2 c / \partial z^2 \approx D_s [c(z+\Delta z) + c(z-\Delta z) - 2c(z)] / \Delta z^2$, where $c(z)$ is the measured

concentration profile and $\Delta z$ is a depth interval. Using the values from the concentration profile #2 around $z$=3 cm, $\Delta z$=0.4 cm, and the diffusion coefficient in the sediment of porosity $\phi = 0.45$ of $D_s$=0.9×10$^{-5}$ $cm^2 s^{-1}$ (Boudreau 1996), the diffusive term amounts to ≈ -0.17 $\mu molL_s^{-1}$ min$^{-1}$. Using the values from profile #5 around z = 0.5 cm and the same $D_s$ and $\Delta z$, the diffusive term amounts to ≈ 0.54 $\mu molL_s^{-1}$ min$^{-1}$. Consequently, a conservative estimation of the inaccuracy of the measured OCR ranges between approximately -0.2 and 0.6 $\mu molL_s^{-1}$ min$^{-1}$ for the deeper parts of the sediment (z ≥ 3 cm) and for the locations close to the sediment-water interface (z ≤ 0.5 cm), respectively. Thus the error induced by diffusion is less than 10%.

Since the OCR values obtained from different pairs of the measured oxygen profiles were similar, the OCR profile can be satisfactorily determined by measuring only two sequential profiles during the flow-off period. Thus, a depth profile of OCR between 0 and 4 cm with a spatial resolution of 2 mm could be determined with a needle-type microsensor within 30–60 min.

*Continuous $O_2$ imaging by planar optode*: The sediment sample was collected from the same site using a steel core with a window containing a planar oxygen optode. Approximately 2/3 of the optode was covered by the sediment and the remaining 1/3 by the overlying water.

The CCD camera was positioned so that the area of the planar optode (25×150 mm) resulted in an oxygen image of size 80×480 pixels, implying a spatial resolution of ≈300 μm. To minimise the noise of the oxygen images, 4 and 8 sequential images were averaged, resulting in a temporal resolution of ≈5 s and 10 s during the flow-on and flow-off periods, respectively.

Penetration of oxygen into the sediment during the flow-on period was observed in real time (see Fig. 4A–D). At a flow speed of 50 cm$^3$min$^{-1}$, an approximately homogeneous distribution of oxygen in the sediment was reached after 8 min. Examples of the images recorded during the flow-off period, which lasted for 40 min, are shown in Fig. 4E–H. To check for the reproducibility of the measurement, the same procedure was repeated two more times.

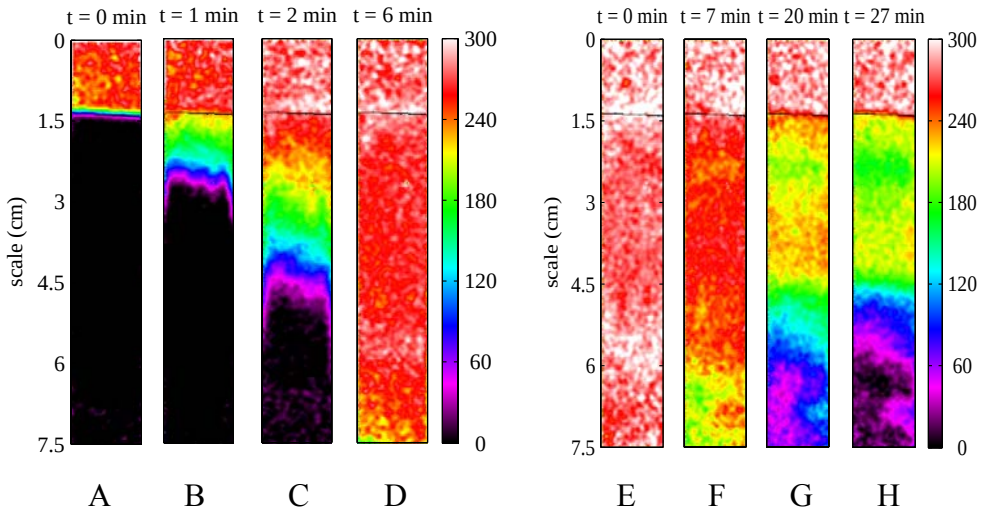


**Figure 4:** Examples of oxygen images during the flow-on (A–D) and flow-off (E–H) periods of the flow-through experiment. The solid lines at approximately 1.5 cm indicate the sediment surface. The color-bar on the right indicates the gradation of oxygen concentrations in $\mu molL_w^{-1}$.

Typical examples of time evolutions of the oxygen concentration in three selected pixels of the oxygen images are shown in Fig. 5. The pixels were selected to demonstrate different types of oxygen dynamics in the sediment. The data denoted as #1 in the bottom graph depict the decrease of oxygen concentration unaltered by diffusion during the entire duration of the flow-off period. On the other hand, the data denoted as #2 and #3 demonstrate how diffusion can increase and decrease the initial rate of oxygen consumption, respectively.

Figure 5 also shows the results of the fitting procedure. For example, the order of the most suitable polynomial fitting the data #1, #2 and #3 was 1, 3, and 2, respectively. The corresponding initial slopes, representing the local OCR, are depicted by the dashed lines. In addition to the local OCR, the fitting procedure also revealed the standard deviation of the initial slope, namely 0.05, 0.5 and 0.25 $\mu molL_s^{-1}\,\mathrm{min}^{-1}$ for data #1, #2 and #3, respectively. Thus the precision of the OCR values in a randomly selected pixel can be conservatively estimated as $\approx \pm 0.5\ \mu molL_s^{-1}\,\mathrm{min}^{-1}$.

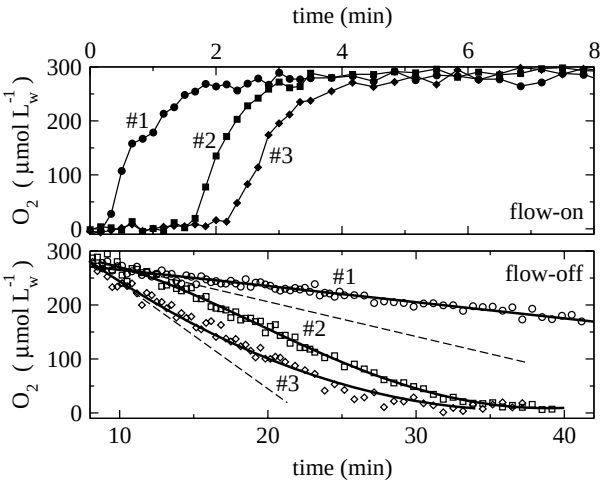


**Figure 5:** Examples of time evolutions of oxygen in three selected pixels as measured by the planar oxygen optode during the flow-on and flow-off periods. Data denoted as #1, #2 and #3 correspond to selected points located at depths of 1, 3 and 5 cm of the sediment, respectively. Symbols represent the experimental data, solid lines in the bottom graph the most suitable fitting polynomial (see text for more details) and dashed lines indicate the initial slope of oxygen decrease, representing the local OCR. For data #1, the dashed line is identical with the fitting line.

After the fitting procedure was carried out in every pixel of the oxygen images, 2D maps of OCR across the entire observed section of the sediment were obtained (Fig. 6). After averaging the images in the horizontal direction, depth profiles of OCR were obtained, as shown in the same figure. The error bars, obtained as the standard deviations of the OCR values at the corresponding horizontal section, indicate the variability of sediment oxygen consumption over small horizontal scales.

The profiles obtained by planar optodes agree well with the profiles determined by the microelectrode based approaches (compare Fig. 6 with Figs. 2 and 3). This demonstrates a consistency of the measurement approaches. The planar optode based approach, however, provides a number of benefits.

Firstly, planar optodes enable the acquisition of a large amount of information during a single flow-on/off cycle of the flow-through measurement (Fig. 1B). In particular, the spatial resolution is optimal (≈300 µm, as compared to 2–5 mm achieved by a microelectrode in approximately the same measuring time) and both the vertical *and* horizontal small-scale variability of oxygen consumption activity of the sediment can be assessed. Secondly, since the planar optodes enable the

observation of the oxygen distributions in real time, the timing of the flow-through measurement can be optimized dynamically.

A drawback of planar optodes is that the signal-to-noise ratio is lower than that of microelectrodes. This may lead to less precise OCR values (in the order of $\approx \pm 0.5\ \mu molL_s^{-1}\ \mathrm{min}^{-1}$, as mentioned above).

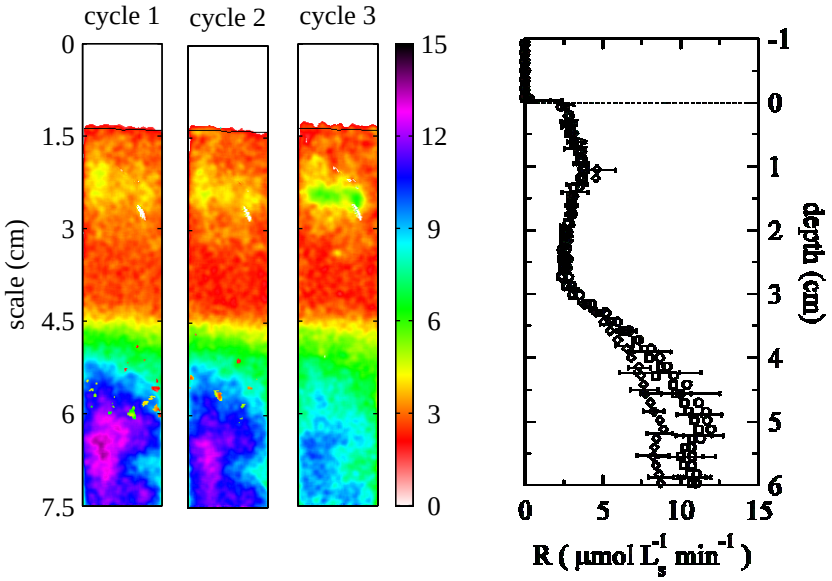


**Figure 6:** Examples of OCR images obtained from three subsequent flow-through cycles. The color-bar to the right of the OCR images indicates the correspondence between the color and OCR in $\mu molL_s^{-1}\ \mathrm{min}^{-1}$. Depth profiles of OCR, obtained by horizontal averaging of the images, are also shown (circles, squares and diamonds correspond to the cycles 1, 2 and 3, respectively). The error bars represent the horizontal variability of the sediment's OCR. For clarity, only every 5th vertical data-point is depicted, i.e., every 1.5 mm.

When using a microelectrode, OCR can be determined at any point in the sediment, which is an advantage in comparison to the planar optode based approach, where the measurement is restricted to the region of the sediment in direct contact with the optode. The OCR obtained by microelectrodes and planar optodes are similar, thus wall effects may be assumed to have been insignificant during this method demonstration.

Another potential drawback related to measurement with optodes is that the determination of oxygen requires intensive blue excitation light. If the sediment contains phototactic micro-organisms, the OCR could be altered if light exposure is long enough to allow for migration of such organisms towards the wall. Also, if

photosynthetic micro-organisms were present in the sediment, oxygen production induced by the measuring light could influence the OCR measurement. However, such problems could be avoided by the use of optically isolated planar optodes (Glud et al. 1998, 1999b).

*$O_2$ profiling during steady-state flow-on period:* The flow-through method employing $O_2$ profiling by a microelectrode during the steady-state flow-on period was tested using the same sediment core characterized with the other microelectrode-based approaches. The water flow was, however, significantly lowered to $v_f$=0.25 $cm^3\,min^{-1}$, which corresponded to a pore water flow velocity of 3.3 cm $h^{-1}$. During the flow-on period, oxygen profiles were determined by a microelectrode at different horizontal positions. After approximately 2 hours, stationary oxygen profiles were measured, as shown in Fig. 7A. Each profile was fitted by a model describing advective transport of oxygen in the sediment (Eq. (2)), leading to a depth profile of OCR. These depth profiles were averaged and the resulting mean values together with the standard deviations are shown by symbols in Fig. 7B.

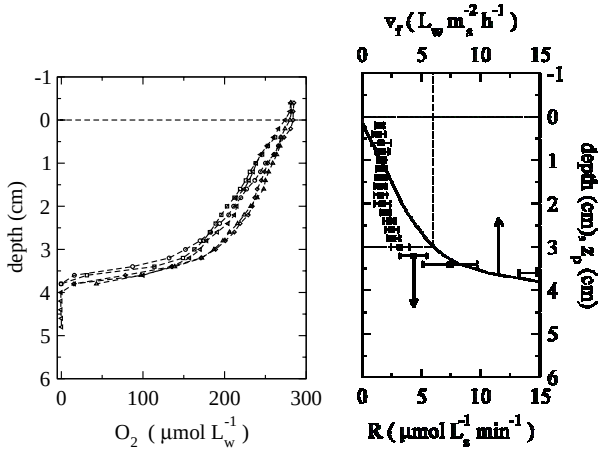


**Figure 7:** (A) Stationary oxygen profiles measured during the flow-on period at various horizontal positions. (B) Depth profile (symbols) of OCR obtained as the average of the OCR depth profiles calculated from Eq. (2) and the stationary profiles in A. The corresponding rate of water filtration through the sediment as a function of oxygen penetration depth $z_p$ is depicted by a solid line.

The OCR values agree very well with those obtained by the alternative microelectrode based methods described above. The effect of diffusion, given by the second derivative of the profile multiplied by the diffusion coefficient, was also evaluated, but no significant influence on the OCR values was found.

Results obtained under steady flow can also be viewed as mimicking in situ oxygen profiles. An important parameter obtained by autonomous in situ profilers is the dynamic penetration depth of oxygen. The question is whether the volumetric exchange rate of water through the sediment could be estimated from this parameter.

Although natural flows are usually more complex (see below), the advective transport of pore water through many permeable sediments can be thought of as similar to that during the flow-on period of the flow-through measurements. During the measurement described above, the oxygen penetration depth of ≈3.7 cm was achieved with the pore water flow of 3.3 cm $h^{-1}$, or the overlying water flow of 1.5 cm $h^{-1}$ = 15 L $m^{-2}$ $h^{-1}$ (see the oxygen profiles in Fig. 7A). Thus, if such a penetration depth was observed by in situ microprofiling, it could be estimated that approximately 15 L of overlying water is hourly filtered through every $m^2$ of the sediment.

If another oxygen penetration depth was measured, additional "mimicking" measurements would not be necessary. Since the depth profile of OCR was already measured, advection-governed oxygen profile and thus the penetration depth can be modeled from Eq. (2). Denoting the oxygen concentration in the overlying water by $c_0$, penetration depth of oxygen by $z_p$, and assuming that the values of the pore water flow and porosity do not vary with depth, integration of Eq. (2) leads to $c_0 v_f / \phi A = \int_0^{z_p} R(z)dz$. Using this equation, which is nothing else than a simple oxygen balance for a steady-state vertical water flow, $v_f$ can be estimated from the measured $z_p$ and OCR profile $R(z)$, or vice versa.

The possible shape of $v_f(z_p)$ was calculated from the measured OCR profile and is shown by a solid line in Fig. 7B. When OCR is approximately constant (depths between 0 and 3 cm), the oxygen penetration depth increases roughly linearly with

the flow rate. At 6 $L_w\ m_s^{-2}\ h^{-1}$, it reaches 3 cm, i.e., approximately 6 L of overlying water is filtered hourly through every $m^2$ of sediment when oxygen penetrates 3 cm deep. OCR rapidly increases below 3 cm and consequently the oxygen penetration depth is much less sensitive to the flow rate. For example, even though $v_f$ doubles from ≈ 7.5 $L_w\ m_s^{-2}\ h^{-1}$ to ≈ 15 $L_w\ m_s^{-2}\ h^{-1}$, the penetration of oxygen increases only by as little as 5 mm (from ≈3.3 to ≈3.8 cm).

These observations suggest that in situ filtration rates of the sediment (pore water flow rates) could be estimated from OCR profiles when in situ oxygen penetration depths are also measured. This could be an interesting and attractive application of the flow-through method, since in situ filtration rates in permeable sediments have only been determined thus far by elaborate measurements of the displacement of an indicator (e.g., fluorescent dye or iodide) injected into the sediment (Precht and Huettel 2004; Reimers et al. 2004). One should, however, bare in mind the difference between the simple down-flow implemented in the flow-through method and the more complex water exchange in natural sediments (see Shum 1992; Shum and Sundby 1996; Huettel et al. 1996; Precht et al. 2004 for more on this topic).

The patterns of oxygen distributions resulting from the complex water exchange in permeable sediments can be determined in two dimensions (Precht et al. 2004; Wenzhöfer and Glud 2004). Provided that the directional field of the pore water flow is known, or can be to some extent reliably estimated, the model of advective transport expanded to two dimensions can be used together with the two-dimensional oxygen images to quantify the flow rate. Specifically, the process would involve (i) the calculation of the spatial derivative of concentration along the direction of the pore water flow vector, i.e., $\nabla_{\vec{s}} c$, where $\vec{s} \parallel \vec{v}_f$, and (ii) the calculation of the time derivative of concentration, $\partial c/\partial t$, determined from oxygen images acquired at different times. Consequently, neglecting the diffusive transport, the magnitude of the local flow rate (in $cm\ h^{-1}$) could be estimated from $v_f / \phi A \approx (\partial c / \partial t - R) \,|\, \nabla_{\vec{s}} c \,|^{-1}$, where $R$ is the two-dimensional OCR distribution determined by the planar optode based flow-through method. The pursuit of such

an interesting application would, however, require further investigation beyond the scope of this article.

*Comparison of the flow-through method with the flux and benthic-chamber methods:* The flow-through method was compared with the commonly used techniques for the determination of the areal oxygen consumption rates, i.e., the flux and benthic-chamber methods, under diffusion-dominated conditions. The purpose of this test was to confirm the consistency among the methods under well controlled conditions, where all methods are directly applicable.

The core with the planar optode was filled with sieved sediment of porosity $\phi$=0.45. The water above the sediment was kept air saturated and stirred with a small propeller attached to a rotating axis. Stirring was minimal to ensure that transport was entirely diffusive.

Firstly, multiple microprofiles were measured by an oxygen microelectrode at different horizontal positions across the sediment surface area. The concentrations, which decreased by 23±3 μmol $L^{-1}$ over the average DBL thickness of 500μm (measured profiles not shown), were fitted by a diffusive model. Using the diffusion coefficient $D_w = 2x10^{-5}$ $cm^2s^{-1}$, the average oxygen flux at the sediment-water interface was $J_{flux} = 5.4 \pm 0.9$ μmol$m^{-2}min^{-1}$.

The second step consisted of a planar optode based flow-through measurement with the flow-on period lasting approximately 2 min. At each horizontal position of the calculated OCR image, the vertical OCR profile was integrated over the penetration depth of oxygen (≈5mm). The penetration depth was determined sufficiently long before and after the flow-through measurement, i.e., when oxygen distribution was governed by diffusion. This way, the obtained values could directly be compared with those from the first and next steps (see below). The resulting rates were averaged, leading to a total areal oxygen uptake rate of $J_{flow\text{-}through} = 5.0 \pm 1.0$ μmol $m^{-2}$ $min^{-1}$.

Finally, a measurement mimicking the benthic-chamber experiment was carried out. Aeration of the overlying water was stopped and the chamber was closed with a lid. Stirring of the overlying water continued in order to maintain the same thickness of the diffusive boundary layer as during the diffusive flux measurement.

The decrease of oxygen in the overlying water was monitored by an oxygen microelectrode positioned 1 cm above the sediment surface as well as by the planar optode, which extended well above the sediment surface. From the decrease, determined by regression analysis, the volume of the overlying water and the area of the sediment surface, the oxygen uptake rate was found to be $J_{chamber} = 5.3 \pm 0.1$ μmol $m^{-2}$ $min^{-1}$.

The obtained values confirm that the three techniques lead to consistent results, when tested under equivalent, well controlled, diffusion-dominated conditions. However, since the flow-through method determines the potential volumetric OCR independently of the oxygenation status of the sediment, its applicability is much broader than that of the flux or benthic-chamber methods (see discussion for more on this topic).

It should be noticed that the standard deviation of the oxygen uptake rate obtained by the benthic-chamber method was approximately 9–10 times smaller than that obtained by the other two methods. This is understandable, as the standard deviations evaluated for the flux and flow-through methods represent the small-scale *horizontal variability* of the sediment with regard to the oxygen uptake rates, which is averaged by the benthic-chamber technique.

*Effects of water percolation on the measurement:* To identify potential artifacts induced by the percolation of air-saturated water through the sediment, results obtained by the planar optode based approach were further analyzed. The OCR images and the corresponding depth profiles of OCR displayed in Fig. 6 demonstrate that the OCR measured in cycle $N$+1 were lower than those measured in cycle $N$ in nearly all pixels. This was a consistently observed effect when the cycles were measured immediately one after the other. On the other hand, if the gap between the cycles was much longer, e.g., over night, a recovery in the measured OCR to the original values was observed (data not shown). The effect was much more pronounced in deeper parts of the sediment (below 3 cm in the example discussed here), which coincided with a distinctly differently colored sediment (dark gray, almost black), as opposed to a light brown sediment of the top 3 cm.

This effect is most likely due to sediment stratification developed under natural conditions as a result of a highly dynamic, advection driven supply of oxygen into

the sediment induced by waves and tidal pumping. Oxygen penetration depths of 2–3 cm are frequently observed by in situ profiler measurements (Walpersdorf, unpublished data), suggesting that the top sediment layer is inhabited mainly by aerobically respiring organisms, whereas reduced compounds accumulated in the deeper sediment. During the flow-through measurement, the pool of reduced compounds that can be easily oxidized contributed to the observed OCR in the deeper part of the sediment. As a result of this chemical oxidation, the size of the pool was reduced, resulting in the decreased contribution to the OCR observed in the subsequent measurement. On the other hand, when the sediment was kept anoxic for a longer time period, the pool could recover, resulting in a higher observed OCR.

Percolation of the sediment sample with aerated water is a prerequisite for the method, leading to a possible flushing out of compounds dissolved in the pore water from the sediment. Furthermore, rather lengthy percolation periods are required when a microelectrode based approach is employed. This may lead to a possible underestimation of the real oxygen consumption activity, as discussed above. However, as shown in Fig. 6, these effects are not significant in the part of the sediment that is naturally exposed to oxic conditions, which is the zone of primary interest.

Reimers et al. (2004) recently reported that the areal consumption rate of the same sediment volume could be enhanced by an increased percolation rate. Greater dispersion and penetration of oxygenated water into anoxic microenvironments within heterogeneous sediment at higher flow rates was suggested as a possible cause of this effect. Our measurements support this view, although additional experiments would be needed to exclude the possibility that respiration activities of microorganisms are enhanced by higher pore water flow rates. Using planar optodes, it was possible to monitor in real time the distribution of oxygen in the sediment. When OCR at some regions (not necessarily microscopic) of the sediment exceeded the supply of oxygen by the percolation at a specific flow rate, the regions remained anoxic. This would result in effectively zero potential volumetric OCR in these regions, leading after integration to lower areal OCR. If the flow rate was increased until the entire sediment in front of the optode was

oxic, the subsequently calculated OCR image showed significantly higher rates at these regions. Therefore, when sufficiently high percolation rates are used, the flow-through method provides an estimate of the maximum areal OCR. The percolation could, however, be modified to reflect the pore water flow conditions observed in situ (if such data exist), thus providing an estimate of the total oxygen uptake by the sediment experiencing close to natural conditions.

**Comments and recommendations**

The flow-through method is in principle a laboratory technique and cannot easily be applied in situ. However, since the experimental setup can be relatively easily assembled, it can be used as a field technique enabling the measurement immediately after the collection of the sample from a studied site.

The measurement procedure is simple and the software tools providing the subsequent analysis of the results were designed so that they could be operated by a trained non-specialist. Only minimal instrumentation (a micropositioner, an oxygen microelectrode and a data acquisition system) is required when the approach based on $O_2(t)$ measurements at discrete depths is employed. An additional automated micropositioning setup is preferable if the approaches based on continuous $O_2$ profiling during the flow-on or flow-off periods are used. With the access to a lifetime imaging system and planar oxygen optodes, full benefits of the flow-through method, namely the rapid determination of OCR in 2D with high spatial resolution, can be exploited. It is preferable to conduct planar optode measurements under dark conditions or at least at low ambient light intensities. No special light conditions are required for the microelectrode based approach, unless potential photosynthesis needs to be avoided. Typical merits characterizing each approach of the flow-through method are summarized in Tab. 1.

Table 1: Duration, spatial resolution and precision of the different approaches of the flow-through measurement for a typical 3–4 cm vertical OCR profile determined by an oxygen microelectrode (ME) or planar optode (PO).

| Measurement approach | Measurement time of one OCR profile | Spatial resolution (mm) | Precision (µmol $L^{-1}$ $min^{-1}$) |
|---|---|---|---|
| $O_2(t)$ at discrete depths (ME) | 2 h | 2–5 | 0.01–0.1 |
| Continuous $O_2$ profiling (ME) | 30–60 min | 2 | 0.5 |
| Continuous $O_2$ imaging (PO) | 20–30 min | 0.3 | 0.5 |
| $O_2$ profiling during steady flow (ME) | 2–4 h | 2 | 0.5 |

The flow-through method has a distinct advantage over the flux and benthic-chamber methods, as it quantifies the spatial distribution of *potential* oxygen consumption rates independently of the in situ conditions in the sediment. To determine actual in situ oxygen uptake rates, the results must be combined with information gathered when in situ oxygen distributions are measured in the sediment. It is not necessary to describe or mimic natural levels of flow complexity when quantifying OCR. It is only necessary to know over what depth to integrate the OCR profile.

Due to the reliance of the flow-through method on supplementary information provided by benthic in situ profilers, its application may be costlier in comparison to, e.g., the benthic-chamber method. However, due to the above mentioned advantage, the flow-through method provides more accurate results in sediments with highly dynamic conditions (flow and oxygen penetration), where the use of benthic-chambers is limited and the flux method is not applicable.

The use of the flow-through method is limited in sediments with abundant burrowing and bioirrigating macrofauna. This is mainly because macrofauna can locally disturb the assessment of the rates by its irregular activity (i.e., water pumping) during the measurement. Another problem is that the respiring macrofauna can be easily missed if microelectrodes are used or if macrofauna are not located in sections of sediment in contact with planar optodes. Even though the

volumetric respiration rates due to macrofauna can be determined, a straightforward quantification of areal OCR of the sediment would be problematic and the benthic-chamber or eddy-correlation technique would provide more reliable results.

The use of planar optodes facilitates a high spatial resolution measurement of OCR in two dimensions. This provides an insight into the sediment and the functional variability of the processes governing the oxygen uptake, e.g., allows to differentiate between the microbial activity and bioturbation or bioirrigation, which is not possible using the benthic-chamber or eddy-correlation techniques.

In conclusion, the proposed method provides a feasible technique for the determination of volumetric oxygen consumption rates with high spatial resolution. The method is most suitable for permeable sediments which can be easily percolated with water and which are naturally exposed to highly dynamic conditions. Of particular interest are sandy sediments, such as coral sands, intertidal or subtidal lithogenous sands, river beds, seep sediments.

**Acknowledgments**

We would like to thank Gaby Eickert, Ines Schröder, Ingrid Dohrmann, Alfred Kutsche, Georg Herz, Volker Mayer, Paul Färber and Herald Osmers for the preparation of oxygen microsensors and the construction of various mechanical and electronic parts necessary for the experimental setup. The crew of the vessel Verandering are thanked for providing pleasant and safe conditions on board. The valuable comments of two anonymous reviewers and especially of Clare Reimers are much appreciated. This study was supported by the Bundesministerium für Bildung und Forschung (BMBF, project number 03F02848).

## References

P. Berg, H. Røy, F. Janssen, V. Meyer, B. B. Jørgensen, M. Huettel, and D. de Beer. Oxygen uptake by aquatic sediments measured with a novel non-invasive eddy-correlation technique. *Marine Ecology—Progress Series*, 261:75–83, 2003.

B. P. Boudreau. The diffusive tortuosity of fine-grained unlithified sediments. *Geochimica et Cosmochimica Acta*, 60(16): 3139–3142, 1996.

J. Crank. *Mathematics of Diffusion*. Oxford University Press, 2nd edition, 1975.

D. de Beer, F. Wenzhöfer, T. D. Ferdelman, S. Boehme, M. Huettel, J. E. E. von Beusekom, M. E. Boettcher, N. Musat, and N. Dubilier. Transport and mineralization rates in North Sea sandy intertidal sediments (Sylt-Rømø basin, Wadden Sea). *Limnology and Oceanography*, 50(1): 113-127, 2005.

H. de Haas, T. C. E van Weering, and H. de Stigter. Organic carbon in shelf seas: sinks or sources, processes and products. *Continental Shelf Research*, 22(5):691–717, 2002.

K. O. Emery. Relict sediments on continental shelves of the world. *Am. Assoc. Petroleum Geologists*, 52:445–464, 1968.

E. H. G. Epping, A. Khalili, and R. Thar. Photosynthesis and the dynamics of oxygen consumption in a microbial mat as calculated from transient oxygen microprofiles. *Limnology and Oceanography*, 44(8): 1936–1948, 1999.

R. N. Glud, S. Forster, and M. Huettel. Influence of radial pressure gradients on solute exchange in stirred benthic chambers. *Marine Ecology-Progress Series*, 141(1–3): 303–311, 1996.

R. N. Glud, J. K. Gundersen, B. B. Jørgensen, N. P. Revsbech, and H. D. Schulz. Diffusive and total oxygen-uptake of deep-sea sediments in the eastern south-atlantic ocean—in-situ and laboratory measurements. *Deep-Sea Research Part I—Oceanographic Research Papers*, 41(11–12):1767–1788, 1994.

R. N. Glud, I. Klimant, G. Holst, O. Kohls, V. Meyer, M. Kühl, and J. K. Gundersen. Adaptation, test and in situ measurements with $O_2$ microopt(r)odes on benthic landers. *Deep-Sea Research Part I—Oceanographic Research Papers*, 46(1):171–183, 1999a.

R. N. Glud, M. Kühl, O. Kohls, and N. B. Ramsing. Heterogeneity of oxygen production and consumption in a photosynthetic microbial mat as studied by planar optodes. *Journal of Phycology*, 35(2):270–279, 1999b.

R. N. Glud, C. M. Santegoeds, D. De Beer, O. Kohls, and N. B. Ramsing. Oxygen dynamics at the base of a biofilm studied with planar optodes. *Aquatic Microbial Ecology*, 14(3):223–233, 1998.

R. N. Glud, A. Tengberg, M. Kühl, P. O. J. Hall, I. Klimant, and G. Holst. An in situ instrument for planar $O_2$ optode measurements at benthic interfaces. *Limnology and Oceanography*, 46(8): 2073–2080, 2001.

G. Holst and B. Grunwald. Luminescence lifetime imaging with transparent oxygen optodes. *Sensors and Actuators B—Chemical*, 74 (1–3):78–90, 2001.

G. Holst, O. Kohls, I. Klimant, B. Konig, M. Kühl, and T. Richter. A modular luminescence lifetime imaging system for mapping oxygen distribution in biological samples. *Sensors and Actuators B—Chemical*, 51 (1–3):163–170, 1998.

M. Huettel and G. Gust. Impact of bioroughness on interfacial solute exchange in permeable sediments. *Marine Ecology Progress Series*, 89(2–3): 253–267, 1992.

M. Huettel, W. Ziebis, and S. Forster. Flow-induced uptake of particulate matter in permeable sediments. *Limnology and Oceanography*, 41(2):309–322, 1996.

D. G. Kleinbaum and L. L. Kupper. *Applied Regression Analysis and other Multivariable Methods*. Duxbury Press, 1st edition, 1978.

D. E. Malan and A. McLachlan. In situ benthic oxygen fluxes in a nearshore coastal marine system: a new approach to quantify the effect of wave action. *Marine Ecology Progress Series*, 73:69–81, 1991.

M. M. Pamatmat. Oxygen consumption by the seabed IV. Shipboard and laborator experiments. *Limnology and Oceanography*, 16:536–550, 1971.

E. Precht, U. Franke, L. Polerecky, and M. Huettel. Oxygen dynamics in permeable sediments with wave-driven pore water exchange. *Limnology and Oceanography*, 49(3):693–705, 2004.

E. Precht and M. Huettel. Advective pore water exchange driven by surface gravity waves and its ecological implications. *Limnology and Oceanography*, 48(4): 1674–1684, 2003.

E. Precht and M. Huettel. Rapid wave-driven advective pore water exchange in a permeable coastal sediment. *Journal of Sea Research*, 51:93–107, 2004.

C. E. Reimers, H. A. Stecher, G. L. Taghon, C. M. Fuller, M. Huettel, A. Rusch, N. Ryckelynck, and C. Wild. In situ measurements of advective solute transport in permeable shelf sands. *Continental shelf research*, 24:183–201, 2004.

N. P. Revsbech. An oxygen microelectrode with a guard cathode. *Limnology and Oceanography*, 34(2):474–478, 1989.

N. P. Revsbech, J. Sørensen, T. H. Blackburn, and J. P. Lomholt. Distribution of oxygen in marine sediments measured with microelectrodes. *Limnology and Oceanography*, 25(3):403–411, 1980.

K. T. Shum. Wave-induced advective transport below a rippled water-sediment interface. *Journal of Geophysical Research—Oceans*, 97: 789–808, 1992.

K. T. Shum and B. Sundby. Organic matter processing in continental shelf sediments — the subtidal pump revisited. *Marine Chemistry*, 53:81–87, 1996.

K. L. Smith. Benthic community respiration in NW Atlantic Ocean—insitu measurements from 40 to 5200 M. *Marine Biology*, 47(4):337–347, 1978.

R. R. Sokal and F. J. Rohlf. *Biometry*. W. H. Freeman and Company, 3rd edition, 1995.

A. Tengberg et al. 1995. Benthic chamber and profiling landers in oceanography—A review of design, technical solutions and functioning. *Progress In Oceanography*, 35(3):253–294, 1995.

E. Viollier, C. Rabouille, S. E. Apitz, E. Breuer, G. Chaillou, K. Dedieu, Y. Furukawa, C. Grenz, P. Hall, F. Janssen, J. L. Morford, J. C. Poggiale, S. Roberts, T. Shimmield, M. Taillefert, A. Tengberg, F. Wenzhöfer, and U. Witte. Benthic biogeochemistry: state of the art technologies and guidelines for the future of in situ survey. *Journal of Experimental Marine Biology and Ecology*, 285–286:5–31, 2003.

F. Wenzhöfer and R. N. Glud. Benthic carbon mineralization in the Atlantic: a synthesis based on in situ data from the last decade. *Deep-Sea Research Part I-Oceanographic Research Papers*, 49(7):1255–1279, 2002.

F. Wenzhöfer and R. N. Glud. Small-scale spatial and temporal variability in coastal benthic $O_2$ dynamics: Effects of fauna activity. *Limnology and Oceanography*, 49:1471–1481, 2004.

# Spatial and temporal patterns of mineralization rates and oxygen distribution in a permeable intertidal sand flat (Sylt, Germany)

Ursula Werner, Markus Billerbeck, Lubos Polerecky, Ulrich Franke, Markus Huettel, Justus van Beusekom and Dirk de Beer

submitted to Limnology and Oceanography

**Abstract**

Oxygen distribution and benthic mineralization rates were investigated in a permeable (3.9 x $10^{-11}$ $m^2$) intertidal sand flat (Hausstrand, Sylt, German Wadden Sea) in a transect from the low- towards the high-waterline. At all stations, oxygen penetration was deep and dynamic during inundation due to pore water advection. During exposure oxygen penetration was reduced. Oxygen consumption rates (OCR) and sulfate reduction rates (SRR) were linked to the inundation time of the stations: Oxygen consumption rates were elevated at the lower flat in summer (lower flat 131 -187; middle- and upper flat 64 -108 mmol C $m^{-2}$ $d^{-1}$). Sulfate reduction rates decreased sharply from the low- to the high-waterline during all seasons (e.g., in summer: lower flat 18 - 40; middle flat 8.8 - 9.4, upper flat 0.5 - 4 mmol C $m^{-2}$ $d^{-1}$). The advective supply of oxygen was a major determinant for the magnitude and pattern found in OCR. Driven by the oxygen availability, 71 - 90% of oxygen consumption took place during inundation. Due to the deep oxygen penetration, aerobic mineralization was the dominant degradation process at all stations. A simple estimate of the organic matter supplied to the sediments by pore water advection only explained a fraction of the mineralization rates. Advective exchange between water column and sediments may thus contribute to high mineralization rates with the supply of oxygen being the chief factor and the supply of organic carbon being subordinate. Mineralization rates were higher in summer than in winter. Only in summer sulfate reduction became a significant process.

## Introduction

Permeable sandy sediments may act as biocatalytic filter systems for organic matter from the water column (Webb and Theodor 1968; Huettel and Gust 1992; Shum and Sundby 1996). Benthic mineralization rates can be high and, consistent with a deep oxygen penetration, aerobic mineralization was found to be dominant (D'Andrea et al. 2002; De Beer et al. 2005). In shallow water sediments, benthic photosynthesis supplies organic material and oxygen to the sediments (Cammen 1991; Berninger and Huettel 1997). However, the magnitude and depth distribution of benthic mineralization processes depend to a large extent on the transport of electron acceptors and electron donors from the water column to the sediment and from the sediment surface to deeper sediment layers. While in cohesive sediments the main transport mechanisms are diffusion and fauna-mediated (bioturbation/bioirrigation), in permeable sediments pore water advection additionally contributes to interfacial exchange (Huettel and Gust 1992; Shum 1992; Shum and Sundby 1996). Pore water advection can exceed diffusive transport rates by orders of magnitude (Huettel and Gust 1992; Boudreau et al. 2001). Pore water advection is considered the major reason for high mineralization rates in the organic poor sands (Webb and Theodor 1968; Shum and Sundby 1996; Huettel and Rusch 2000) as it provides solutes such as oxygen (Forster et al. 1996; Ziebis et al. 1996) and particulate organic carbon (Rusch and Huettel 2000; Ehrenhauss and Huettel 2004) to the sediments while removing potentially inhibitory end-products of mineralization processes.

At an inundated intertidal sand flat advection is driven by pressure gradients caused by the interaction of tidal and wind driven currents and waves with sediment topography, (Riedl et al. 1972; Huettel and Gust 1992; Precht and Huettel 2003), or by density changes (Webster et al. 1996; Rocha 1998). At an exposed intertidal sand flat advection may occur as pore water drainage, driven by a hydraulic gradient developing between the sea water level and the slower dropping pore water level (Nielsen 1990). Thus, at intertidal sand flats, the advective exchange rates may vary over the tidal cycle. During inundation, pressure gradients are generated by hydrodynamics that are reduced or absent during exposure. The advective supply of oxygen and organic matter from the water column should

therefore depend on the inundation time of the sediment and, thus, on the distance to the low water line. This may lead to a spatial heterogeneity in mineralization rates, with mineralization rates increasing towards the low water line.

Field studies on transport and mineralization rates in permeable intertidal sediments (Rusch and Huettel 2000; D'Andrea et al. 2002; De Beer et al. 2005) are rare, as the dynamic nature of permeable sediments complicates in situ measurements (Reimers et al. 2004). A deep oxygen penetration was found during the inundation period of an intertidal flat due to pore water advection (De Beer et al. 2005), however, at another intertidal flat, a deeper oxygen penetration was found during the exposure period due to air intrusion (Brotas et al. 1990). An in situ study found that the advective supplied organic carbon was in balance with the organic carbon required for benthic mineralization (Rusch and Huettel 2000). However, as the activity of permeable sands may be closely linked to pore water advection, the choice of the methods for mineralization rates measurements is critical. Stirred benthic chambers generate pressure gradients and pore water circulation patterns, resembling those generated by currents interacting with topography (Huettel and Rusch 2000), but, in order to mimic natural pore water advection rates, intensive studies on local hydrodynamics and sediment topography are necessary. For the measurement of oxygen consumption rates (OCR) that include the effects of pore water advection, we chose a recently introduced method that combines in situ time series of oxygen depth measurements with laboratory measurements of potential volumetric sedimentary OCR (De Beer et al. 2005; Polerecky et al. 2005).

Our aim was to investigate in situ the influence of pore water advection on mineralization rates and on sediment oxygenation. We investigated whether inundation time of the sediments leads to spatial patterns of oxygen distribution and dynamics and mineralization rates across an intertidal sandflat. We, therefore, measured oxygen dynamics, sedimentary oxygen consumption rates and sulfate reduction rates at three stations along a transect stretching from the low water line towards the high water line during different seasons. We discuss the role of transport processes that are connected to inundation time, such as pore advection and drainage, for the determination of magnitude and patterns of mineralization rates.

## Material and Methods

*The study site*- The study was conducted on the intertidal sand flat "Hausstrand" in the Sylt/Rømø Basin in the North Frisian Wadden Sea, Germany (Fig. 1). The basin is a semi-enclosed lagoon, connected to the North Sea through a channel (Lister Tief) in the north. The influence of freshwater in the basin via atmospheric input or fresh water runoff is small, being less than one thousandth of the tidal water exchange with the North Sea. The investigated intertidal flat is situated south of List Harbour and stretches over approx. 500 m in north south direction. From the low water line the tidal flat stretches over a 100 m wide, rather level zone, followed by a 30 m wide, steeper sloping beach face. The tidal flat is protected from the prevailing westerly winds by the island and from currents by a short dam. Current velocities reach 0.5 m $s^{-1}$.The tidal amplitude is ca. 1-2 m. The origin of the sand is mainly eolic.

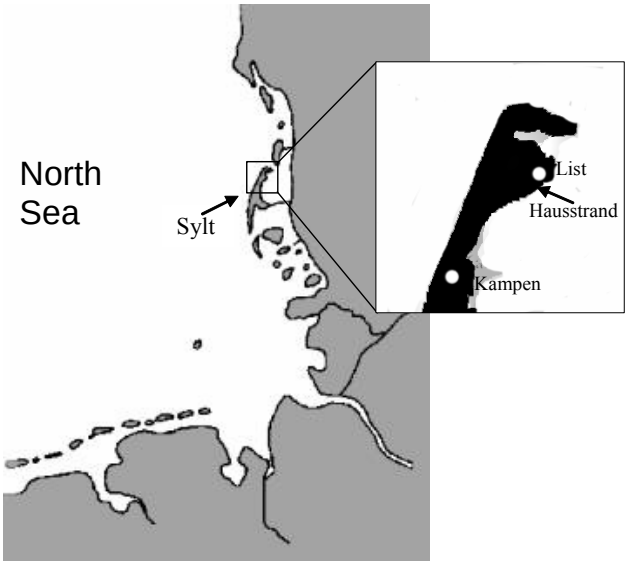


Figure 1: Location of the island Sylt in the North Sea and close up on the northern part with the investigated intertidal flat Hausstrand.

The investigation campaigns covered three seasons, and were conducted in April and August 2002 and February and June 2003. Investigations were conducted on the level part of the tidal flat, where sediments remain water saturated during exposure due to capillary forces. Three stations were chosen, with a distance of ca. 40 m between stations. The lower flat station was situated close to the mean low

water line (N 55°00'52.8; E 008°26'16.9), the middle flat station was situated in the middle of the transect and was in February and June 2003 influenced by a shallow (ca.0.5-2 cm deep) but broad (up to 5 m wide) tidal gully. The upper flat station was located at the upper end of the dissipative zone (ca. 10 m in front of the mean high water line). The mean water level above the sediment during inundation was 1.9 m at the lower station, 1.50 m at the middle station and 1.30 m at the upper station. The abundance of macrofauna at the Hausstrand is rather low (7 individuals per 10 $cm^2$), whereas meiofauna is abundant (6000 individuals per 10 $cm^2$) (Armonies and Hellwig-Armonies 1987).

*Sampling*- If not stated differently below, sediment samples for laboratory analysis or experiments were taken with plastic core liners with an inner diameter of 3.6 cm. Sampling depth was 10 to 15 cm. All samples at one station were randomly taken within 2 $m^2$. The investigated parameters, number of replicates and incubation temperature used for rate assessment are summarized in Table 1.

*Sediment characteristics*- Grain sizes were determined by sieving sediments through a calibrated sieve stack. Sediments were pooled over 0-3, 4-10 and 11-15 cm depth intervals. Porosity was calculated from the weight loss of a known volume of wet sediment after drying at 60°C until weight constancy (1 cm depth resolution). Permeability was measured using the constant head method (Klute and Dirksen 1986) on cores of ca. 15 cm length. Four different pressure heads were applied per replicate core.

*In situ sensor studies*- For in situ profiles, microsensors were mounted on a deep-sea profiler as described previously (Glud et al. 1999; Wenzhöfer et al. 2000). Oxygen was measured using Clark type oxygen microelectrodes (Revsbech 1989) with a tip diameter of 300 µm to prevent damage by the coarse grains, an actual sensing surface of 5 µm and a response time ($t_{90}$) of less than 5 seconds. Temperature was measured with a Pt100 electrode (tip diameter: 3 mm; Umweltsensortechnik, Germany). For the monitoring of the sediment surface, a resistivity sensor was employed. The profiling device was positioned on the sediment with the microsensors initially 1-2 cm above the sediment surface. Downward profiles were continuously measured over several tidal cycles (up to 56 h) to a sediment depth of 6 to 7 cm, (step size of 1 mm). One profile was

recorded within 25-35 min, with a minimum pause of 5 min between the profiles to reduce effects of holes formed by the intruding microsensors.

Table 1: Overview of investigated parameters per station for the four investigation campaigns. Numbers in parentheses identify the number of replicate sediment cores or seawater samples taken for analysis. Number in brackets for water column current velocities and pore water flow velocities identify the number of inundation or exposure periods where measurements were conducted. For additional details see text.

| Parameter | April 2002 | August 2002 | February 2003 | June 2003 |
|---|---|---|---|---|
| in situ $O_2$ | all | all | all | all |
| OCR | MF (3) | LF, MF (1); UF (2) | all (3-4) | all (3)SRR |
| | all (3) | all (3) | all (2) | all (3) |
| Add. OCR | | | LF, UF (1) | all (1) |
| Add. SRR | | | all (2) | all (2-3) |
| Incub. T (°C) | 10 | 20 | 2 | 18 |
| Porosity | all (2) | all (3) | all (2) | |
| Grain sizes | all (2) | all (2) | all (2) | |
| Permeability | LF, MF (2[a]) | MF (3[a]) | | |
| TOC (sed.) | all (2) | all (2-3) | all (2) | all (2) |
| PW solutes | LF, MF(3[b]) | LF, MF(3[b]);UF (2) | LF,MF(3[b]);UF (2) | all (1) |
| SW sol./OC | (3) | (4) | (4) | (3) |
| Water column current velocity | | | LF, MF [2] | MF [2] |
| Pore water flow velocity at sediment depth: | | | | |
| 2 cm | | | | MF, LF [2-3] |
| 5 cm | | | | MF [3] |
| 10 cm | | | | MF [1] |

Abbreviations:
all = all stations; LF= lower flat station; MF= middle flat station; UF= upper flat station; Add. = addition experiment OCR and SRR; Incub. T= incubation temperature for OCR and SRR, PWsolutes= pore water solutes (DOC, nutrients, sulfate, salinity); SW sol./OC =sea water column solutes and particulate organic matter

[a] 4 different pressure heads were applied per replicate core

[b] 5-6 cores pooled per replicate; replicates taken at three time points over the tidal cycle

*Oxygen consumption rates*- Measurements of potential volumetric oxygen consumption rates (pOCR) were performed in the laboratory on freshly collected intact sediment cores as described previously (De Beer et al. 2005; Polerecky et al. 2005). Experiments were conducted in the dark at the average in situ temperature of the respective month (Table 1). Air-saturated ambient sea water was percolated through the sediment cores until oxygen was present in high concentrations at the depth of measurement. After the percolation was stopped, the decrease of oxygen in time was monitored by an oxygen microsensor (April 2002) or a planar oxygen

optode (all other campaigns). The initial oxygen concentration decrease at the measuring depths was taken as the potential OCR. For the assessment of pOCR with planar optodes, we used rectangular stainless steal cores (inner dimensions 70 x 75 mm, height 250 mm, wall thickness 2 mm) that had at one side a polycarbonate window to which a semi-transparent oxygen optode was glued. The planar optode technique allowed the calculation of pOCR with a resolution of ≈ 300 µm over the entire optode area (ca.25 x 150 mm; resulting oxygen image size 80 x 480 pixels). For the assessment of pOCR with oxygen microsensors, the microsensor was positioned at a defined depth within the sediment cores and the cores were repetitively percolated to obtain a profile of pOCR with depth intervals of 2 mm (0-3 cm depth) to 5 mm (below 3 cm).

The obtained volumetric data represent the potential oxygen consumption, whenever oxygen is present at the specific sediment depth. To obtain the areal OCR of the sediments, the rates were integrated over the various depths of oxygen penetration as obtained in situ from the automatic profiler as described previously (De Beer et al. 2005). We assumed pOCR to follow zero order kinetics with respect to oxygen (Thamdrup et al. 1998). For the assessment of daily areal OCR, all oxygen penetration depths measured over full tidal cycles were used, so that daily areal OCR reflect the oxygen availability of the distinctive inundation and exposure periods of the three stations.

*Sulfate reduction rates*- Potential sulfate reduction rates (pSRR) were measured with the whole core $^{35}SO_4^{2-}$ radiotracer incubation method (Jørgensen 1978) modified for permeable sediments (De Beer et al. 2005). Radiolabeled $^{35}SO_4^{2-}$ (Amersham) was added to 70 mL of ambient seawater to a specific activity of 340MBq/mol $SO_4^{2-}$. The seawater-tracer solution was allowed to percolate into the core. The permeability of the sediment allowed an even distribution of tracer in the pore water within 1 min. After an incubation of 4 to 6 h at the average in situ temperature (Table 1), sediments were sliced in 1 cm sections and incubation was terminated by transferring the sediments into 20% ZnAc. Samples were processed using the cold chromium distillation procedure (Kallmeyer et al. 2004). Radioactivity of $^{35}SO_4^{2-}$ and Total Reduced Inorganic Sulfur (TRIS) was determined with a liquid scintillation counter (Packard 2500 TR), using Lumasafe Plus® (Lumac BV, Holland) scintillation cocktail.

Sulfate reduction rates were assessed in the laboratory under stagnant flow conditions, the supply of oxygen was thus restricted to molecular diffusion. In the field oxygen penetrates much deeper into the sediments and may lower sulfate reduction rates. The anoxic conditions during incubation may lead to an overestimation of sulfate reduction rates, although sulfate reduction has been measured in oxidised and oxic sediments (Jørgensen 1977; Jørgensen and Bak 1991). Because of the uncertainty about the inhibitory effects of oxygen, we made maximum and minimum estimations. The maximum depth integrated sulfate reduction rates ($SRR_{max}$) were not corrected for possible oxygen inhibition. To obtain a minimum assessment of depth integrated SRR ($SRR_{min}$), i.e., assuming that oxygen completely inhibits sulfate reduction, pSRR were integrated over the anoxic sediment depths only, as deduced from the in situ oxygen measurements.

*Estimation of aerobic mineralization rates*- Aerobic mineralization cannot be directly measured and was, therefore, calculated from areal OCR and $SRR_{max}$. Oxygen consumption rates represent the sum of aerobic mineralization and oxidation of reduced substances from anaerobic decay (e.g., $Fe^{2+}$ and $H_2S$). The sulfides produced by sulfate reduction are oxidized back to sulfate within the sediments, using oxygen as the ultimate electron acceptor. Therefore the aerobic mineralization rates were calculated by subtracting the sulfate reduction rates (expressed in equivalents of oxygen used for the oxidation of sulfides to sulfate) from the measured oxygen consumption rates. We considered sulfate reduction to be the most important anaerobic respiration process (Jørgensen 1982), the others were not considered.

*Organic matter addition experiments*- The percolation methods for the measurement of pOCR and pSRR allow the addition of water soluble substances together with the seawater solution to the whole sediment cores. We added glucose (2 mmol $L^{-1}$) to determine a stimulation of pOCR by organic substances, whereas acetate (2 mmol $L^{-1}$) was added to determine a stimulation of pSRR. The assessment of pOCR before and after addition were performed in the same core, for pSRR separate cores were taken.

*Estimated bottom water filtration rates*- The estimation of bottom water filtration rates (L $m^{-2}$ $d^{-1}$) during inundation was based on the simplified assumption that the oxygen penetration depth is controlled by the balance between

a vertical downward transport of oxygen and the sedimentary pOCR. By combining the oxygen penetration depth and pOCR data the rate of oxygen supply to the sediment was calculated. From the supply rate of oxygen, one can calculate how much water is pumped through the sediments (bottom water filtration rates) by using the oxygen concentration in the overlying water (Polerecky et al. 2005):

$$v_f = \int_0^{z_p} OCR(z)dz \times c_o^{-1}$$

with $v_f$ being the flow rate in L $m^{-2}$ $h^{-1}$, $\int_0^{z_p} OCR(z)dz$ being the oxygen consumption rates integrated over the oxygen penetration depth ($z_p$) in mol $m^{-2}$ $h^{-1}$ and $c_0$ being the oxygen concentration in the overlying water in mol $L^{-1}$. By using the bottom water filtration rate and the POC content or the chlorophyll *a* concentrations of the water column, one estimate the amount of organic carbon that is transferred to the sediments by pore water advection.

*Water column current velocities*-Water currents 5 cm above the sea floor were measured using a Nortek™ Acoustic Doppler Velocimeter (ADV) that measures 3 components (*x*, *y*, *z*) of the flow velocities within a cylindrical sampling volume (ca. 6 mm in diameter and 6 mm in height) located 100 mm below the probe. Flow velocities were recorded with a sampling frequency of 0.5 Hz during February 2003 and with 25 Hz during June 2003. The water current velocity was calculated for each sampling using the scalar of the 3 velocity components and averaged over 1 minute intervals.

*Pore water flow velocity*- Pore water flow velocity was measured on the middle station and at the lower flat station in June 2003 using a slight modification of the method described by Precht and Huettel (2004). The passage of a fluorescent dye tracer (Fluorescein, 100 mg $L^{-1}$) through the sediments was followed by 6 optical glass fibre sensors (tip diameter 140µm, Radiall®) fixed to a plane wire mesh. As the in situ dye signal intensity is influenced by the pore space in front of the sensor, values are given as normalized sensor signals. Prior to measurements of the drainage flow during exposure, dye was injected directly into the sand and dug out later, to visually determine the main flow direction. Then, a small incision was cut into the sediment to the desired depth (see Table 1) and the set-up was carefully inserted horizontally several cm into the undisturbed part of the sediment. After rebuilding the sediment surface, 1 mL of dye solution was injected through a

syringe needle that was fixed to the upstream end of the mesh. The average pore water flow velocity was calculated for all measurements from the time interval between the geometric centroids of the signal curves at consecutive sensors. Dye was injected during exposure at falling tide, at low tide and rising tide and on the transition to inundation. Experiments during inundation were tested with the set-up being inserted into the sediments with various angles with respect to the sediment surface.

*Sedimentary organic carbon and pore water solutes*- Sediment samples for TOC analysis were sectioned into 1 cm slices and stored at -20°C. Before analysis, samples were freeze dried, ground, and acidified with 1 N HCL to remove the inorganic carbon. The samples were transferred into tin cups and [TOC] was measured using a Heraeus CHNO-rapid elemental analyzer with sulfanilamid as a calibration standard.

Pore water was extracted from all stations (1 cm depth intervals, 5 - 6 cores pooled) for the analysis of DOC, pore water nutrients (ammonium, nitrate, nitrite, phosphate, and silicate), sulfate and salinity. The sediment samples were placed into a Buechner-funnel on top of a nylon mesh. The funnel was inserted into a pressure chamber with the outflow of the funnel protruding from the chamber. Inert gas was then blown into the chamber and the pore water was collected at the outflow of the funnel. The pore water was filtered through a nylon syringe filter with 0.2 µm pore size (Millex GN, Millipore) and transferred into pre-combusted glass vials (DOC) or plastic vials (nutrients, sulfate, salinity). The whole procedure was conducted under anoxic conditions in a glove box. Pore water samples were stored at -20°C until analysis. For the calculation of DOC, total dissolved carbon (TDC) and dissolved inorganic carbon (DIC) concentration was measured by high temperature catalytic oxidation using a Shimadzu$^{TM}$ TOC-5050A analyzer connected to a Shimadzu ASI 5000A autosampler. Bicarbonate and phthalate were used as calibration standards. DOC was obtained by subtracting DIC from TDC. Pore water nutrients were analysed spectrophotometrically with a Skalar Continuous-Flow-Analyzer according to (Grasshoff et al. 1999). For the upper flat station, pore water had to be stored in glass vials in some cases, therefore, silicate measurements for the first campaigns were not considered. Pore water sulfate concentrations were determined by non-suppressed ion-chromatography and

conductivity detection with a Waters 510 HPLC pump, Waters WISP 712 autosampler, Waters IC-Pak anion exchange column (50 x 4.6 mm) and a Waters 430 Conductivity detector. The eluant was 1 mM isophthalate buffer in 10% methanol, adjusted to pH 4.5. Salinity was measured using a refractometer. To test whether advective exchange of pore and overlying water is reflected in altering DOC and nutrients concentrations, pore water was extracted on different times during the tidal cycle on the lower and the middle flat. The first sampling was 20 min after incoming tide, the second sampling at high tide and the third sampling at low tide.

*Water column parameters*- Water samples for the analysis of particulate organic carbon (POC) and suspended matter (SM) were filtered on weighted and pre-combusted (600°C, 6h), Whatman GF/F filters (0.7 µm pore size), rinsed with Milli Q to remove the sea salt and stored frozen until analysis. Before analysis of POC, samples were pre-treated with 1N HCL to remove the inorganic carbon, dried and transferred into tin cups. POC was analyzed using a Heraeus CHNO-rapid elemental analyzer with sulfanilamid as a calibration standard. SM was determined by the weight differences of the empty and loaded dry filter. The filtrate was further filtrated through a nylon syringe filters (see above) and analyzed for DOC and nutrients as described above.

Water samples for the analysis of chlorophyll a content were filtered on Whatman GF/C filters (0.7µm pore size). Acetone was used as extraction solvent (extraction time 18h at 4°C) and the chlorophyll a content was determined photometrically. Samples were taken every 3-5 days within an annual sampling campaign of water column parameters at Sylt.

## Results

*General site description*- The average daily inundation time was 7.5 h longer at the lower flat station than at the upper flat station (Table 2). In June, inundation times were longest at all stations. The inundation times were calculated over a 4 week period, including the three weeks of the investigation campaigns (tide gauge List, with permission of Wasser- und Schifffahrtsamt Tönning, Germany). The sediment properties did not vary between stations nor between seasons. The sediments consisted of silicate grains with a median grain size of 380 µm and were very well sorted medium sands (Wentworth 1922). Porosity was on average (± S.D.) 41 (± 3) % in the upper 2 cm of the sediment and 35 (± 3) % below. The sediments were highly permeable, on average 3.9 x $10^{-11}$ (± 0.3) $m^2$.

Table 2. Averaged inundation times, bottom water filtration and organic carbon infiltration during inundation at the three transect stations. For the calculation of daily bottom water filtration rates (L $m^{-2}$ $d^{-1}$) for each station, the average bottom water filtration rate from all stations recorded in April, June and August (19 L $m^{-2}$ $d^{-1}$) and the averaged inundation times of the respective stations were used. The amount of infiltrated organic carbon per station was calculated from the daily bottom water filtration rate and an averaged water column POC content of 0.06 mol $L^{-1}$.

| Inundation time (h $d^{-1}$) | upper flat | middle flat | lower flat |
|---|---|---|---|
| April | 12.9 | 15.2 | 20.2 |
| June | 15 | 17.8 | 22.4 |
| August | 14.1 | 16.6 | 22.4 |
| February | 13 | 15.7 | 20.4 |
| Bottom water filtration rate (L $m^{-2}$ $h^{-1}$) | | | |
| April | | 12 ± 2 | |
| August | 25 ± 5 | 16 ± 6 | 34 ± 13 |
| June | 13 ± 5 | 15 ± 6 | 21 ± 7 |
| February | 1.8 ± 0.5 | 3.3 ± 0.6 | 1.4 ± 0.4 |
| Daily bottom water filtration rate (L $m^{-2}$ $d^{-1}$) | | | |
| | 260 | 310 | 405 |
| Organic carbon infiltration (mmol C $m^{-2}$ $d^{-1}$) | | | |
| | 15 | 18 | 24 |

The average water temperatures during the measurement campaigns are presented in Table 3. Highest temperatures were measured in August 2002.

Table 3: Water column temperature, water column and pore water salinity, water column and pore water sulfate concentrations, water column POC, suspended matter (SM) and water column chlorophyll *a* content. Numbers after ± indicate standard deviation.

| | Temp. (°C) | Salinity | $SO_4^{2-}$ (mmol $L^{-1}$) | POC (µmol $L^{-1}$) | SM (mg $L^{-1}$) | Chl a (µg $L^{-1}$) |
|---|---|---|---|---|---|---|
| February | - 0.1 ± 0.4 | 28 | 22.2 ± 0.6 | 108 ± 20 | 84 ± 12 | 2.6 ± 0.4 |
| April | 8.5 ± 1.2 | 26-27 | 21.0 ± 0.6 | 60 ± 21 | 26 ± 4 | 16.6 ± 7.8 |
| June | 16.5 ± 1.0 | 31 | 24.1 ± 0.4 | 51 ± 4 | 74 ± 4 | 2.6 ± 1.9 |
| August | 21.0 ± 0.7 | 29-30 | 23.2 ± 0.5 | 56 ± 6 | 34 ± 25 | 3.6 ± 0.8 |

*Oxygen penetration depth and dynamics*- Oxygen penetrated deep and varied dynamically in time at all stations. The oxygen penetration depths were significantly different (non parametric U-test, $p < 0.01$, all stations, except at lower flat in February) between inundation and exposure periods of the flat, with the oxygen penetration being deeper and more variable during inundation. Exemplary time series of oxygen profiles are shown in Figure 2a-c and a summary of all oxygen penetration depths during exposure and inundation is given in Figure 3.
The simultaneous employment of the ADV and the automatic profiler clearly showed a covariance of the oxygen penetration depth and current velocity of the overlying water during inundation (Fig. 4). Oxygen penetration and dynamics during inundation were also enhanced during strong winds and waves (Fig. 5). The oxygen profiles that were measured during inundation often had a sigmoidal shape (Fig. 6 a). During the exposure of the flat, some oxygen profiles had a nearly parabolic shape (Fig. 6 b). During exposure benthic photosynthesis could increase oxygen penetration depth (Fig. 6 b).

The oxygen penetration depths and dynamics were comparable between the three transect stations during the inundation period within a campaign (Fig. 3). Also the oxygen penetration depths were similar between the three transect stations during exposure periods of a campaign (Fig. 3). Only in April, oxygen penetrated deeper at the lower flat during both inundation and exposure.

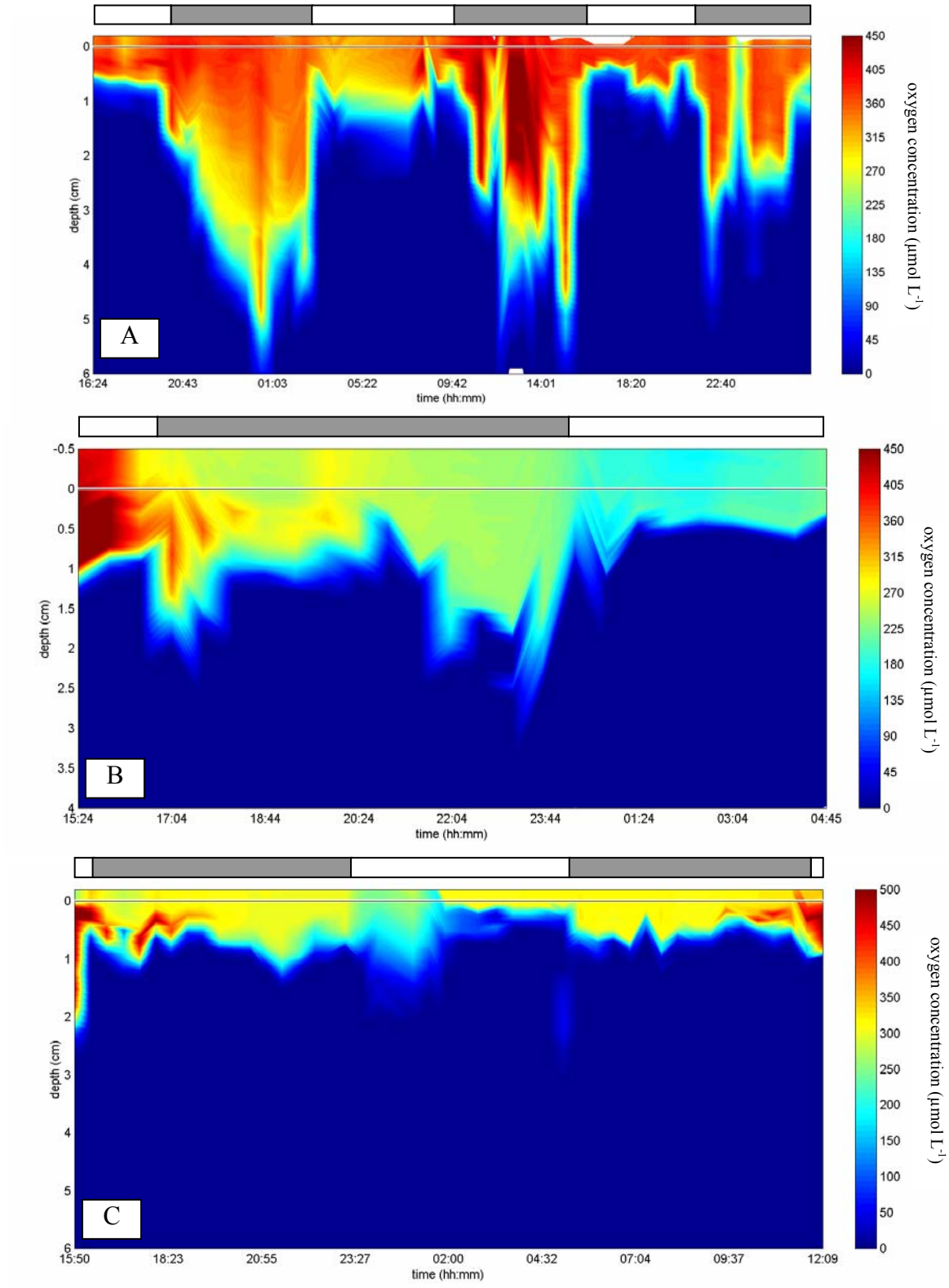


Figure 2 a-c: Time series of oxygen concentration profiles in the upper flat station in a) February, b) April and c) June. White and grey bars indicate exposure and inundation periods at the stations, respectively. Note that the total duration of the time series differs in all graphs.

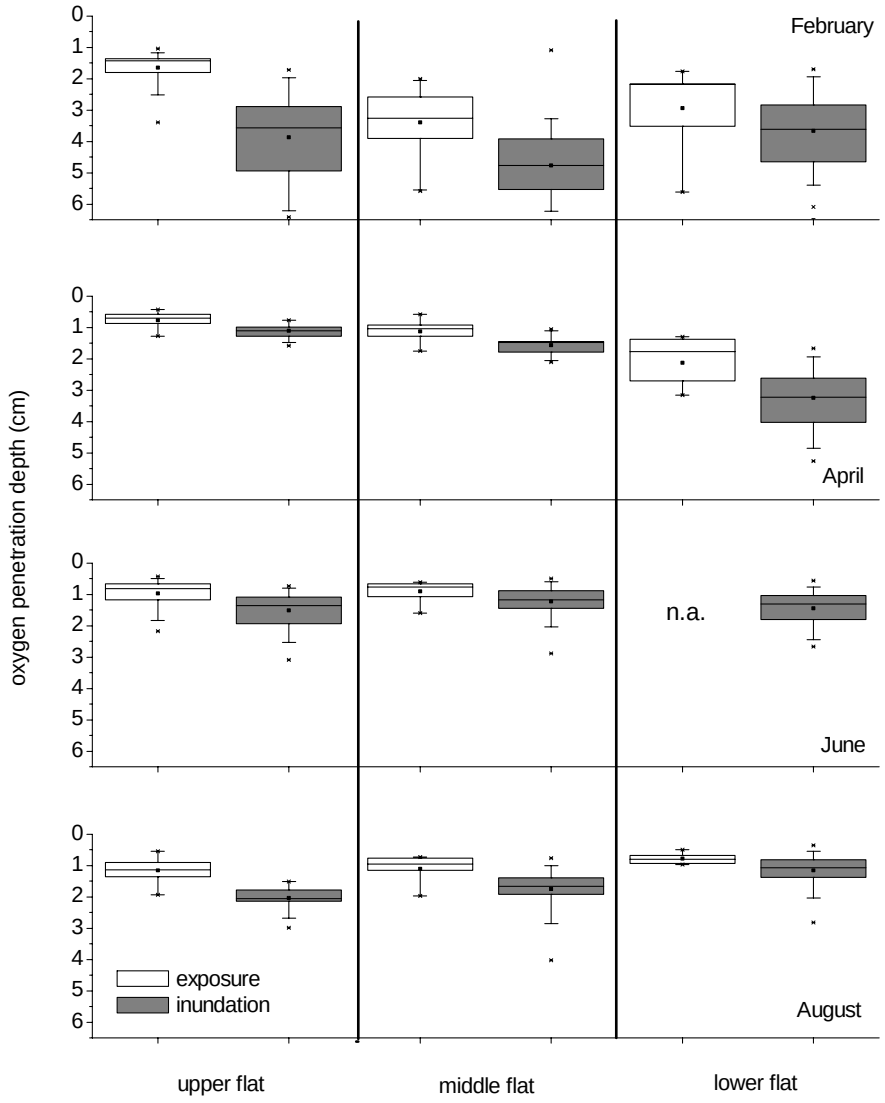


Figure 3: Oxygen penetration depths measured at the three transect stations during exposure and inundation of the flat. The horizontal lines of the box denote the 25th, 50th, and 75th percentiles, the square dot side the box represents the mean. The error bars denote the 5th and 95th percentiles, the symbols above and below the whiskers represent the extremes. The lower station was not exposed in June to the high water level in the Sylt/ Rømø Basin.

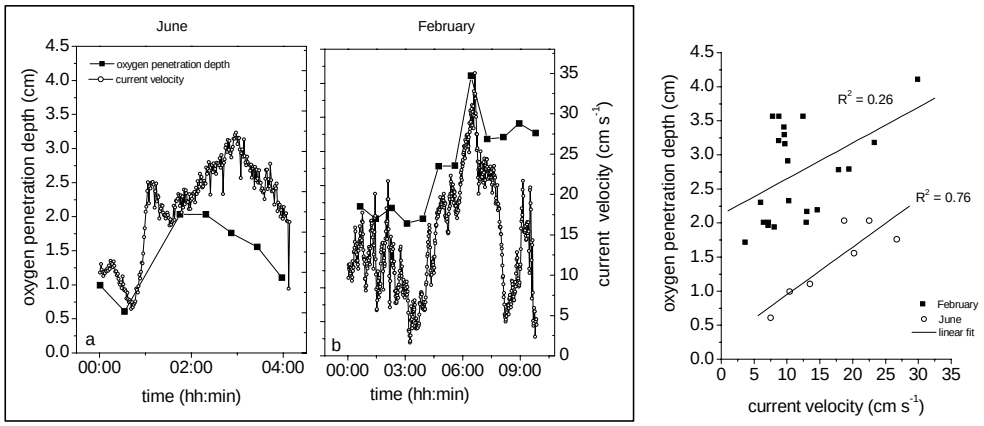


Figure 4: Current velocity measured at 5 cm above the sediment in relation to oxygen penetration depth for June (a) and of one exemplary data set for February (b). Linear regression plots of oxygen penetration depth against current velocity for June and for all February data.

There was a strong dependency of oxygen penetration depth with season (e.g., Fig. 3). With similar current velocities of the overlying water oxygen penetrated deeper in winter than in summer (Fig. 4).

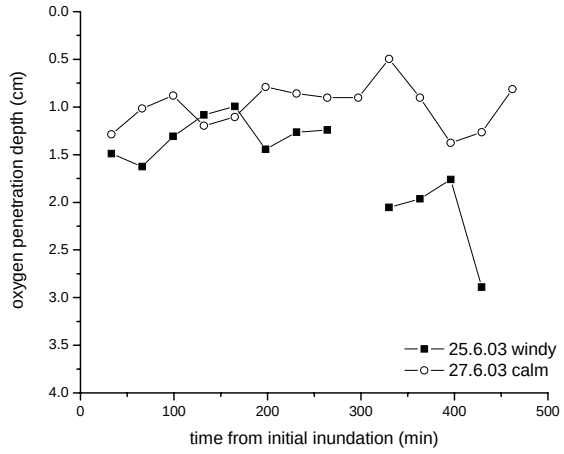


Figure 5: Dependence of oxygen penetration depth on the weather conditions, measured during inundation at the middle flat station in June.

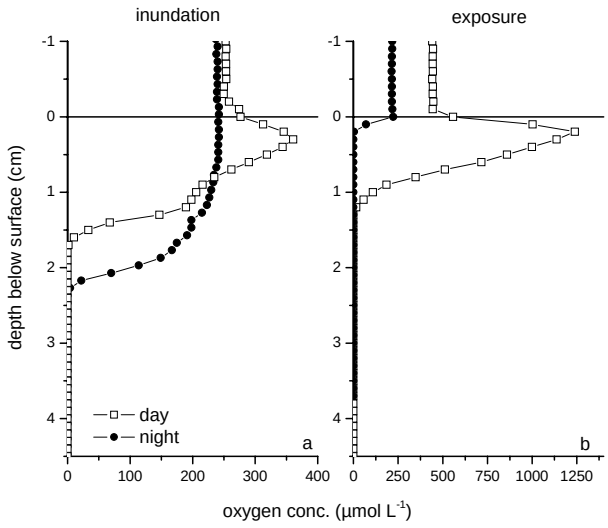


Figure 6: Exemplary day (open symbols) and night (filled symbols) oxygen profiles during inundation (a) and exposure (b) measured at the upper station (June). The subsurface oxygen peak of the day profiles indicates oxygen production by benthic photosynthesis. The night profile during inundation shows the oxygen supply to deep sediment layers by advection, whereas the oxygen distribution measured during exposure at night is dominated by diffusion.

*Oxygen consumption rates*- The potential OCR in the oxygenated sediment layers are presented in Figure 7. Most of the potential OCR profiles had a small peak in the top centimeter of the sediment, and were otherwise rather constant with depth. In the summer months June and August, the highest potential OCR were found near the low water line. The potential OCR rates were strongly influenced by season, being approx. 10 to 20 times higher in the summer months than during winter. Areal OCR were higher during inundation than during exposure because oxygen penetrated deeper when water was present over the sediment (Fig. 8). At all stations, 71 to 90% of the daily areal OCR took place during inundation (Fig. 9). In August and June, highest areal OCR were found at the lower flat station, in February, the intermediate station showed the highest rates (Fig. 9 and Table 4). The differences between the remaining stations were not pronounced. Areal OCR showed a pronounced seasonal variability, with lowest rates found in winter. In spring and summer areal OCR were comparably high.

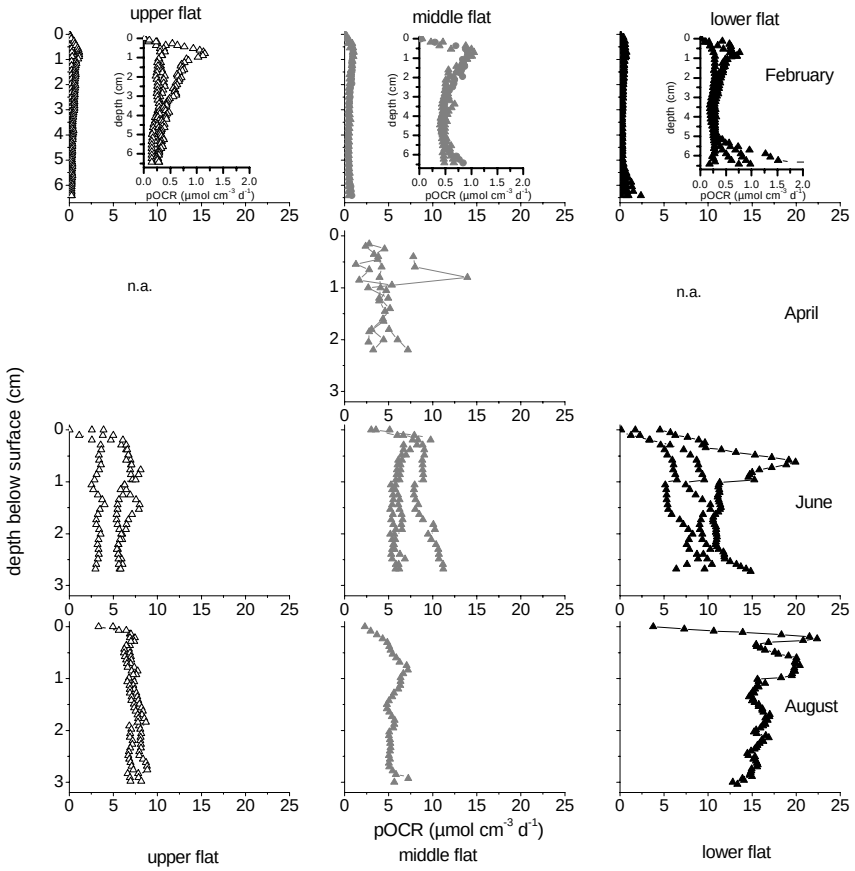


Figure 7: Depth profiles of volumetric potential OCR (pOCR) in the oxygenated sediment layer at the three transect stations during the four measurement campaigns. The different lines per layer represent replicate cores. The inserted graphs for February show the pOCR values in different scale.

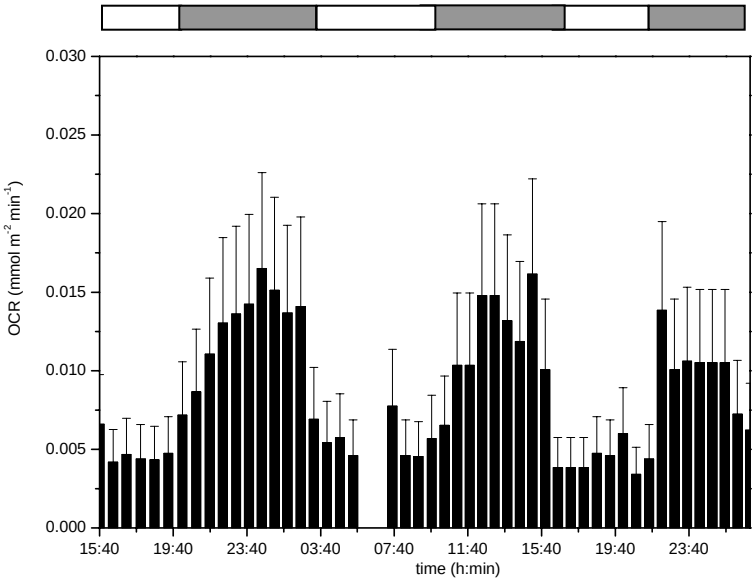


Figure 8: Effect of inundation on areal OCR shown for three tidal cycles at the upper flat in February. White and grey bars above the figure indicate exposure and inundation period of the station, respectively.

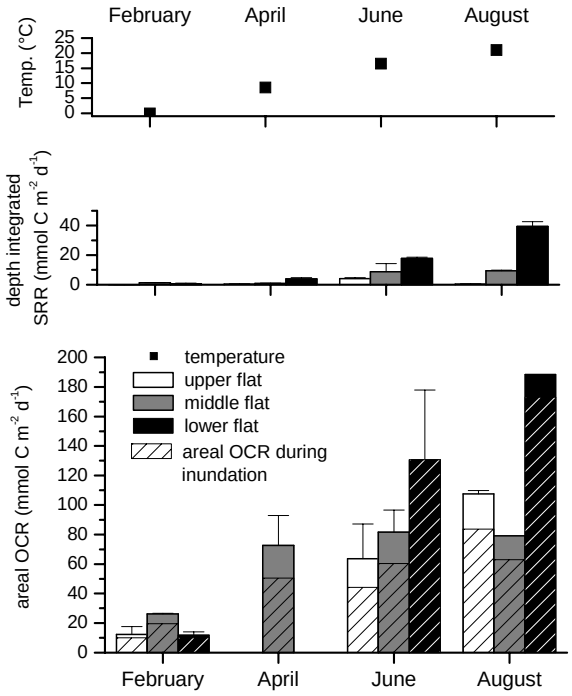


Figure 9: Areal OCR and depth integrated SRR calculated for the actual daily inundation and exposure times at the three stations, and average water column temperature. The hatched parts of the column show the part of the daily areal OCR that takes place during inundation. Note that in June the lower flat station remained inundated.

*Sulfate reduction rates*- Potential sulfate reduction rates decreased from the lower flat station towards the upper flat during all seasons (Fig. 10). The differences between stations were most pronounced in August. Potential SRR had a peak or increased below 1-2 cm depth in spring and summer, with the peak width increasing towards the lower flat. In winter, pSRR increased below 4-5 cm depth. The pSRR were the highest in summer. In contrast to the pOCR, pSRR were low in spring. The extent of seasonal variability depended on the station (Fig. 10, Table 4), with highest seasonal variability found at the lower flat and smallest seasonal differences at the upper flat. Pore water sulfate concentrations at all depths were equal to sea water concentrations at all stations (Table 4) and were, thus, not limiting pSRR. Differences between the depth integrated maximum and minimum SRR ($SRR_{max}$ and $SRR_{min}$) were small (Table 4).

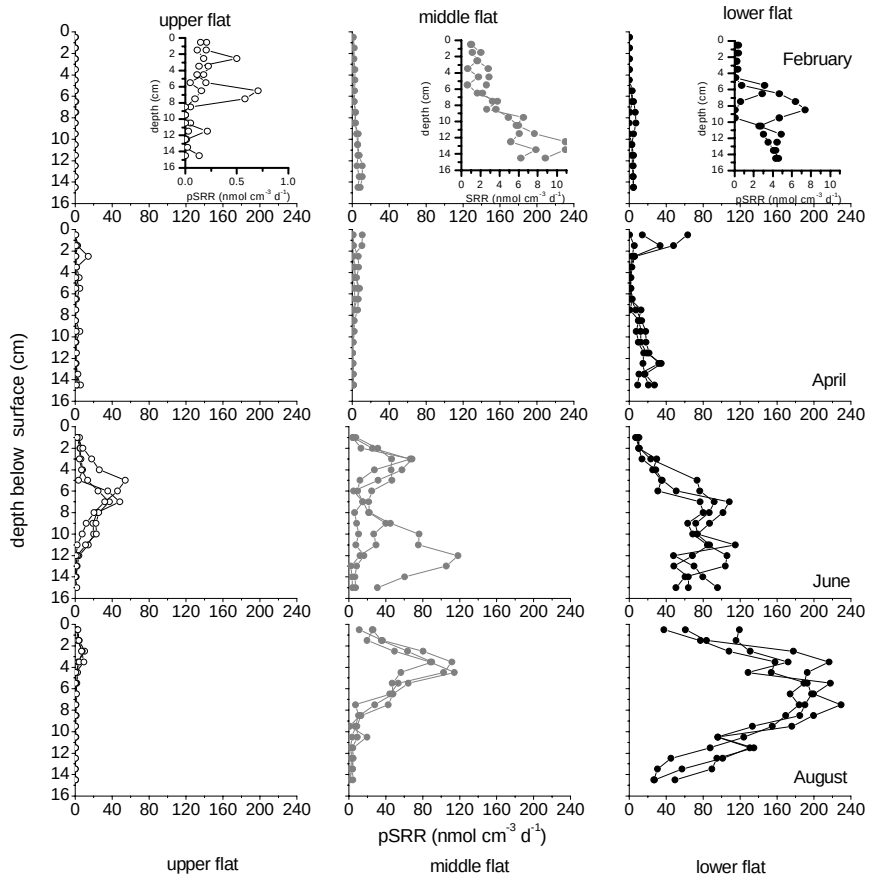


Figure 10: Potential SRR at the three transect stations during the four measurement campaigns. The different line graphs represent replicate cores. The inserted graphs in February show the pSRR in different scale.

The contribution of sulfate reduction to total mineralization increased towards the low water line (Table 4). A maximum contribution of 21% was found in August at the lower flat station. At the upper flat station sulfate reduction contributed less than 1% to total mineralization in August and February, but 6% in June. These estimates assume that other anaerobic processes had only negligible influence on mineralization.

*Aerobic mineralization*- The calculated areal aerobic mineralization rates (areal OCR corrected for the oxygen uptake by the $H_2S$ produced by sulfate reduction) were high and deviated less than 10% from areal OCR (Table 4), as SRR were comparably low.

Table 4. Average areal OCR, estimated aerobic mineralization rates and depth integrated SRR (mmol C $m^{-2}$ $d^{-1}$), and contribution of SRR to total mineralization (in %). $SRR_{max}$ are SRR integrated over the top 15 cm of sediments, whereas $SRR_{min}$ are SRR integrated only over the anoxic layers of the sediment. The contribution of SRR to total mineralization is based on $SRR_{max}$. Numbers after ± indicate standard deviation.

| Min. rates (mmol C $m^{-2}$ $d^{-1}$) | upper flat | middle flat | lower flat |
|---|---|---|---|
| February | | | |
| OCR | 12.2 ± 5.3 | 26.2 ± 0.3 | 11.9 ± 2.3 |
| aerobic min. | 12 | 25 | 11 |
| $SRR_{max}$ | 0.04[a] ± 0.02 | 1.24[a] ± 0.24 | 0.71[a] ± 0.28 |
| $SRR_{min}$ | 0.03 ± 0.02 | 1.11 ± 0.22 | 0.69 ± 0.28 |
| contribution SRR (%) | 0.3 | 4.7 | 6.0 |
| April | | | |
| OCR | | 72.5 ± 20.3 | |
| aerobic min. | | 71 | |
| $SRR_{max}$ | 0.47 ± 0.18 | 0.78 ± 0.18 | 3.8 ± 0.9 |
| $SRR_{min}$ | 0.44 ± 0.19 | 0.37 ± 0.28 | 2.7 ± 0.2 |
| contribution SRR (%) | | 1.1 | |
| June | | | |
| OCR | 63.6 ± 23.5 | 81.5 ± 15.0 | 130.7 ± 47.2 |
| aerobic min. | 59 | 73 | 113 |
| $SRR_{max}$ | 4.1 ± 0.5 | 8.8 ± 5.5 | 17.7 ± 0.9 |
| $SRR_{min}$ | 3.9 ± 0.4 | 8.6 ± 5.5 | 17.4 ± 0.9 |
| contribution SRR (%) | 6.4 | 10.8 | 13.6 |
| August | | | |
| OCR | 107.6 ± 2.1[a] | 79.2[b] | 188.6[b] |
| aerobic min. | 107 | 70 | 149 |
| $SRR_{max}$ | 0.51 ± 0.07 | 9.4 ± 0.4 | 39.4 ± 3.2 |
| $SRR_{min}$ | 0.40 ± 0.05 | 8.6 ± 0.5 | 37.6 ± 2.2 |
| contribution SRR (%) | 0.5 | 11.9 | 20.9 |

[a] n=2, [b] n=1

*Stimulation of OCR and SRR by organic matter addition*- Addition of dissolved organic carbon usually stimulated OCR and SRR (Table 5), except for February, where no stimulation of OCR was measurable. Glucose addition in June enhanced OCR 1.3 to 1.5-fold. The stimulation of SRR was most pronounced at the lower flat, where in February an almost 7-fold increases of SRR was recorded after acetate addition. The increase of pSRR varied with sediment depth, with rates being particularly enhanced in the sediment layers where pSRR already had been high prior to the addition of dissolved organic carbon.

Table 5. Organic matter addition experiment. Areal OCR control and areal OCR after the addition of 2 mmol $L^{-1}$ glucose and depth integrated SRR control and depth integrated SRR after the addition of 2 mmol $L^{-1}$ acetate. Numbers after ± indicate standard deviation.

| Rates (mmol C $m^{-2}$ $d^{-1}$) | | upper flat | middle flat | lower flat |
|---|---|---|---|---|
| OCR (Feb. 2003) | control | 18 | | 11 |
| | addition | 16 | | 8 |
| OCR (June 2003) | control | 45 | 82 | 110 |
| | addition | 68 | 104 | 147 |
| SRR (Feb. 2003) | control | 0.04 ± 0.02 | | 0.7 ± 0.3 |
| | addition | 0.08 ± 0.01 | | 4.7 ± 2.9 |
| SRR (June 2003) | control | 4.1 ± 0.3 | 8.8 ± 5.5 | 17.7 ± 0.9 |
| | addition | 5.2 ± 2.1 | 16.5 ± 4.8 | 36.1 ± 2.6 |

*Bottom water filtration rates*- The advective filtration rates of bottom water through the sediments were calculated from oxygen penetration depths and sedimentary pOCR and ranged from 1.4 to 34 L $m^{-2}$ $h^{-1}$. Differences in calculated bottom water filtration rates per hour inundation time (Table 2) were small between the three transect stations in April, June and August. However, the total daily volume of water pumped through the sediments decreased from 405 to 260 L $m^{-2}$ $d^{-1}$ towards the upper station due to decreasing inundation periods. In winter, the bottom water filtration rates showed unrealistically low results and were not included in further calculations. In winter the oxygen penetration depths were mainly influenced by the pressure field across the sediment surface and not by the low sedimentary OCR, thus the basic concept of the estimation could not be applied. Therefore, the winter data were not included in the calculations of advective organic matter supply to the sediments.

The total amount of advective carbon received by the sediments from the water column by advective filtration increased towards the lower flat station (Table 2). This calculation is based on the simplifying assumption that all POC in the infiltrated water volume is captured by the sediments (based on an averaged water POC content of 0.06 mol $L^{-1}$). If the infiltration rates are based on the water column chlorophyll a content, the amount of easily degradable organic carbon supplied to the sediments would in most months be even lower: During the plankton bloom in April, 18, 21 and 28 mmol C $m^{-2}$ $d^{-1}$, in the other month 3, 4 and 5 mmol C $m^{-2}$ $d^{-1}$

were filtered at the high, middle and lower station, respectively (assuming 1 µg chlorophyll a represents algae cells of 50 µg organic carbon).

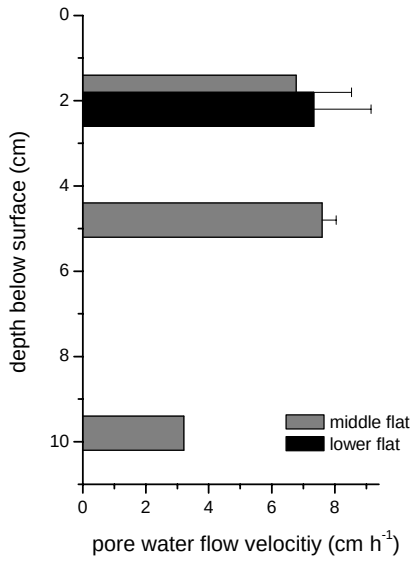


Figure 11: Pore water flow velocities during exposure at 2, 5 and 10 cm sediment depth at the middle and in 2 cm sediment depth at the lower flat station in June.

*Surface pore water flow velocities*- As concluded from the dye experiments, pore water drained towards the low water line during exposure of the flat (Fig. 11). At 10 cm sediment depth the pore water flow velocity (3-4 cm $h^{-1}$) was only half of that in the layers above 5 cm (6-8 cm $h^{-1}$) (Fig.11). The pore water flow velocities were the same at falling and low tide at 2 and 5 cm depth, only at 2 cm depth the flow velocities decreased shortly before re-inundation of the station (data not shown). The flow direction reversed not before the incoming tide was nearly above the measuring set up. During inundation the tracer dye quickly dispersed and was no longer detected by the planar sensor set-up.

*Sediment and water column parameters*- The average TOC content of the sediments was below 0.1% at all stations. The lowest TOC content was always found at the upper station (0.04 ± 0.02% for all investigations). At the middle and lower flat stations the average TOC content varied between 0.05 and 0.09%. The TOC content was highest in the upper 2 cm of the sediments and usually decreased with depth. There was no clear seasonal trend.

Water column POC concentrations were similar in all investigated months except for high values in February (Table 3). There, the high POC content coincided with a high load of suspended matter that may be related to a storm

event. The chlorophyll *a* content in the water column was highest in April and comparable between the other investigation months.

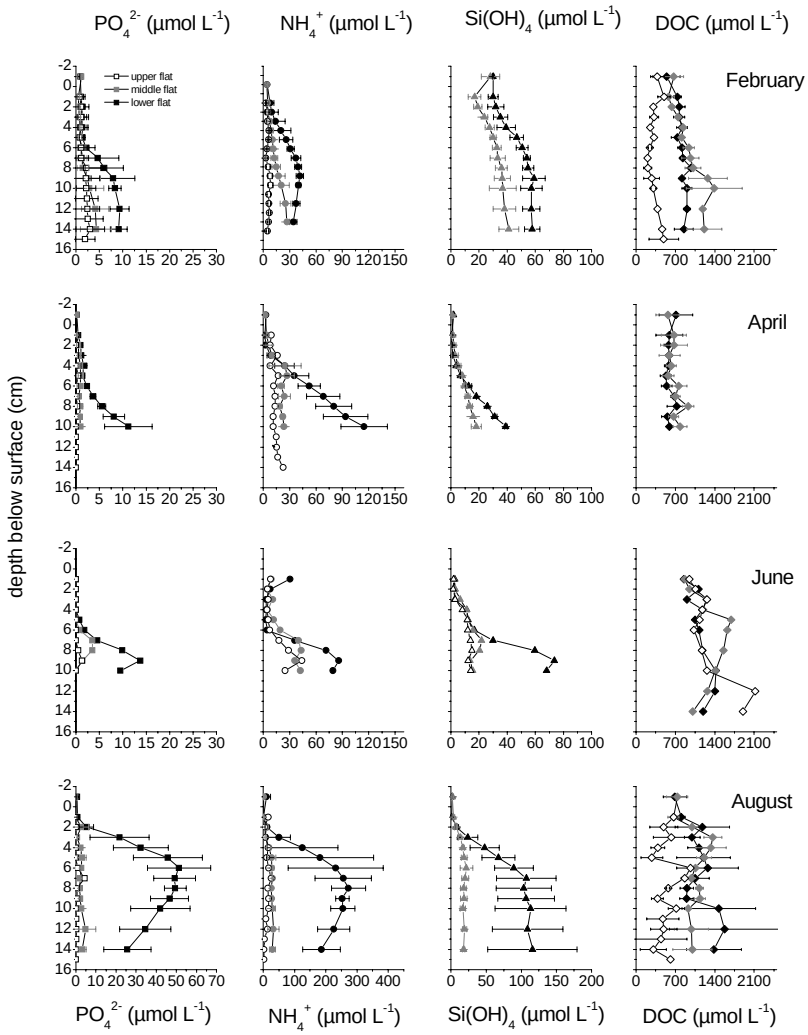


Figure 12: Nutrient and DOC concentrations in pore- and overlying water of the three investigation sites during the four sampling campaigns.

The pore water concentrations of DOC, phosphate, ammonium, and silicate (Fig. 12), did not vary over the tidal cycle, thus measurements were taken as replicates. Pore water DOC in the top centimeter of sediment was close to the DOC content of the water column, below, pore water DOC increased slightly with depth in most measurements. In August and in February, the lower and middle flat station had similar DOC contents, while the upper station had lower DOC concentrations.

In June, DOC content was similar at all stations. DOC was lower in winter than in summer.

Phosphate, ammonium and silicate concentrations in the pore water were highest at the lower flat station and showed a distinct increase below 2-4 cm depth. At the other two stations, this increase was less pronounced or absent. A seasonal effect in pore water nutrient concentrations was only detectable at the lower flat where higher concentrations were found in the summer months. The determination of nitrate and nitrite gave peculiar results. The concentrations were high over the entire sediment depths (in 10 cm depth ca. 35 µmol $L^{-1}$ nitrate or up to 1µmol $L^{-1}$ nitrite, data not shown). Although these solutes may be transported to deeper sediment layers by pore water advection, ground water inflow or faunal transport, these data may as well be artefacts from the pore water extraction or analysis. The nitrate and nitrite concentrations were thus not included in the data set.

**Discussion**

*The significance of pore water advection for the oxygen distribution in the sediments*- The sediments at the investigation site are highly permeable and facilitate pore water advection (e.g. (Riedl and Machan 1972; Thibodeaux and Boyle 1987; Huettel and Gust 1992). The sandy deposits were homogeneous along the transect as concluded from our data on grain size distribution, permeability and porosity. The flow rate of fluids in highly permeable sediments is proportional to the pressure gradient driving the flow and sediment permeability (Darcy 1856). Given similar hydrodynamical conditions over the length of the transect, pore water advection at the three stations should be comparable in magnitude. Indeed, during inundation, the oxygen penetrations depths and the estimated bottom water filtration rates were similar between the three stations for most measurements. Thus, differences in hydrodynamics that may exist between the stations due to different water depths or due to a decrease of the flow velocity towards the shore, had no detectable influence on the oxygen penetration depths between stations.

The oxygen distribution and dynamics were strongly linked to the presence or absence of pore water advection. During inundation, oxygen penetrated deeper and varied more dynamically than during the exposure of the flat. The co-variance of oxygen penetration depth with the current velocity of the overlying water (Fig. 4) indicates that the dynamics and deep penetration of oxygen were linked to pore water advection. Constraints in the correlation between oxygen penetration depths and water current velocity are due to the influence of sediment topography on pore water advection and the influence of location on our one dimensional oxygen penetration depths measurements: While highest oxygen penetration occurs below zones of high pressure (i.e. ripple troughs), where the oxygen rich bottom water is forced into the sediment, low penetration depths are found below zones of low pressure (i.e., ripple crests), where anoxic pore water is drawn to the sediment surface (Huettel and Gust 1992; Shum and Sundby 1996; Precht et al. 2004). Nevertheless, the average oxygen penetration depth increases due to advective pore water exchange because in a sediment surface with wave or current ripples, as found at our study site, the area of bottom water intrusion is approximately 6-times larger than the area of pore water emergence (Precht et al. 2004). In winter, the low

correlation of oxygen penetration and water current velocity may partly be a result of the low OCR, as the sediments remained oxygenated for some time, even if current velocities decreased (Fig. 4). Pore water advection can also be inferred from the sigmoid shape of the oxygen profiles during inundation (Revsbech et al. 1980). The quick response of the oxygen penetration depth to wind-enhanced currents and waves emphasizes the strong coupling of these permeable sediments and the overlying water by physical (or hydraulic) forcing.

During the exposure of the flat, oxygen penetration remained dynamic but was less than during inundation time, even when the upper sediment layers were directly exposed to air. In some measurements the oxygen profiles exhibited the nearly parabolic shape of diffusion dominated profiles (Fig. 6 b) as also found in retrieved cores, where diffusion was the only transport mechanism (oxygen penetration depth ca. 2 mm in summer; data not shown). A major cause of a deeper oxygen penetration during exposure of the flat was the oxygen production by benthic photosynthesis. However, other factors may contribute to the oxygen dynamics during exposure, such as an inflow of oxygen rich water below superficial water runoff or pore water drainage.

During inundation and exposure of the flat, oxygen is transported into the sediments by bioirrigating benthic fauna (Aller 2001; Wenzhöfer and Glud 2004). Evidence for bioirrigation are oxygen profiles that showed irregularities within the oxygenated layer or ephemeral oxygen peaks below the oxygen penetration depth. These deep oxygen peaks were not included in the determination of oxygen penetration depth, as a quantification of bioirrigation from one dimensional oxygen measurements is not possible. This may lead to an underestimation of areal OCR.

Our findings on the variability of oxygen dynamics over the tidal cycle differ from previous findings (Brotas et al. 1990), that showed deepest oxygen penetration during exposure of an intertidal sand flat due to air intrusion. The oxygen penetration depth measurements in that study were, however, conducted in sediment cores, and thus without an impact of in situ hydrodynamics.

*Significance of pore water advection for benthic mineralization rates: oxygen*- The advective supply of oxygen and organic matter from the water column to the benthic system is considered a major reason for high mineralization rates in permeable sediments (Webb and Theodor 1968; Huettel and Gust 1992; Shum and

Sundby 1996). The advective supply of oxygen was a major factor for the magnitude and patterns found in benthic mineralization rates in our measurements. Mineralization rates were high and due to the deep oxygen penetration aerobic mineralization rates dominated organic matter degradation processes at all stations (Table 4), as previously concluded from a more limited data set from the same site (De Beer et al. 2005). The high aerobic mineralization rates are in contrast to findings in finer grained coastal sediments, where the aerobic mineralization is restricted to a few millimetres and sulfate reduction can account for up to 50% of total mineralization (Jørgensen 1982). That the deep oxygen supply promoted aerobic organisms in the oxygenated sediment layer may also be seen in the potential OCR, which were at each measuring depth at least an order of magnitude higher as the potential SRR. Although in the oxygenated layer reduced substances should not contribute significantly to the pOCR, a quantification of aerobic mineralization remains difficult. In permeable sediments, the contribution of reduced substances may be even more complicated, as pore water advection may transport reduced substances to the upper sediment layer (Huettel et al. 1998; Precht et al. 2004) or to sediment regions remote of their origin. Also, the magnitude of iron and manganese reduction is not known.

The oxygen penetration depth determined how much of the potential aerobic mineralization could actually take place. The varying oxygen supply over the tidal cycle resulted in a pronounced temporal variability of areal OCR (Fig. 8). Due to the deeper oxygen penetration during inundation, between 71 to 90% of the total mineralization took place during inundation of the flat. The advective supply of oxygen may be a major factor for the pattern found in mineralization rates: due to the longer inundation time, the amount of oxygen flushed through the sediments was highest at the lower flat station and this should contribute to the high potential and areal OCR, which exceeded those recorded in the other stations (beneficial conditions for aerobes over longer time periods). The variability of areal OCR over the tidal cycle as presented in Figure 8 reflects the influence of the variable oxygen availability on total mineralization. Other factors leading to a variability of aerobic mineralization over the day such as dial rhythm of faunal activity (e.g. (Wenzhöfer and Glud 2004) were beyond the scope of this study.

*Significance of pore water advection for benthic mineralization rates: filtration of organic carbon*- The second reason why inundation time influences benthic mineralization rates is the supply of organic matter from the water column to the sediments. Due to the longer inundation time in the lower station, more organic matter from the water column can reach the sediments at the lower flat station. The inundation-coupled filtration and sedimentation time along the transect may explain the low sedimentary TOC and DOC content in the upper station. Further, OCR and SRR increased upon the addition of dissolved organic carbon. Thus, the decreasing supply of organic matter due to decreasing inundation times along the transect may significantly contribute to the pattern found in the benthic mineralization rates. The differences in mineralization rates between stations were most pronounced for SRR. Sulfate was not limiting and similar between stations, thus our data indicate an increasing limitation of SRR by suitable organic substances towards the upper flat. The low SRR and the low absolute increase of SRR after acetate addition at the upper flat point to a low abundance of sulfate reducing bacteria (SRB). The environmental conditions for SRB must, therefore, be unfavourable over long time periods, preventing the development of SRB. For OCR, differences between sites were less pronounced as for SRR, which may be explained by a variety of factors. The organic material at the upper station may be more refractory and thus aerobic mineralization may be faster as anaerobic mineralization (Hulthe et al. 1998; Kristensen and Holmer 2001). There may be an increasing contribution of meio- and macrofauna to the utilization of oxygen towards the upper flat stations, as highest abundances of meio- and macrofauna were found at the middle and upper intertidal flat at the Hausstrand (Armonies and Hellwig-Armonies 1987).

The increase of mineralization rates in parallel with inundation time (i.e., time of pore water advection) point towards the importance of pore water advection for benthic mineralization. However, our estimation on bottom water filtration rates indicates that the organic matter supply through bottom water filtration cannot solely explain the magnitude of benthic mineralization rates (Table 2 and 4). As the stoichiometry of organic carbon oxidation is roughly 1 mol C-org: 1 mol $O_2$, the results suggest that in the summer months areal OCR at the respective sites are more than 4 to 8 times higher (up to 38 times higher, when calculated from

chlorophyll *a*) than the amount of infiltrated organic matter. One reason for the relatively small estimated contribution of pore water advection to the required organic carbon is that the simple model used to calculate bottom water filtration rates underestimates the actual amount of filtrated water. The concept behind the estimation is that the oxygen penetration depth is controlled by the balance between a vertical downward transport of oxygen and the sedimentary oxygen consumption rates. For permeable sediments this is a strong simplification as the flow of filtered water through the sediments follows a more curved path between in- and outflow areas and these horizontal flow components are neglected in the chosen approach. The more U-shaped flow path means that in the upper sediment layers the oxygen entering the sediments will leave it before it is used, and this infiltrated water volume is not comprised in the estimation. Particulates, however, transported by the same water bodies, will efficiently be trapped and subsequently be transported deeper in the sediment, e.g. by bioturbation (Krantzberg 1985) or wave-driven sediment reworking. Thus, the bottom water filtration rates calculated from oxygen supply are underestimated because the solute oxygen behaves differently than the particulate organic carbon. However, a suitable modelling of pore water advection rates is still missing (Boudreau et al. 2001). An indication that our bottom water filtration rates are a reasonable approximation, is that the rates are in line with other studies (Precht and Huettel 2003; Precht and Huettel 2004).

The misfit of respired to filtered organic carbon may also indicate that other processes than pore water advection are significant sources for organic carbon at the intertidal flat. These may be gravitational sedimentation, benthic photosynthesis and transport of organic matter from the water column by filter feeding macrofauna. Benthic photosynthesis may be of major importance for the supply of organic matter in permeable sediments. At the middle flat, benthic photosynthesis supplied organic material in the order of 35 to 50 mmol C $m^{-2}$ $d^{-1}$ (net rates) in the summer and autumn (De Beer et al. 2005; Billerbeck, unpublished data). Thus, ca. 50% of the organic carbon used in benthic mineralization could be provided by benthic photosynthesis. On a nearby sublittoral station, the sands were found to be net-autotrophic and photosynthesis rates even increased with increasing pore water advection rates (P. Cook, unpublished data). However, more measurements are needed that compare patterns of benthic photosynthesis with patterns of benthic

mineralization rates. Generally low abundances of macrofauna and the decrease of macrofaunal abundance towards the low water line (Armonies and Hellwig-Armonies 1987) may suggest that faunal transport of organic matter from overlying water to the sediments is not the dominant source of organic carbon at the investigation site. Other sources for organic material such as terrestrial-, groundwater- or eolic fluxes may be of minor importance for the pattern and magnitude found in benthic mineralization rates in surface sediments, e.g. a groundwater inflow was not detected in the surface sediments.

The input of organic material form the water column or from the top sediment layer by photosynthesis is reflected in the depth distribution of the potential OCR and SRR. In some measurements peaking pOCR were found above the pSRR peaks (Fig. 7 and 10). Highest pSRR where often measured at the interface of oxygenated and anoxic sediment layers, i.e., in an almost anoxic zone where the supply of organic carbon from above was maximal. Most sedimentary bacteria are attached to sand grains, thus a horizontal stratification of microbial populations in the top sediment layers was not expected due to the regular reworking of sediments by migrating ripples and bioturbation. Our results indicate, nevertheless, that a zonation of pOCR and pSRR can establish.

*Significance of pore water advection for the distribution of pore water nutrients*- The low concentrations of ammonium, phosphate and silicate in the upper sediment layers nutrients indicate an uptake by organisms, the removal by pore water advection and oxidation processes. Over the tidal cycle, no differences in pore water nutrient concentrations were found. This is in contrast to previous findings (Rocha 1998), where increasing pore water ammonium concentrations during exposure were observed. At our study site the missing contrast in pore water solute concentrations between inundation and exposure time may be caused by the reduced mineralization rates during exposure and ensuing slow nutrient concentration build-up. Also, diatoms and other autotrophic organisms are able to accumulate and store nutrients as soon as they become available. Below 3 to 5 cm sediment depth the pore water nutrient concentrations increased. The higher nutrient concentration found below 3 to 5 cm at the lower flat station may be supported by the pore water drainage flow during exposure, that was directed towards the low water line. During this transport organic matter may become

further mineralised and end products can accumulate in the pore water below the regularly flushed sediment layer, as found for another intertidal flat (Billerbeck, unpublished). The elevated nutrient concentrations may stimulate mineralization rates and photosynthesis at the lower station, thus additionally supporting higher mineralization rates at the lower flat station.

The measurements of the electron acceptor nitrate showed unreliable results. Anaerobic processes like nitrate reduction can be of major important in sediments (Canfield et al. 1993a; Canfield et al. 1993b) and may be of special importance in permeable sediments due to the dynamic oxygen distribution. We could not clarify whether the measurements are artefacts caused by the pore water extraction procedure (e.g., due to ammonium oxidation), a result from the interfering substances during analysis or whether they represent the real situation (caused, e.g., by pore water advection and faunal activity). High nitrate concentrations have been measured in other permeable sediments down to 15 cm depth (e.g. (Ehrenhauss et al. 2004), however, in situ measurements with nitrate biosensors are necessary to clarify the results.

*Seasonal pattern of mineralization rates and oxygen distribution*- As reported by numerous studies, benthic mineralization rates vary in the sediments of the Wadden Sea over the year due to a direct stimulation of chemical and biological processes by temperature and due to a variation of the organic matter load in the water column (Kristensen et al. 1997). Our results support these observations, as OCR, aerobic mineralization and SRR were highest in the warmer months. From the two summer months, June had lower mineralization rates, which can be explained by the lower ambient temperatures and the low carbon content in the overlying water column. At the upper flat, however, SRR did not vary over season, stressing the limitation of SRR by organic matter at this station. In April measurements were preceded by the spring bloom (van Beusekom, unpublished data). The high load of easily degradable organic carbon promoted OCR in April, which were comparable to OCR measured in summer, although temperatures were still lower. The response of SRR seems to be more delayed, as SRR in April showed only a small peak in the upper sediment layer but was generally still low.

Although hydrodynamics were comparable between summer and winter (Fig. 4), oxygen penetrated deeper in winter than in summer, due to increased

oxygen solubility and reduced sedimentary pOCR. The low areal OCR during winter show that the deeper penetration of oxygen could not compensate the lower volumetric pOCR.

Lower temperatures and lower pOCR may explain the in comparison to the other stations deeper oxygen penetration depths at the lower flat station in April. The oxygen distribution measurements at the lower flat were conducted first within the campaign, at the outset of the spring bloom and 3 to 4°C lower ambient temperatures as compared to the remaining time of the campaign.

*Conclusions*- Our results stress the overall importance of pore water advection for benthic mineralization rates. We found highest areal and volumetric OCR and SRR at the lower flat station, were the inundation time and thus the exposure time of the sediments to pore water advection were longest. The advective supply of oxygen shifted total benthic mineralization towards aerobic processes. It is likely that this advective effect is not restricted to the intertidal but extends to the shallow shelf where permeable beds permit flushing of the upper sediment layer (Marinelli et al. 1998; Jahnke et al. 2000; Reimers et al. 2004). The importance of oxygen supply by pore water advection for total benthic mineralization was reflected in the elevated OCR during inundation as compared to exposure time of the sand flat. However, the contribution of organic matter supply by pore water advection for total benthic mineralization remains to be investigated. The high benthic mineralization rates emphasize the importance of sands for the coastal marine carbon cycle.

**Acknowledgments**: We thank Martina Alisch, Christiane Hueerkamp and Kyriakos Vamvakopoulos for the support during fieldwork. Gabriele Eickert, Ines Schröder, Karin Hohmann, Ingrid Dohrmann, and Cecilia Wiegand are thanked for making the sensors and their help. Volker Meyer, Paul Färber, Harald Osmers, Alfred Kutsche and Georg Herz are acknowledged for the technical help. A big thank goes to the staff of the Wadden Sea Station on Sylt (Alfred Wegener Institute) for their support and great hospitality. Thomas Krieger of Wasser- und Schifffahrtsamt Tönning - Gewässerkunde- for the friendly permission of Sylt tide gauge data. This study was financed by the Max Planck Society (MPG), Germany.

## References

Aller, R. C. 2001. Transport and Reactions in the Bioirrgated Zone, p. 269-301. *In* Boudreau. B.P. and Jørgense. B.B. [eds.], The Benthic Boundary Layer. Oxford University Press.

Armonies, W., and M. Hellwig-Armonies. 1987. Synoptic Patterns of Meiofaunal and Macrofaunal Abundances and Specific Composition in Littoral Sediments. Helgol. Meeresunters. **41:** 83-111.

Berninger, U. G., and M. Huettel. 1997. Impact of flow on oxygen dynamics in photosynthetically active sediments. Aquat. Microb. Ecol. **12:** 291-302.

Boudreau, B., M. Huettel, R. Forster, A. Jahnke, J. McLachlan, J. Middelburg, P. Nielsen, F. Sansone, G. Taghon, W. Van Raaphorst, I. Webster, J. Weslawski, P. Wiberg, and B. Sundby. 2001. Permeable Marine Sediments: Overturning an Old Paradigm. EOS, TransAGU **82:** 133-136.

Brotas, V., A. Amorimferreira, C. Vale, and F. Catarino. 1990. Oxygen Profiles in Intertidal Sediments of Ria Formosa (S Portugal). Hydrobiologia **207:** 123-129.

Cammen, L. M. 1991. Annual Bacterial Production in Relation to Benthic Microalgal Production and Sediment Oxygen-Uptake in an Intertidal Sandflat and an Intertidal Mudflat. Mar. Ecol.-Prog. Ser. **71:** 13-25.

Canfield, D. E., B. B. Jørgensen, H. Fossing, R. Glud, J. Gundersen, N. B. Ramsing, B. Thamdrup, J. W. Hansen, L. P. Nielsen, and P. O. J. Hall. 1993a. Pathways of Organic-Carbon Oxidation in three Continental-Margin Sediments. Mar Geol **113:** 27-40.

Canfield, D. E., B. Thamdrup, and J. W. Hansen. 1993b. The Anaerobic Degradation of Organic-Matter in Danish Coastal Sediments - Iron Reduction, Manganese Reduction, and Sulfate Reduction. Geochim. Cosmochim. Acta **57:** 3867-3883.

D'Andrea, A. F., R. C. Aller, and G. R. Lopez. 2002. Organic matter flux and reactivity on a South Carolina sandflat: The impacts of porewater advection and macrobiological structures. Limnol. Oceanogr. **47:** 1056-1070.

Darcy, H. 1856. Les Fontaines Publiques de la Ville de Dijon. Dalmont.

de Beer, D., F. Wenzhoefer, T. G. Ferdelman, S. E. Boehme, M. Huettel, J. E. E. van Beusekom, M. E. Boettcher, N. Musat, and N. Dubillier. 2005. Transport and mineralization rates in North Sea sandy intertidal sediments, Sylt-Rømø Basin, Wadden Sea. Limnol. Oceanogr. **50:** 113-127.

Ehrenhauss, S., and M. Huettel. 2004. Advective transport and decomposition of chain-forming planktonic diatoms in permeable sediments. J. Sea Res. **52:** 179-197.

Ehrenhauss, S., U. Witte, F. Janssen, and M. Huettel. 2004. Decomposition of diatoms and nutrient dynamics in permeable North Sea sediments. Cont. Shelf Res. **24:** 721-737.

Forster, S., M. Huettel, and W. Ziebis. 1996. Impact of boundary layer flow velocity on oxygen utilisation in coastal sediments. Mar. Ecol.-Prog. Ser. **143:** 173-185.

Glud, R. N., I. Klimant, G. Holst, O. Kohls, V. Meyer, M. Kuhl, and J. K. Gundersen. 1999. Adaptation, test and in situ measurements with O-2 microopt(r)odes on benthic landers. Deep-Sea Res. Part I-Oceanogr. Res. Pap. **46:** 171-183.

Grasshoff, K., K. Kremling, and M. Ehrhardt. 1999. Methods of seawater analysis. Wiley-VCH Verlag.

Huettel, M., and G. Gust. 1992. Impact of Bioroughness On Interfacial Solute Exchange in Permeable Sediments. Mar. Ecol.-Prog. Ser. **89:** 253-267.

Huettel, M., and A. Rusch. 2000. Transport and degradation of phytoplankton in permeable sediment. Limnol. Oceanogr. **45:** 534-549.

Huettel, M., W. Ziebis, S. Forster, and G. W. Luther. 1998. Advective transport affecting metal and nutrient distributions and interfacial fluxes in permeable sediments. Geochim. Cosmochim. Acta **62:** 613-631.

Hulthe, G., S. Hulth, and P. O. J. Hall. 1998. Effect of oxygen on degradation rate of refractory and labile organic matter in continental margin sediments. Geochim. Cosmochim. Acta **62:** 1319-1328.

Jahnke, R. A., J. R. Nelson, R. L. Marinelli, and J. E. Eckman. 2000. Benthic flux of biogenic elements on the Southeastern US continental shelf: influence of pore water advective transport and benthic microalgae. Cont. Shelf Res. **20:** 109-127.

Jørgensen, B. B. 1977. Bacterial Sulfate Reduction Within Reduced Microniches of Oxidized Marine-Sediments. Mar. Biol. **41:** 7-17.

---. 1978. Comparison of Methods For the Quantification of Bacterial Sulfate Reduction in Coastal Marine-Sediments .1. Measurement With Radiotracer Techniques. Geomicrobiology Journal **1:** 11-27.

---. 1982. Mineralization of Organic-Matter in the Sea Bed - the Role of Sulfate Reduction. Nature **296:** 643-645.

Jørgensen, B. B., and F. Bak. 1991. Pathways and Microbiology of Thiosulfate Transformations and Sulfate Reduction in a Marine Sediment (Kattegat, Denmark). Appl. Environ. Microbiol. **57:** 847-856.

Kallmeyer, J., T. G. Ferdelman, A. Weber, H. Fossing, and B. B. Jørgensen. 2004. A cold chromium distillation procedure for radiolabeled sulfide applied to sulfate reduction measurements. Limnology and Oceanography: Methods. **2:** 171-180.

Klute, A., and C. Dirksen. 1986. Hydraulic Conductivity and Diffusivity: Laboratory Methods, p. 687 ff. *In* A. Klute [ed.], Method of Soil Analysis - part 1 - physical and mineralogical methods. American Society of Agronomy.

Krantzberg, G. 1985. The Influence of Bioturbation on Physical, Chemical and Biological Parameters in Aquatic Environments - a Review. Environ Pollut. A - Ecol. Biol. **39:** 99-122.

Kristensen, E., and M. Holmer. 2001. Decomposition of plant materials in marine sediment exposed to different electron accepters (O-2, NO3-, and SO42-), with emphasis on substrate origin, degradation kinetics, and the role of bioturbation. Geochim. Cosmochim. Acta **65:** 419-433.

Kristensen, E., M. H. Jensen, and K. M. Jensen. 1997. Temporal variations in microbenthic metabolism and inorganic nitrogen fluxes in sandy and muddy sediments of a tidally dominated bay in the northern Wadden Sea. Helgol. Meeresunters. **51:** 295-320.

Marinelli, R. L., R. A. Jahnke, D. B. Craven, J. R. Nelson, and J. E. Eckman. 1998. Sediment nutrient dynamics on the South Atlantic Bight continental shelf. Limnol. Oceanogr. **43:** 1305-1320.

Nielsen, P. 1990. Tidal Dynamics of the Water-Table in Beaches. Water Resour. Res. **26:** 2127-2134.

Polerecky, L., U. Franke, U. Werner, B. Grunwald, and D. de Beer. 2005. High spatial resolution measurement of oxygen consumption rates in permeable sediments. Limnology and Oceanography: Methods **3:** 75-85.

Precht, E., U. Franke, L. Polerecky, and M. Huettel. 2004. Oxygen dynamics in permeable sediments with wave-driven pore water exchange. Limnol. Oceanogr. **49:** 693-705.

Precht, E., and M. Huettel. 2003. Advective pore-water exchange driven by surface gravity waves and its ecological implications. Limnol. Oceanogr. **48:** 1674-1684.

---. 2004. Rapid wave-driven advective pore water exchange in a permeable coastal sediment. J. Sea Res. **51:** 93-107.

Reimers, C. E., H. A. Stecher, G. L. Taghon, C. M. Fuller, M. Huettel, A. Rusch, N. Ryckelynck, and C. Wild. 2004. In situ measurements of advective solute transport in permeable shelf sands. Cont. Shelf Res. **24:** 183-201.

Revsbech, N. P. 1989. An Oxygen Microsensor With a Guard Cathode. Limnol. Oceanogr. **34:** 474-478.

Revsbech, N. P., B. B. Jørgensen, and T. H. Blackburn. 1980. Oxygen in the Sea Bottom Measured With a Microelectrode. Science **207:** 1355-1356.

Riedl, R. J., and R. Machan. 1972. Hydrodynamic Patterns in Lotic Intertidal Sands and Their Biolimatological Implications. Mar. Biol. **13:** 179-209.

Riedl, R. J., R. Machan, and N. Huang. 1972. Subtidal Pump - Mechanism of Interstitial Water Exchange By Wave Action. Mar. Biol. **13:** 210-221.

Rocha, C. 1998. Rhythmic ammonium regeneration and flushing in intertidal sediments of the Sado estuary. Limnol. Oceanogr. **43:** 823-831.

Rusch, A., and M. Huettel. 2000. Advective particle transport into permeable sediments - evidence from experiments in an intertidal sandflat. Limnol. Oceanogr. **45:** 525-533.

Shum, K. T. 1992. Wave-Induced Advective Transport Below a Rippled Water-Sediment Interface. J. Geophys. Res.-Oceans **97:** 789-808.

Shum, K. T., and B. Sundby. 1996. Organic matter processing in continental shelf sediments - The subtidal pump revisited. Mar. Chem. **53:** 81-87.

Thamdrup, B., J. W. Hansen, and B. B. Jørgensen. 1998. Temperature dependence of aerobic respiration in a coastal sediment. FEMS Microbiol. Ecol. **25:** 189-200.

Thibodeaux, L. J., and J. D. Boyle. 1987. Bedform-Generated Convective-Transport in Bottom Sediment. Nature **325:** 341-343.

Webb, J. E., and J. Theodor. 1968. Irrigation of Submerged Marine Sands Through Wave Action. Nature **220:** 682-683.

Webster, I. T., S. J. Norquay, F. C. Ross, and R. A. Wooding. 1996. Solute exchange by convection within estuarine sediments. Est. Coast. Shelf Sci .**42:** 171-183.

Wentworth, C. K. 1922. A scale of grade and class terms for clastic sediments. J. Geol. **30:** 377-392.

Wenzhöfer, F., and R. N. Glud. 2004. Small-scale spatial and temporal variability in coastal benthic O-2 dynamics: Effects of fauna activity. Limnol. Oceanogr. **49:** 1471-1481.

Wenzhöfer, F., O. Holby, R. N. Glud, H. K. Nielsen, and J. K. Gundersen. 2000. In situ microsensor studies of a shallow water hydrothermal vent at Milos, Greece. Mar. Chem. **69:** 43-54.

Ziebis, W., M. Huettel, and S. Forster. 1996. Impact of biogenic sediment topography on oxygen fluxes in permeable seabeds. Mar. Ecol.-Prog. Ser. **140:** 227-237.

# Surficial and deep pore water circulation governs spatial and temporal scales of nutrient recycling in intertidal sand flat sediment

Markus Billerbeck, Ursula Werner, Lubos Polerecky, Eva Walpersdorf, Dirk de Beer and Markus Huettel

submitted to Marine Ecology Progress Series

**Abstract**

We studied aerobic and anaerobic mineralization in permeable sediment of a sloping intertidal sand flat near the island of Spiekeroog, southern North Sea. One site near the water line and one site on the upper flat were studied on a tidal and seasonal basis to assess the temporal and spatial scales of mineralization. Hydrodynamic forcing during inundation of the tidal flat caused deeper oxygen penetration through flushing of the uppermost sediment layer. This flushing resulted in higher areal oxygen consumption and lower depth integrated sulfate reduction rates in the submerged flat than during exposure. Mineralization rates in the top 15 cm of the sediment were similar between both study sites and ranged from 38 (winter) to 280 mmol C $m^{-2}$ $d^{-1}$ (summer), with sulfate reduction contributing 3 to 25 % to total mineralization, depending on the season. At the upper flat, the seasonal differences were reflected in the pore water concentrations of nutrients, DIC and DOC. Near the low water line, however, pore water nutrient and DIC concentrations were independent of the season and up to 15-times higher compared to the upper flat. The differences in concentrations of metabolic products between the two sites resulted from a low tide drainage extending deep below the uppermost flushed layer and causing seepage of pore water near the low water line. Mineralization and nutrient release in these permeable intertidal sediments is affected by two filtration processes that work on distinctly different temporal and spatial scales: 1) rapid “skin filtration” through the uppermost sediment layer during inundation that is characterized by short flow paths, low pore water residence time and immediate feedback to the ecosystem; 2) slow “body filtration” through deeper sediment layers during low tide that is characterized by long flow paths and pore water residence times, and is acting as a buffered nutrient source to the ecosystem.

## Introduction

Sandy sediments prevail in the intertidal regions of the German Wadden Sea (Flemming and Ziegler 1995). Despite rather small bacterial numbers and low organic matter content of sandy sediments (Bergamaschi et al. 1997, Llobet-Brossa et al. 1998, Rusch et al. 2003), their high mineralization capacity has been recognized in recent studies (Cammen 1991, D'Andrea et al. 2002, Huettel et al. 2003). The permeability of the sand facilitates advective pore water transport through the upper sediment layers in contrast to muddy sediments, where diffusional processes are dominating (Huettel and Gust 1992, Huettel and Webster 2001). The advective pore water transport can exceed diffusion by orders of magnitude (Lohse et al. 1996, Boudreau et al. 2001).

During inundation of intertidal sand flats, the percolation of water through the sediment is driven by pressure gradients generated by the interaction of bottom currents with the sediment topography (Thibodeaux and Boyle 1987, Glud et al. 1996) and by waves passing over the permeable bed (Van der Loeff 1981, Precht and Huettel 2003). This hydrodynamic forcing provides oxygen to the upper sediment layers and enhances aerobic mineralization of organic matter during inundation (Forster et al. 1996, Dauwe et al. 2001, Werner et al. submitted). The high aerobic mineralization capacity in the upper sediment layers and anaerobic degradation processes deeper in the sediment are fuelled by the filtration of suspended particles and dissolved organic matter from the water column into the permeable bed (Huettel et al. 1996, Rusch et al. 2001). Furthermore, bioturbation and bioirrigation by benthic macrofauna adds to the supply of electron acceptors and organic matter to the sediment (Graf and Rosenberg 1997, Aller 2001). Inorganic nutrients, the products of mineralization, are removed from the sand by the advective flushing (Huettel et al. 1998) and can support primary production in the water column. The depth of the advective flushing is dependent on the permeability of the sediment and usually is restricted to the top few mm to cm of the sand bed (Brotas et al. 1990, de Beer et al. 2005). Within this surface layer of the tidal flat, organic matter can be recycled quickly and immediate feedback may be provided to the ecosystem in a matter of hours to days by the removal of the metabolic products from the sediment.

The lack of advective flushing during low tide exposure of the intertidal flat leads to accumulation of metabolic products in the sediment (Rocha 1998, Kuwae et al. 2003). Transport, however, is not restricted to diffusion during exposure. Some benthic bioturbators are still active during exposure (Orvain and Sauriau 2002). Also, pore water may be drained through the permeable sand driven by the buildup of a hydraulic gradient between the sea water level and the slower dropping pore water level (Nielsen 1990). The drainage mechanism transports pore water mainly laterally through the sediment towards the low water line, where pore water discharge can be observed also at the exposed sediment surface constituting an important nutrient input to coastal waters (Howes and Goehringer 1994, Osgood 2000, Jahnke et al. 2003). Sediment layers extending deep below the regularly flushed upper layer can be affected by the drainage over horizontal distances between tens and hundreds of meters (Whiting and Childers 1989, Jahnke et al. 2003). Due to the long residence time and pathways of the pore water within these deeper layers of the intertidal flat, the feedback of mineralization products to the ecosystem is delayed. This large body of the sand flat, thus, may act as a source of nutrients that can support primary production in the system during times of low nutrient concentrations in the sea water.

We hypothesize that in an intertidal sand flat the recycling of sedimentary mineralization products is governed by two main pore water circulation patterns operating on distinctly different temporal and spatial scales: 1) a rapid “skin circulation” within the top sediment layer, characterized by short flow paths and residence times of the pore water with an immediate feedback to the system; 2) a slower “body circulation” through the surface and deeper layers of the sediment with long flow paths and pore water residence times. Due to the relatively long time interval between organic matter input and mineralization product release, this “body circulation” may act as a large buffer system for nutrients. In order to test this hypothesis, measurements of oxygen consumption and sulfate reduction were conducted on a sloping intertidal sand flat in the German Wadden Sea and combined with measurements of oxygen penetration depth and pore water concentrations of metabolic products. In order to assess the temporal scales of the mineralization processes, one study site near the low water line and one site at the upper flat were studied on a tidal and seasonal basis.

## Methods

*Site description*: Sampling and in situ measurements were carried out at the north eastern margin of the 11 km² large Janssand tidal flat (53°44`07`` N, 007°41`57`` E), an intertidal sand flat located in the backbarrier area of the island of Spiekeroog, North Sea, Germany (Fig. 1A). The marginal area of this tidal flat is sloping on average 1.6 cm $m^{-1}$ towards the low water line, and the tidal flat is covered by 1.5-2 m of water during high tide (Fig. 1B).

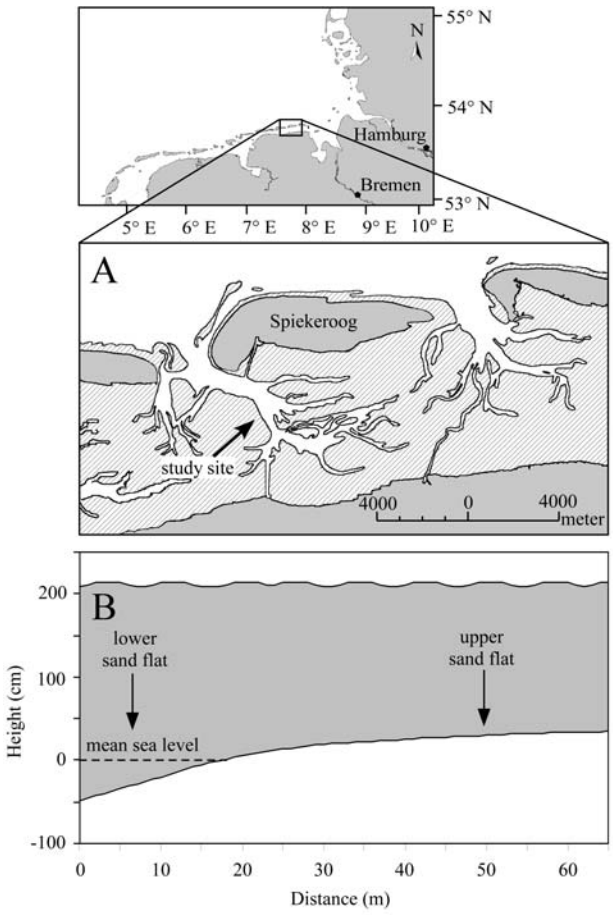


Figure 1: (A) Study site near the island of Spiekeroog, Wadden Sea, Germany. (B) Tidal flat topography as surveyed during July 2003 relative to mean sea level.

During low tide, the sand flat becomes exposed for approximately 6 to 8 hours, depending on tidal range. A “lower sand flat” site close to the low water line and an “upper sand flat” site approximately 45 m upslope the tidal flat (Fig. 1B) were chosen as the main study areas and investigated on a seasonal basis between December 2001 and March 2004 (Table 1). The lower flat site is

inundated approximately 3-4 h $d^{-1}$ longer than at the upper flat due to the tidal flat topography (Fig. 1B).

*Sediment characteristics*: Grain size was analyzed by dry-sieving the top 10 cm of the sediment and classified according to Wentworth (1922). The porosity of the top 15 cm of the sediment was determined in 1 cm intervals from the weight loss of a known volume of sediment after drying at 60° C until weight constancy. In July 2003, porosity of the top10 cm of the sediment was measured every 2 hours during exposure at the upper tidal flat. The permeability of the top 15 cm of the sediment was measured using the constant head method described in Klute and Dirksen (1986).

*Pore water solutes*: For pore water analysis (nutrients, DIC, DOC and sulfate), four to six sediment cores were collected with a 36 mm core liner during low tide from the upper and lower sand flat site. Additional sediment cores were collected over a tidal cycle from the upper sand flat site (20 minutes after inundation, high tide peak and low tide) between March and December 2002. The sediment cores were processed immediately after collection inside a glove box that was flushed with inert argon gas. The cores were sectioned to a depth of 10 to 20 cm (1 cm intervals to 10 cm depth, 2 cm intervals below), and sediment slices of the same depth were pooled to obtain a sufficient volume of pore water. The pooled sediment was transferred to a plastic Buechner-funnel with a nylon mesh preventing loss of sediment through the funnel. The funnel with sediment was inserted into a pressure container such that the outflow end of the funnel protruded from lower end of the container. An inlet on the opposite side of the funnel permitted gas flow into the container. The pore water was separated from the sediment matrix by flushing the pressure container for ca. 20 seconds with argon gas. In December 2001, pore water was sampled down to 15 cm sediment depth in 2.5 cm intervals with a pore water sipper as described in Huettel (1990).

Table 1: Measurements conducted during the field campaigns between December 2001 and March 2004. Numbers in brackets denote replicate measurements.

| | Sediment characteristics | | | Porewater solutes | | | In situ measurements and rates | | |
|---|---|---|---|---|---|---|---|---|---|
| Campaign | Porosity | Permeability | Grain size | Nutrients | DIC | DOC | Oxygen penetration | Oxygen consumption | Sulfate reduction |
| December 2001 | | | | upper (12) | | upper (1) | upper (1) * | | upper (3) |
| 03 - 14.12.01 | | | | lower (6) | | lower (1) | lower (1) | | lower (3) |
| March 2002 | upper (1) | | | upper (4) | upper (3) | upper (4) | upper (1) | | upper (3) |
| 11 - 20.03.02 | | | | | | | | | |
| June 2002 | upper (2) | upper (5) | | upper (4) | upper (2) | upper (4) | upper (1) | upper (2) microsensor | upper (3) |
| 04 - 15.06.02 | lower (1) | lower (4) | | lower (1) | lower (1) | lower (1) | lower (1) | lower (2) microsensor | lower (3) |
| September 2002 | upper (1) | | | upper (4) | upper (3) | upper (3) | upper (1) | upper (2) optode | upper (3) |
| 25 - 29.09.02 | lower (1) | | | lower (1) | lower (1) | lower (1) | lower (1) | lower (2) optode | lower (2) |
| December 2002 | upper (2) | | | upper (4) | upper (2) | | | upper (2) optode | |
| 03 - 09.12.02 | lower (1) | | | lower (1) | lower (1) | | | | |
| July 2003 | upper (2) † | upper (6) | upper (1) | upper (2) | upper (2) | upper (2) | upper (1) | upper (3) optode | |
| 22 - 31.07.03 | lower (1) | lower (6) | | lower (1) | lower (1) | lower (1) | lower (1) | | |
| March 2004 | | | | upper (1) | upper (1) | upper (1) | upper (1) | upper (2) microsensor | |
| 25 - 31.03.04 | | | | lower (1) | lower (1) | lower (1) | lower (1) | | |

* combined with Acoustic Doppler Velocimeter measurement † 4 additional porosity measurements over exposure period

Pore water profiles were replicated 12 times at the upper flat and 6 times at the lower flat with the sipper. All pore water samples were passed through 0.2 µm nylon syringe filters. Aliquots for DIC analysis were then preserved with 20 µl of a saturated mercury chloride solution in 2 ml Zinnser™ vials without headspace and kept refrigerated until further processing. Volumes of 3 to 5 ml of pore water were transferred to pre-combusted glass vials for DOC analysis or into plastic vials for nutrient and sulfate measurements and kept frozen.

Pore water nutrients were measured spectrophotometrically with a Skalar Continuous-Flow-Analyzer according to Grasshoff et al. (1999). Pore water DIC was determined by flow injection analysis (Hall and Aller 1992) with freshly prepared $NaHCO_3$ calibration standards. For the analysis of DOC, total dissolved carbon and DIC were measured by high temperature catalytic oxidation on a Shimadzu TOC-5050A analyzer connected to a Shimadzu ASI 5000A autosampler using bicarbonate and phthalate as calibration standards. DOC concentration was obtained by subtraction of DIC from total dissolved carbon. Pore water sulfate concentration was determined with a Dionex® ion chromatograph using IonPac® AS9-HC analytical and IonPac® AG9-HC guard columns.

*In situ sensor measurements*: In situ measurements of oxygen penetration depth were performed by microsensors mounted on an autonomous profiler as described in Glud et al. (1999) and Wenzhöfer et al. (2000). Oxygen concentration was measured with Clark type oxygen microelectrodes (Revsbech 1989) with 300 µm tip diameter, an actual sensing surface of 5 µm and less than 5 seconds response time ($t_{90}$). The profiler was set up during low tide on the sediment with the microsensors initially positioned 1-2 cm above the sediment surface. Downward oxygen profiles were measured over at least one tidal cycle to a sediment depth of 6 cm in 1 mm intervals. Repeated profiles were measured every 20 to 60 minutes. The oxygen sensors sometimes produced persisting holes in the sediment during low tide and such profiles were discarded from the data set.

*Measurement of oxygen consumption rates (pOCR and aOCR)*: Volumetric oxygen consumption rates were measured at in situ temperatures on freshly collected sediment cores in the laboratory. The sediment cores were percolated with aerated ambient sea water until oxygen was present in high concentrations at the desired measurement depth. After stopping the percolation, the decrease in

oxygen concentration was monitored either with a Clark type oxygen microelectrode or a planar optode (de Beer et al. 2005, Polerecky et al. 2005) (Table 1). Consistency of both methods was demonstrated by Polerecky et al. (2005). The initial decrease in oxygen concentration was considered as the potential volumetric oxygen consumption rate (pOCR). Assessment of pOCR with the microsensor was carried out by positioning the sensor in the sediment core at defined depths in 2 mm to 5 mm intervals and repetitively percolating water through the same core. The planar optode technique permitted the calculation of respiration rates with a resolution of ≈ 300 µm over the optode area (ca. 25 x 150 mm; resulting oxygen image size 80 x 480 pixels). All measurements were performed on two replicate cores down to 8 cm sediment depth and in the dark to prevent photosynthesis.

Areal oxygen consumption rates (aOCR) were obtained by integrating the measured pOCR over the oxygen penetration depths measured in situ by the autonomous profiler. As pOCR data were only available from June 2002, pOCR determined during December 2002 and March 2004 were combined with oxygen penetration depths measured in December 2001 and March 2002, respectively, to estimate areal OCR for the latter months. Areal oxygen consumption was estimated to be equal to total mineralization, assuming that reduced substances from anaerobic decay (e.g. sulfide from sulfate reduction) contributed to the measured oxygen consumption rates (Jørgensen 1982).

*Potential (pSRR) and maximum/minimum sulfate reduction rates (SRRmax and SRRmin)*: Sulfate reduction rates were measured in two to three replicate sediment cores with the tracer whole core incubation method (Jørgensen 1978) modified for permeable sediments (de Beer et al. 2005) (Table 1). Radiolabeled $^{35}SO_4^{2-}$ (Amersham™) was added to 70 ml of ambient seawater in the laboratory to obtain a specific activity of 340 MBq per mol $SO_4^{2-}$. The seawater-tracer solution was allowed to percolate into the sediment from the top of the core leading to a homogenous distribution of tracer within the permeable sand. After incubating the sediment at average in situ temperatures for 4 to 6 hours, the core was sliced into 1 cm sections and the incubation stopped by placing the slices into 20% ZnAc. The samples were processed with the cold chromium distillation procedure (Kallmeyer et al. 2004) that is based on the single step chromium reduction method (Fossing

and Jørgensen 1989). Radioactivity of $^{35}SO_4^{2-}$ and Total Reduced Inorganic Sulfur (TRIS) was measured with a liquid scintillation counter (Packard™ 2500 TR) using the Lumasafe Plus® scintillation cocktail. The calculation of sulfate reduction rates accounted for the measured porosities and pore water sulfate concentrations. Sediment horizons that are regularly supplied with oxygen by in situ advective transport can become anoxic during the stagnant incubation conditions and the measured sulfate reduction rates may, therefore, represent an overestimation of actual in situ rates. On the other hand, pore water flow conditions cannot be applied during the incubation due to the resulting relocation of the radiolabeled sulfides from their place of production. Hence, in situ sulfate reduction rates were estimated in a maximum/minimum scenario, with the maximum (SRRmax) estimated by integrating pSRR over the entire measurement depth. The minimum (SRRmin) was obtained by integrating pSRR only over the varying anoxic sediment depths down to 15 cm, as inferred from the in situ oxygen penetration depths.

*Measurement of near bottom flow velocities*: Near bottom water flow was measured using a Nortek™ Acoustic Doppler Velocimeter (ADV) combined with the in situ determination of oxygen penetration depths in December 2001. The ADV measured 3 component (x, y, z) flow velocities at a sampling frequency of 25 Hz within a cylindrical sampling volume (ca. 6mm Ø x 6mm) located 100 mm below the probe. The ADV was mounted on a tripod with a profiling unit and flow velocities were measured stepwise for 30 seconds in 1 cm intervals from 1 to 25 cm above the sea floor over the inundation period. The average water current velocities were calculated for each height as the scalar of the 3 velocity vectors averaged over the 30 second measurement intervals.

*Data analysis*: Statistical analysis of differences between sampling sites and seasons were performed at a 95 % confidence level ($p<0.05$). Pore water data as well as rates of oxygen consumption and sulfate reduction were analyzed with the nonparametric Mann-Whitney U-Test for pairwise comparisons and the Kruskal-Wallis H-Test for between-group analysis. After detection of significance in the group analysis, the $\chi^2$ approach was used as a post hoc test to identify the significance between the populations.

**Results**

*Sediment characteristics*: The Janssand tidal flat is characterized by well sorted ($\sigma$<0.38 phi) fine quartz sands with a mean grain size of 176 µm (2.5 phi). With permeabilities ranging between 7.2 – 9.5 x $10^{-12}$ m² at the upper flat and 0.5 – 3.1 x $10^{-12}$ m² at the lower flat, the sediment at both study sites permitted advective pore water flows. The porosity of the top 15 cm of the sediment was 34.7 and 39.5 % at the upper and lower flat, respectively. The porosity measurements taken at 2 hour intervals in July 2003 showed that the porosity of the top 10 cm of the sediment remained almost constant during the entire exposure period (range between 36.4 and 38.6 %). A glassy sediment surface and visual observation of water runoff at the lower flat site during exposure indicated a discharge of drained pore water. This was not observed at the upper sand flat site, where the sediment surface had a "dry" appearance during low tide.

*Potential volumetric rates of oxygen consumption (pOCR) and sulfate reduction (pSRR)***:** Interestingly, pOCR at the lower sand flat was similar to that measured at the upper flat during June and September 2002 (Fig. 2), except in a zone of higher pOCR activity that was detected between 0.8 and 1.6 cm sediment depth in June 2002 ($p<0.001$). During September 2002, mean pOCR were slightly lower at the lower sand flat site ($p<0.01$) but very variable between cores in the top cm of sediment (Fig. 2). After a repeated flushing of the sediment core from the lower flat that exhibited highest pOCR, the rates decreased considerably, suggesting that oxidation of reduced solutes or particle bound material largely contributed to the higher rates during the first measurement in September 2002. No reduction in pOCR in the regularly oxygenated sediment layer was observed during repeated measurements of sediment cores from the upper sand flat (see also Polerecky et al. 2005).

In the regularly oxygenated sediment layer down to the maximum oxygen penetration depth, the volumetric rates of oxygen consumption (pOCR) showed a clear seasonal trend at the upper sand flat (Fig. 3) with lower rates during the winter months (December, March) than during summer (June, September, July) ($p<0.001$). While pOCR did not differ between June and September 2002, highest pOCR were measured during the extraordinarily warm July in 2003. Below the

maximum oxygen penetration depth, pOCR increased at both study sites during most months, but remained constant or decreased during September 2002 at the upper and lower flat, respectively (data not shown).

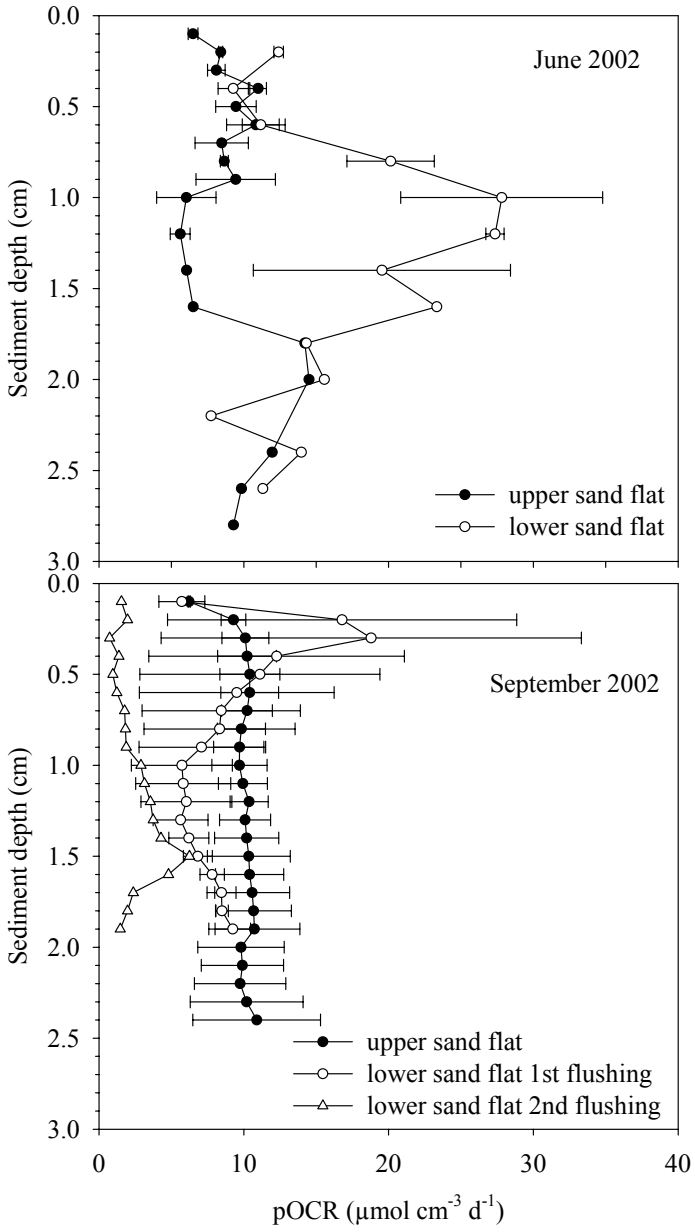


Figure 2: Potential volumetric oxygen consumption rates (pOCR) at the upper and lower sand flat during June and September 2002. Rates are plotted as the mean of 2 cores with the range as error bars down to the maximum penetration depth of oxygen for the respective months. For clarity, only every third datapoint (every 1 mm) is shown from the planar optode measurements in September.

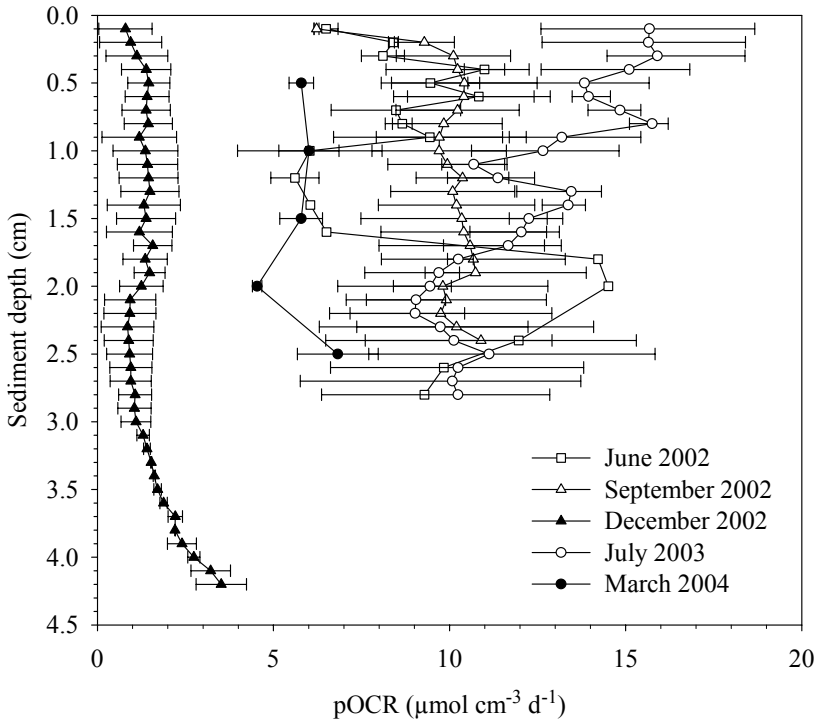


Figure 3**:** Potential volumetric oxygen consumption rates (pOCR) at the upper sand flat between June 2002 and March 2004. All rates are plotted as the mean of 2 cores (3 cores in July 2003) with the range as error bars down to the maximum oxygen penetration depth for the respective months. For clarity, only every third datapoint (every 1 mm) is shown from the planar optode measurements in September, December and July.

Similar to the pOCR measurements, site differences in pSRR were small between the upper and lower flat (Fig. 4). The pSRR rates were only marginally higher at the lower sand flat site ($p<0.05$) during December 2001 and June 2002 and did not differ between the upper and lower flat during September 2002.

As compared to pOCR, the seasonal trend was less pronounced for pSRR (Fig. 4). Highest SRR were measured in September 2002 in 2 to 3 cm sediment depth at both study sites. Except this zone of higher activity, no difference in pSRR was detected between September 2002, June 2002, and December 2001 for the upper and lower sand flat sites. Significantly lower potential of sulfate reduction was, however, measured at the upper sand flat during March 2002 ($p<0.001$). The highest potential of sulfate reduction was usually measured in sediment layers located near the maximum depth of oxygen penetration (Fig. 4). Below this zone of higher activity, pSRR decreased with sediment depth in most profiles.

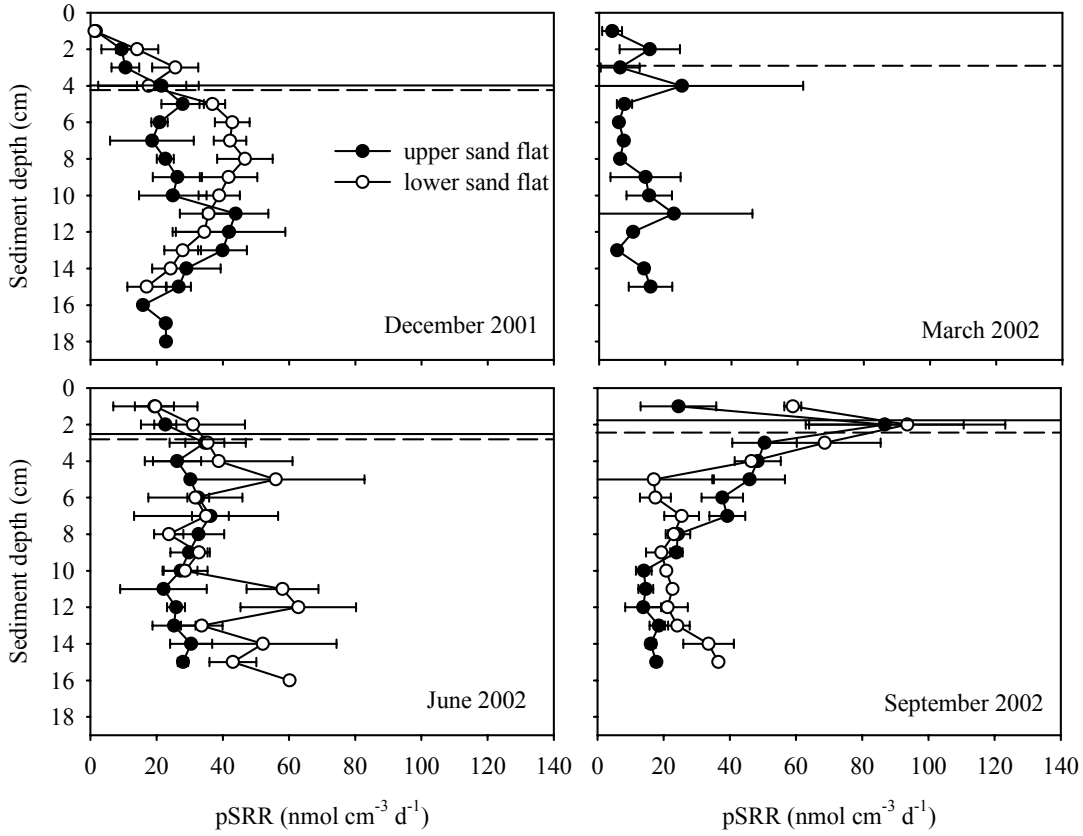


Figure 4: Volumetric sulfate reduction rates (pSRR) at the upper and lower sand flat sites between December 2001 and September 2002 (March 2002 only upper flat). Mean and standard deviation (error bars) were calculated from 3 replicate cores. The maximum oxygen penetration depth is marked with dashed (upper flat) and solid (lower flat) lines.

*Areal rates of oxygen consumption (aOCR) and depth integrated sulfate reduction (SRRmax; SRRmin)*: In situ areal rates of oxygen consumption (aOCR) and sulfate reduction (SRRmin) were calculated from the measured potential rates (pOCR, pSRR) and in situ oxygen penetration depths, since oxygen can inhibit the activity of sulfate reducers (Marschall et al. 1993). The maximum value for depth integrated sulfate reduction (SRRmax) is not corrected for oxygen penetration depth, as sulfate reduction activity has also been measured within the regularly oxygenated sediment layer (Jørgensen 1977, Jørgensen and Bak 1991).

Oxygen generally penetrated deeper into the sediment during inundation than during exposure of the tidal flat. At the upper sand flat, the maximum penetration depth of oxygen into the sediment was 4.2 cm in December and varied between 2.4 – 2.8 cm for all other investigated months. Due to the deeper oxygen penetration, aOCR (Fig. 5 and 6A) was significantly higher during inundation as

compared to exposure (at least $p<0.05$). Areal OCR followed a seasonal trend at the upper flat with lowest rates during December 2001, intermediate during March, June, September 2002 and March 2004 and highest rates during the very warm July 2003 (Fig. 6).

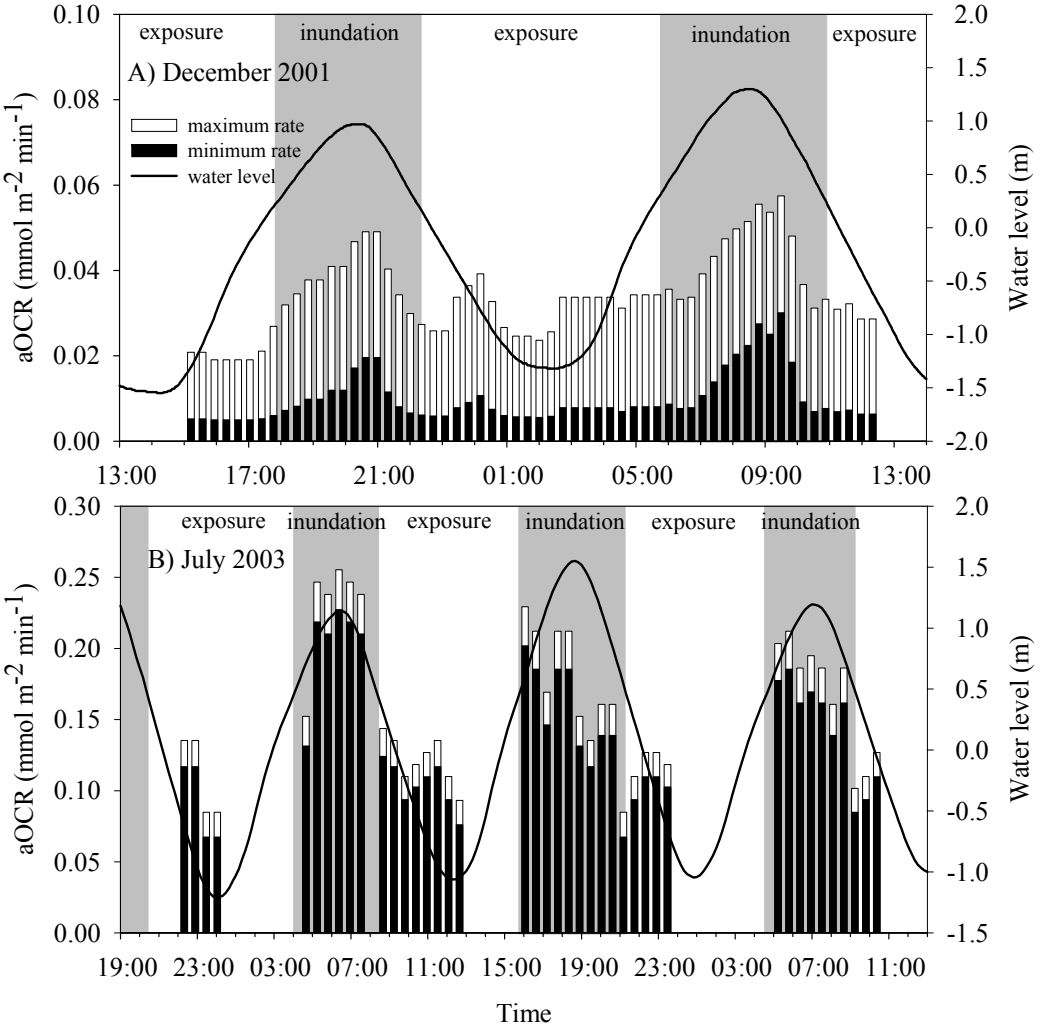


Figure 5: Areal oxygen consumption rates (aOCR) and sea water level over several tidal cycles during (A) December 2001 and (B) July 2003 (Note different scalings for aOCR). Rates are given as minimum and maximum of two replicate pOCR measurements (3 replicates in July 2003). December rates were calculated from oxygen penetration measured in December 2001 and pOCR measured in December 2002.

Also at the lower sand flat, the maximum oxygen penetration depth was 2.4 – 2.8 cm. The aOCR at the lower flat was higher during June 2002 and similar to the upper flat during September 2002 (Fig. 6B).

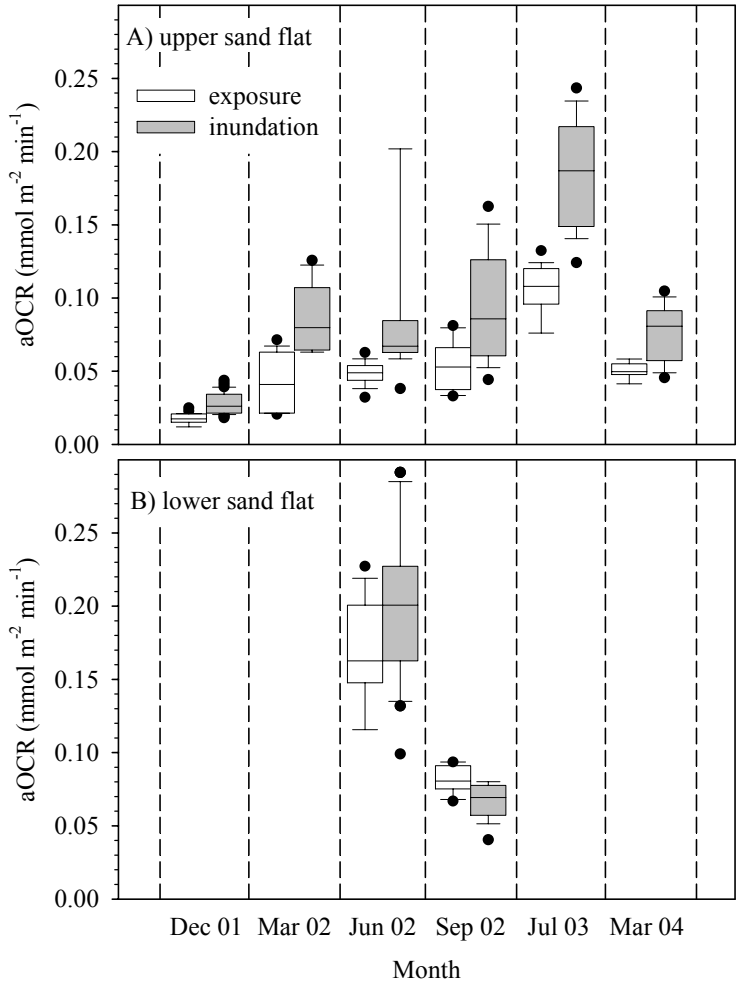


Figure 6**:** Areal oxygen consumption rates during exposure (white boxes) and inundation (grey boxes) at the (A) upper and (B) lower sand flat between December 2001 and March 2004. The boxes comprise the 25$^{th}$ and 75$^{th}$ percentiles and the line within the boxes represents the median. The 10$^{th}$ and 90$^{th}$ percentiles are represented by whiskers and outliers by filled circles.

The conservative minimum value for depth integrated sulfate reduction (SRRmin) was obtained by integrating pSRR over the anoxic sediment depth down to 15 cm. Thus, SRRmin rates were inversely related to OCR with slightly lower rates during inundation than during exposure (Fig. 7). SRRmin were low during

March 2002 and rather constant during all other months. The depth integrated sulfate reduction rates at the upper and lower flat were similar.

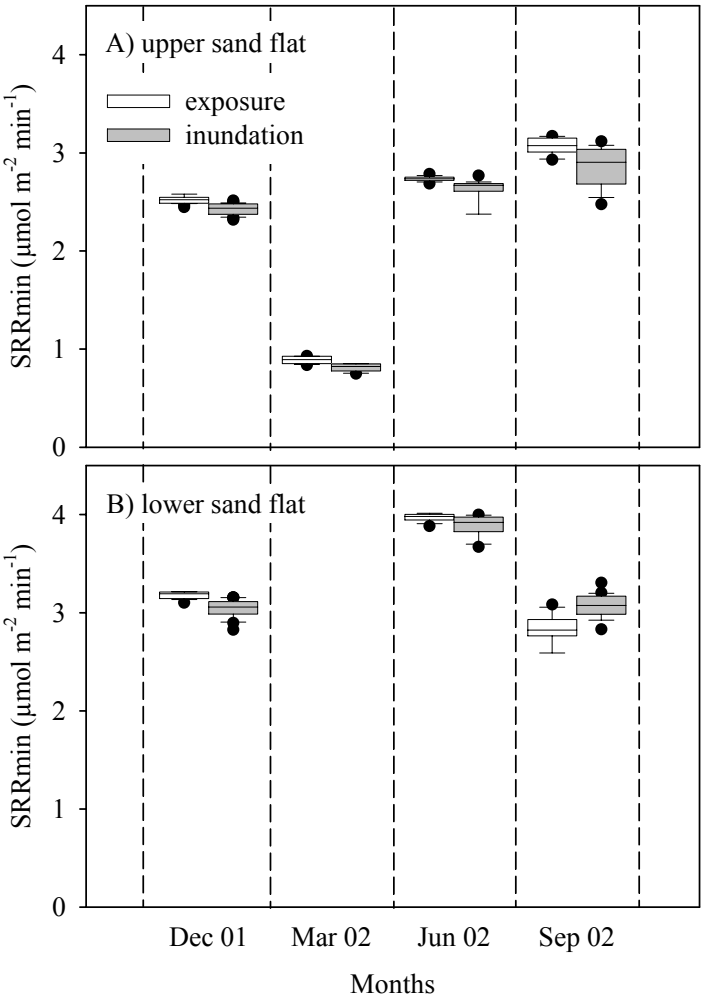


Figure 7**:** Sulfate reduction rates integrated over the anoxic sediment up to 15 cm depth (SRRmin) during exposure (white boxes) and inundation (grey boxes) at the (A) upper and (B) lower sand flat. The boxes comprise the 25$^{th}$ and 75$^{th}$ percentiles and the line within the boxes represents the median. The 10$^{th}$ and 90$^{th}$ percentiles are represented by whiskers and outliers by filled circles.

Daily rates of areal oxygen consumption and depth integrated sulfate reduction for all investigated months are presented for a full day and for exposure and inundation periods in Table 2. Daily oxygen consumption rates at the lower sand flat were 2.8 times higher during June 2002 as compared to the upper flat as a result of the higher

Table 2: Daily rates of areal oxygen consumption and sulfate reduction between December 2001 and March 2004 at the upper and lower sand flat site with respective inundation and exposure times. All rates represent mineralization in mmol C $m^{-2}$ $d^{-1}$ with the range in parentheses.

| Upper sand flat | December 01/02 | March 02 | June 02 | September 02 | July 03 | March 04 |
|---|---|---|---|---|---|---|
| Exposure (hrs:min) | 14:55 | 14:20 | 13:50 | 11:50 | 13:50 | 19:20 |
| Inundation (hrs:min) | 09:05 | 09:40 | 10:10 | 12:10 | 10:10 | 04:40 |
| Exposure /Inundation | 1.6 | 1.5 | 1.4 | 1.0 | 1.4 | 4.1 |
| aOCR (total mineral.) daily | 30.5 (13.5 - 47.6) * | 84.8 (81.6 - 87.9) † | 93.9 (87.7 - 100.1) | 106.0 (88.9 - 123.1) | 200.1 (186.5 - 215.9) | 80.6 (78.9 - 82.2) |
| aOCR (total mineral.) exposure | 15.8 (6.0 - 25.6) * | 40.5 (39.2 - 41.9) † | 43.1 (39.9 - 46.3) | 37.9 (32.9 - 43.0) | 90.1 (84.0 - 98.9) | 57.5 (56.7 - 58.4) |
| aOCR (total mineral.) inundation | 14.7 (7.4 - 22.0) * | 44.2 (42.4 - 46.1) † | 50.7 (47.7 - 53.8) | 68.1 (56.0 - 80.2) | 110.1 (102.6 - 117.0) | 23.1 (22.3 - 23.9) |
| SRRmax daily | 7.6 (6.6 - 8.8) | 2.8 (1.8 - 4.2) | 8.2 (7.4 - 9.0) | 9.5 (9.0 - 10.2) | | |
| SRRmax exposure | 4.8 (4.2 - 5.6) | 1.8 (1.1 - 2.7) | 5.0 (4.5 - 5.5) | 4.7 (4.4 - 5.0) | | |
| SRRmax inundation | 2.8 (2.4 - 3.2) | 1.0 (0.6 - 1.5) | 3.2 (2.9 - 3.5) | 4.9 (4.6 - 5.2) | | |
| SRRmin daily | 7.2 (6.0 - 8.2) | 2.5 (1.6 - 3.8) | 7.7 (6.9 - 8.5) | 8.5 (8.2 - 8.9) | | |
| SRRmin exposure | 4.6 (3.9 - 5.3) | 1.6 (1.0 - 2.5) | 4.8 (4.3 - 5.3) | 4.3 (4.2 - 4.6) | | |
| SRRmin inundation | 2.6 (2.1 - 2.9) | 0.8 (0.5 - 1.3) | 2.9 (2.6 - 3.2) | 4.2 (4.1 - 4.4) | | |
| % SRRmin;max of aOCR daily | 23.4 - 24.9 | 2.9 - 3.3 | 8.3 - 8.8 | 8.0 - 9.0 | | |
| % SRRmin;max of aOCR exposure | 29.2 - 30.5 | 4.1 - 4.4 | 11.1 - 11.7 | 11.4 - 12.3 | | |
| % SRRmin;max of aOCR inundation | 17.3 - 18.8 | 1.9 - 2.2 | 5.8 - 6.3 | 6.2 - 7.2 | | |
| **Lower sand flat** | | | | | | |
| Exposure (hrs:min) | 11:20 | | 10:40 | 09:40 | | |
| Inundation (hrs:min) | 12:40 | | 13:20 | 14:20 | | |
| Exposure /Inundation | 0.9 | | 0.8 | 0.7 | | |
| aOCR (total mineral.) daily | | | 268.8 (257.5 - 280.1) | 105.6 (35.9 - 175.4) | | |
| aOCR (total mineral.) exposure | | | 105.8 (99.6 - 112.0) | 48.6 (18.0 - 79.2) | | |
| aOCR (total mineral.) inundation | | | 163.0 (157.9 - 168.1) | 57.1 (18.0 - 96.2) | | |
| SRRmax daily | 9.4 (8.6 - 10.4) | | 11.7 (9.9 - 13.6) | 10.3 (9.2 - 11.5) | | |
| SRRmax exposure | 4.4 (4.0 - 4.9) | | 5.3 (4.5 - 6.2) | 4.1 (3.7 - 4.6) | | |
| SRRmax inundation | 5.0 (4.5 - 5.5) | | 6.4 (5.4 - 7.4) | 6.2 (5.5 - 6.9) | | |
| SRRmin daily | 8.9 (7.9 - 9.9) | | 11.3 (9.7 - 12.8) | 8.6 (7.7 - 9.6) | | |
| SRRmin exposure | 4.3 (3.9 - 4.8) | | 5.2 (4.4 - 5.9) | 3.3 (2.9 - 3.7) | | |
| SRRmin inundation | 4.6 (4.1 - 5.1) | | 6.1 (5.2 - 6.9) | 5.3 (4.7 - 5.9) | | |
| % SRRmin;max of aOCR daily | | | 4.2 - 4.4 | 8.2 - 9.8 | | |
| % SRRmin;max of aOCR exposure | | | 4.9 - 5.0 | 6.8 - 8.5 | | |
| % SRRmin;max of aOCR inundation | | | 3.7 - 3.9 | 9.3 - 10.9 | | |

* pOCR measured in December 2002, OPD measured in December 2001

† pOCR measured in March 2004, OPD measured in March 2002

volumetric OCR rates, but did not differ between the two sites during September 2002 (Table 2, Fig. 2). During average tidal cycles with about 14 hours of exposure per day, daily rates of oxygen consumption were approximately the same during exposure and inundation (Table 2), but this ratio shifted corresponding to longer inundation (September 2002) or exposure periods (March 2004). Daily sulfate reduction rates were only slightly higher at the lower sand flat site. Assuming that sulfate reduction was the dominant anaerobic mineralization process, sulfate reduction contributed between 3 and 25 % to total mineralization (aOCR), depending on the season (Table 2).

*Pore water solute concentrations*: The pore water nutrient and DIC concentrations were one order of magnitude higher at the lower sand flat than at the upper flat during most months (Fig. 8). This difference was most distinct during December 2001 and from December 2002 until March 2004 ($p<0.001$) but less pronounced during June and September 2002 ($p<0.001$, $p<0.01$ for silicate). Pore water DOC concentrations were, on the other hand, never different between both study sites.

At the upper sand flat, the solute concentrations (nutrients, DIC, DOC) showed a seasonal trend with higher concentrations during the warmer months (June, July, September) and lower concentrations during the colder months (March, December) ($p<0.001$). Surprisingly, no seasonality was apparent for the lower sand flat, as nutrient and DIC concentrations were lower in Summer 2002 than in Winter 2002 and a further increase in concentrations was observed in summer 2003 and spring 2004.

The pore water solute concentrations varied only slightly between the tidal cycle samplings at the upper sand flat and no particular pattern could be observed. All upper sand flat profiles were regarded as replicates, as they did not differ significantly ($p>0.05$).

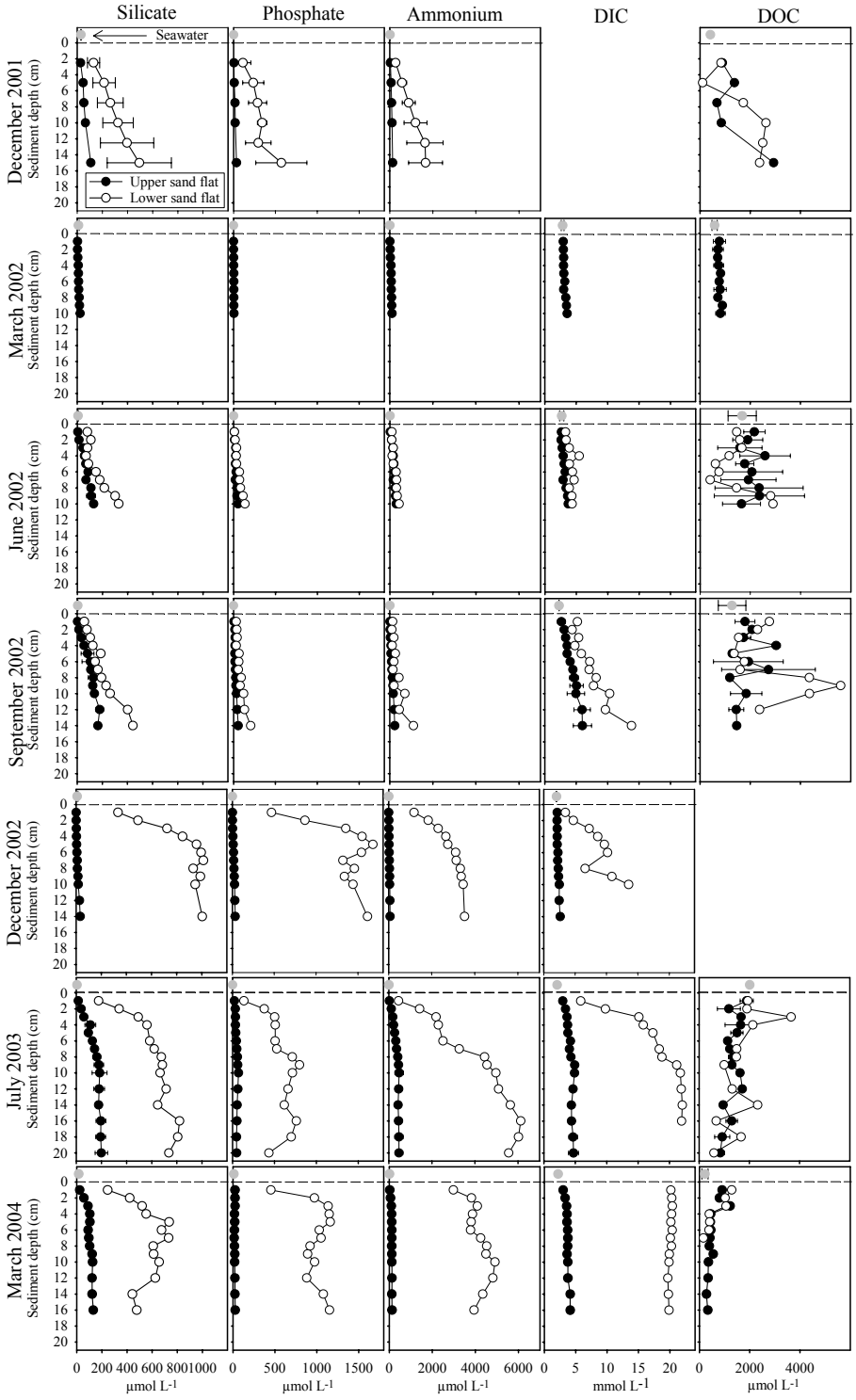


Fig. 8: Pore water nutrient, DIC and DOC concentrations at the upper and lower sand flat sites

**Discussion**

*Variability of areal OCR and depth integrated SRR over the tidal cycle*: Oxygen generally penetrated deeper into the sediment during inundation of the Janssand tidal flat. The deeper oxygen penetration resulted in higher areal oxygen consumption and lower sulfate reduction rates (minimum assessment) during submergence of the tidal flat.

In laboratory measurements, however, Brotas et al. (1990) attributed a deeper oxygen penetration into exposed sandy sediment to intrusion of air and this was also postulated by Usui et al. (1998) for an intertidal flat based on the observation that upper sediment layers became undersaturated in water content. Porosity measurements during July 2003 at the Janssand tidal flat, however, did not reveal a significant decrease in water content during low tide. In fine sands such as the Janssand tidal flat, the sediment stays completely water saturated during exposure due to capillary forces (Drabsch et al. 1999, Atherton et al. 2001) preventing intrusion of air. Nevertheless, in situ oxygen penetration was much deeper (down to 15 mm in July 2003 and March 2004) than in retrieved laboratory cores (2 to 3.5 mm for July and March, respectively).

Although benthic photosynthesis can generate high oxygen concentrations in the surface layer of the sediment (Revsbech et al. 1980, Berninger and Huettel 1997), we never observed consistently deeper oxygen penetration and, hence, higher OCR during daylight exposure than during nighttime exposure (Fig. 5). Macrofauna can strongly enhance interfacial exchange processes (Rhoads 1974, Huettel 1990, Graf and Rosenberg 1997), but faunal activity is heterogeneous and unlikely to completely stop during the laboratory measurements. Thus, other mechanisms were responsible for the deeper in situ penetration of oxygen during low tide than in the laboratory. We observed that during exposure the Janssand sand flat continuously drains pore water that flows through the sediment towards the low water line. This drainage permits intrusion of the oxygen-rich water that remained as puddles on the sediment surface into the sand and also penetration of oxygen contained in surface layer pore water deeper into the bed. Dispersion of the pore water flow within the porous sediment matrix may further enhance oxygen

penetration depth. These mechanisms are not active in the retrieved cores, explaining the lesser oxygen penetration in the laboratory.

During inundation of the tidal flat, the interaction of unidirectional or oscillating water currents with sediment topography induces advective flow of pore water through the permeable bed (Webb and Theodor 1968, Thibodeaux and Boyle 1987, Huettel and Gust 1992). Pressure oscillations caused by waves passing over the permeable sediment also contribute to the pore water flow (Riedl et al. 1972, Van der Loeff 1981). Bottom currents and waves lead to a continuous change of sediment topography, e.g. by ripple migration. Oscillating flow interacting with sediment ripples generates an intrusion of oxygenated water into the ripple faces and outflow of anoxic pore water near the ripple crests (Precht and Huettel 2003). This leads to varying oxygen penetration depths at small spatial scales corresponding to the ripple length. Along with ripple migration during inundation, as observed in several oxygen profiles from the study site, the intrusion/outflow-zones move along the sediment surface (Precht et al. 2004, Franke et al. submitted). Additionally, the bioirrigation activity of benthic macrofauna during submergence can lead to a deeper transport of oxygen into the sediment (Aller 2001, Wenzhöfer and Glud 2004). Benthic photosynthesis, on the other hand, may decrease with increasing water depth due to diminishing light penetration in the turbid Wadden Sea waters (Colijn and Cadee 2003).

Combined measurements of near bottom water flow and oxygen profiles at the Janssand tidal flat revealed a deeper oxygen penetration with increasing average flow velocities (Fig. 9). The observation of the same co-variance in a recent study of another permeable, intertidal sand flat (Werner et al. submitted) suggests that hydrodynamic forcing is the determining factor for the variability of oxygen penetration. The hydrodynamically induced advective transport of oxygenated water into the sediment, therefore, is responsible for the higher areal OCR and lower depth integrated SRR during indundation of the Janssand tidal flat.

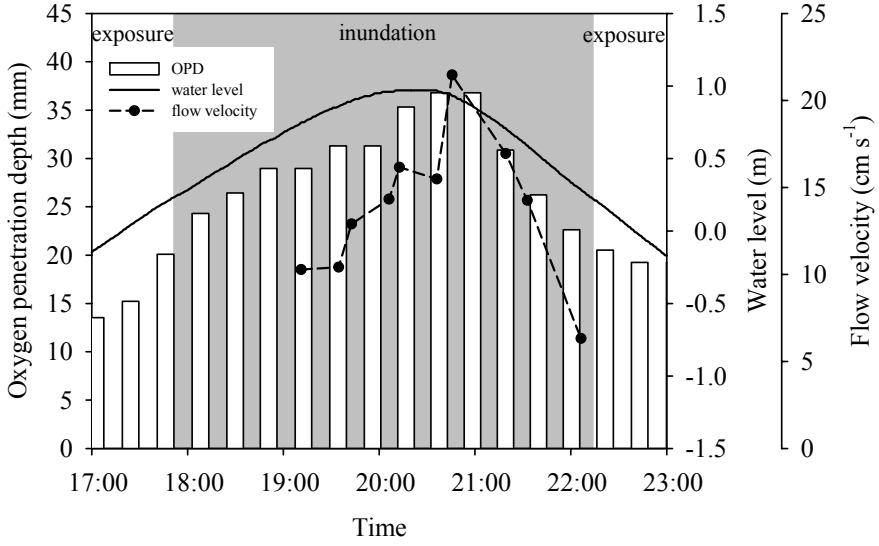


Figure 9: Relationship between the average water flow velocity 5 cm above the sea floor and oxygen penetration depth (OPD) during December 2001. The solid line denotes the change of the sea water level relative to mean sea level.

The importance of advective pore water exchange and resultant oxygen supply to the sediment for the mineralization of organic matter is reflected by the potential oxygen consumption rates that were at least one order of magnitude higher than the potential sulfate reduction rates (compare Fig. 3 and Fig. 4). Consequently, the share of depth integrated sulfate reduction to total mineralization was relatively low in the investigated top 15 cm of the Janssand sediment (3 to 10 % during most months). The microbial community can access the high energy yield of aerobic mineralization as soon as oxygen is supplied to the respective sediment layers. Despite the enhancement of potential mineralization rates by the advective oxygen supply during submergence and the lower potential rates during exposure, total mineralization during low tide can be as high as during submergence due to the relatively long exposure of the Janssand during an average tidal cycle. This may also partially explain why no tidal differences in pore water nutrient and DIC concentrations were measured. Tidal differences in pore water nutrients and DIC were not evident even during extraordinarily long (September 2002) and short (March 2004) inundation periods. Possible pore water concentration differences were probably too small within this short timeframe and may have been masked by spatial heterogeneity.

*Seasonal variability of OCR and SRR*: The oxygen consumption rates were consistent with the temperature dependence of aerobic mineralization (Thamdrup et al. 1998). A higher availability and degradability of organic matter during the summer months may have contributed to the observed seasonality of oxygen consumption. For sulfate reduction, seasonality was only partially evident in the low March values, but December rates were close to the summer measurements. This is surprising, as the temperature dependence for sulfate reduction is even stronger than that of aerobic mineralization (Thamdrup et al. 1998). In September 2002, high rates of sulfate reduction in the uppermost sediment layers of both study sites suggest a recent input of fresh organic matter, possibly by an autumn algal bloom. In December 2001, the sulfate reducers possibly profited from the mineralization of such an algal bloom as reflected in only slightly lower pore water DOC concentrations in winter as compared to June and September 2002 (see Fig. 8).

*Differences between the upper and lower sand flat sites*: Higher mineralization rates should lead to more degradation products such as DIC and nutrients. Indeed, the seasonal trend of oxygen consumption rates was reflected in the solute concentrations at the upper sand flat site. Interestingly, this was not the case for the lower sand flat, where nutrient and DIC concentrations were not linked to season. Depth integrated sulfate reduction and areal OCR were comparable between both study sites and thus cannot explain the observed 5-15 times higher concentrations of degradation products at the lower flat. Benthic chamber incubations confirmed the similar oxygen consumption rates for both study sites (Billerbeck et al. in prep.) and comparable sulfate reduction rates between both sites were also measured in another study at this tidal flat (Bosselmann in prep.). The higher oxygen consumption at the lower flat in June 2002 was restricted to a 1 cm thick sediment layer (see Fig. 2) suggesting the presence of buried organic material such as macroalgae and may reflect spatial variability. In order to produce the large difference in solute concentrations between the two sites in July 2003 and March 2004, mineralization rates (as estimated from aOCR) need to be about 10 times higher at the lower flat. As this clearly was not the case, the high concentration of metabolic products and seasonal independence of these

concentrations at the lower sand flat points to a non-local source for the nutrients and DIC at this site.

As the Janssand sediment has a permeability permitting pore water flow, the exposure of the tidal flat during low tide and ensuing hydraulic gradient between the pore water table and sea water level lead to drainage transport of pore water through the sediment from the upper flat directed towards the low water line (Nielsen 1990). Tracer injections revealed that this drainage affects at least the sediment layers down to 50 cm depth with drainage transport velocities of 0.07 to 0.12 m $d^{-1}$ (Billerbeck et al. in prep.) Sedimentary decomposition processes and drainage transport result in a concentration increase of metabolic products towards the low water line (Billerbeck et al. in prep.). With the rather slow drainage transport, about 1 to 2 years are needed for the pore water to travel the distance of 50 m from the upper flat to the lower flat. Due to mixing and dispersion within the sediment during this passage, seasonal fluctuations in concentrations of metabolic products are evened out and, thus, are absent at the point of emergence. Slow pore water flows likely exist also below 50 cm sediment depth with degradation products originating from the large inner area of the tidal flat. Such deep flows may additionally contribute to the high pore water solute concentrations at the lower flat sampling site.

In contrast to nutrients and DIC, DOC concentrations followed a seasonal trend at the lower flat, similar to the situation at the upper flat. We explain this observation with the different transport characteristics of dissolved and particulate material in the sand (Huettel et al. 1996) and the tight link between particulate and dissolved organic matter concentrations observed in marine sediments (Ehrenhauss et al. 2004). Degradable organic particles, e.g. phytoplankton cells, are retained in the uppermost sediment layer in permeable sediment when water is filtered through the bed due to drainage or bottom current driven sediment percolation (Pilditch et al. 1997, Huettel and Rusch 2000). The degradation of this material may cause only a non-significant change in the nutrient concentration at the lower flat site due to the relatively high background concentrations, however, it may have caused the noticeable seasonal changes in the DOC concentration at that site and also at the upper flat site.

At the lower sand flat, drained pore water is discharged via the sediment surface from a seepage face that extends from the low water line about 30 meters upslope the tidal flat. As a consequence of this discharge, reduced substances are highly concentrated also in the upper sediment layer that is regularly flushed with sea water during inundation (Billerbeck et al. in prep.). The contribution of chemical oxidation to measurements of total oxygen consumption in the regularly oxygenated sediment layer of the lower flat needs to carefully be accounted for, especially during periods with high concentration of reduced substances at this site. This was evident in the September 2002 measurement of pOCR at the lower flat, where the repeated flushing of the sediment resulted in a distinct decrease in oxygen consumption. Probably, the rates measured after flushing the large pool of reduced substances out of the sediment may best represent the actual aerobic mineralization. At the upper sand flat, the contribution of chemical oxidation to total oxygen consumption is likely small in the regularly oxygenated sediment layer (Polerecky et al. 2005).

Our results demonstrate that the nutrient recycling by the biocatalytical filtration system sand flat works on two distinctly different temporal and spatial scales (Fig. 10):

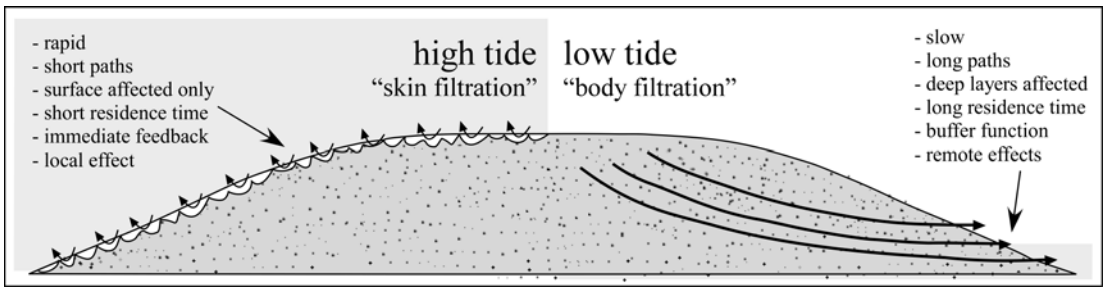


Figure 10: "Skin" and "Body" filtration in an intertidal sand flat. During high tide, boundary flow-topography interaction causes flushing of the surface sediment layer. Organic particles are filtered from the water, degraded and nutrients are returned promptly. During low tide, drainage removes nutrient-rich pore water from the entire sand flat, providing a season-independent nutrient source acting as a buffer.

(1) Filtration of water through the surface layer (<10cm) of the sediment, due to bottom flow-topography interaction, flushes the upper few centimeters of the sand bed resulting in retention of degradable organic particles in the surface layer and flushing of metabolic products (inorganic nutrients, DIC) from this layer. The spatial scale of these "skin circulation cells" is in the order of centimeters and the time scale is in the order of hours to days. The process is active only during inundation. Solute concentrations in these small and rapid circulation cells reflect tidal, daily and seasonal patterns. The recycling of nutrients of the small cells, thus, provides immediate feedback to the ecosystem during inundation.

(2) Filtration of water through the sand flat due to a tidal drainage process that is active only during exposure. This "body circulation cell" filters a large water volume (total discharge in Janssand about 80,000 to 130,000 L on each tidal cycle, Billerbeck et al. in prep.) through the entire body of the sand flat at a relatively small pore flow velocity. Since the spatial scales of this large flow cell are in the order of tens to hundreds of meters, the residence time is rather long with time scales in the order of years to tens of years. This recycling, thus, is independent of seasonal oscillations and can act as a nutrient reservoir and nutrient source during times of low nutrient concentrations in the water column.

With the combination of a fast and a slow nutrient recycling system, the tidal biocatalytical sand filter rapidly responds to organic matter input by instantaneous nutrient regeneration and release, while at the same time the sand flat acts as a buffer for nutrients that is independent of short-term and seasonal fluctuations. The rapid "skin filtration" feeds back nutrients only during inundation and thus supports benthic and pelagic primary production within the intertidal area. The slow "body filtration" returns nutrients only during exposure of the tidal flat and contributes to the increase in nutrient concentration of the Wadden Sea water during low tide (Niesel and Günther 1999). The export of this nutrient rich water by tidal currents and a decreased turbidity in the open North Sea can lead to high primary production in a belt of coastal waters seaward of the barrier islands (Colijn et al. 1987, Colijn and Cadee 2003). The ecological consequence of such a recycling system operating on two different alternating time scales is a dampening of short term and seasonal fluctuations in primary productivity through immediate feed back as well as continuous nutrient return to the system. Because the slow

"body filtration" releases pore water only during low tide, this process may act also as an efficient pump that removes metabolic products from the intertidal zone to the North Sea with the tidal currents. This removal may be essential for maintaining the biocatalytical filtration capacity of the intertidal sands.

**Acknowledgments:** We thank M. Alisch for the assistance in field and laboratory work and acknowledge the hospitality and help of the Plattboden-ship crews during the cruises. We thank G. Schüssler, S. Menger, D. Franzke and S. Pabel for their help with laboratory work. We acknowledge G. Eickert, I. Schröder, K. Hohmann, I. Dohrmann and C. Wiegand for making the sensors and thank J. Langreder, A. Nordhausen, G. Herz, A. Kutsche, P. Färber, V. Meyer and H. Osmers for technical assistance.

W. Anton of the WSA Emden kindly provided tide gauge data. This study was supported by the Deutsche Forschungsgemeinschaft (DFG) within the research group "Biogeochemistry of the Wadden Sea" (FG 432-5), coordinated by Prof. J. Rullkötter. We are grateful to Prof. B. B. Jørgensen and Dr. M. E. Böttcher for their support of this work and coordination of the sub-project "Biogeochemical processes at the sediment-water interface of intertidal sediments".

## References

Aller R.C. (2001) Transport and reactions in the bioirrigated zone. In: Boudreau B.P., Jørgensen B.B. (eds) The Benthic Boundary Layer. Oxford University Press, Oxford, p 269-301

Atherton R.J., Baird A.J., Wiggs G.F.S. (2001) Inter-tidal dynamics of surface moisture content on a meso-tidal beach. J. Coast. Res. 17:482-489

Bergamaschi B.A., Tsamakis E., Keil R.G., Eglinton T.I., Montlucon D.B., Hedges J.I. (1997) The effect of grain size and surface area on organic matter, lignin and carbohydrate concentration, and molecular compositions in Peru Margin sediments. Geochim. Cosmochim. Acta 61:1247-1260

Berninger U.G., Huettel M. (1997) Impact of flow on oxygen dynamics in photosynthetically active sediments. Aquat. Microb. Ecol. 12:291-302

Boudreau B., Huettel M., Forster R., Jahnke A., McLachlan J., Middelburg J., Nielsen P., Sansone F., Taghon G., Van Raaphorst W., Webster I., Weslawski J., Wiberg P., Sundby B. (2001) Permeable Marine Sediments: Overturning an Old Paradigm. EOS Trans. Am. Geophys. Union 82:133-136

Brotas V., Amorim-Ferreira A., Vale C., Catarino F. (1990) Oxygen profiles in intertidal sediments of Ria Formosa (S. Portugal). Hydrobiologia 207:123-129

Cammen L.M. (1991) Annual Bacterial Production in Relation to Benthic Microalgal Production and Sediment Oxygen-Uptake in an Intertidal Sandflat and an Intertidal Mudflat. Mar. Ecol. Prog. Ser. 71:13-25

Colijn F., Admiraal W., Baretta J.W., Ruardij P. (1987) Primary production in a turbid estuary, the Ems-Dollard: field and model studies. Cont. Shelf Res. 7:1405-1409

Colijn F., Cadee G.C. (2003) Is phytoplankton growth in the Wadden Sea light or nitrogen limited? J. Sea Res. 49:83-93

D'Andrea A.F., Aller R.C., Lopez G.R. (2002) Organic matter flux and reactivity on a South Carolina sandflat: The impacts of porewater advection and macrobiological structures. Limnol. Oceanogr. 47:1056-1070

Dauwe B., Middelburg J.J., Herman P.M.J. (2001) Effect of oxygen on the degradability of organic matter in subtidal and intertidal sediments of the North Sea area. Mar. Ecol. Prog Ser. 215:13-22

de Beer D., Wenzhoefer F., Ferdelman T.G., Boehme S.E., Huettel M., van Beusekom J.E.E., Boettcher M.E., Musat N., Dubillier N. (2005) Transport and mineralization rates in North Sea sandy intertidal sediments, Sylt-Rømø Basin, Wadden Sea. Limnol. Oceanogr. 50:113-127

Drabsch J.M., Parnell K.E., Hume T.M., Dolphin T.J. (1999) The capillary fringe and the water table in an intertidal estuarine sand flat. Estuar. Coast. Shelf Sci. 48:215-222

Ehrenhauss S., Witte U., Buhring S.L., Huettel M. (2004) Effect of advective pore water transport on distribution and degradation of diatoms in permeable North Sea sediments. Mar. Ecol. Prog. Ser. 271:99-111

Flemming B.W., Ziegler K. (1995) High-resolution grain size distribution patterns and textural trends in the backbarrier environment of Spiekeroog Island (southern North Sea). Senckenb. Marit. 26:1-24

Forster S., Huettel M., Ziebis W. (1996) Impact of boundary layer flow velocity on oxygen utilisation in coastal sediments. Mar. Ecol. Prog. Ser. 143:173-185

Fossing H., Jørgensen B.B. (1989) Measurement of Bacterial Sulfate Reduction in Sediments - Evaluation of a Single-Step Chromium Reduction Method. Biogeochemistry 8:205-222

Franke U., Polerecky L., Precht E., Huettel M. Wave tank study of particulate organic matter degradation in permeable sediments. submitted to Limnol. Oceanogr.

Glud R.N., Forster S., Huettel M. (1996) Influence of radial pressure gradients on solute exchange in stirred benthic chambers. Mar. Ecol. Prog. Ser. 141:303-311

Glud R.N., Klimant I., Holst G., Kohls O., Meyer V., Kuehl M., Gundersen J.K. (1999) Adaptation, test and in situ measurements with O-2 microopt(r)odes on benthic landers. Deep-Sea Res. Part I-Oceanogr. Res. Pap. 46:171-183

Graf G., Rosenberg R. (1997) Bioresuspension and biodeposition: A review. J. Mar. Syst. 11:269-278

Grasshoff K., Kremling K., Ehrhardt M. (1999) Methods of seawater analysis, Vol. Wiley-VCH Verlag

Hall P.O.J., Aller R.C. (1992) Rapid, small-volume, flow injection analysis for $\Sigma CO_2$ and $NH_4^+$ in marine and freshwaters. Limnol. Oceanogr. 37:1113-1119

Howes B.L., Goehringer D.D. (1994) Porewater drainage and dissolved organic carbon and nutrient losses through the intertidal creekbanks of a New England salt marsh. Mar. Ecol. Prog. Ser. 114:289-301

Huettel M. (1990) Influence of the lugworm *Arenicola marina* on porewater nutrient profiles of sand flat sediments. Mar. Ecol. Prog. Ser. 62:241-248

Huettel M., Gust G. (1992) Impact of bioroughness on interfacial solute exchange in permeable sediments. Mar. Ecol. Prog. Ser. 89:253-267

Huettel M., Røy H., Precht E., Ehrenhauss S. (2003) Hydrodynamical impact on biogeochemical processes in aquatic sediments. Hydrobiologia 494:231-236

Huettel M., Rusch A. (2000) Transport and degradation of phytoplankton in permeable sediment. Limnol. Oceanogr. 45:534-549

Huettel M., Webster I.T. (2001) Porewater flow in permeable sediments. In: Boudreau B.P., Jørgensen B.B. (eds) The Benthic Boundary Layer. Oxford University Press, Oxford, p 144-179

Huettel M., Ziebis W., Forster S. (1996) Flow-induced uptake of particulate matter in permeable sediments. Limnol. Oceanogr. 41:309-322

Huettel M., Ziebis W., Forster S., Luther G.W. (1998) Advective transport affecting metal and nutrient distributions and interfacial fluxes in permeable sediments. Geochim. Cosmochim. Acta 62:613-631

Jahnke R.A., Alexander C.R., Kostka J.E. (2003) Advective pore water input of nutrients to the Satilla River Estuary, Georgia, USA. Estuar. Coast. Shelf Sci. 56:641-653

Jørgensen B.B. (1977) Bacterial sulfate reduction within reduced microniches of oxidized marine-sediments. Mar. Biol. 41:7-17

Jørgensen B.B. (1978) Comparison of methods for the quantification of bacterial sulfate reduction in coastal marine-sediments .1. Measurement with radiotracer techniques. Geomicrobiol. J. 1:11-27

Jørgensen B.B. (1982) Mineralization of organic-matter in the sea bed - the role of sulfate reduction. Nature 296:643-645

Jørgensen B.B., Bak F. (1991) Pathways and microbiology of thiosulfate transformations and sulfate reduction in a marine sediment (Kattegat, Denmark). Appl. Environ. Microbiol. 57:847-856

Kallmeyer J., Ferdelman T.G., Weber A., Fossing H., Jørgensen B.B. (2004) A cold chromium distillation procedure for radiolabeled sulfide applied to sulfate reduction measurements. Limnol. Oceanogr.: Methods 2:171-180

Klute A., Dirksen C. (1986) Hydraulic conductivity and diffusivity: Laboratory methods. In: Klute A. (ed) Methods of soil analysis - part 1 - Physical and mineralogical methods. American Society of Agronomy, p 687-700

Kuwae T., Kibe E., Nakamura Y. (2003) Effect of emersion and immersion on the porewater nutrient dynamics of an intertidal sandflat in Tokyo Bay. Estuar. Coast. Shelf Sci. 57:929-940

Llobet-Brossa E., Rossello-Mora R., Amann R. (1998) Microbial community composition of Wadden Sea sediments as revealed by flourescence in situ hybridization. Appl. Environ. Microbiol. 64:2691-2696

Lohse L., Epping E.H.G., Helder W., van Raaphorst W. (1996) Oxygen pore water profiles in continental shelf sediments of the North Sea: Turbulent versus molecular diffusion. Mar. Ecol. Prog. Ser. 145:63-75

Marschall C., Frenzel P., Cypionka H. (1993) Influence of oxygen on sulfate reduction and growth of sulfate-reducing bacteria. Arch. Microbiol. 159:168-173

Nielsen P. (1990) Tidal dynamics of the water table in beaches. Water Resour. Res. 26:2127-2134

Niesel V., Günther C.P. (1999) Distribution of nutrients, algae and zooplankton in the Spiekeroog backbarrier system. In: Dittmann S. (ed) The Wadden Sea Ecosystem - Stability properties and mechanisms. Springer-Verlag, Berlin Heidelberg New York, p 77-94

Orvain F., Sauriau P.G. (2002) Environmental and behavioural factors affecting activity in the intertidal gastropod *Hydrobia ulvae*. J. Exp. Mar. Biol. Ecol. 272:191-216

Osgood D.T. (2000) Subsurface hydrology and nutrient export from barrier island marshes at different tidal ranges. Wetlands Ecol. Manage. 8:133-146

Pilditch C.A., Emerson C.W., Grant J. (1997) Effect of scallop shells and sediment grain size on phytoplankton flux to the bed. Cont. Shelf Res. 17:1869-1885

Polerecky L., Franke U., Werner U., Grunwald B., de Beer D (2005) High spatial resolution measurement of oxygen consumption rates in permeable sediments. Limnol. Oceanogr.: Methods 3:75-85

Precht E., Franke U., Polerecky L., Huettel M. (2004) Oxygen dynamics in permeable sediments with wave-driven pore water exchange. Limnol. Oceanogr. 49:693-705

Precht E., Huettel M. (2003) Advective pore-water exchange driven by surface gravity waves and its ecological implications. Limnol. Oceanogr. 48:1674-1684

Revsbech N.P. (1989) An oxygen microsensor with a guard cathode. Limnol. Oceanogr. 34:474-478

Revsbech N.P., Sørensen J., Blackburn T.H., Lomholt J.P. (1980) Distribution of oxygen in marine-sediments measured with microelectrodes. Limnol. Oceanogr. 25:403-411

Rhoads D.C. (1974) Organism-sediment relations on the muddy sea floor. Oceanogr. Mar. Biol., Annu. Rev. 12:263-300

Riedl R.J., Huang N., Machan R. (1972) The subtidal pump: Mechanism of interstitial water exchange by wave action. Mar. Biol. 13:210-221

Rocha C. (1998) Rhythmic ammonium regeneration and flushing in intertidal sediments of the Sado Estuary. Limnol. Oceanogr. 43:823-831

Rusch A., Forster S., Huettel M. (2001) Bacteria, diatoms and detritus in an intertidal sandflat subject to advective transport across the water-sediment interface. Biogeochemistry 55:1-27

Rusch A., Huettel M., Reimers C.E., Taghon G.L., Fuller C.M. (2003) Activity and distribution of bacterial populations in Middle Atlantic Bight shelf sands. FEMS Microbiol. Ecol. 44: 89-100

Thamdrup B., Hansen J.W., Jørgensen B.B. (1998) Temperature dependence of aerobic respiration in a coastal sediment. FEMS Microbiol. Ecol. 25:189-200

Thibodeaux L.J., Boyle J.D. (1987) Bedform-generated convective transport in bottom sediment. Nature 325:341-343

Usui T., Koike I., Ogura N. (1998) Tidal effect on dynamics of pore water nitrate in intertidal sediment of a eutrophic estuary. J. Oceanogr. 54:205-216

Van der Loeff M.M.R. (1981) Wave effects on sediment water exchange in a submerged sand bed. Neth. J. Sea Res. 15:100-112

Webb J.E., Theodor J. (1968) Irrigation of Submerged Marine Sands through Wave Action. Nature 220:682-683

Wentworth C.K. (1922) A scale of grade and class terms for clastic sediments. J. Geol. 30:377-392

Wenzhöfer F., Glud R.N. (2004) Small-scale spatial and temporal variability in coastal benthic O-2 dynamics: Effects of fauna activity. Limnol. Oceanogr . 49:1471-1481

Wenzhöfer F., Holby O., Glud R.N., Nielsen H.K., Gundersen J.K. (2000) In situ microsensor studies of a shallow water hydrothermal vent at Milos, Greece. Mar. Chem. 69:43-54

Werner U., Billerbeck M., Polerecky L., Franke U., Huettel M., van Beusekom J.E.E., de Beer D. Spatial and temporal pattern of mineralization rates and oxygen distribution in a permeable intertidal sandflat (Sylt, Germany). submitted to Limnol. Oceanogr.

Whiting G.J., Childers D.L. (1989) Subtidal advective water flux as a potentially important nutrient input to southeastern U.S.A. saltmarsh estuaries. Estuar. Coast. Shelf Sci. 28:417-431

# Spatial patterns of aerobic and anaerobic mineralization rates and oxygen penetration dynamics in coral reef sediments (Heron Island, Australia)

Ursula Werner, Paul Bird, Christian Wild, Timothy Ferdelman, Lubos Polerecky, Gabriele Eickert, Ron Jonstone, Ove Hoegh-Guldberg, and Dirk de Beer

submitted to Marine Ecology Progress Series

**Abstract**

Oxygen consumption rates (OCR), aerobic mineralization and sulfate reduction rates (SRR) were studied in the permeable carbonate reef sediments of Heron Reef, Australia. Four stations with different hydrodynamic regimes were selected for this study. In situ oxygen penetration dynamics into the sediments were measured with an autonomous microsensor profiler. Areal OCR were quantified from the measured oxygen penetration depth and volumetric OCR. Oxygen penetration and dynamics (median penetration depths at the four stations ranged between 0.3 and 2.2 cm), OCR (median 57 to 196 mmol C $m^{-2}$ $d^{-1}$), aerobic mineralization (median 24 to 176 mmol C $m^{-2}$ $d^{-1}$) and SRR (median 9 to 42 mmol C $m^{-2}$ $d^{-1}$) were highly variable between sites. The supply of oxygen by pore water advection was a major cause for high mineralization rates by stimulating aerobic mineralization at all sites. However, estimated bottom water filtration rates could not explain the pattern in volumetric OCR and SRR found between the four stations. This suggest that local mineralization rates are additionally controlled by other factors than current driven pore water advection, e.g., on the distribution of the benthic fauna, or by local differences in labile organic carbon supply from sources such as benthic photosynthesis. Carbon mineralization rates were among the highest reported for coral reef sediments, stressing the role of these sediments for reef ecosystem functioning.

## Introduction

In shallow coral reef systems, the carbonate sediments and the reef framework are sites where a large fraction of the organic matter produced in the water column or by benthic primary production is mineralized (Clavier and Garrigue 1999, Richter et al. 2001, Wild et al. 2004b). Consequently, sediments contribute strongly to an efficient element cycling within the reef system (Andrews and Hans 1983, Rasheed et al. 2002, Wild et al. 2004a), which is the reason why coral reefs maintain their high biomass and high gross primary productivity, despite being situated in oligotrophic waters (Crossland and Barnes 1983) .

Unconsolidated carbonate sediments cover large areas within a coral reef (Capone et al. 1992, Clavier and Garrigue 1999), however, little is known about aerobic and anaerobic mineralization processes within these sands. Sedimentary mineralization processes depend on transport mechanisms that provide electron donors and electron acceptors to the benthic system. Transport processes between water column and sediments include molecular diffusion, pore water advection, gravitational settling of particles, burial due to lateral sediment transport and biological transport (bioturbation/bioirrigation) (Huettel and Gust 1992, Shum and Sundby 1996, Aller 2001). Coral reef sediments are highly permeable, reaching permeabilities of $10^{-9}$ $m^2$ (Enos and Sawatsky 1981, Wheatcraft and Buddemeier 1981, Rasheed et al. 2003). In permeable sediments, the advective circulation of bottom water through the sediments (i.e. pore water advection) is considered a major transport mechanism (Buddemeier and Oberdorfer 1988, Huettel et al. 2003), that may largely exceed transport by diffusion (Boudreau et al. 2001). Pore water advection is considered a major reason for high mineralization rates in permeable sediments (Webb and Theodor 1968, Huettel and Gust 1992, Shum and Sundby 1996), by providing oxygen and organic carbon from the water column to the benthic system, while removing potentially inhibitory end products of mineralization processes (Ziebis et al. 1996, Falter and Sansone 2000, Rusch et al. 2000). Pore water advection is generated by pressure gradients across the sediment as resulting from the interaction of currents or waves with uneven bed-topography (Buddemeier and Oberdorfer 1988, Huettel and Gust 1992, Precht and Huettel 2003), or from density fluctuations (Webster et al. 1996). In coral reefs, tide-

induced pressure gradients resulting from water level differences across the reef crest may cause a significant water flow through sediments and reef framework (Oberdorfer and Buddemeier 1986, Parnell 1986).

The supply of oxygen to and its penetration depth into the sediments determines whether aerobic and anaerobic processes are dominant. Oxygen consumption, the sum of aerobic mineralization and the oxygen consumption by reduced substances from the anaerobic decay, increases with an increasing advective supply of oxygen (Forster et al. 1996). Measurements of oxygen distribution in coral reef sediments are rare. King et al. (1990) measured an oxygen penetration depth of 0.5 to 1 cm and an oxygen penetration exceeding 1.5 cm when water movement was high. In another coral reef sediment oxygen was reported to penetrate 15 to 50 cm, which was attributed to wave action (Falter and Sansone 2000). A deep oxygen penetration may support benthic aerobic and suboxic metabolism. In coral reef sediments aerobic mineralization is dominant over anaerobic degradation (Boucher et al. 1994, Alongi 1998).

The dominant anaerobic mineralization process in most coastal marine sediments is sulfate reduction, typically responsible for up to 50% of the mineralization of organic matter (Jorgensen 1982, Canfield et al. 1993). Little is known about sulfate reduction in permeable sediments, such as those from coral reefs. It is difficult to predict whether the permeability enhances or limits sulfate reduction: advective transport from the water column supplies organic carbon to fuel sulfate reduction rates, as well as oxygen that may lower sulfate reduction rates.

In order to evaluate the metabolic activity of sands, the choice of method is crucial. As the activity of permeable sands may be closely linked to pore water advection, the methods used to measure benthic activity should not block the local pore water advection (Buddemeier and Oberdorfer 1988). Oxygen consumption rates (OCR) are used since the late 1960s as an integrating measure of sedimentary metabolism (Hargrave 1969). However, for the assessment of OCR, slurry incubations and flux calculations from pore water oxygen profiles are of limited use in sands, as they do not account for advective exchange. Stirred benthic chambers generate pressure gradients and pore water circulation patterns, resembling those generated by currents interacting with topography (Huettel and

Rusch 2000), however, intensive studies on local hydrodynamics and sediment topography are necessary in order to mimic natural pore water advection rates. To obtain oxygen consumption rates that account for pore water advection, we chose a recently introduced method that combines in situ time series of oxygen penetration depth measurements with laboratory measurements of volumetric sedimentary OCR (de Beer et al. 2005, Polerecky et al. 2005).

One focus of this study was the in situ measurement of oxygen penetration and dynamics in the carbonate sediments of Heron Reef, Australia. A second focus was the determination of oxygen consumption, aerobic mineralization and sulfate reduction with methodological approaches that account for effect of pore water advection. Four study sites were selected with strongly different hydrodynamic regimes, to examine whether pore water advection is the main controlling parameter for benthic mineralization rates and to examine the ratio between aerobic and anaerobic mineralization.

## Material and Methods

*The study site*: The study was carried out at Heron Island, Australia (23°27' S, 151°55'E). The island is located in the lagoonal platform reef Heron Reef, on the southern boundary of the Great Barrier Reef (Fig.1a). Average tidal range is 2 m (spring) and 1 m (neap) with westerly current set during flood and an easterly currents set during the ebb. The average wind direction is south-east. The mean annual air temperature is 24.1°C (T. Upton, pers. com.). Field experiments were conducted at four sublitoral stations (Fig. 1b). North Beach (NB), a shallow site exposed to strong currents and Shark Bay (SB), a sheltered site exposed to weak currents were located within the pseudolagoon close to the island. Here unconsolidated sediments occupy 78% of the surface area (calculated using unpublished data from A. Klueter) and corals form only small discrete patches.

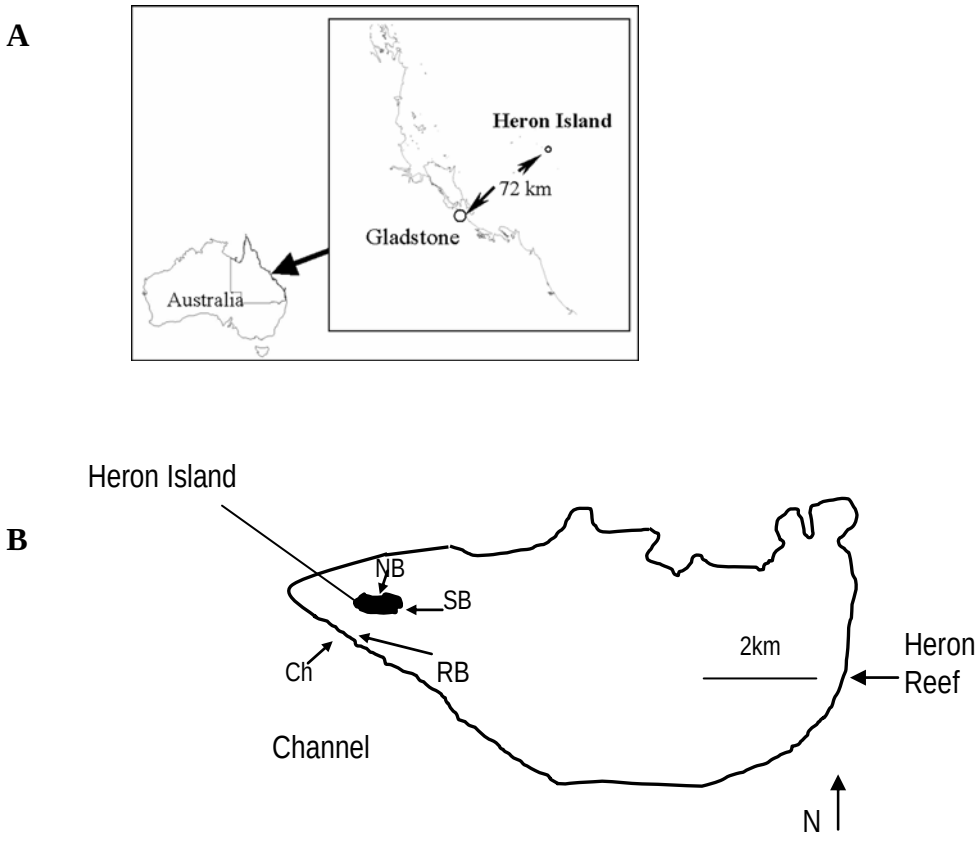


Figure 1: A) Location of Heron Island, B) Location of the four sampling sites North Beach (NB), Shark Bay (SB), the Reef Belt (RB) and the Channel Station (Ch) at Heron Reef

More remote from the island were the Reef Belt Station (RB) and the Channel Station (Ch), where unconsolidated sediments occupy 60% of the area and corals are almost continuous. The Reef Belt Station was situated at the coral belt surrounding the pseudolagoon and was exposed to strong currents and breaking waves. The Channel Station was located outside the reef platform, close to the reef edge in the channel between Heron Reef and Wistari Reef (water depth: 5 m depth). Here currents were calm. The sediments at all stations consisted of carbonate sands of biogenic origin. At Shark Bay and North Beach highest abundance of sediment mounds and burrows created by faunal organisms were detectable by eye, and by careful digging highest numbers of macrofauna were exposed, when comparing sites. At the Reef Belt Station lowest macrofaunal abundances were found. Within sites, we took care to measure and sample in areas that were low in abundances of faunal sediment structures. At Shark Bay a larger area inhabited with *Callianassa sp.* was found ca. 20 m remote from our sampling site.

*Sampling*: Most of the sampling and measurements were carried out in January 2002. During the sampling period sea water temperature varied between 27 and 33°C and salinity ranged between 28 and 33. Measurements and sampling were conducted within an area of 2 $m^2$ at each site. Sampling for the analysis of sediment characteristics, oxygen consumption rates and sulfate reduction rates was done with plastic cores (inner diameter 3.6 cm). Sampling depth was usually 10 cm, but in some cases less due to buried rocks and compacted underground.

*Sediment characteristics*: Porosity and total organic carbon (TOC) content were determined in 1 cm subsections from 2 sediment cores per station. Samples for TOC were stored at -20°C and freeze dried before analysis. [TOC] was determined by subtracting the total inorganic carbon [TIC] content from the total carbon [TC] content. TIC was measured by coulometric titration on a CM 5012 UIC coulometer. TC was measured using a Heraeus CHNO-rapid elemental analyzer with sulfanilamid as a calibration standard. Porosity was calculated from the weight loss of a known volume of wet sediment after drying at 60°C until a constant weight was reached. Grain sizes were determined by sieving the pooled sediment of 2 cores through a calibrated sieve stack and classified according to (Wentworth 1922).

Permeability of the upper 7 cm of the sediment was measured using the constant head method (Klute and Dirksen 1986) on 2 replicate cores. The cores were stored frozen until analysis.

*In situ oxygen distribution*: In situ oxygen profiles were measured using Clark type oxygen microelectrodes (Revsbech 1989) with a tip diameter of 300 µm to prevent damage by the coarse grains, an actual sensing area of 5 µm diameter and a response time ($t_{90}$) of less than 5 seconds. The oxygen microsensors were mounted on an autonomous profiler as described previously (Glud et al. 1999, Wenzhofer et al. 2000). The device was positioned on the sediment with the microsensors initially 1-2 cm above the sediment surface. Downward profiles were continuously measured over ca. 24 h to a sediment depth of 6 cm, with a step size of 250 µm. One profile was recorded within 30 min, with a minimum pause of 5 min between the profiles. At North Beach and Shark Bay the 24 h measurements were repeated 3 times to assess longer scale temporal changes and assess reproducibility, at the other stations the 24 hour cycles were done once.

*Oxygen consumption rates*: Measurements of volumetric oxygen consumption rates were performed in the lab as described previously (de Beer et al. 2005, Polerecky et al. 2005). Experiments were conducted at 28°C, the average in situ temperature of the sediments in January 2002. Oxygen microsensors were positioned at a defined depth within the sediment cores. Sediments were oxygenated by percolating ambient aerated sea water through the sediment cores until a steady state was reached at the depth of measurement. Then the percolation was stopped, and the decrease of oxygen in time was monitored. The initial concentration decrease was taken as the potential volumetric oxygen consumption rate (pOCR). The measurements were conducted in 2 mm steps within the first centimeter of the sediment and in 0.5 cm steps between 1 and 4 cm. Two replicate profiles per core and two cores per station were measured. The measurements were performed in the dark to prevent photosynthesis.

The obtained volumetric values represent the potential oxygen consumption rates, whenever oxygen is present at the specific sediment depth. To obtain the areal OCR of the sediments, the rates were integrated over the depths of oxygen penetration as obtained in situ from the profiler (for more details see de Beer et al.

(2005) and Polerecky et al. (2005)). We assumed that OCR follow zero-order kinetics with respect to oxygen (Thamdrup et al. 1998).

*Sulfate reduction rates*: Sulfate reduction rates were measured with the whole core $^{35}SO_4^{2-}$ radiotracer incubation method (Jorgensen 1978) modified for permeable sediments (de Beer et al. 2005). For each treatment a minimum of 3 replicate sediment cores was incubated (incubation temperature of 28°C). Radiolabeled $^{35}SO_4^{2-}$ (Amersham) was added to 70 mL of ambient seawater to a specific activity of 340MBq/mol$SO_4^{2-}$. The seawater-tracer solution was placed on top of the sediment and allowed to drain into the core. The permeability of the sediment allowed an even distribution of tracer in the pore water. After 6 h incubation (unless specified differently below), the sediments were frozen at –20°C. The frozen sediments were then sliced in 0.5 (0-3 cm depth) or 1 cm sections (below 3 cm) and fixed in 20% ZnAc. Samples were processed using the cold chromium distillation procedure (Kallmeyer et al. 2004). The method was slightly modified by first adding HCl until all carbonates were dissolved. Radioactivity of $^{35}SO_4^{2-}$ and Total Reduced Inorganic Sulfur (TRIS) was determined with a liquid scintillation counter (Packard 2500 TR), using Lumasafe Plus® (Lumac BV, Holland) scintillation cocktail. Pore water sulfate concentrations were determined by non-suppressed ion-chromatography and conductivity detection with a Waters 510 HPLC pump, Waters WISP 712 autosampler (100µL injection volume), Waters IC-Pak anion exchange column (50 x 4.6 mm) and a Waters 430 Conductivity detector. The eluant was 1 mM isophthalate buffer in 10% methanol, adjusted to pH 4.5 with sodium tetraborate.

In permeable sediments, the thus determined sulfate reduction rates may not be the in situ rates, as the supply of oxygen is restricted to molecular diffusion during incubation. In the field oxygen penetrates much deeper into the sediments and may lower sulfate reduction rates, although this anaerobic process has been measured in oxidized and oxic sediments (Jorgensen 1977, Jorgensen and Bak 1991). Because of the uncertainty about the inhibitory effects of oxygen, we made maximum and minimum estimations. The maximum sulfate reduction rates ($SRR_{max}$) were not corrected for possible oxygen inhibition. To obtain minimum sulfate reduction rates ($SRR_{min}$), i.e. assuming oxygen completely inhibits sulfate

reduction, rates were integrated over the anoxic sediment depths only, as deduced from the in situ oxygen measurements.

*Addition experiment*: To asses a possible limitation of SRR by organic matter, we added glucose (2 mmol $L^{-1}$), acetate (2mmol $L^{-1}$) or fresh coral mucus (0.72 mmol C $L^{-1}$) to sediments cores taken from Shark Bay together with the seawater-tracer solution (3 replicates per treatment).

*Influence of photosynthesis*: To asses the effect of photosynthesis on sulfate reduction, we incubated sediments from Shark Bay and North Beach in the dark and under light (PAR: 800 µmol Photons $m^{-2}$ $s^{-1}$; lamp: KL 1500 electronic, Schott, Germany). To assess the effect of a full light period the incubation times were 12 h (3 replicates per treatment).

*Silver foil technique*: By trapping radiolabeled $H_2{}^{35}S$ on a silver foil as $Ag^{35}S$, two-dimensional images of $H_2{}^{35}S$ distribution were obtained (e.g., Krumholz et al. 1997, Visscher et al. 2000). Strips of silver foil (30 x 85 mm and 0.1 mm thick; Johnson Matthey GmbH, UK) were prepared as described in Krumholz et al. (1997). The silver foil was attached to the inner wall of cores before sampling of sediments from North Beach and Shark Bay (4 replicates per station). The radiotracer incubation was then performed as described above and cores were incubated for 12-14 h. After incubation the cores were frozen , slightly thawed on the outside and pushed out of the core, together with the foil. The foil was removed from the still frozen sediment, washed with sea water to remove residual $^{35}SO_4{}^{2-}$. Distribution of radioactivity of $Ag^{35}S$ precipitates on the foils were analyzed using a phosphor imager (Phosphor imager SI, Molecular Dynamics). Three profiles were assessed with a vertical data points resolution of 50 µm. For direct comparison with the silver foil data, the incubated sediments were further used for determination of SRR with the tracer whole core incubation method as described above.

*Aerobic mineralization rates*: Oxygen consumption is the sum of aerobic mineralization and oxidation of reduced substances from anaerobic decay (e.g., $Fe^{2+}$ and $H_2S$). The sulfide produced during sulfate reduction is oxidized back to sulfate within the sediments, using oxygen as the ultimate electron acceptor. Therefore areal aerobic mineralization rates were calculated by subtracting the SRR (expressed in equivalents of oxygen used for the oxidation of sulfides to sulfate)

from the measured OCR. We assumed sulfate reduction to be the most important anaerobic respiration process, the others were ignored. We ignored burial of iron-sulfides, as iron concentrations in coral reef sediments are low (Alongi et al. 1996, Chambers et al. 2001).

*Estimated bottom water filtration rates*: The oxygen penetration depth is controlled by the balance between a downward transport of oxygen and the sedimentary OCR. Therefore, from the combined oxygen penetration depth and OCR data the supply rate of oxygen to the sediment can be calculated that is needed to lead to the measured oxygen penetration depth given the local OCR. From the supply rate of oxygen, one can further calculate the water volume that is pumped through the sediments (bottom water filtration rates in L $m^{-2}$ $h^{-1}$ ) by using the oxygen concentration in the overlying water as summarized in the following formula (Polerecky et al. 2005):

$$v_f = \int_0^{z_p} OCR(z)dz \times c_o^{-1} \quad (1)$$

with $v_f$ being the bottom water filtration rate in L $m^{-2}$ $h^{-1}$, $\int_0^{z_p} OCR(z)dz$ being the oxygen consumption rates integrated over the oxygen penetration depth ($z_p$) in mmol $m^{-2}$ $h^{-1}$ and $c_0$ being the oxygen concentration in the overlying water in mmol $L^{-1}$. This calculation is based on the simplifying assumption that the advective supply resembles a downward percolation. In reality, the water enters the sediment at the ripple troughs and flanks and leaves the sediments near the ripple crest, thus the flow of filtered water through sediments follows a more curved path between in- and out flow areas (Huettel et al. 1996, Shum and Sundby 1996). These horizontal components of the flow are ignored in the chosen approach and the estimated bottom water filtration rates may thus underestimate natural pore water advection rates.

**Results**

*Sediment characteristics*: Sediments from all station were highly permeable (Table 1). The permeability was highest at Shark Bay. At North Beach and at the Reef Belt Station a similar permeability was determined, whereas the permeability of the Channel Station was lowest (Table 1). North Beach and Shark Bay were composed of coarse sand, whereas the Reef Belt Station and the Channel Station were composed of medium sands (medium and poorly sorted, respectively) according to Wentworth (1922). The content of grains in the silt and clay size class at the three platform stations was below 6% and at the Channel Station below 11%. Porosity was similar for the three platform station and decreased with depth at all stations.

The TOC content was low, constant with depth and comparable at most stations. At North Beach the TOC content in the upper 3 cm was higher than at the other stations (Table 1).

Table 1: Sediment properties at North Beach (NB), Shark Bay (SB), Reef Belt Station (RB) and the Channel Station (Ch). Except for grain size, data are averages ± standard deviation.

| | | permeability ( $10^{-11}$ $m^2$) | median grain size (µm) | porosity (%) | TOC (% DW) |
|---|---|---|---|---|---|
| NB | 0-7 cm | 8.4 ± 1.1 | 591 | | |
| NB | 0-3 cm | | | 66.8 ± 4.7 | 1.82 ± 0.2 |
| NB | 3-7 cm | | | 55.8 ± 3.5 | 0.74 ± 0.4 |
| SB | 0-7 cm | 13.6 ± 0.2 | 718 | 47.7 ± 2.7 | 0.50 ± 0.3 |
| RB | 0-7 cm | 6.5 ± 0.1 | 426 | 54.6 ± 0.9 | 0.75 ± 0.2 |
| Ch | 0-7 cm | 0.3 ± 0.001 | 227 | 64.5 ± 1.0 | 0.59 ± 0.2 |

*In situ oxygen distribution and dynamics*: During all measurements of in situ oxygen distribution the weather conditions were calm and comparable. Indeed, the three replicate measurements at Shark Bay and North Beach showed a high reproducibility (Fig. 2). Oxygen dynamics and oxygen penetration depths were different between stations (Fig. 2 & 3). At North Beach and at the Reef Belt Station oxygen penetrated deepest and oxygen dynamics were pronounced (Fig. 2 & 4). At

the Reef Belt Station breaking waves and strong currents lead to a dynamic seafloor topography and migrating ripples, therefore the oxygen penetration depth could not be determined for all profiles (Fig. 2). At Shark Bay and at the Channel Station the oxygen penetration depth was shallow and dynamics were small (Fig. 2, 3, 5).

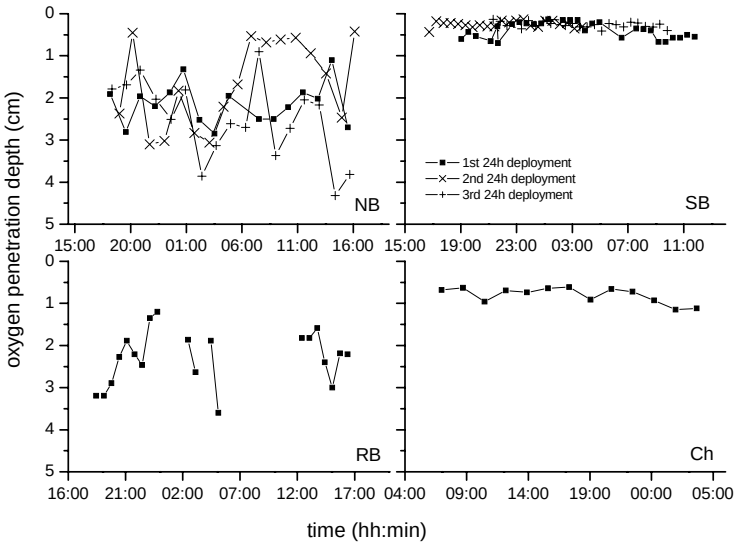


Figure 2. Oxygen penetration depth at the four investigated sites North Beach (NB), Shark Bay (SB), the Reef Belt (RB) and the Channel Station (Ch). Zero represents the sediment surface.

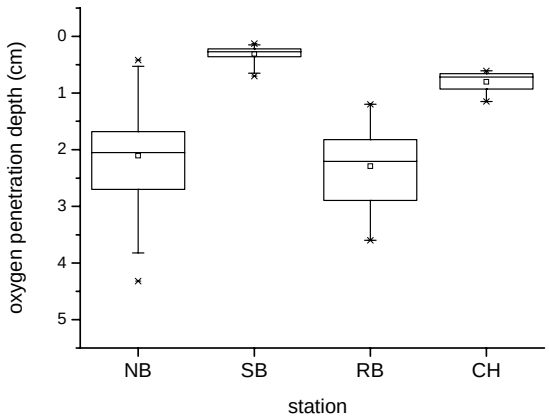


Figure 3: Statistical chart (box charts) of the oxygen penetration depths at North Beach (NB), Shark Bay (SB), the Reef Belt (RB) and the Channel Station (Ch). The horizontal lines in the box represent the 25$^{th}$, 50$^{th}$ (median), and 75$^{th}$ percentile values. The error bars represent the 5$^{th}$ and 95$^{th}$ percentile values. The symbols below and above the error bar denote the extreme values. The average is shown as a square symbol in the box.

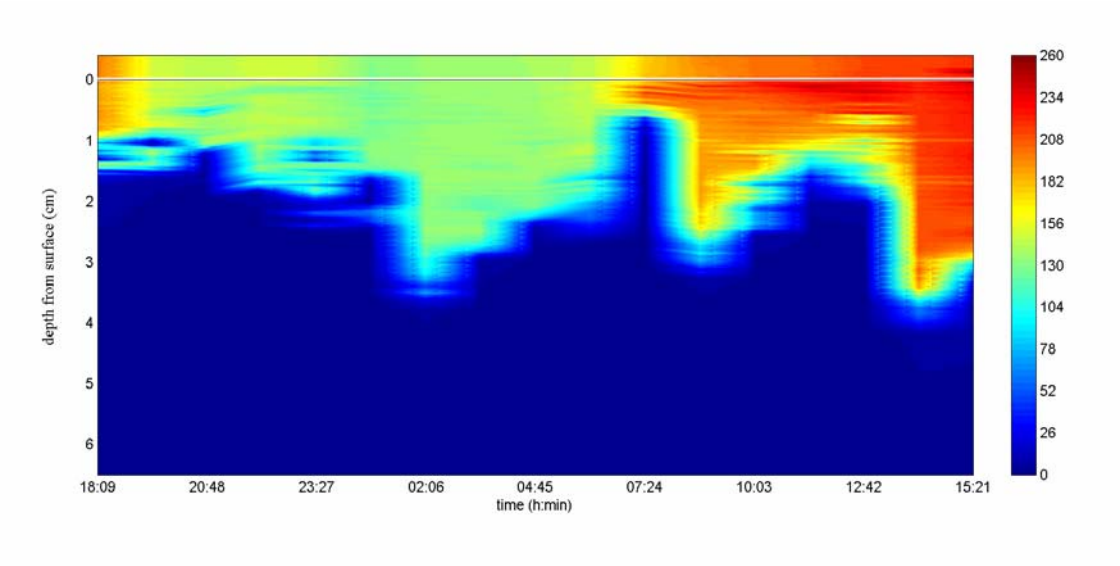


Figure 4.Time series of oxygen profiles at North Beach. The graph shows measurements of one day. The color scheme represent oxygen concentration in µmol $L^{-1}$. The horizontal line at zero represents the sediment surface. Note that oxygen saturation is approx. 200 µmol $L^{-1}$, indicating oxygen oversaturation of the overlying water and the upper sediment layers during the day.

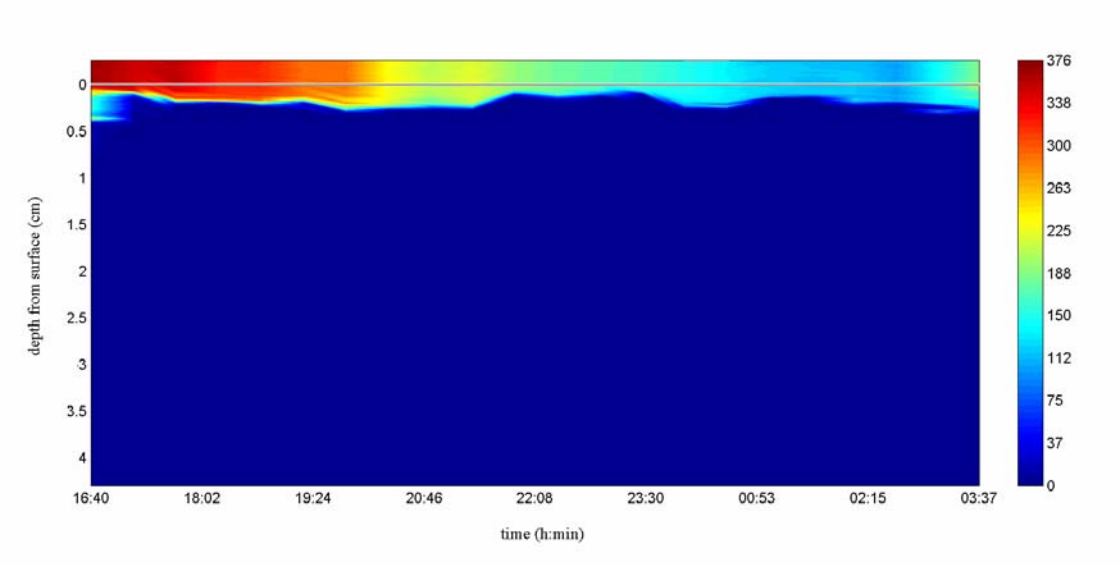


Figure 5: Time series of oxygen profiles at Shark Bay. The graph shows measurements of one day. The color scheme represent oxygen concentration in µmol $L^{-1}$. The horizontal line at zero represents the sediment surface.

In Figure 6a in situ oxygen profiles are displayed which show that photosynthesis and bioturbation can supply oxygen to the sediments. Photosynthesis causes the near surface oxygen peak, with concentrations above that of the overlaying water. Bioturbation may have caused the deeper ephemeral oxygen peak. Figure 6b shows a pore water advection dominated, rather sigmoid shaped oxygen profile (Revsbech et al. 1980) measured in situ, with a deep oxygen penetration and a constant oxygen concentration in the upper 2.7 cm. In contrast, the diffusion dominated oxygen profile measured in the lab (Fig. 6b), showed a shallow oxygen penetration and the nearly parabolic shape of diffusion dominated profiles.

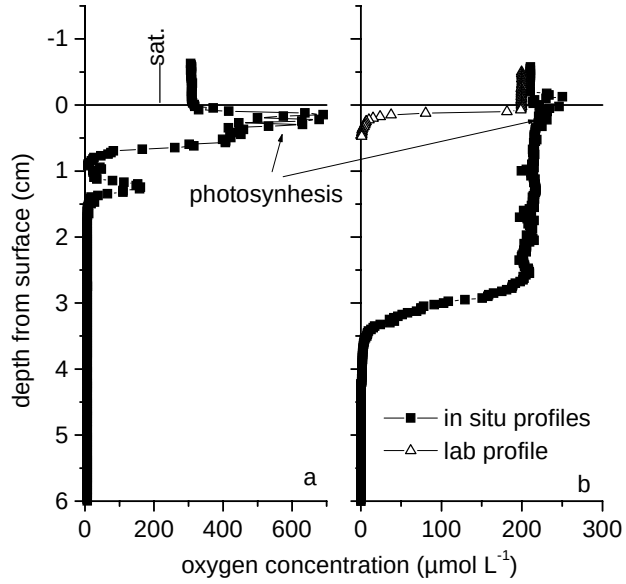


Figure 6: Examples of oxygen concentration profiles measured at North Beach. Profiles with filled symbols are in situ oxygen profiles. Oxygen production by benthic photosynthesis is indicated. The deep oxygen peak in Figure 6 a may result from faunal pumping activity. For comparison of pore water advection and diffusion dominated oxygen profiles, a diffusive lab profile is shown in Figure 6 b (open symbol). Sat. denotes the saturation of oxygen at ambient temperature and salinity.

*Oxygen consumption rates*: The highest pOCR (above the maximal oxygen penetration depth) were measured at the Channel Station (Fig. 7). The two stations close to the island showed intermediate and similar pOCR, whereas the Reef Belt Station had lowest pOCR.

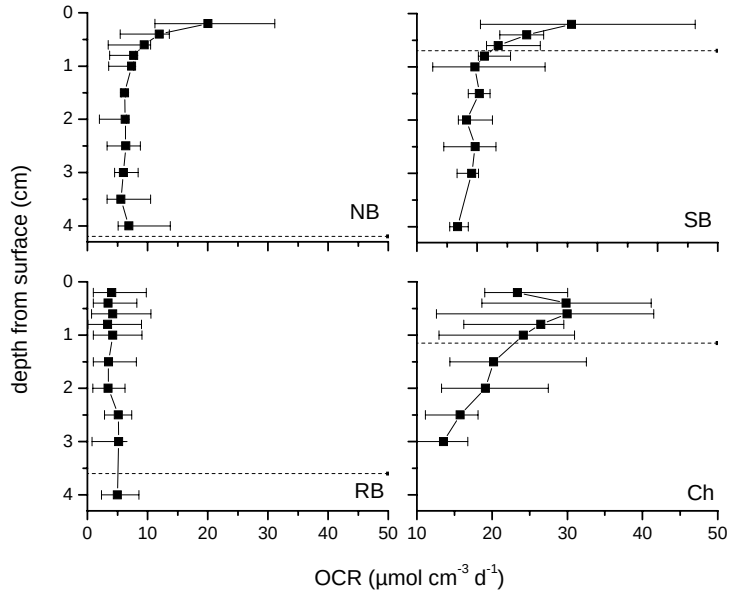


Figure 7: Median volumetric oxygen consumption rates (OCR). The error bars for the volumetric oxygen consumption rates indicate the measured data range. The hatched line indicates the maximum oxygen penetration depth.

The areal OCR (Fig. 8 & Table 2) are obtained by integrating the pOCR over the varying oxygen penetration depths. Although pOCR were comparable at North Beach and Shark Bay, the different oxygen penetration at these stations resulted in different areal OCR. The areal OCR at North Beach with its deep oxygen penetration and at the Channel Station with its shallow oxygen penetration were comparable, so the deep oxygen penetration compensated for lower volumetric activities. At the Reef Belt Station areal OCR were intermediate.

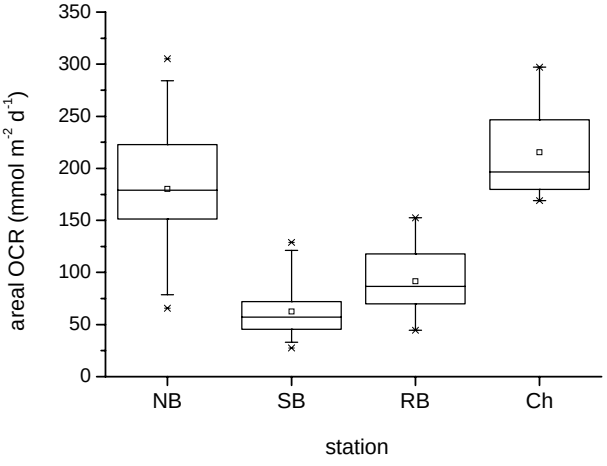


Figure 8: Box chart of the areal oxygen consumption rates (OCR) at North Beach (NB), Shark Bay (SB), the Reef Belt (RB) and the Channel Station (Ch). For detailed description of the box chart refer to Figure 5.

Table 2: Areal oxygen consumption rates (OCR), estimated areal aerobic mineralization, maximum and minimum depth integrated sulfate reduction rates ($SRR_{max}$ and $SRR_{min}$) and contribution of sulfate reduction to total carbon mineralization. First value of estimated aerobic mineralization is based on OCR and $SRR_{max}$ , the second value is based on OCR and $SRR_{min}$. The first value of the contribution of SRR to total carbon mineralization is based on $SRR_{min}$, the second value is based on $SRR_{max}$. Integration depth for SRR is 7 cm.

| Station | North Beach | Shark Bay | Reef Belt | Channel Station |
|---|---|---|---|---|
| OCR (mmol C $m^{-2}$ $d^{-1}$) | | | | |
| median | 183.5 | 57.1 | 88.2 | 196.6 |
| range | 66-305 | 27-129 | 44-153 | 169-297 |
| est. aerobic mineralization (mmol C $m^{-2}$ $d^{-1}$) | | | | |
| median | 142-160 | 21-24 | 79-83 | 173-176 |
| $SRR_{max}$ (mmol C $m^{-2}$ $d^{-1}$) | | | | |
| median | 41.8 | 36.1 | 9.1 | 24.2 |
| range | 38-58 | 26-44 | 6-11 | 20-28 |
| $SRR_{min}$ (mmol C $m^{-2}$ $d^{-1}$) | | | | |
| median | 23.2 | 33.4 | 5.4 | 20.8 |
| range | 19-40 | 23-41 | 2-7 | 17-25 |
| Contrib. SRR to carbon mineralization (%) | | | | |
| | 15-27 | 69-74 | 6-10 | 12-14 |

*Sulfate reduction rates*: The sulfate concentrations were in the range of 28-30 mmol $L^{-1}$, and did not vary with depth or between stations. Volumetric SRR (Fig. 9) at all sites were highest in the upper 2-3 cm of the sediment. Depth integrated SRR varied between sites (Tab. 2), with highest potential sulfate reduction rates ($SRR_{max}$) found at North Beach and Shark Bay. The Channel Station had intermediate $SRR_{max}$, whereas the Reef Belt Station had the lowest $SRR_{max}$ of all stations. The minimum estimate of the sulfate reduction rates ($SRR_{min}$) differed from $SRR_{max}$, especially at the stations with the deep oxygen penetration (North Beach and the Reef Belt Station) (Tab. 2). The relative contribution of sulfate reduction to total mineralization (Tab. 2), varied between the sites. At most stations anaerobic mineralization contributed 10 to 20%, only in Shark Bay most organic matter was mineralized anaerobically.

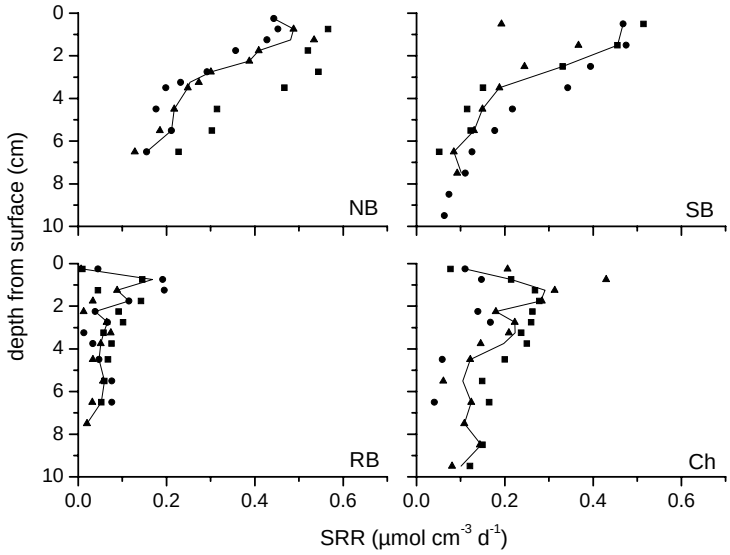


Figure 9: Sulfate reduction rates (SRR) at North Beach (NB), Shark Bay (SB), the Reef Belt (RB) and the Channel Station (Ch). The black symbol represent the three replicate measurements, the line represents the median of the data set.

*Aerobic mineralization rates*: The pattern of aerobic mineralization rates (Tab. 2) was comparable to the pattern of the areal OCR, with high rates found at North Beach and at the Channel Station, intermediate rates at the Channel station and low rates at Shark Bay.

OCR and SRR were repeatedly measured in August 2003 (data not shown) at all stations except the Channel Stations. Similar volumetric rates and comparable trends between the stations were found.

*SRR in response to organic carbon addition*: The addition of glucose and acetate (2 mmol C $L^{-1}$) increased SRR at all depths, showing a limitation of SRR by dissolved organic carbon. Surprisingly, the addition of fresh, homogenized coral mucus (0.72 ± 0.03 mmol C $L^{-1}$) did not increase, but decreased SRR (Fig. 10).

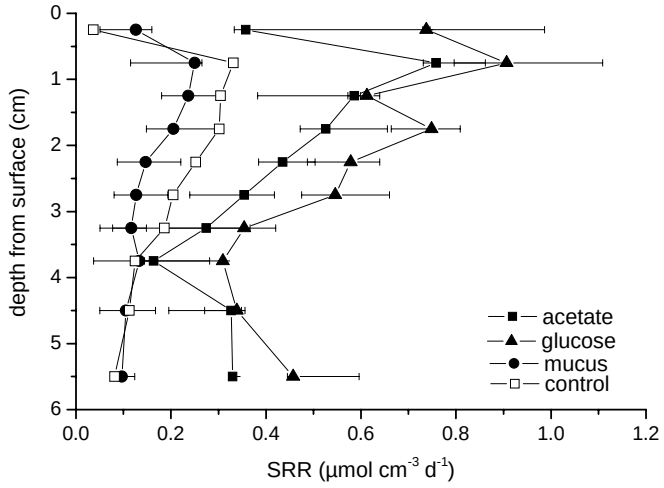


Figure 10: Median sulfate reduction rates after the addition of glucose, acetate and homogenized coral mucus and control. The error bars represent the data range.

*Effect of light on SRR*: Illumination did not affect SRR (data not shown). Thus, photosynthetically produced organic substances or oxygen, did not result in a detectable effect on SRR within a 12 h period.

*$H_2S$ production measurement by the silver foil technique*: The variability among the three replicate profiles of $Ag^{35}S$ measured per silver foil was small and the shapes of the replicate profiles per foil were similar with depth for all cores from Shark Bay and North Beach (Fig. 11).The depth distribution of radioactive $H_2S$ trapped on the silver foil showed, however, in 7 out of 8 data sets, no agreement with the depth distribution of SRR measured with the tracer whole core incubation method in the same core (Fig. 11).

*Estimated bottom water filtration rates*: Estimated bottom water filtration rates were similar at North Beach and the Channel Station (NB: median 33 L $m^{-2}$ $h^{-1}$, range 4-70 L $m^{-2}$ $h^{-1}$; Ch: median 34 L $m^{-2}$ $h^{-1}$, range 20-62 L $m^{-2}$ $h^{-1}$). Pore water advection rates at Shark Bay and at the Reef Belt Station were lower (SB: median 10 L $m^{-2}$ $h^{-1}$, range 3-30 L $m^{-2}$ $h^{-1}$; RB: median 12 L $m^{-2}$ $h^{-1}$, range 3-53 L $m^{-2}$ $h^{-1}$).

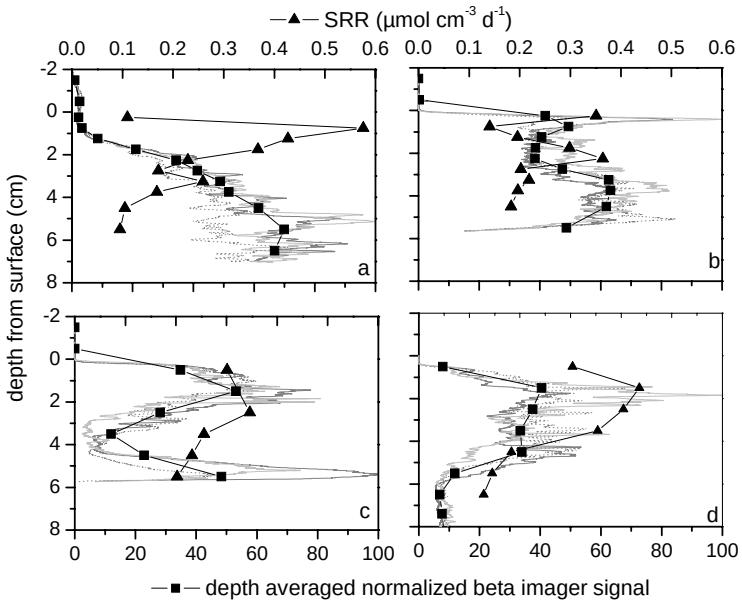


Figure 11: Comparison of normalized beta imager signal of $Ag^{35}S$ on silver foil and sulfate reduction rates obtained with the tracer whole core incubation method of four representative sediment cores. The grey lines indicate three distinct beta imager signal profiles that were measured per silver foil, the line graph with the square symbol represents their median, averaged over 0.5 cm depth intervals. The sulfate reduction rates (SRR) obtained with the tracer whole core method are shown by a line graph with triangle symbols.

**Discussion**

*Oxygen distribution*: At all stations, pore water advection was a major factor for the transport of oxygen into the sediments as can be derived from the sigmoid shape of the oxygen profiles and the deep and variable in situ oxygen penetration depths compared to diffusion controlled laboratory experiments (oxygen penetration depth <3mm, data not shown).

Oxygen penetration and dynamics were different between sites. Oxygen penetrated deep and dynamically at the two exposed sites North Beach and Reef Belt Station, whereas at the more sheltered stations Shark Bay and the Channel Station the oxygen penetration was shallow and uniform. The sequence for oxygen penetration depths at the four station may be summarized as NB = RB > Ch > SB. All stations were composed of sediments typical for permeable sediments. There was, however, no correlation between the oxygen penetration depth and permeability. Shark Bay had, for example, the highest permeability but the lowest oxygen penetration depths. The differences in oxygen penetration and dynamics may thus to a large extend be explained by differences in the local hydrodynamics. The deep and variable oxygen penetration at North Beach and at the Reef Belt Station showed a fast and pronounced oxygenation and de-oxygenation caused by the strong and variable bottom currents and by wave action. Additionally, the local hydrodynamics led to migrating roughness elements (e.g., ripples) at these stations and the pressure gradients developing at these topographical structures are resulting in migrating zones of down and upwelling pore water (Huettel and Gust 1992, Precht et al. 2004), contributing to the alterations in the oxygen penetration depths. The shallower and more uniform oxygen penetration at the Channel Station and at Shark Bay indicate more stationary pressure gradients, which may result from weaker hydrodynamics or from more stationary sediment topography. At the Channel Station the effect of surface gravity waves on advective exchange may be smaller compared to the other stations due to the deeper water depth. At Shark Bay the development of microalgal mats has been observed, when currents were calm. Less turbulent hydrodynamics may lower resuspension and thus favor the development of microalgal mats (Demers et al. 1987), that may temporarily lower the sediment permeability. Benthic photosynthesis supplied oxygen to the top

sediment layers, often causing oxygen oversaturation, however, there was no obvious increase of the oxygen penetration depth caused by benthic photosynthesis. Our data do not show a variable oxygen penetration due to tide-induced pressure gradients across the reef crest (Oberdorfer and Buddemeier 1986, Parnell 1986).

The sequence of estimated bottom water filtration rates according to Eq. 1 is Ch = NB > RB = SB, North Beach and the Reef Belt Station (stations that may be rather comparable concerning sediment topography) thus are showing similar oxygen penetration depths but distinct pore water advection rates. The pore water advection rate was high at the Channel Station, which may be caused by a special topography or by bottom water currents being accelerated between coral patches. The bottom water filtration rates are estimates as the horizontal components of the pressure gradient driven flow of water through the sediments is neglected.

*Benthic mineralization rates*: Pore water advection is considered a major controlling factor for high mineralization rates in permeable sediments as the bottom water entering the sediments transports oxygen to deep sediments layers and organic matter of the water can be filtered out by the sediments (Webb and Theodor 1968, Pamatmat 1971, Huettel and Gust 1992, Shum and Sundby 1996). The method for the assessment of OCR used in this work allows the distinction between volumetric and areal OCR, as it is possible for SRR. The sequence of the volumetric OCR (in the oxygenated sediment layers) can be written as Ch > NB = SB > RB and for sulfate reduction as NB = SB > Ch > RB. Thus, the pattern of volumetric OCR and SRR found between sites does not relate to the estimated pore water advection rates. Volumetric OCR and SRR at Shark Bay and North Beach are, for example, similar, although pore water advection rates differ. The volumetric mineralization rates represent the turnover potential at the specific site, resulting from the activity, size and composition of the local benthic assemblages. High volumetric mineralization rates result from beneficial environmental conditions for benthic organisms at the respective stations, e.g., in the supply of oxygen and organic carbon. Thus, for the observed pattern and magnitude of volumetric mineralization rates other factors than pore water advection have to be major contributors. To examine the role of pore water advection for the magnitude and pattern of mineralization rates, one has to distinguish between the advective supply of oxygen and the advective supply of water column organic matter. The

supply of oxygen by pore water advection is of major importance for the magnitude of mineralization rates at our sites, as it fuels the high aerobic mineralization rates. The volumetric OCR were at least an order of magnitude higher as the volumetric SRR, indicating a high contribution of aerobic mineralization to total mineralization at all depths within of the oxygenated sediment layer Additionally, the advective supply of oxygen to the sediments is a major determinant of the oxygen penetration depth, thus determines how much of the potential aerobic mineralization can actually proceed (determination of the magnitude of areal OCR).

The availability of easily degradable organic carbon is a major factor determining benthic mineralization rates. However, the filtration of organic carbon from the water column by pore water advection seems to be of secondary importance for the magnitude and pattern found in mineralization rates. The deviating pattern of volumetric mineralization rates and pore water advection rates may be explained by other organic carbon sources, such as benthic photosynthesis or transport of organic matter to the sediments by fauna. High biomasses of meio- and macrofauna were found in coral reef sediments (Wilkinson 1987, Riddle et al. 1990) and benthic animals are known to contribute to the particulate and solute fluxes across the sediment-water interface and within sediments (Graf and Rosenberg 1997, Kristensen 2000). The presence of burrow-building, bioirrigating fauna, i.e. filter-feeding organisms, will increase the solute exchange by enlarging the potential effective exchange area from the visible sediment surface also to the burrows walls within the sediment (Aller 2001), which influences pathways and magnitude of benthic mineralization processes (Aller and Aller 1998, Banta et al. 1999). Bioturbation can change sediment composition and increase sediment surface microtopography, which has a significant impact on oxygen and organic matter exchange rates (Krantzberg 1985, Ziebis et al. 1996). Also, the deposition of particles by animal constructions and the feeding behavior of demersal plankton and fish (e.g., Bishop and Greenwood 1994, Marnane and Bellwood 2002) are important mechanisms of transporting organic matter to the sediments. In a short distance to our sampling site in Shark Bay large numbers of mounds built by the mud shrimp *Callianassa sp.* were present. These structures have been shown to increase advective transport when compared to sediments with a smooth surface

(Ziebis et al. 1996). Distribution patterns of benthic fauna and their activities were beyond the scope of this study. Upon digging in the top 10 to 15 cm of sediments, large numbers of sediment dwelling worms, shrimps, bivalves were exposed at North Beach, but much less at the Reef Belt Station. It may be speculated that the low mineralization rates at the reef belt may be a consequence of physical stress induced by the intense water and sediment movement, making it an unfavorable place for infauna (Hall 1994). Conversely, steadier hydrodynamics in the channel, may be favorable for benthic filter feeders and be a refuge for defecating fish. High aerobic mineralization rates as compared to the moderate SRR at the Channel Station may thus be explained by a high contribution of respiring meio- and macrofauna to oxygen uptake.

High volumetric OCR and SRR were measured close to the island, and may be caused by a better supply of organic carbon at these stations. At Shark Bay high benthic primary production rates of 165 mmol $m^{-2}$ $d^{-1}$ were measured (Rasheed et al. 2004). King et al. (1990) suggests that the close coupling between benthic algal production and heterotrophic metabolism may be a factor controlling SRR in coral reef sediments. However, we did not observe a response of SRR to light in North Beach and Shark Bay sediments. An inhibition of SRR or photosynthetically produced oxygen may have compensated a positive stimulation by excreted or produced organic carbon. An important carbon source around the Island is coral mucus. Coral mucus, described as an energy carrier and planktonic particle trap in coral reefs, was found to be concentrated by tidal currents in the lagoon around Heron Island. There, it sediments to the seafloor, leading to an enhancement of benthic mineralization processes (Wild et al. 2004a). Additionally, sedimentary processes at North Beach and Shark Bay may be enhanced by terrestrial input from the island (Smith and Johnson 1995).

*The role of sulfate reduction*: Although SRR were high, aerobic mineralization dominated sediment mineralization processes at most sites, as found in previous studies (Boucher et al. 1994, Alongi 1998). Sulfate reduction can be dominant in some areas within the reef, as in Shark Bay, where local pore water advection was low and sediment oxygenation restricted to a few millimeters. SRR were limited by organic carbon as the addition of dissolved glucose and acetate led to an enhancement of SRR. Interestingly, fresh coral mucus did not increase SRR.

This could indicate that fresh mucus is not a suitable energy source for sulfate reducing bacteria, but may as well result from cytotoxic substances found in freshly released coral mucus (Fung et al. 1997). An inhibition of SRR by anti-microbial substances in fresh mucus is not described yet and may deserve more detailed investigations. SRR measured in sediment cores six hours after mucus exposure, were found to be elevated (Wild et al. 2004b). Thus, with time and exposure to degradation processes, coral mucus may become an appropriate electron donor for sulfate reducing bacteria.

The sulfide produced during sulfate reduction can, both in dissolved and iron-bound forms, be oxidized to sulfate over a complex series of processes (e.g., Jorgensen 1990). Sulfide oxidation processes are likely to play an important role at the investigation site. Sulfide oxidation may explain the differing results of $Ag^{35}S$ distribution obtained with the silver foil technique and the SRR obtained with the tracer whole core method. All of the sulfide produced by sulfate reduction was not necessarily bound to the silver foil. Only free sulfide reacts with the silver, whereas the chromium distillation method detects all major inorganic sulfur compounds (e.g., $H_2S$, FeS, $FeS_2$, $S_8$, $S_2O_3^{2-}$) excluding sulfate (Kallmeyer et al. 2004). Rapid oxidation of sulfide (or in iron-rich environments, a rapid precipitation of iron sulfides) thus prevents an efficient trapping of sulfides by the silver foil. Additionally, the two techniques integrate over different sediment volumes, which may contribute to the measured differences. These are drawbacks of the silver foil technique when used for the quantitative assessment of sedimentary SRR. In combination with the tracer whole core incubation method the silver foil technique may be used to show zones of sedimentary sulfide oxidation and binding, however, it has to be kept in mind, that unknown processes may contribute to the observed pattern.

*Comparison of oxygen penetration and mineralization rates with other studies*: In situ measurements of oxygen distribution within coral reef sediments are rare. The comparably low oxygen penetration depths measured at Shark Bay and the Channel Station were similar to in situ oxygen data presented by King et al. (1990), who measured an oxygen penetration exceeding 15 mm only during a period of high water movement. Entsch et al. (1983) and Williams et al. (1985) measured reducing conditions below 5 cm with redox electrodes, indicating

permanent anoxia below this sediment depth. In contrast to these and our results, Falter and Sansone (2000) measured an oxygen penetration of 15-50 cm by taking pore water samples from well points. The deep oxygen penetration was attributed to wave induced pore water advection.

The areal OCR measured at North Beach and at the Channel Station are, to our knowledge, among the highest reported in carbonate reef sediments. This may be explained by the method used, as the OCR measured in this paper allow for the relation of oxygen penetration depth to hydrodynamics. At a temperate sandflat the OCR measured with this method were double as high as OCR measured with stirred benthic chambers (de Beer et al. 2005). However, whether these two methods result in different OCR may depend largely on the currents speeds in the investigated area. This may explain why in the sheltered area of Shark Bay simultaneous measurements with stirred benthic chambers in January 2002 (Wild et al. 2004b) and previous measurements (Rasheed et al. 2004) with stirred benthic chambers, gave OCR that were comparable to our measurements. The rates obtained for Shark Bay and the Reef Belt Station are comparable to rates found in other coral reef sediments (Boucher et al. 1994, Clavier and Garrigue 1999, Grenz et al. 2003).

The high SRR measured at the two stations close to the island are comparable only to SRR measured in carbonate reef sediments which were surrounded by mangroves (Hines and Lyons 1982) or highly influenced by terrigenious input (King et al. 1990). The SRR measured at the reef belt and in the channel were as low as described previously for coral sands (Skyring and Chambers 1976, Skyring 1985, Nedwell and Blackburn 1987, King et al. 1990, Alongi et al. 1996). However, comparing SRR with previous investigations is limited, as methods used before 1985 may underestimate SRR by underestimating the chromium reducible sulfur pool (CRS; mainly $S^0$ and $FeS_2$).

*Importance of sediments:* The high aerobic and anaerobic mineralization rates confirmed that the reef sediments can be very active and contribute significantly to element cycling within the reef ecosystem. The heterogeneity of reef system makes an extrapolation of our data to the Heron Island lagoon delicate. However, if the three platform stations are considered representative for the reef area around Heron Island, the sediments turn over approx. between 500 and 1800

kg C $km^{-2}$ $d^{-1}$. A rough estimate of the turnover rates of total area of Heron Reef occupied by sediments (sediment area: 19.5 $km^2$), is in the order of 3700000-13000000 kg C $a^{-1}$ (neglecting the seasonal differences).

**Acknowledgements**: We thank all technicians from the microsensor group for making the excellent microsensors. The people from HIRS are thanked for their logistic help and hospitality. A big thank goes to C. Schoenberg and E. Walpersdorf for taking and shipping samples. We thank B.B. Jørgensen and M Huettel and H. Røy for very helpful discussion and support. This study was financed by the Max Planck Society (MPG), Germany.

## References

Aller, R. C. 2001. Transport and reactions in the bioirrgated zone, p. 269-301. *In* B. P. Boudreau and B. B. Jørgensen [eds.], The benthic boundary layer. Oxford University Press.

Aller, R. C., and J. Y. Aller. 1998. The effect of biogenic irrigation intensity and solute exchange on diagenetic reaction rates in marine sediments. J Mar Res **56:** 905-936.

Alongi, D. M. 1998. Coastal ecosystem processes. pp. 419. Marine Science Series. CRC Press. New York.

Alongi, D. M., F. Tirendi, and A. Goldrick. 1996. Organic matter oxidation and sediment chemistry in mixed terrigenous-carbonate sands of Ningaloo Reef, Western Australia. Mar. Chem. **54:** 203-219.

Andrews, J. C., and M. Hans. 1983. Space-time variability of nutrients in a lagoonal patch reef. Limnol. Oceanogr. **28:** 215-227.

Banta, G. T., M. Holmer, M. H. Jensen, and E. Kristensen. 1999. Effects of two polychaete worms, *Nereis diversicolor* and *Arenicola marina*, on aerobic and anaerobic decomposition in a sandy marine sediment. Aquat. Microb. Ecol. **19:** 189-204.

Bishop, J. W., and J. G. Greenwood. 1994. Nitrogen-excretion by some demersal macrozooplankton in Heron and One-Tree Reefs, Great-Barrier-Reef, Australia. Mar. Biol. **120:** 447-453.

Boucher, G., J. Clavier, and C. Garrigue. 1994. Oxygen and carbon-dioxide fluxes at the water-sediment interface of a tropical lagoon. Mar. Ecol.-Prog. Ser. **107:** 185-193.

Boudreau, B., M. Huettel, R. Forster, A. Jahnke, J. McLachlan, J. Middelburg, P. Nielsen, F. Sansone, G. Taghon, W. Van Raaphorst, I. Webster, J. Weslawski, P. Wiberg, and B. Sundby. 2001. Permeable marine sediments: Overturning an old paradigm. EOS,TransAGU **82:** 133-136.

Buddemeier, R., and J. Oberdorfer. 1988. Hydrogeology and hydrodynamics of coral reef pore waters. Proc. Sixth Internat. Coral Reef Symp. **2:** 485-490.

Canfield, D. E., B. Thamdrup, and J. W. Hansen. 1993. The anaerobic degradation of organic-matter in danish coastal sediments - iron reduction, manganese reduction, and sulfate reduction. Geochim. Cosmochim. Acta **57:** 3867-3883.

Capone, D. G., S. E. Dunham, S. G. Horrigan, and L. E. Duguay. 1992. Microbial nitrogen transformations in unconsolidated coral-reef sediments. Mar. Ecol.-Prog. Ser. **80:** 75-88.

Chambers, R. A., J. W. Fourqurean, S. A. Macko, and R. Hoppenot. 2001. Biogeochemical effects of iron availability on primary producers in a shallow marine carbonate environment. Limnol. Oceanogr. **46:** 1278-1286.

Clavier, J., and C. Garrigue. 1999. Annual sediment primary production and respiration in a large coral reef lagoon (sw new caledonia). Mar. Ecol.-Prog. Ser. **191:** 79-89.

Crossland, C. J., and D. J. Barnes. 1983. Dissolved nutrients and organic particulates in water flowing over coral reefs at Lizard-Island. Aust. J. Mar. Freshw. Res. **34:** 835-844.

de Beer, D., F. Wenzhoefer, T. G. Ferdelman, S. E. Boehme, M. Huettel, J. E. E. van Beusekom, M. E. Boettcher, N. Musat, and N. Dubillier. 2005. Transport and mineralization rates in north sea sandy intertidal sediments, Sylt-Rømø Basin, Wadden Sea. Limnol. Oceanogr. **50:** 113-127.

Demers, S., J. C. Therriault, E. Bourget, and A. Bah. 1987. Resuspension in the shallow sublittoral zone of a macrotidal estuarine environment - wind influence. Limnol. Oceanogr. **32:** 327-339.

Enos, P., and L. H. Sawatsky. 1981. Pore networks in holocene carbonate sediments. J. Sediment. Petrol. **51:** 961-985.

Entsch, B., K. G. Boto, R. G. Sim, and J. T. Wellington. 1983. Phosphorus and nitrogen in coral-reef sediments. Limnol. Oceanogr. **28:** 465-476.

Falter, J. L., and F. J. Sansone. 2000. Hydraulic control of pore water geochemistry within the oxic-suboxic zone of a permeable sediment. Limnol. Oceanogr. **45:** 550-557.

Forster, S., M. Huettel, and W. Ziebis. 1996. Impact of boundary layer flow velocity on oxygen utilisation in coastal sediments. Mar. Ecol.-Prog. Ser. **143:** 173-185.

Fung, F. M. Y., S. Tachibana, L. M. Chou, and J. L. Ding. 1997. Cytotoxic and anticancer agents in mucus of *Galaxea fascicularis*: Purification and characterization. Journal of Marine Biotechnology **5:** 50-57.

Glud, R. N., I. Klimant, G. Holst, O. Kohls, V. Meyer, M. Kuhl, and J. K. Gundersen. 1999. Adaptation, test and in situ measurements with O-2 microopt(r)odes on benthic landers. Deep-Sea Res. Part I-Oceanogr. Res. Pap. **46:** 171-183.

Graf, G., and R. Rosenberg. 1997. Bioresuspension and biodeposition: A review. J. Mar. Syst. **11:** 269-278.

Grenz, C., L. Denis, G. Boucher, L. Chauvaud, J. Clavier, R. Fichez, and O. Pringault. 2003. Spatial variability in sediment oxygen consumption under winter conditions in a lagoonal system in New Caledonia (South Pacific). J. Exp. Mar. Biol. Ecol. **285:** 33-47.

Hall, S. J. 1994. Physical disturbance and marine benthic communities - life in unconsolidated sediments. Oceanogr. Mar. Biol. Annu. Rev. **32:** 179-239.

Hargrave, B. T. 1969. Similarity of oxygen uptake by benthic communities. Limnol. Oceanogr. **14:** 801-805.

Hines, M. E., and W. B. Lyons. 1982. Biogeochemistry of nearshore Bermuda sediments .1. Sulfate reduction rates and nutrient generation. Mar. Ecol.-Prog. Ser. **8:** 87-94.

Huettel, M., and G. Gust. 1992. Impact of bioroughness on interfacial solute exchange in permeable sediments. Mar. Ecol.-Prog. Ser. **89:** 253-267.

Huettel, M., H. Røy, E. Precht, and S. Ehrenhauss. 2003. Hydrodynamical impact on biogeochemical processes in aquatic sediments. Hydrobiologia **494:** 231-236.

Huettel, M., and A. Rusch. 2000. Transport and degradation of phytoplankton in permeable sediment. Limnol. Oceanogr. **45:** 534-549.

Huettel, M., W. Ziebis, and S. Forster. 1996. Flow-induced uptake of particulate matter in permeable sediments. Limnol. Oceanogr. **41:** 309-322.

Jørgensen, B. B. 1977. Bacterial sulfate reduction within reduced microniches of oxidized marine-sediments. Mar. Biol. **41:** 7-17.

---. 1978. Comparison of methods for the quantification of bacterial sulfate reduction in coastal marine-sediments .1. Measurement with radiotracer techniques. Geomicrobiology Journal **1:** 11-27.

---. 1982. Mineralization of organic-matter in the sea bed - the role of sulfate reduction. Nature **296:** 643-645.

---. 1990. A thiosulfate shunt in the sulfur cycle of marine-sediments. Science **249:** 152-154.

Jørgensen, B. B., and F. Bak. 1991. Pathways and microbiology of thiosulfate transformations and sulfate reduction in a marine sediment (Kattegat, Denmark). Appl. Environ. Microbiol. **57:** 847-856.

Kallmeyer, J., T. G. Ferdelman, A. Weber, H. Fossing, and B. B. Jørgensen. 2004. A cold chromium distillation procedure for radiolabeled sulfide applied to sulfate reduction measurements. Limnology and Oceanography: Methods. **2:** 171-180.

King, G. M., R. G. Carlton, and T. E. Sawyer. 1990. Anaerobic metabolism and oxygen distribution in the carbonate sediments of a submarine-canyon. Mar. Ecol.-Prog. Ser. **58:** 275-285.

Klute, A., and C. Dirksen. 1986. Hydraulic conductivity and diffusivity: Laboratory methods, p. 687 ff. *In* A. Klute [ed.], Method of soil analysis - part 1 - Physical and mineralogical methods. American Society of Agronomy.

Krantzberg, G. 1985. The influence of bioturbation on physical, chemical and biological parameters in aquatic environments - a review. Environmental Pollution Series a-Ecological and Biological **39:** 99-122.

Kristensen, E. 2000. Organic matter diagenesis at the oxic/anoxic interface in coastal marine sediments, with emphasis on the role of burrowing animals. Hydrobiologia **426:** 1-24.

Krumholz, L. R., J. P. McKinley, F. A. Ulrich, and J. M. Suflita. 1997. Confined subsurface microbial communities in cretaceous rock. Nature **386:** 64-66.

Marnane, M. J., and D. R. Bellwood. 2002. Diet and nocturnal foraging in cardinalfishes (Apogonidae) at One Tree Reef, Great Barrier Reef, Australia. Mar. Ecol.-Prog. Ser. **231:** 261-268.

Nedwell, D. B., and T. H. Blackburn. 1987. Anaerobic metabolism in lagoon sediments from Davies Reef, Great-Barrier-Reef. Est Coast Shelf Sci **25:** 347-353.

Oberdorfer, J. A., and R. W. Buddemeier. 1986. Coral-reef hydrology - field studies of water-movement within a barrier-reef. Coral Reefs **5:** 7-12.

Pamatmat, M. M. 1971. Oxygen consumption by seabed. 4. Shipboard and laboratory experiments. Limnol. Oceanogr. **16:** 536-&.

Parnell, K. E. 1986. Water-movement within a fringing-reef flat, Orpheus-Island, North-Queensland, Australia. Coral Reefs **5:** 1-6.

Polerecky, L., U. Franke, U. Werner, B. Grunwald, and D. de Beer. 2005. High spatial resolution measurement of oxygen consumption rates in permeable sediments. Limnology and Oceanography: Methods **3:** 75-85.

Precht, E., U. Franke, L. Polerecky, and M. Huettel. 2004. Oxygen dynamics in permeable sediments with wave-driven pore water exchange. Limnol. Oceanogr. **49:** 693-705.

Precht, E., and M. Huettel. 2003. Advective pore-water exchange driven by surface gravity waves and its ecological implications. Limnol. Oceanogr. **48:** 1674-1684.

Rasheed, M., M. I. Badran, and M. Huettel. 2003. Particulate matter filtration and seasonal nutrient dynamics in permeable carbonate and silicate sands of the Gulf of Aqaba, Red Sea. Coral Reefs **22:** 167-177.

Rasheed, M., M. I. Badran, C. Richter, and M. Huettel. 2002. Effect of reef framework and bottom sediment on nutrient enrichment in a coral reef of the Gulf of Aqaba, Red Sea. Mar. Ecol.-Prog. Ser. **239:** 277-285.

Rasheed, M., C. Wild, U. Franke, and M. Huettel. 2004. Benthic photosynthesis and oxygen consumption in permeable carbonate sediments at Heron Island, Great Barrier Reef, Australia. Est. Coast. Shelf Sci. **59:** 139-150.

Revsbech, N. P. 1989. An oxygen microsensor with a guard cathode. Limnol. Oceanogr. **34:** 474-478.

Revsbech, N. P., B. B. Jørgensen, and T. H. Blackburn. 1980. Oxygen in the sea bottom measured with a microelectrode. Science **207:** 1355-1356.

Richter, C., M. Wunsch, M. Rasheed, I. Kotter, and M. I. Badran. 2001. Endoscopic exploration of red sea coral reefs reveals dense populations of cavity-dwelling sponges. Nature **413:** 726-730.

Riddle, M. J., D. M. Alongi, P. K. Dayton, J. A. Hansen, and D. W. Klumpp. 1990. Detrital pathways in a coral-reef lagoon .1. Macrofaunal biomass and estimates of production. Mar. Biol. **104:** 109-118.

Rusch, A., M. Huettel, and S. Forster. 2000. Particulate organic matter in permeable marine sands - dynamics in time and depth. Est. Coast. Shelf Sci. **51:** 399-414.

Shum, K. T., and B. Sundby. 1996. Organic matter processing in continental shelf sediments - the subtidal pump revisited. Mar. Chem. **53:** 81-87.

Skyring, G. 1985. Anaerobic microbial processes in coral reef sediments. Proc. Fifth Int. Coral Reef symp. **3**. p. 421–425

Skyring, G. W., and L. A. Chambers. 1976. Biological sulfate reduction in carbonate sediments of a coral-reef. Aust. J. Mar. Freshw. Res. **27:** 595-602.

Smith, J. S., and C. R. Johnson. 1995. Nutrient inputs from seabirds and humans on a populated coral cay. Mar. Ecol.-Prog. Ser. **124:** 189-200.

Thamdrup, B., J. W. Hansen, and B. B. Jørgensen. 1998. Temperature dependence of aerobic respiration in a coastal sediment. FEMS Microbiol. Ecol. **25:** 189-200.

Visscher, P. T., R. P. Reid, and B. M. Bebout. 2000. Microscale observations of sulfate reduction: Correlation of microbial activity with lithified micritic laminae in modern marine stromatolites. Geology **28:** 919-922.

Webb, J. E., and J. Theodor. 1968. Irrigation of submerged marine sands through wave action. Nature **220:** 682-683.

Webster, I. T., S. J. Norquay, F. C. Ross, and R. A. Wooding. 1996. Solute exchange by convection within estuarine sediments. Est. Coast. Shelf Sci. **42:** 171-183.

Wentworth, C. K. 1922. A scale of grade and class terms for clastic sediments. J. Geol. **30:** 377-392.

Wenzhofer, F., O. Holby, R. N. Glud, H. K. Nielsen, and J. K. Gundersen. 2000. In situ microsensor studies of a shallow water hydrothermal vent at Milos, Greece. Mar. Chem. **69:** 43-54.

Wheatcraft, S. W., and R. W. Buddemeier. 1981. Atoll-island hydrology. Ground Water **19:** 311-320.

Wild, C., M. Huettel, A. Klueter, S. G. Kremb, M. Y. M. Rasheed, and B. B. Jørgensen. 2004a. Coral mucus functions as an energy carrier and particle trap in the reef ecosystem. Nature **428:** 66-70.

Wild, C., M. Rasheed, U. Werner, U. Franke, R. Johnstone, and M. Huettel. 2004b. Degradation and mineralization of coral mucus in reef environments. Mar. Ecol.-Prog. Ser. **267:** 159-171.

Wilkinson, C. R. 1987. Microbial ecology on a coral-reef. Search **18:** 31-33.

Williams, S. L., S. M. Yarish, and I. P. Gill. 1985. Ammonium distributions, production, and efflux from backreef sediments, St-Croix, United-States Virgin Islands. Mar. Ecol.-Prog. Ser. **24:** 57-64.

Ziebis, W., M. Huettel, and S. Forster. 1996. Impact of biogenic sediment topography on oxygen fluxes in permeable seabeds. Mar. Ecol.-Prog. Ser. **140:** 227-237.

# Photosynthesis in coral reef sediments (Heron Reef, Australia)

Ursula Werner, Anna Blazejak, Paul Bird, Gabriele Eickert and Dirk de Beer

in preparation for submission to Marine Ecology Progress Series

**Abstract**

In a laboratory study, we investigated microphytobenthic photosynthesis on four stations in the coral reef sediments at Heron Reef, Australia. The microphytobenthos was dominated by diatoms, dinoflagellates and cyanobacteria, as deduced from biomarker pigment analysis. Episammic colonies that were similar in appearance and that had a diameter of ca. 100 µm, were highly diverse with respect to cyanobacterial 16S rDNA sequences. Net photosynthesis varied between 1.9 and 8.5 mmol $O_2$ $m^{-2}$ $h^{-1}$ and was strongly correlated with chlorophyll-a content of the stations, which lay between 31 and 84 mg $m^{-2}$. The approximate microphytobenthic production for the entire reef was in the order of magnitude of the production estimated for corals. Photosynthesis stimulated calcification at all investigated sites (0.2-1.0 mmol $Ca^{2+}$ $m^{-2}$ $h^{-1}$). The sediments of at least three stations were net calcifying. Sedimentary $N_2$-fixation rates (measured as acetylene reduction at two sites) ranged between 0.9 to 3.9 mmol $N_2$ $m^{-2}$ $h^{-1}$ and were highest in the light, indicating the importance of heterocystous cyanobacteria. In coral fingers no $N_2$-fixation was measurable, which stresses the importance of the sediment compartment for reef nitrogen cycling.

## Introduction

High rates of primary production in coral reef ecosystems are often associated with corals (zooxanthellae), turf algae or larger benthic macroalgae (Kinsey 1985; Gattuso et al. 1997; Gattuso et al. 1998). However, benthic microphytobenthos (e.g. diatoms, dinoflagellates and cyanobacteria), living in unconsolidated reef sediments, may also contribute significantly to reef ecosystem primary production (Charpy et al. 1998; Clavier and Garrigue 1999; Heil et al. 2004). Per unit surface area the primary production rates of microphytobenthos may be low in comparison to the rates of corals (Kinsey 1985; Gattuso et al. 1998), nevertheless, sediments often occupy large areas within the reef (Clavier and Garrigue 1999). Thus, on the whole reef ecosystem scale the contribution of microphytobenthos and corals to reef primary production may be equally important (Clavier and Garrigue 1999).

Photosynthesis may stimulate calcification and, thereby, influence the cycling of inorganic carbon and promotes sediment building and cementation. The calcification rate depends on the saturation state of the pore water with respect to carbonate and calcium. Calcification (or from right to left, the dissolution of $CaCO_3$) can be written as

$$Ca^{2+} + 2HCO_3^- \leftrightarrow CaCO_3 + CO_2 + H_2O \quad (1)$$

Calcification decreases DIC by one and total alkalinity (TA) by two units. The release of $CO_2$ lowers the pH.

The simplified reaction of photosynthesis (and from the right aerobic respiration) is given in equation 2:

$$CO_2 + H_2O \leftrightarrow CH_2O + O_2 \quad (2)$$

The uptake of $CO_2$ by photosynthesis shifts the carbonate equilibrium towards the carbonate species and increases the pH and TA. Thus, net photosynthesis increases the saturation state of the solution with respect to calcium carbonate and stimulates calcification. Calcification may act as a buffer against a photosynthesis-driven pH increase, which is beneficial for phototrophic organisms, as most of them preferentially take up $CO_2$, which is more abundant at lower pH (Zeebe and Gladrow 2005).

$CaCO_3$ may dissolve during organic matter mineralization, which can be very active in coral reef sediments (Werner et al. in prep.; Wild et al. 2004b). Aerobic mineralization (equation 2 from the right to the left) promotes the dissolution of $CaCO_3$ (Canfield and Raiswell 1991) by the release of $CO_2$, which lowers the pH and the saturation state of the solution with respect to calcium carbonate.

The oceanic water around coral reefs is typically depleted in nitrogen relative to phosphorous (Gattuso et al. 1998). Thus, fixation of $N_2$ from the atmosphere by $N_2$-fixing reef organisms is of major importance for the nitrogen supply for coral reefs (Wilkinson et al. 1984; Larkum et al. 1988; Oneil and Capone 1989). $N_2$-fixation occurs exclusively by prokaryotes, with cyanobacteria and sulfate reducing bacteria being most important in marine environments. Therefore sediments, in which these organisms are abundant, could be important for the supply of nitrogen in the reef ecosystem.

We investigated microphytobenthic photosynthesis at Heron Reef, Australia. Previously reported chlorophyll-a concentrations at Heron Reef were amongst the highest found in marine sediments (up to 1153mg chl-a $m^{-2}$) (Roelfsema et al. 2002; Heil et al. 2004). Our goal was to quantify microphytobenthic photosynthesis and to investigate the impact of microphytobenthic photosynthesis on sedimentary calcification and $N_2$-fixation rates. We addressed the heterogeneity of the microphytobenthic community by investigating the biomarker photopigments distribution and by investigating episammic colonies for 16S rDNA diversity.

## Material and methods

*Site description*: The study was carried out at Heron Island, Australia (23°27' S, 151°55'E). The island is located in the lagoonal platform reef Heron Reef, on the southern boundary of the Great Barrier Reef (Fig.1a). Investigations were conducted on four stations (Fig. 1b). Two stations were chosen close to the island at North Beach. North Beach 1 (NB1) was located ca. 40 m offshore (water depth at low tide was 1 m). North Beach 2 (NB2) was situated close to the Beach (water depth at low tide was ca. 0.5 m). At the reef edge, where hydrodynamic forcing was strongest, the reef belt station (RB) was chosen (water depth at low tide was ca. 1 m).

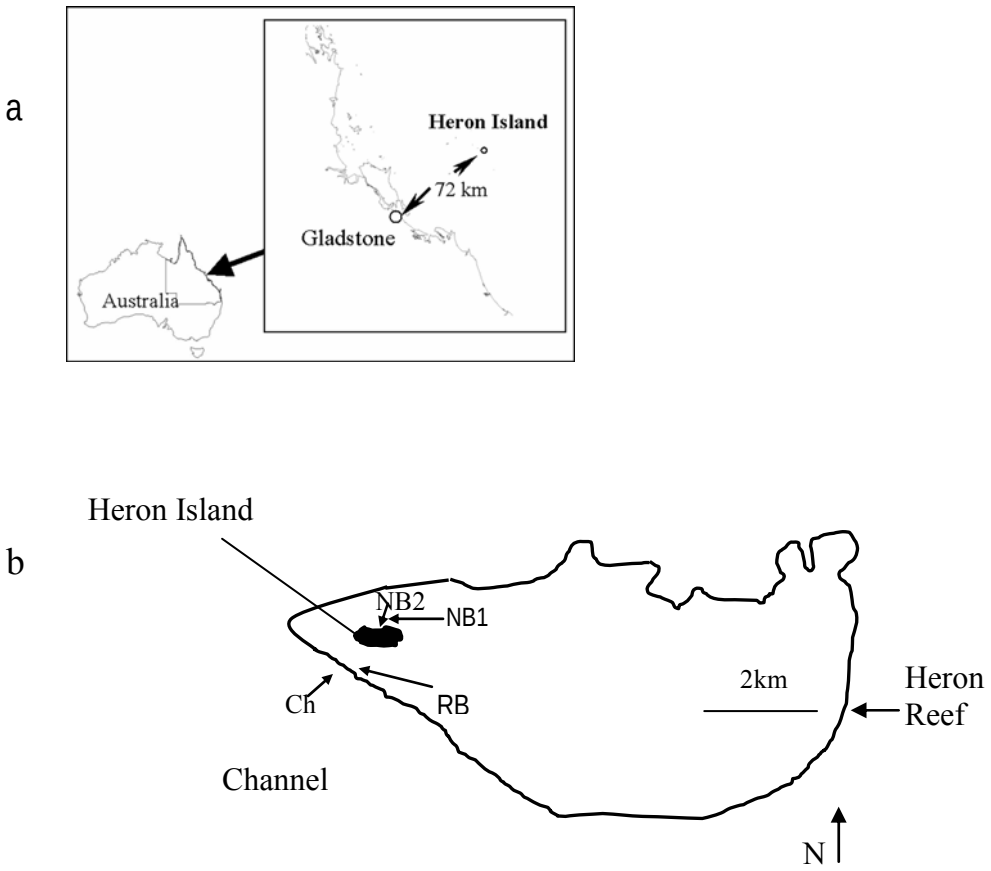


Figure 1: a) Location of Heron Island and b) location of the four investigation sites at Heron Reef. NB is North Beach, RB is the reef belt and Ch the Channel station.

The channel station (Ch) was located outside the reef platform close to the reef edge, within the channel between Heron Reef and Wistari Reef (water depth at low tide ca. 5 m). The sediment characteristics of North Beach 2, the reef belt and the channel station are given in Table 1.

Table 1: Sediment characteristics of the investigated stations (sampling depth 7 cm). Apart from grain sizes, data are given as averages ± standard deviation. NB 2 is the near-shore station at North Beach, RB is the reef belt and Ch the channel station.

| | permeability ( $10^{-11}$ $m^2$) | median grain size (µm) | porosity (%) | TOC (% DW) |
|---|---|---|---|---|
| NB2 | 8.4 ± 1.1 | 591 | 60.9 ± 11.4 | 1.39 ± 0.6 |
| RB | 6.5 ± 0.1 | 426 | 54.6 ± 0.9 | 0.75 ± 0.2 |
| Ch | 0.3 ± 0.001 | 227 | 64.5 ± 1.0 | 0.59 ± 0.2 |

*Sampling*: Sampling and measurements were carried out in January 2002. During the sampling period sea water temperature varied between 27 and 33°C and salinity ranged between 28 and 33. The top 10 cm of sediments were investigated. If not stated otherwise, the sediments were taken with plastic core liners with an inner diameter of 3.6 cm, incubation temperature was 28°C. An overview of the experiments is given in Table 2.

Table 2: Sampling scheme. For further details see text. NB 1 and 2 are stations at North Beach, RB is the reef belt and Ch the channel station.

| | NB2 | NB1 | RB | Ch |
|---|---|---|---|---|
| algal pigments: | x | | x | x |
| Episammic colonies diversity: | top/bot. | | | |
| Microsen. studies ($O_2$, $Ca^{2+}$, pH): | x | x | x | x |
| $^{14}C$ in situ photosynthesis | | x | | |
| Light-dark-shift (colonies) | various depths | | | |
| $N_2$ fixation (ARR) | top/bot.* | top/bot.* | | |

* top/bot.: sediments from the top 3 cm and from 8 to 10cm depth were sampled.

*Algal pigment analysis*: Duplicate sediments cores from North Beach 2, reef belt and the channel station were analysed for photopigment concentrations and composition. In these sediment cores the microsensor measurements (see below) were conducted beforehand. The sediments were sliced in 0.5 cm sections (0-5 cm depth) or in 1 cm sections (5-10 cm depth). Sediments were stored frozen at -20°C. Sediments were freeze dried before analysis and subsamples (1–2 g) were transferred to 15 ml polypropylene centrifuge tubes that contained 3 ml of 100% acetone. To break the cells, the mixture was sonicated (7 x 1 minute) on ice. For the extraction of the pigments the mixture was stored 24h in a freezer at -20°C. Shortly before analysis the extract was filtered (Acrosdisc CR syringe filter; 0.45 µm pore size, PALL, Gellman Laboratory) and diluted with water to a final concentration of 70% acetone (Buffan-Dubau and Carman 2000). Photopigments were subsequently separated on a Water HPLC (2690 Separation module), equipped with a Eurospher-100 C18, 5 µm Vertex column (Knauer Berlin, Germany), according to the method proposed by Wright et al. (1991). Absorption spectra of the separated compounds were measured on a Waters 996 Photo Diode Array detector and pigments were quantified and identified by comparison to pigment standards (DHI Waters and Environment, Denmark).

*Microsensor measurements*: We measured $O_2$, $Ca^{2+}$ and pH concentration profiles with microsensors in duplicate sediment cores taken at the four sampling sites. Measurements were performed in the laboratory immediately after sampling. The water layer on top of the sediment was gently stirred to develop a defined diffusive boundary layer (DBL). Measurements were performed in the light (PAR: 600 µmol Photons $m^{-2}$ $s^{-1}$; lamp: KL 1500 electronic, Schott, Germany) and in the dark. Profiles were measured with a step size of 250 µm. Per investigated parameter

3 to 6 replicate profiles were measured at each station. The $O_2$ microsensors were amperometric Clark type electrodes with a guard (Revsbech 1989), an actual sensing area of 5 µm diameter and a response time ($t_{90}$) of less than 5 seconds. The microsensors were thick walled so that the tip diameter was approx.. 300 µm. The pH and $Ca^{2+}$ electrodes were liquid ion-exchange membrane (LIX) glass microsensors as described in (De Beer et al. 2000) with a response time ($t_{90}$) of less than 1 second.

Net photosynthesis, diffusive oxygen uptake (DOU), calcification and decalcification rates were calculated from light and dark $O_2$ and $Ca^{2+}$ profiles (Jørgensen and Revsbech 1985; Kuehl et al. 1996), using Fick´s first law:

$$J = - D_{0,i} (dC/dz) \quad (1)$$

where J = the flux, $D_0$ = molecular diffusion coefficient of the solute in water (Li and Gregory 1974) (corrected for temperature and salinity) and dC/dz = the linear gradient of the measured solute. Diffusive fluxes of oxygen and calcium within the sediment were calculated from the profiles using equation (1) as well as the empirical relations for diffusion coefficients in the sediment:

$$J = - \phi D_{s,i} (dC/dz) \quad (2)$$

and

$$D_{s,i} = D_0 \phi^{m-1} \quad (3)$$

where $D_{s,i}$ = the diffusion coefficient in sediments of the species i corrected for temperature and pressure, $\phi$ = the measured porosity and m =3 (Li and Gregory 1974; Ullman and Aller 1982).

Net photosynthesis was calculated from oxygen profiles measured in the light by evaluating the sum of up- and downward oxygen fluxes away from the photosynthetic active sediment zone. The DOU of the sediment was calculated from interfacial oxygen fluxes in the dark. From $Ca^{2+}$ profiles measured in the light, areal calcification rate was determined by calculating the $Ca^{2+}$ fluxes from the water column and from deep sediment to the photosynthetic active sediment layer, where $Ca^{2+}$ concentrations were lower. Sedimentary decalcification was calculated from dark $Ca^{2+}$ effluxes from the sediments to the overlying water.

*Gross photosynthesis measurements on colonies (light-dark-shift method)*: We used the light-dark-shift method for the assessment of gross photosynthesis rates (Revsbech et al. 1981) in sediments cores, using oxygen microsensors with a sensing surface of 5µm and a 90% response time of 0.2s. At North Beach 2 green colonies attached to the sand grains were abundant. These colonies had a dome shape with diameter of ca. 100µm, the outer layer was hard and intercepted by radial structures. These colonies were also investigated for gross photosynthesis rates with the light-dark-shift method. We therefore isolated single sand grains and positioned the sensor directly at the colony surface. The grains were taken from

different sediment layers (from 0-1.5 cm, 1.5 - 3 cm, 3 - 4 cm and from 4 – 6 cm depth), in the deeper layers they were more brownish in colour. To obtain photosynthesis versus irradiance curves (PI curves) of these colonies the light-dark-shift method was applied at light intensities between 2 and 1100 µmol Photons $m^{-2}$ $s^{-1}$ and the oxygen concentration change after darkening was monitored.

*In situ photosynthesis rate with the $^{14}C$ incubation method*: At North Beach 1 photosynthesis ($CO_2$ fixation) was measured in situ under ambient light conditions using the $^{14}C$ incubation method. Radiolabeled $H^{14}CO_3^-$ was injected into sediment cores (plastic core liners with an inner diameter of 2.6 cm) through injection ports in the core wall, with 0.5 cm depth intervals to result in a specific activity of ca. 700 MBq/mol DIC. Measurements were started at 6 AM by injecting the tracer. Cores were sealed with parafilm and carefully inserted into the sediments of origin. 3 replicate cores were incubated for 2 h. The injection was terminated by freezing the cores. After freezing the sediments were sectioned into 0.2 cm thick layers (0-1 cm). From each core the remaining $H^{14}CO_3^-$ radio tracer was removed by adding HCl, dissolving also all carbonaceous sediments. The radioactivity of the remaining liquid was determined with a liquid scintillation counter (Packard 2500 TR), using Lumasafe Plus® (Lumac BV, Holland) scintillation cocktail.

*Cyanobacterial 16S rDNA diversity of episammic photosynthetic colonies*: The green episammic colonies like those investigated for gross photosynthesis rates (see above), were analysed for 16S rRNA gene diversity at North Beach 2. Colonies from the top sediment layer and from 8-10 cm depth (more brownish in appearance) were separately investigated. Up to 50 colonies from each sediment layer were scratched off the sand grains in order to obtain enough material for 16S rRNA gene sequence analysis. The samples were rinsed with sterile water and stored frozen at -20°C until analysis.

DNA extraction and polymerase chain reaction (PCR) amplification: DNA from the cyanobacterial colony samples was chemically extracted (addition of 20µl Tris KCL buffer (pH 8.3) and 2 µL proteinase K (1mg $ml^{-1}$)) followed by subsequent incubation at 55°C for 1 h) and a mechanical treatment (homogenization in a 0.1 ml homogenizator). Amplification of cyanobacterial 16S rDNA genes was performed using cyanobacteria-specific primers (CYA 106F

and CYA 781R; (Nuebel et al. 1997)). 1-2µl of the isolated DNA was used as template after preheating the PCR mix (100 µl total volume) to 80°C to avoid non-specific annealing of the primers to non-target DNA. The following thermocycling conditions were used: 1 cycle at 80°C for 5 min; 27 cycles at 95°C for 1 min, 60°C for 1 min, and 72°C for 3 min; and 1 cycle at 72°C for 10 min.

Cloning and sequencing: 16S rRNA PCR fragments (~ 675 bp) were cloned using the TA Cloning Kit (Invitrogen, Breda, Netherlands) according to the manufacturer's protocol. Clones were randomly picked and checked for the correct insert size by PCR with the vector primers M13F and M13R. For this purpose small amount of cells from each clone colony was picked with a sterile toothpick and resuspended in 10 µl sterile water. After preheating of this suspension to 95°C for 5 min, the released DNA was used as template and amplified by PCR as described above with an annealing temperature of 42°C. PCR products of clones of the correct size were purified with the QiAquick PCR Purification Kit (Qiagen, Hilden, Germany) and subsequently sequenced with the vector primers M13F and M13R. Sequencing reactions were run using ABI BigDye on an ABI PRISM® 3100 Genetic Analyzer (Applied Biosystems, Foster City, USA). Sequences were aligned and compared using the Bioedit Program (www.mbio.ncsu.edu/BioEdit/bioedit.html).

Phylogenetic analysis: The 16S rRNA gene sequences were analyzed using the ARB software package (Ludwig et al. 1998). A maximum-likelihood cyanobacterial tree was calculated using long (> 1300 bp) published cyanobacterial sequences. The partial sequences obtained in this study were aligned to the sequences in the ARB database using the alignment tool of the ARB software package. These sequences were then inserted into the pre-established tree using the maximum parsimony method.

*$N_2$-fixation (acetylene reduction) rates*: $N_2$-fixation rates of sediments from North Beach 1 and 2 were measured in the laboratory using the acetylene reduction method (Stewart et al. 1967; Larkum et al. 1988). Sediment samples from the top 3 cm were incubated in light and dark. Sediment samples from 10 cm depth were only incubated in the dark. 2.5 mL sediment and 1 mL seawater were transferred into 6 mL glass vials. Through the rubber seal 0.5 mL acetylene ($C_2H_2$) were

injected. The samples were gently stirred and incubated in a flow through aquaria that received 50% of ambient light via neutral density screening, at 28°C. The glass vials were incubated upside down to allow the penetration of light, glass vials used for dark incubations were wrapped in aluminium foil. Triplicate samples were incubated up to 7 h, with 1-2 h intervals between treatments. The incubation was stopped by the addition of 250 µL glutaraldhyde (25%). Within 4 weeks, the samples were analysed for ethylene ($C_2H_4$) and $C_2H_2$ concentrations by using a GC.

$N_2$-fixation rates were calculated from acetylene reduction rates (ARR) using a ratio of 3 mol $C_2H_2$ reduced to 1 mol $N_2$ fixed, a ratio found for white coral sands dominated by diatoms and dinoflagellates (Charpy-Roubaud et al. 2001).

Coral fingers from the abundant hard corals *Acropora sp*. were placed into 28 mL glassvials, and seawater was added until coral and seawater had a final volume of 14 mL and 2.5 mL $C_2H_2$ was added to the gas space. The samples (3 replicates per treatment) were incubated for 8 and 12 h in the light and in the dark, respectively and further processed as described above.

## Results

*Microphytobenthic biomass and diversity*: The sedimentary chlorophyll-a content was lowest at the channel station, and comparable at North Beach 2 and reef belt (Fig. 2). The chlorophyll-a content decreased with depth at all stations. The concentrations of the biomarker fucoxanthin, peridinin and zeaxanthin (Fig. 3), showed a different microphytobenthic community at North Beach 2 as compared to the reef belt and the channel station: Only at North Beach 2 high concentrations of peridinin were found and the ratio of zeaxanthin to chlorophyll-a was highest. The depth distribution of fucoxanthin followed the depth distribution of chlorophyll-a at the reef belt and the channel station, this is also true for the depth distribution of peridinin at North Beach 2. Fucoxanthin is characteristic for diatoms, whereas peridinin is a marker for dinoflagellates. Zeaxanthin can be found in cyanobacteria and chlorophytes, however, the absence of chlorophyll b in the sediments indicates that zeaxanthin originated from cyanobacteria.

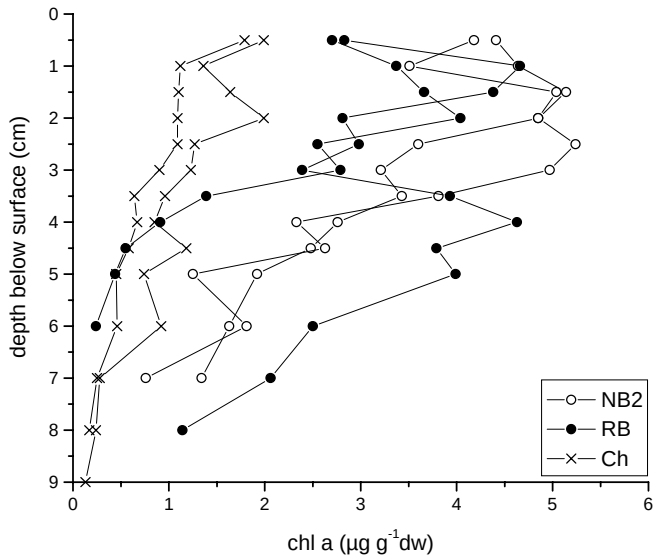


Figure 2: Sedimentary chlorophyll a content at NB2, RB and at the channel station (given per gram dry weight of the sediment), duplicate measurements are shown.

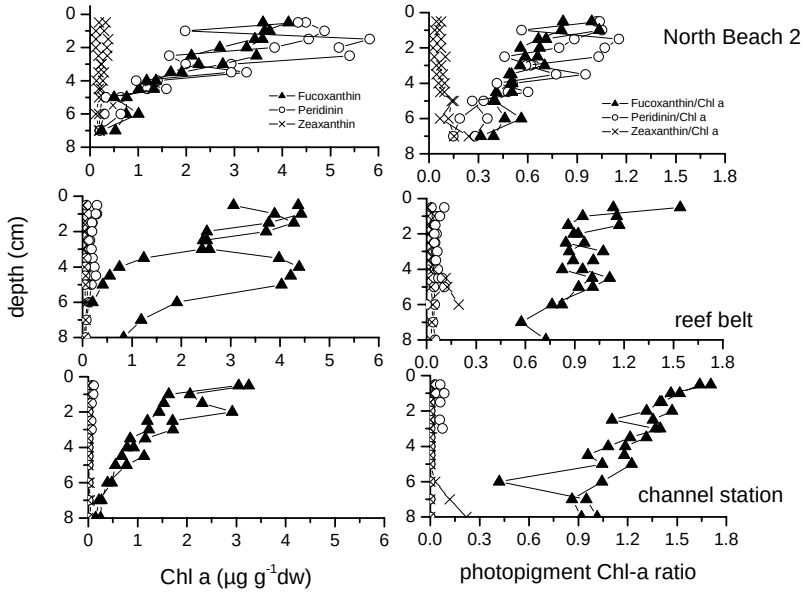


Figure 3: Concentration of the biomarker pigments fucoxanthin, peridinin and zeaxanthin (left panel) and their ratio to chlorophyll-a (right panel) at North Beach 2, the reef belt and the channel station.

The cyanobacteria of the episammic colonies were highly diverse, as shown by the phylogentic reconstruction of the obtained cyanobacterial 16S rRNA gene sequences from the colonies of the top sediment layer and from 8 to 10 cm depth (Fig. 4). The obtained sequences are spread over the cyanobacterial tree in eight distinct clusters. In Cluster 1, four sequences fell within the monophyletic group of heterocystous cyanobacteria (such as *Calothrix sp.*) that often form large filaments. Cluster 2 and 4 included cyanobacteria that belong to typically thin filamentous types, like the genera *Leptolyngbya, Phormidium* and *Halomicronema*. Interestingly, Cluster 5 included one sequence that belongs to the marine picoplanktonic cyanobacteria, although these colonies were benthic.

Cluster 6, 7 and 8 constituted unicellular cyanobacteria related to *Myxosarcina* and *Xenococcus* species (5 sequences), *Synechococcus* and *Gleocapsa* species (5 sequences) and *Microcystis* (2 sequences). The sequences of Cluster 7 were more than 9% divergent from each other and had more than 16.5% dissimilarity to the closest relative. This may indicate that the sequences belong to new species or even a new

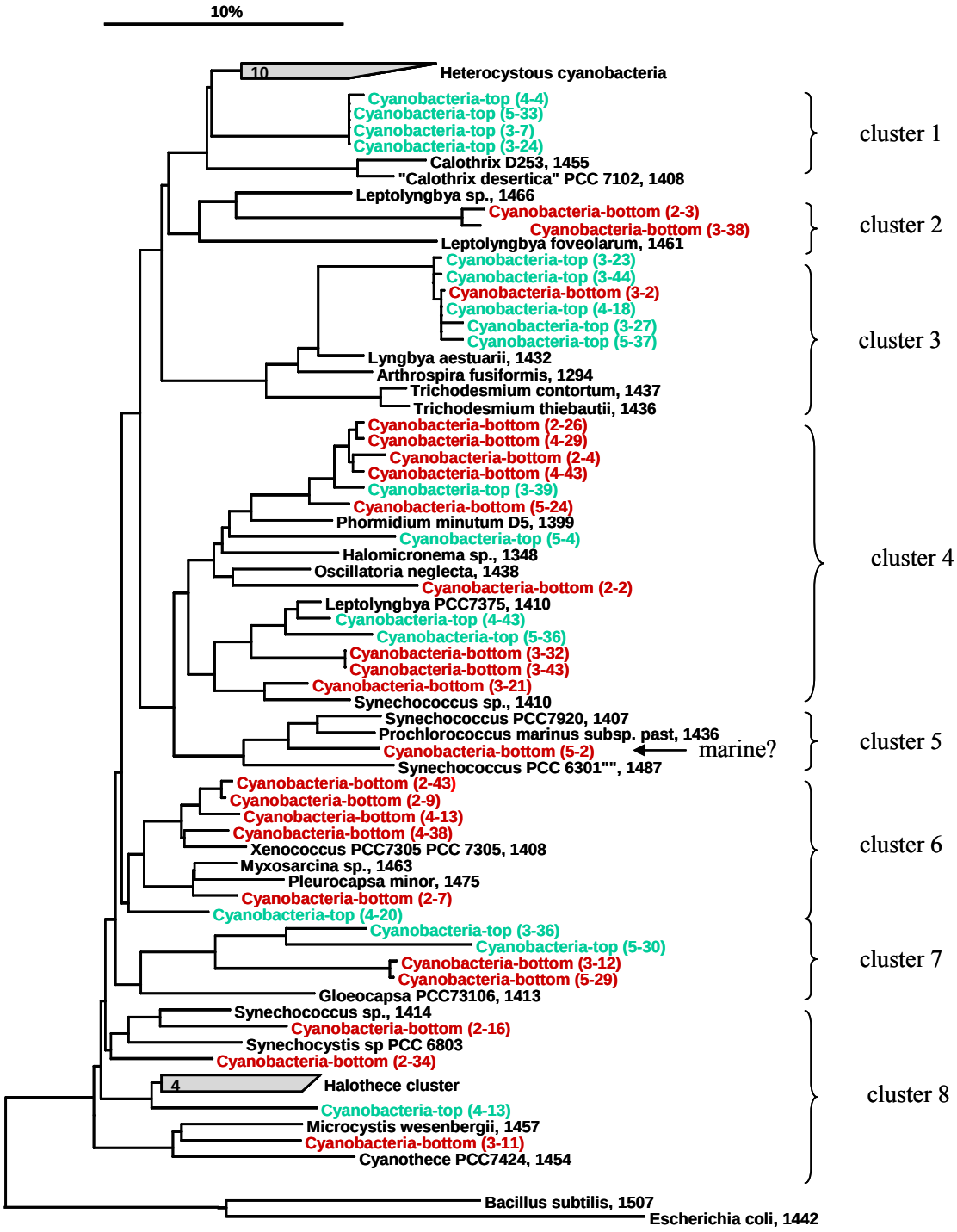


Figure 4: Cyanobacterial 16S rDNA gene sequences of the episammic colonies from the top sediment layer (green) and from 8 to 10 cm depth (red). The numbers in parentheses are clone numbers.

genus. In general, most of the obtained sequences had between 5 to 16.5% dissimilarity to previously described species, indicating richness in novel species.

Clear differences between the top and bottom colonies were found, for example, the sequences in cluster 1 were only found in the top layer of the sediments, whereas most of sequences from cluster 6 were from bottom sediment.

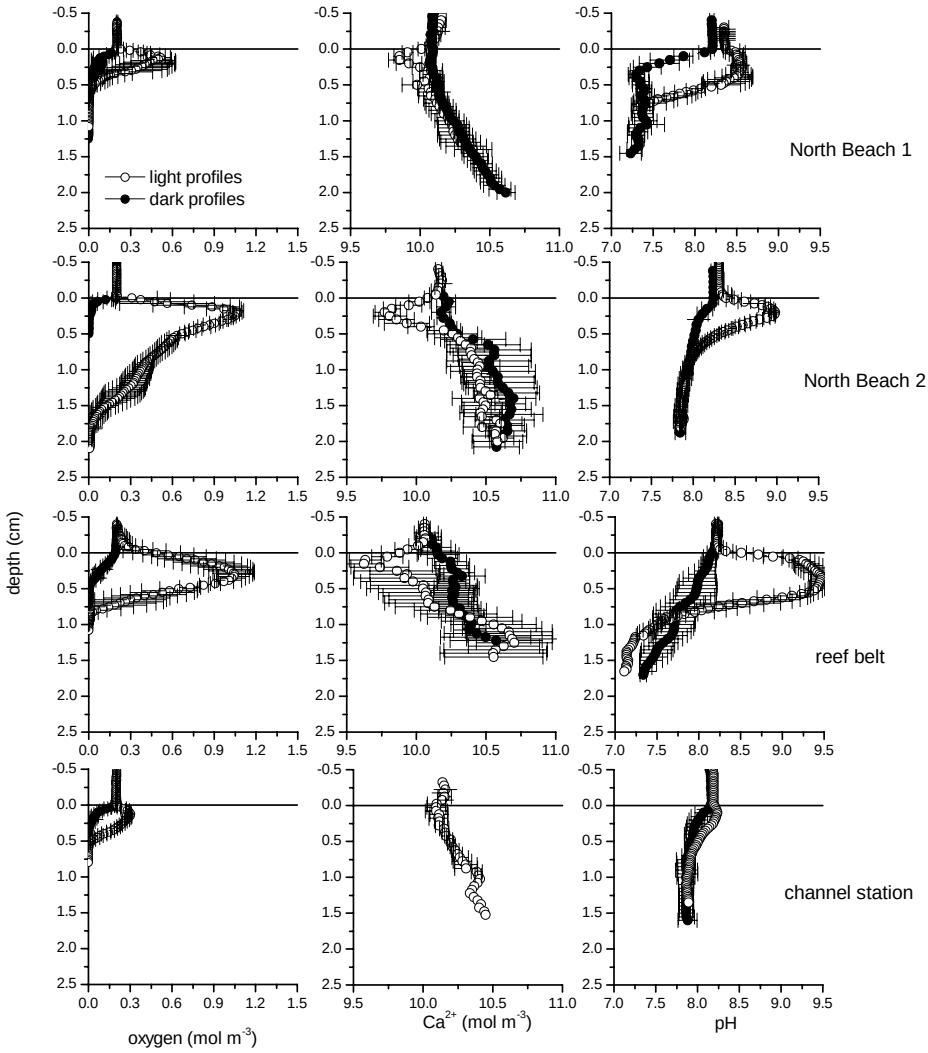


Figure 5. Profiles of $O_2$, $Ca^{2+}$ and pH measured in the light and in the dark at the four investigation sites.

*Microphytobenthic photosynthesis*: Microphytobenthic photosynthesis was found at all stations, since oxygen profiles measured in the light showed oxygen oversaturation below the sediment surface (Fig. 5). However, oxygen

concentrations and peak widths varied between stations. Highest areal net photosynthesis rates were assessed at North Beach 2, followed by the reef belt, North Beach 1 and the channel station (Table 3). The areal net photosynthesis rates correlated strongly with the chlorophyll-a content of the first sediment centimeter (Fig. 6). Areal photosynthesis rates ($CO_2$ fixation with the $^{14}C$ method) measured in the field at North Beach 1 were with 4.9 ± 1.0 mmol C $m^{-2}$ $h^{-1}$ comparable to the areal net photosynthesis rates obtained in the lab. Highest photosynthesis rates were measured in the top 4 mm (data not shown), similarly to the laboratory microsensor measurements.

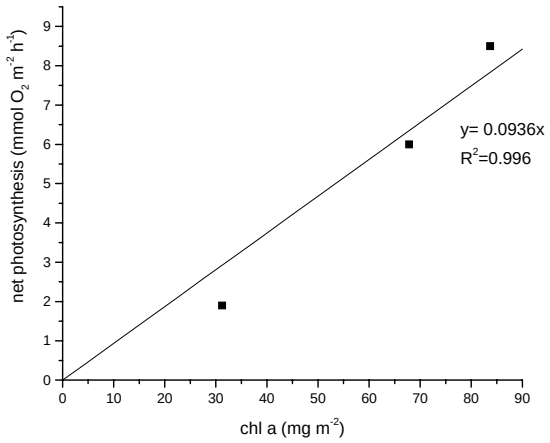


Figure 6: Correlation of net photosynthesis and chlorophyll-a concentrations of the top sediment centimeter of North Beach 2, the reef belt and the channel station.

The measurement with the light-dark-shift method to estimate gross photosynthesis rates showed surprising results. Although clearly net photosynthesis was demonstrated in the sediments, no immediate oxygen concentration decrease was detected upon darkening the sediments in steady state of photosynthesis (data not shown). In the following text, gross photosynthesis rates were thus estimated by adding the DOU to net photosynthesis rates.

The light-dark-shift method was also used on individual episammic colonies (Fig. 7 a and b). At some of the colonies an increase in oxygen concentration was measured upon darkening (Fig. 7a). This increase rate was linearly related to light intensity and did not saturate at high light intensities (Fig. 7a). Other colonies showed the expected decrease in oxygen after the light was switched off (Fig. 7b).

These PI curves showed saturated photosynthesis above 200 µmol Photons $m^{-2}$ $s^{-1}$ and no photoinhibition at high light intensities. Highest photosynthesis rates were measured in a colony from the top sediment layer. To obtain more information on the unexpected oxygen concentration increase upon darkening, we randomly picked several colonies from different sediments depths and investigated them using the light-dark-shift method and a light intensity of 580 µmol Photons $m^{-2}$ $s^{-1}$. The number of colonies that showed an oxygen increase upon darkening, increased with depths (data not shown).

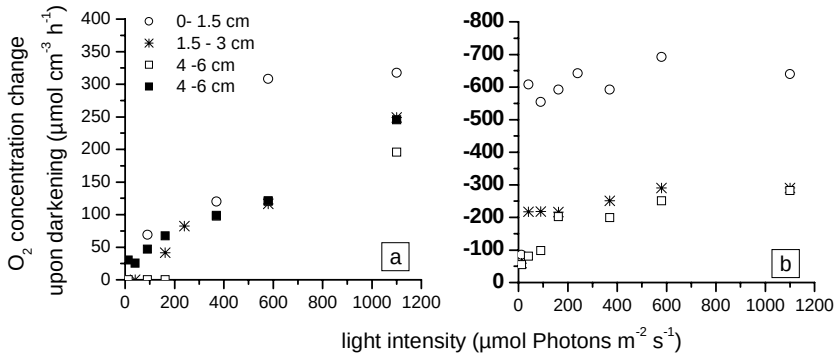


Figure 7: Oxygen concentration changes at episammic colonies upon darkening, using the light-dark shift method at different light intensities. The left panel (a) shows results from colonies of various depths where the oxygen concentration increased after darkening. The right panels (b) shows results from colonies where the oxygen decreased, as expected, after darkening (note positive y-values in a and negative values in b)

*Influence of photosynthesis on pore water pH and calcification*: The pH profiles determined during light incubation showed a peak, which coincided with a dip in the $Ca^{2+}$ profiles below the sediment surface at all stations (Fig. 5). The pH was highest at the reef belt and North Beach 2, where highest net photosynthesis rates were measured (Fig. 5). Areal net photosynthesis rates of the four stations correlated strongly with the calcification rates obtained from $Ca^{2+}$ flux calculations (Fig. 8 a).

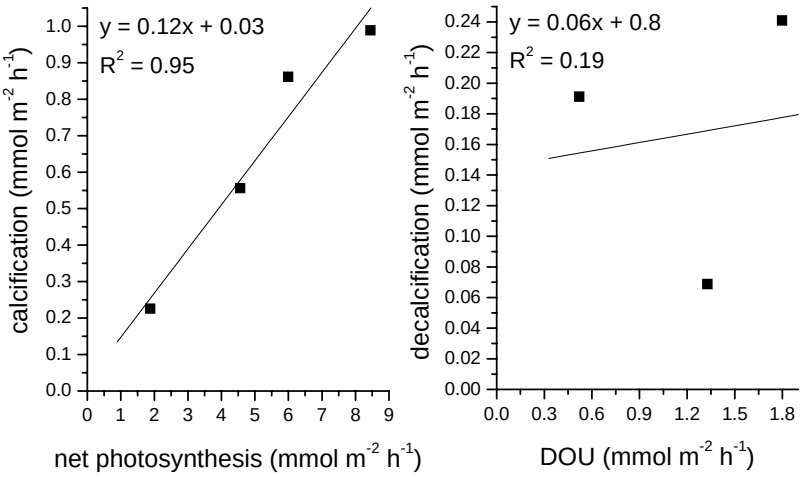


Figure 8: a) Correlation of net photosynthesis and calcification rate and b) of dissolved oxygen uptake (DOU) and decalcification rate.

*Relationship between DOU and pH and $Ca^{2+}$ concentrations*: Sedimentary $O_2$, pH and $Ca^{2+}$ concentrations changed in the upper 0.5 to 1 cm in the absence of photosynthesis (Fig. 5). During dark incubation, the thickness of the oxygenated layer was reduced as compared to the light incubations. The DOU varied between stations, highest rates were measured at North Beach 2, lowest rates at the reef belt, and at North Beach 1 and the channel station the DOU were comparable (Table 3). At North Beach 2 the high DOU resulted in the shallowest oxygen penetration, whereas the low DOU at the reef belt allowed the deepest oxygen penetration (Fig. 5).

The pH of the sediments decreased below seawater values during dark incubations (Fig. 5). The pH decreased sharpest in the sediment layer where oxygen was consumed. $Ca^{2+}$ concentrations in dark incubated sediments were above sea water concentrations in the top sediment layer and also below the oxygenated sediment layer (similar in the dark and in the light). However, interfacial $Ca^{2+}$ fluxes showed only a low correlation with areal DOU (Fig. 8 b). Per mol oxygen produced during photosynthesis more $CaCO_3$ precipitated than it was dissolved per mol DOU in the dark incubations.

*$N_2$-fixation rates*: In North Beach 1 and North Beach 2 sediments highest ARR were measured in the top layer during light incubations (Fig. 9). At North

Beach 1, ARR was also detected in the dark. In the deeper sediment depths ARR were low at both stations. The areal $N_2$-fixation rate (integrated over the depth of 10 cm) were highest at North Beach 1 (Table 3). In contrast to the sediments, ARR in the coral fingers was below the detection limits (data not shown).

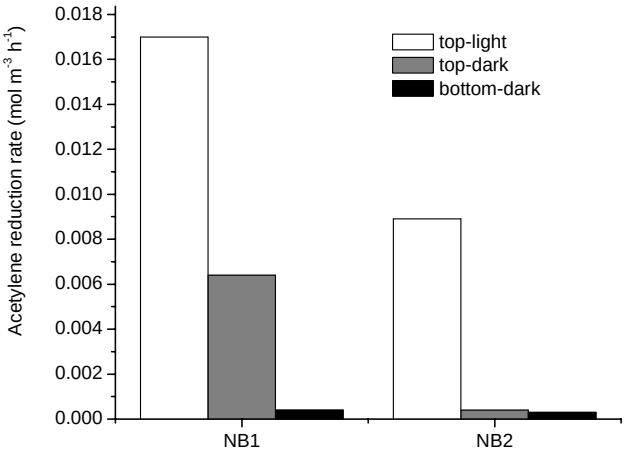


Figure 9: Acetylene reduction rates at North Beach1 (NB1) and North Beach 2 (NB 2) in the light and in the dark in the top sediment layer (0-3cm depth) and in the dark in the bottom sediment layer (10 cm depth).

Table 3: Net photosynthesis, diffusive oxygen uptake (DOU), light and dark calcium fluxes, chlorophyll-a content and $N_2$-fixation rates of the investigated sites. Data are given as average ± standard deviation. NB 1 & 2 are stations at North Beach, RB is the reef belt and Ch the channel station.

| | NB1 | NB2 | RB | Channel |
|---|---|---|---|---|
| Net photosynthesis rate<br>mmol $m^{-2}$ $h^{-1}$ | 4.6 ± 1.0 | 8.5 ± 0.2 | 6.0 ± 0.3 | 1.9 ± 0.1 |
| DOU<br>mmol $m^{-2}$ $h^{-1}$ | 1.3 ± 0.3 | 1.8 ± 0.2 | 0.5 ± 0.1 | 1.3 ± 0.1 |
| $Ca^{2+}$ light fluxes (calcification)<br>mmol $m^{-2}$ $h^{-1}$ | 0.6 ± 0.1 | 1.0 ± 0.1 | 0.7 ± 0.2 | 0.2 ± 0.2 |
| $Ca^{2+}$ dark fluxes (decalcification)<br>mmol $m^{-2}$ $h^{-1}$ | 0.07 ± 0.03 | 0.24 ± 0.13 | 0.19 ± 0.10 | |
| Ratios<br>Calc./net photosynth. | 0.12 | 0.17 | 0.14 | 0.12 |
| decalc./DOU | 0.05 | 0.13 | 0.37 | |
| Chla (mg $m^{-2}$)* | | 84 ± 10 | 68 ± 10 | 31 ± 3 |
| total $N_2$ fixation (ARR)**<br>mmol N $m^{-2}$ $h^{-1}$ | 3.9 | 0.9 | | |
| $N_2$ fixation (ARR) in light***<br>mmol N $m^{-2}$ $h^{-1}$ | 0.08 | 0.04 | | |

* integrated over the top first cm of the sediment, ** intergated over 10 cm *** top 5 mm

## Discussion

*Microphytobenthic diversity and activity:* The microphytobenthos was dominated by diatoms, dinoflagellates and cyanobacteria. With respect to cyanobacteria the episammic colonies were markedly divers. Sequences from a large variety of cyanobacterial groups were found in these only small (ca. 100 µm diameter) colonies.

The chlorophyll-a concentrations found at all investigated stations were low when compared to previously reported investigations at Heron Reef, where concentrations varied between 23 to 1153 mg chl a $m^{-2}$ (Roelfsema et al. 2002) and 92-995 mg chl a $m^{-2}$ (Heil et al. 2004). Still, the photosynthesis rate per unit chlorophyll-a (upper 0.5 cm) was high, indicating an active microphytobenthic community. Values ranged between 3.7 and 11 mg $O_2$ $mg^{-1}$Chl a $h^{-1}$. The high activity of the microphytobenthic community may be promoted by the strong hydrodynamic forcing in coral reefs (Buddemeier and Oberdorfer 1988; Hamner and Wolanski 1988). Dead microphytobenthos may be efficiently removed from the sediments by sediment resuspension resulting from tidal and wind induced currents and waves, whereas the living and active, e.g., episammic microphytobenthos, is likely to remain in the sediments. Coral reef sands are often characterized by a high permeability (Enos and Sawatsky 1981; Rasheed et al. 2003) and facilitate pore water advection though the interstices, where the exchange of solutes between sediments and water column can be greatly enhanced as compared to diffusion (Huettel and Gust 1992; Shum 1992). Pore water advection may stimulate microphytobenthic photosynthesis by removing inhibitory substances such as $H_2S$ from the pore water (Boudreau et al. 2001; Huettel et al. 2003) or by supplying $CO_2$ to the sediments (Cook and Røy in prep.).

Per unit surface area microphytobenthic photosynthesis is at least 6 times lower as photosynthesis rates reported for corals (average 600 mmol C $m^{-2}$ $d^{-1}$, up to 1380 mmol C $m^{-2}$ $d^{-1}$) (Kinsey 1985), and lower as most rates reported for macroalgae dominated reef flats (83 - 1660 C $m^{-2}$ $d^{-1}$) (Kinsey 1985). However, on the whole ecosystem scale the large areal extent of sandy sediments (not colonized by algae or corals) may compensate the lower photosynthetic activity. At Heron Reef 19.5 $km^2$ are covered by sands whereas only 6.9 $km^2$ are covered by corals

(Wild et al. 2004a). If the average photosynthesis rate of North Beach1, North Beach 2 and the reef belt station is considered representative for the entire reef flat area covered by sands, our data indicate that microphytobenthic photosynthesis (1770 mol C $d^{-1}$) is in the order of magnitude with an estimated production of corals (4140 mol C $d^{-1}$, based on an average production of 600 mmol C $m^{-2}$ $d^{-1}$) at Heron Reef.

Biomass (as derived from chlorophyll-a concentrations) and photosynthetic activity of the microphytobenthos varied between stations, as found for other reefs (Boucher et al. 1998; Garrigue 1998; Clavier and Garrigue 1999). Benthic photosynthesis is controlled by phycobenthic biomass and irradiance, for tropical sediments a limitation of benthic photosynthesis by nutrients is also reported (Heil et al. 2004). Net microphytobenthic photosynthesis rates at the investigated sites were highly correlated with the chlorophyll-a content of the respective stations, which may partly be due to the fact that all samples were measured under the same light conditions. Differences in microphytobenthic biomass and net photosynthesis rates reflect past environmental conditions for the microphytobenthos at the different stations. The channel station was the deepest of all stations and thus experienced lower light intensities. Net photosynthesis rates were different at the close-by stations North Beach 2 and North Beach 1. North Beach 2, which was closest to the island, may receive higher loadings of nutrients from land produced by humans and birds (Smith and Johnson 1995), which may favour benthic photosynthesis. A nutrient limitation at North Beach 1 may also be deduced from the higher light and dark $N_2$-fixation rates at this station as compared to the more shoreward station North Beach 2. However, remote from the island, the reef belt station had also high photosynthesis rates and chlorophyll-a concentrations. The high net photosynthesis rates at the reef belt coincided interestingly with the lowest DOU of all stations. Lowest oxygen consumption rates at this station (compared to the other stations) were also determined by another method that accounts for the effect of a deep oxygen supply by pore water advection (Werner et al. in prep.). Low oxygen consumption rates at a site with high primary production may indicate that the produced organic carbon is efficiently removed from the sediments by sediment reworking at this hydrodynamically very exposed station. The hydrodynamic forcing may also contribute to the low oxygen consumption rates as

the physical stress of the intense water and sediment movement makes it an unfavourable place for respiring infauna (Hall 1994).

*Consequences of microphytobenthic photosynthesis:* Microphytobenthic photosynthesis was not only important for the production of organic carbon but also affected the pore water pH and $Ca^{2+}$ concentrations in the top sediment layers of all stations. The pH peak in the photosynthetic sediment layer resulted from the $CO_2$ uptake by benthic microalgae and a consequential shift of the carbonate equilibrium towards $CO_3^{2-}$. This increases the saturation state of the pore water with respect to calcium carbonate and promotes calcium carbonate precipitation, as shown by the low $Ca^{2+}$ concentrations in the photosynthetic sediment layer. By buffering against strong pH increases, calcification may interact beneficially with benthic photosynthesis and support high photosynthesis rates within the reef sediments. In this study, the ratio of mol $CaCO_3$ precipitated per mol oxygen produced was 0.1 for all reef stations and 0.06 for the Channel station. These numbers compare well with estimates based on data given in the review by (Kinsey 1985), which ranged between ca. 0.3 and 1.1 for both, corals and sands.

The above seawater $Ca^{2+}$ concentration in the pore water and the positive calcium efflux to the overlying water in the dark indicate that benthic mineralization stimulated decalcification in the sediments. The aerobic oxidation of organic matter results in a lowering of the pH (as seen in Fig. 4 in the upper mm of sediments) and lowers total alkalinity (Tribble 1993; Sanders 2003). Aerobic mineralization, thus, creates a microenvironment which may be undersaturated with respect to calcium carbonate, resulting in a dissolution of $CaCO_3$. However, the magnitude of $Ca^{2+}$ fluxes were not significantly related to the magnitude of DOU (Fig. 8b). Below the sediment layers where aerobic mineralization contributed to $CaCO_3$ dissolution, $Ca^{2+}$ concentrations were also elevated above seawater concentrations during both light and dark incubations and a low pore water pH was measured. Some fermentation processes, some pathways of sulfate reduction and the oxidation of the end product $H_2S$ can induce a drop in pH (Tribble 1993; Sanders 2003). This may promote decalcification in these sediments, as previously described for iron poor reef sediments (Morse et al. 1985; Tribble 1993).

Under the flow conditions applied in the lab, the sediments of at least three stations were net calcifying over a full light/dark cycle, as calcification rates were 3-10 times higher than the decalcification rates (Table 3). The net calcification rates per day (light fluxes minus dark fluxes) were, with rates between 12 and 19 mmol $CaCO_3$ $m^{-2}$ $d^{-1}$, in line with literature data from other reefs sands that range between -4 and 100 mmol $CaCO_3$ $m^{-2}$ $d^{-1}$ (Kinsey 1985; Gattuso et al. 1998).

In situ measurements with pH and $Ca^{2+}$ LIX microsensor attached to an autonomous profiler were unfortunately not successful during our field campaign, but would be of importance to clarify in situ processes under natural hydrodynamics. The effect of pore water transport on calcification/decalcification may be ambivalent. During the diffusive experimental conditions, zones may develop in the sediments, where concentrations (e.g., $H^+$, $Ca^{2+}$) are above of those found in nature. In the presence of pore water advection, however, solutes are efficiently transported within and out of the sediments. This may alter the saturation state of the pore water with respect to calcium carbonate in various sediment layers and thus alter calcification and decalcification rates. Pore water advection was found to stimulate benthic mineralization processes and photosynthesis (Cook and Røy in prep.), which also may alter calcification and decalcification rates. Oxygen consumption rates in the presence of pore water advection were 4 to 6 times higher at the investigated stations (Werner et al. in prep.) as the DOU measured in this study, thus, sediments, instead of being net calcifying, may be net decalcifying.

*$N_2$-fixation:* $N_2$-fixation by microorganisms is considered a major source for nitrogen in coral reefs (Gattuso et al. 1998; Charpy-Roubaud et al. 2001). $N_2$-fixation may thus support high reef gross production rates in oligotrophic waters. The importance of the sediment compartment for the reef ecosystem was stressed by the $N_2$-fixation experiments, as it showed that the sedimentary organisms were active in atmospheric $N_2$-fixation, in contrast to the investigated coral samples. The high rates of $N_2$-fixation in light indicate the importance of heterocystous cyanobacteria that protect the oxygen-sensitive enzyme nitrogenase against the produced oxygen in specialised cells. The presence of cyanobacteria was shown by the biomarker zeaxanthin (and the concurrent absence of chlorophyll-b) and 16S rRNA gene sequences related to heterocystous cyanoacteria were found in the

green episammic colonies (see cluster 1 in Fig. 4). Also some non-heterocystous cyanobacteria can fix $N_2$, but only few of them in the presence of oxygen. At North Beach 1 dark $N_2$-fixation was significant. $N_2$ fixation in the dark may be conducted by sulfate reducing bacteria and by heterocystous and non-heterocystous cyanobacteria, as long as their internal photosynthate storage pools are not depleted (Bebout et al. 1993). As stated above, the higher $N_2$-fixation at North Beach 1 in comparison to North Beach 2 may be due to a higher nitrogen demand at this station.

The $N_2$-fixation rates measured in our study (North Beach 1: 0.26 mg N $m^{-2}$ $d^{-1}$; North Beach 2: 0.06 mg N $m^{-2}$ $d^{-1}$) compare well with $N_2$-fixation rates measured in other coral reefs (summarized in Charpy-Roubaud et al. 2001) that mostly ranged between 0.1 and 8.6 mg N $m^{-2}$ $d^{-1}$.

Microphytobenthic algae are assumed to produce biomass with the Redfield C:N ratio of of 106:16. At North Beach 1 the gross photosynthesis rate of 5.6 mmol C $m^{-2}$ $h^{-1}$ would thus require 0.9 mmol N $m^{-2}$ $h^{-1}$. The $N_2$-fixation rate of 0.08 mmol N $m^{-2}$ $h^{-1}$ in the light would provide ca. 9% of the required nitrogen for the build up of cell material. At North Beach 2 the estimated gross photosynthesis rate of 10.3 mmol C $m^{-2}$ $h^{-1}$ would require 1.6 mmol N $m^{-2}$ $h^{-1}$, only ca 3% are provided by $N_2$-fixation in the light (0.04 mmol N $m^{-2}$ $h^{-1}$). The remaining nitrogen may be taken up from the pore waters. Additionally, may microphytobenthos secret excess carbon produced as low nitrogen containing extrapolymeric substances (Goto et al. 1999; Yallop et al. 2000). At North Beach 1 the daily, total light and dark $N_2$-fixation rates (Table 3) exceeded the nitrogen requirements of the microphytobenthos, which stresses the importance of this nitrogen source for sediment nutrient cycling and benthic microbial processes.

*Results from light dark-shift method:* Gross photosynthesis rates measurements in the sediments and at the episammic colonies gave unexpected results. The concept behind the light dark shift method is that during illumination a steady state between the oxygen production rate, the oxygen consumption rate and the diffusive transport is achieved. When the light is switched off only photosynthesis stops, while respiration and diffusive transport are thought to continue unchanged in the first seconds. Then, the $O_2$ decrease would be equal to gross $O_2$ production before darkening. At some colonies, however, an increase of

oxygen concentrations was measured upon darkening. As oxygen is not produced in the dark, the measured increase can only be explained by diffusive flux of oxygen from the surrounding water towards the sensor tip. This means, however, that in the light an oxygen gradient must have established with lower concentrations close to the colonies than in the surrounding water. This can only be achieved when the colonies are net oxygen consuming in light. This points towards higher respiration rates in the light than in the dark, which is supported by the fact that the unexpected oxygen increase upon darkening increased with rising light intensities also above 200 µmol Photons $m^{-2}$ $s^{-1}$ where photosynthesis was saturated in the colonies that showed the expected decrease in oxygen concentration upon darkening.

An increase of oxygen upon darkening was also found using the light-dark shift method in deep, distinct layers within a cyanobacterial mat (Jørgensen et al. 1988). The oxygen increase upon darkening was with a maximum of 0.27 mmol $O_2$ $cm^{-3}$ $h^{-1}$ (at 600 µmol Photons $m^{-2}$ $s^{-1}$) similar to what we found at the colonies (Fig. 7 a) and the oxygen increase also raised with increasing light intensities. Jørgensen et al. (1988) proposed several explanations for an enhanced oxygen consumption in the light, with the Mehler reaction likely being of importance. At high light intensities the electron flow from photosystem II may exceed the electron demand for $CO_2$ assimilation. To cope with the excess electrons generated in the light reaction, mechanisms are needed that channel the electron flow and, further, reduce high levels of oxygen. In the first steps of the Mehler reaction ½ $O_2$ is reduced and hydrogen peroxide is generated. The Mehler reaction is saturated only at high light intensities, which fits to the observations that the measured oxygen increase upon darkening was not saturated at high light intensities (Fig. 7 a). However, when the enzyme catalase is present and active, the net oxygen uptake by the Mehler reaction is zero as ½ $O_2$ is produced from hydrogen peroxide ($H_2O_2 \rightarrow H_2O + ½\ O_2$). The Mehler reaction is then not useful to explain elevated oxygen consumption in the light. But, the measured increase of oxygen upon darkening was found mostly in colonies from deeper depths, which may have a low photosynthetic activity and a reduced content of the enzyme catalase.

Photorespiration is unlikely to be the cause for an enhanced oxygen consumption in the light, as photorespiration does not decrease in the first seconds upon darkening (Glud et al. 1992). In most aquatic plants, particular unicellular algae and cyanobacteria, photorespiration is suppressed by the intracellular accumulation of inorganic carbon by active uptake of $HCO_3^-$ and $CO_2$ from the external medium (Colman 1989; Ghoshal and Goyal 2001; Ogawa and Kaplan 2003).

Different respiration rates in light and in the dark and the potential impact of the Mehler reaction are critical in the interpretation of results from the light-dark shift method. Different respiration rates in light and dark are only detected, when the investigated organisms are net oxygen consuming in the light and an increase of oxygen is measured upon darkening. In case of only moderately elevated levels of oxygen consumption in light (net production of oxygen in the light), a decrease of oxygen upon darkening would be measured, which would however, lead to an underestimation of gross photosynthesis rates.

*Conclusion:* Although the chlorophyll-a content was much lower in the sediments than expected from previous investigations, microphytobenthic photosynthesis was remarkably high per unit chlorophyll-a. On the whole reef ecosystem scale the contribution of microphytobenthic photosynthesis to total reef production was estimated to be in the same order of magnitude as the production estimated for corals. The importance of the sediment compartment for matter cycling was demonstrated by the $N_2$-fixation experiments, as in sediments $N_2$-fixation was substantial, whereas in corals it was not detectable. The unexpected results with the light-dark-shift method pose questions concerning the physiology of the microalgae. Diverse 16S RNA gene sequences from episammic colonies indicated many unknown cyanobacteria in the reef sediments.

**Acknowledgments:** We are very thankful for the great support by Raid Abed in the evaluation of the 16S rDNA sequences data. Rebecca Ludwig and Henk Jonkers are acknowlegded for their support and for discussion. The staff from the Heron Island research station is thanked for their logistic help and hospitality. We thank

B.B. Jørgensen for support of this study and for discussion. This study was financed by the Max Planck Society (MPG), Germany.

## References

Bebout, B. M., M. W. Fitzpatrick, and H. W. Paerl. 1993. Identification of the sources of energy for nitrogen-fixation and physiological characterization of nitrogen-fixing members of a marine microbial mat community. Appl. Environ. Microbiol. **59:** 1495-1503.

Boucher, G., J. Clavier, C. Hily, and J. P. Gattuso. 1998. Contribution of soft-bottoms to the community metabolism (primary production and calcification) of a barrier reef flat (Moorea, French Polynesia). J. Exp. Mar. Biol. Ecol. **225:** 269-283.

Boudreau, B., M. Huettel, R. Forster, A. Jahnke, J. McLachlan, J. Middelburg, P. Nielsen, F. Sansone, G. Taghon, W. Van Raaphorst, I. Webster, J. Weslawski, P. Wiberg, and B. Sundby. 2001. Permeable marine sediments: Overturning an old paradigm. EOS,TransAGU **82:** 133-136.

Buddemeier, R., and J. Oberdorfer. 1988. Hydrogeology and Hydrodynamics of Coral Reef Pore Waters. Proc. Sixth Internat. Coral Reef Symp. **2:** 485-490.

Buffan-Dubau, E., and K. R. Carman. 2000. Extraction of benthic microalgal pigments for HPLC analyses. Mar. Ecol.-Prog. Ser. **204:** 293-297.

Canfield, D. E., and R. Raiswell. 1991. Carbonate precipitation and dissolution: Its relevance to fossil preservation. p. 411–453. In Allison, P.A., and D.E.G. Briggs [eds]: Taphonomy: Releasing the data locked in the fossil record: Plenum Press, New York

Charpy, L., C. Charpy-Roubaud, and P. Buat. 1998. Excess primary production, calcification and nutrient fluxes of a patch reef (Tikehau atoll, French Polynesia). Mar. Ecol.-Prog. Ser. **173:** 139-147.

Charpy-Roubaud, C., L. Charpy, and A. W. D. Larkum. 2001. Atmospheric dinitrogen fixation by benthic communities of Tikehau Lagoon (Tuamotu Archipelago, French Polynesia) and its contribution to benthic primary production. Mar. Biol. **139:** 991-997.

Clavier, J., and C. Garrigue. 1999. Annual sediment primary production and respiration in a large coral reef lagoon (SW New Caledonia). Mar. Ecol.-Prog. Ser. **191:** 79-89.

Colman, B. 1989. Photosynthetic carbon assimilation and the suppression of photorespiration in the cyanobacteria. Aquat. Bot. **34:** 211-231.

Cook, P., and H. Røy. Advective relief of inorganic carbon limitation in highly productive sandy sediments. submitted Limnol. Oceanogr.

de Beer, D., M. Kuhl, N. Stambler, and L. Vaki. 2000. A microsensor study of light enhanced Ca2+ uptake and photosynthesis in the reef-building hermatypic coral *Favia sp*. Mar. Ecol.-Prog. Ser. **194:** 75-85.

Enos, P., and L. H. Sawatsky. 1981. Pore Networks in Holocene Carbonate Sediments. J. Sediment Petrol. **51:** 961-985.

Garrigue, C. 1998. Distribution and biomass of microphytes measured by benthic chlorophyll a in a tropical lagoon (New Caledonia, South Pacific). Hydrobiologia **385:** 1-10.

Gattuso, J. P., M. Frankignoulle, and R. Wollast. 1998. Carbon and carbonate metabolism in coastal aquatic ecosystems. Annu. Rev. Ecol. Syst. **29:** 405-434.

Gattuso, J. P., C. E. Payri, M. Pichon, B. Delesalle, and M. Frankignoulle. 1997. Primary production, calcification, and air-sea CO2 fluxes of a macroalgal-dominated coral reef community (Moorea, French Polynesia). J. Phycol. **33:** 729-738.

Ghoshal, D., and A. Goyal. 2001. Carbon concentration mechanism(s) in unicellular green algae and cyanobacteria. J. Plant Biochem. Biotechnol. **10:** 83-90.

Glud, R. N., N. B. Ramsing, and N. P. Revsbech. 1992. Photosynthesis and photosynthesis-coupled respiration in natural biofilms quantified with oxygen microsensors. J. Phycol. **28:** 51-60.

Goto, N., T. Kawamura, O. Mitamura, and H. Terai. 1999. Importance of extracellular organic carbon production in the total primary production by tidal-flat diatoms in comparison to phytoplankton. Mar. Ecol.-Prog. Ser. **190:** 289-295.

Hall, S. J. 1994. Physical Disturbance and Marine Benthic Communities - Life in Unconsolidated Sediments. Oceanogr. Mar. Biol. Annu. Rev. **32:** 179-239.

Hamner, W., and E. Wolanski. 1988. Hydrodynamic forcing functions and biological processes on coral reefs: a status review. Proc. Sixth Internat. Coral Reef Symp. **1:** 103-113.

Heil, C. A., K. Chaston, A. Jones, P. Bird, B. Longstaff, S. Costanzo, and W. C. Dennison. 2004. Benthic microalgae in coral reef sediments of the southern Great Barrier Reef, Australia. Coral Reefs **23:** 336-343.

Huettel, M., and G. Gust. 1992. Impact of Bioroughness On Interfacial Solute Exchange in Permeable Sediments. Mar. Ecol.-Prog. Ser. **89:** 253-267.

Huettel, M., H. Røy, E. Precht, and S. Ehrenhauss. 2003. Hydrodynamical impact on biogeochemical processes in aquatic sediments. Hydrobiologia **494:** 231-236.

Jørgensen, B. B., Y. Cohen, and N. P. Revsbech. 1988. Photosynthetic Potential and Light-Dependent Oxygen-Consumption in a Benthic Cyanobacterial Mat. Appl. Environ. Microbiol. **54:** 176-182.

Jørgensen, B. B., and N. P. Revsbech. 1985. Diffusive Boundary-Layers and the Oxygen-Uptake of Sediments and Detritus. Limnol. Oceanogr. **30:** 111-122.

Kinsey, D. 1985. Metabolism, Calcification and Carbon Production, I, System Level Studies. Proc. **4:** 506-526.

Kuehl, M., R. N. Glud, H. Ploug, and N. B. Ramsing. 1996. Microenvironmental control of photosynthesis and photosynthesis-coupled respiration in an epilithic cyanobacterial biofilm.
J. Phycol. **32:** 799-812.

Larkum, A. W. D., I. R. Kennedy, and W. J. Muller. 1988. Nitrogen-Fixation on a Coral-Reef. Mar. Biol. **98:** 143-155.

Li, Y. H., and S. Gregory. 1974. Diffusion of Ions in Sea-Water and in Deep-Sea Sediments. Geochim. Cosmochim. Acta **38:** 703-714.

Ludwig, W., O. Strunk, S. Klugbauer, N. Klugbauer, M. Weizenegger, J. Neumaier, M. Bachleitner, and K. H. Schleifer. 1998. Bacterial phylogeny based on comparative sequence analysis. Electrophoresis **19:** 554-568.

Morse, J. W., J. J. Zullig, L. D. Bernstein, F. J. Millero, P. Milne, A. Mucci, and G. R. Choppin. 1985. Chemistry of calcium carbonate rich shallow-water sediments in the Bahamas. Am. J. Sci. **285:** 147-185.

Nuebel, U., F. GarciaPichel, and G. Muyzer. 1997. PCR primers to amplify 16S rRNA genes from cyanobacteria. Appl. Environ. Microbiol. **63:** 3327-3332.

Ogawa, T., and A. Kaplan. 2003. Inorganic carbon acquisition systems in cyanobacteria. Photosynth. Res. **77:** 105-115.

Oneil, J. M., and D. G. Capone. 1989. Nitrogenase activity in tropical carbonate marine-sediments. Mar. Ecol.-Prog. Ser. **56:** 145-156.

Rasheed, M., M. I. Badran, and M. Huettel. 2003. Influence of sediment permeability and mineral composition on organic matter degradation in three sediments from the Gulf of Aqaba, Red Sea. Est. Coast. Shelf Sci. **57:** 369-384.

Revsbech, N. P. 1989. An Oxygen Microsensor With a Guard Cathode. Limnol. Oceanogr. **34:** 474-478.

Revsbech, N. P., B. B. Jørgensen, and O. Brix. 1981. Primary production of microalgae in sediments measured by oxygen microprofile, H-CO-14(3)-Fixation, and oxygen-exchange methods. Limnol. Oceanogr. **26:** 717-730.

Roelfsema, C. M., S. R. Phinn, and W. C. Dennison. 2002. Spatial distribution of benthic microalgae on coral reefs determined by remote sensing. Coral Reefs **21:** 264-274.

Sanders, D. 2003. Syndepositional dissolution of calcium carbonate in neritic carbonate environments: geological recognition, processes, potential significance. J. Afr. Earth Sci. **36:** 99-134.

Shum, K. T. 1992. Wave-induced advective transport below a rippled water-sediment interface. J. Geophys. Res.-Oceans **97:** 789-808.

Smith, J. S., and C. R. Johnson. 1995. Nutrient inputs from seabirds and humans on a populated coral cay. Mar. Ecol.-Prog. Ser. **124:** 189-200.

Stewart, W. D. P., Fitzgera.Gp, and R. H. Burris. 1967. In situ studies on nitrogen fixation with acetylene reduction technique. Science **158:** 536-&.

Tribble, G. W. 1993. Organic-matter oxidation and aragonite diagenesis in a coral-reef. J. Sediment Petrol. **63:** 523-527.

Ullman, W. J., and R. C. Aller. 1982. Diffusion-coefficients in nearshore marine-sediments. Limnol. Oceanogr. **27:** 552-556.

Werner, U., P. Bird, C. Wild, T. G. Ferdelman, L. Polerecky, G. Eickert, R. Jonstone, and O. Hoegh-Guldberg. Spatial patterns of aerobic and anaerobic mineralization rates and oxygen penetration dynamics in coral reef sediments (Heron Island, Australia). submitted to Limnol. Oceanogr.

Wild, C., M. Huettel, A. Klueter, S. G. Kremb, M. Y. M. Rasheed, and B. B. Jørgensen. 2004a. Coral mucus functions as an energy carrier and particle trap in the reef ecosystem. Nature **428:** 66-70.

Wild, C., R. Tollrian, and M. Huettel. 2004b. Rapid recycling of coral mass-spawning products in permeable reef sediments. Mar. Ecol.-Prog. Ser. **271:** 159-166.

Wilkinson, C. R., D. M. Williams, P. W. Sammarco, R. W. Hogg, and L. A. Trott. 1984. Rates of Nitrogen-Fixation on Coral Reefs across the Continental-Shelf of the Central Great Barrier-Reef. Mar. Biol. **80:** 255-262.

Wright, S. W., S. W. Jeffrey, R. F. C. Mantoura, C. A. Llewellyn, T. Bjornland, D. Repeta, and N. Welschmeyer. 1991. Improved HPLC method for the analysis of chlorophylls and carotenoids from marine-phytoplankton. Mar. Ecol.-Prog. Ser. **77:** 183-196.

Yallop, M. L., D. M. Paterson, and P. Wellsbury. 2000. Interrelationships between rates of microbial production, exopolymer production, microbial biomass, and sediment stability in biofilms of intertidal sediments. Microb. Ecol. **39:** 116-127.

Zeebe, R. E., and D. A. Gladrow. 2005. CO2 in seawater: equilibrium, kinetics, isotopes. 65, pp. 346. Elsevier Oceanography Series. Amsterdam.

**Conclusions and outlook**

In this thesis microbial processes and the role of pore water advection in benthic metabolism of permeable coastal sediments were investigated. The core part of this thesis focuses on the magnitude and relative importance of benthic aerobic and anaerobic mineralization processes and on the role of advective oxygen and organic carbon supply for mineralization. These were investigated in situ at three different sites, two temperate, intertidal sands and carbonate sediments in a coral reef. Between these site clear similarities existed, but simultaneously, these sites exhibited pronounced differences, stressing the uniqueness and heterogeneity of permeable coastal sands.

At all sites oxygen penetrated up to several centimeters into the sediments and oxygen penetration varied with time. This temporal variation was shown by repetitive measurements of oxygen profiles with the autonomous profiler over extended time periods. Oxygen penetration and dynamics were, at all sites, linked to pore water advection. This was derived from the following observations: a) At the intertidal flats, the Hausstrand (Sylt) and Janssand (near Spiekeroog), oxygen penetrated deeper during inundation than during exposure of the flat. The heavily replicated dataset describing oxygen penetration over the tidal cycle supports the previous findings of De Beer et al. (2005). b) The simultaneous measurements of bottom flow velocities and oxygen profiles showed a strong coupling of oxygen penetration to the hydrodynamic forcing in the overlying water column at both intertidal sites, thereby confirming results from laboratory studies (Forster et al. 1996; Precht et al. 2004). c) In the coral reef sediments oxygen penetration and dynamics varied strongly between sites, according to their exposure to hydrodynamic forcing. d) The impact of pore water advection on sedimentary oxygen distribution was also observed in the oxygen profiles of all sites. In the presence of pore water advection, oxygen often penetrated several millimetres without significant concentration decrease and often exhibited a sigmoidal, rather than a parabolic shape, as it has been described for advection and diffusion dominated oxygen profiles, respectively (Revsbech et al. 1980; Forster et al. 1996; Lohse et al. 1996).

Benthic mineralization rates were high at the three investigated sites. Oxygen consumption rates (OCR) ranged between 57 and 269 mmol $O_2$ $m^{-2}$ $d^{-1}$

(only summer OCR of the intertidal flats). One reason for these high mineralization rates was the advective supply of oxygen to the sediments. The deep supply of oxygen during flat inundation led to higher OCR during these periods at both intertidal flats. At the Hausstrand 71 to 90% of total daily mineralization took place during inundation, at Janssand ca. 50% (while the flat was inundation less than 50% of the day). Due to the deep oxygen penetration aerobic mineralization rates were high at all sites.

The importance of pore water advection for benthic mineralization was further stressed by the increase of OCR and sulfate reduction rates (SRR) towards the low water line at the intertidal flat Hausstrand. This indicates that at the lower station, environmental conditions (e.g., supply of oxygen and organic matter) were beneficial for benthic mineralization due to a longer inundation time. Transport of organic carbon into the sediments by pore water advection is another important factor for high benthic mineralization rates in the organic poor sands (Webb and Theodor 1968; Huettel and Gust 1992; Shum 1992). However, estimated organic carbon supply to the sediments by bottom water filtration was not sufficient to fuel the high measured mineralization rates at all sites. This can be explained by the presence of other organic carbon sources or by an error in the estimation of organic carbon fluxes from the overlying water. Other sources of organic matter are likely important for the pattern found in benthic mineralization rates at Heron Reef. The two stations close to the island had very similar volumetric OCR and SRR, the oxygen penetration and dynamics were, however, markedly different between the stations. With similar potential oxygen uptake in the upper sediment layer, the different oxygen penetration must be due to a different rate of oxygen supply, thus, a different pore water advection rate. Comparable volumetric OCR in the presence of different pore water advection rates at the two stations may stress the importance of benthic photosynthesis or faunal transport in these sediments.

The model used to estimate bottom water filtration rates is based on oversimplification, i.e., by assuming vertical 1D –advection (see discussion in chapter 3). The potential errors may lead to an underestimation of bottom water filtration rates. Methods for the determination of in situ bottom water filtration rates are still lacking, or are very laborious. One option is the modelling of pore water flow rates after extensive measurements of bottom current flow and of

sediment topography. This is currently the aim of an ongoing project (F. Janssen, pers. communication).

The three investigated sites also showed clear differences. Different to what was found at the Hausstrand, mineralization rates were equal at the lower and the upper flat at the Janssand, i.e., they were independent of inundation time. This may result from a lower impact of pore water advection due to shorter inundation times and a lower permeability at the Janssand. At Janssand nutrient concentrations were highly elevated at the lower flat as compared to the upper flat and pore water was discharged from the sediments above the low water line (for $H_2S$ release see also E. Walpersdorf, unpublished). The concentration difference could not be explained by the surface sediment mineralization, as mineralization rates were similar between the two sites. Therefore two filtration layers were proposed for the Janssand, the "skin" and the "body" filtration layers, with different pore water residence times and flow path lengths. In principle, this is likely to be true for the Hausstrand as well. At this site also the highest nutrients were measured at the lower flat, although differences were small when compared to the Janssand. This may be due to the different sizes of the intertidal flats. Due to the narrow proportions of the Hausstrand (130 m widths) the catchment area for organic carbon is much smaller as the 3 km wide Janssand and pore water flow paths are longer. Due to the coarser sediments, the pore water pressure is not sufficient to achieve pore water discharge above the low water line at the Hausstrand, thus, nutrients may be discharged in the sublitoral zone. This sublitoral nutrient discharge may support the high photosynthesis rates that were measured at a nearby sublitoral station (Cook and Røy, in prep.).

In this thesis, the percolation method, as characterized in Chapter 2, was applied for the determination of volumetric and areal OCR. This method uses oxygen penetration depths that are obtained under natural hydrodynamic conditions. Oxygen penetration is heavily driven by local hydrodynamics that cannot be mimicked in benthic chambers. Thus, the areal OCR obtained during this thesis were at the upper end or higher than OCR assessed before in sands. In previous studies transport during measurements was restricted to diffusion or benthic chambers were used. The such obtained OCR were between 2 to 170 mmol $O_2$ $m^{-2}$ $d^{-1}$ in intertidal temperate sands (e.g., Cammen 1991; Kristensen

et al. 1997; Rusch et al. 2001; D'Andrea et al. 2002; Magalhaes et al. 2002) and in the range of 11 - 75 mmol $O_2$ $m^{-2}$ $d^{-1}$ for coral reefs (e.g., Boucher et al. 1998; Clavier and Garrigue 1999; Grenz et al. 2003; Rasheed et al. 2004; Wild et al. 2004).

The volumetric OCR profiles measured in this study show the mineralization potential and past environmental conditions with respect to oxygen and organic carbon for the organisms. The volumetric OCR also allowed the comparison of depth distribution patterns of volumetric OCR and SRR. For SRR a zone of high activity was found at the oxic/anoxic interface, where best conditions in terms of organic carbon supply from above and in terms of anoxia can be found. SRR at the interface may also benefit from redox oscillations. OCR were, in some measurements, highest in the first millimetres below the sediment surface, these observations point towards a "net" vertical transport, even in these pore water advection dominated sediments.

The importance of sediments for ecosystem functioning is not restricted to the mineralization of organic matter and release of nutrients from the sediments to the overlying water. This was also demonstrated here in the investigations on microphytobenthos in the coral reef sediments. Microphytobenthic photosynthesis was high, and calculations indicated that it may account for 40% the estimated coral production on the whole reef scale. The high microphytobenthic photosynthesis rates per unit chlorophyll-a indicate an active microphytobenthic community, which may again be a result of the intense hydrodynamic forcing at the investigated sediments. Local hydrodynamics support the efficient mineralization or may support an efficient removal of dead cells from the sands. Pore water advection may also stimulate photosynthesis by increasing the $CO_2$ availability in permeable sediments (Cook and Røy, in prep.). Photosynthesis stimulated calcification and sediments were net calcifying at the chosen experimental settings. By fixing $N_2$ from the atmosphere benthic microbes contribute to reefal nitrogen cycling.

Outlook: The results of the investigations confirm the importance of permeable sediments for coastal carbon and nutrient cycling. However, in situ techniques for the determination of microbial processes and for the determination

of sediment-water column transport need further development for better understanding of pore water advection influenced sediments.

The contribution of organic carbon supply by pore water advection to benthic mineralization in relation to other potential carbon sources needs to be assessed. Therefore, direct measurement of bottom water filtration rates in situ are essential. Benthic photosynthesis and the relation to inundation time/pore water advection needs to be determined in situ. The measurements on microphytobenthic photosynthesis and its consequences for other sedimentary processes in the carbonate sediments (chapter 6) were restricted to diffusive conditions. In situ sensor measurements were not successful due to technical problems. Thus, in situ measurements or experiments with advective transport are still mandatory to clarify processes under more natural flow conditions, e.g., to solve the question whether sediments remain net calcifying in the presence of pore water advection. The episammic colonies were highly diverse with respect to cyanobacterial 16S rDNA gene sequences. Sequences from a large variety of cyanobacterial groups were found in these only small (100µm diameter) colonies. These microorganisms, their physiology and potential interactions within the colonies are interesting objects for future research.

## References


Boucher, G., J. Clavier, C. Hily, and J. P. Gattuso. 1998. Contribution of soft-bottoms to the community metabolism (primary production and calcification) of a barrier reef flat (Moorea, French Polynesia). J. Exp. Mar. Biol. Ecol. **225:** 269-283.

Cammen, L. M. 1991. Annual Bacterial Production in Relation to Benthic Microalgal Production and Sediment Oxygen-Uptake in an Intertidal Sandflat and an Intertidal Mudflat. Mar. Ecol.-Prog. Ser. **71:** 13-25.

Clavier, J., and C. Garrigue. 1999. Annual sediment primary production and respiration in a large coral reef lagoon (SW New Caledonia). Mar. Ecol.-Prog. Ser. **191:** 79-89.

Cook, P., and H. Røy. Advective relief of inorganic carbon limitation in highly productive sandy sediments. submitted to Limnol. Oceanogr.

D'Andrea, A. F., R. C. Aller, and G. R. Lopez. 2002. Organic matter flux and reactivity on a South Carolina sandflat: The impacts of porewater advection and macrobiological structures. Limnol. Oceanogr. **47:** 1056-1070.

de Beer, D., F. Wenzhoefer, T. G. Ferdelman, S. E. Boehme, M. Huettel, J. E. E. van Beusekom, M. E. Boettcher, N. Musat, and N. Dubillier. 2005. Transport and mineralization rates in North Sea sandy intertidal sediments, Sylt-Rømø Basin, Wadden Sea. Limnol. Oceanogr. **50:** 113-127.

Forster, S., M. Huettel, and W. Ziebis. 1996. Impact of boundary layer flow velocity on oxygen utilisation in coastal sediments. Mar. Ecol.-Prog. Ser. **143:** 173-185.

Grenz, C., L. Denis, G. Boucher, L. Chauvaud, J. Clavier, R. Fichez, and O. Pringault. 2003. Spatial variability in Sediment Oxygen Consumption under winter conditions in a lagoonal system in New Caledonia (South Pacific). J Exp Mar Biol Ecol **285:** 33-47.

Huettel, M., and G. Gust. 1992. Impact of bioroughness on interfacial solute exchange in permeable sediments. Mar. Ecol.-Prog. Ser. **89:** 253-267.

Kristensen, E., M. H. Jensen, and K. M. Jensen. 1997. Temporal variations in microbenthic metabolism and inorganic nitrogen fluxes in sandy and muddy sediments of a tidally dominated bay in the northern Wadden Sea. Helgol. Meeresunters. **51:** 295-320.

Lohse, L., E. H. G. Epping, W. Helder, and W. van Raaphorst. 1996. Oxygen pore water profiles in continental shelf sediments of the North Sea: Turbulent versus molecular diffusion. Mar. Ecol.-Prog. Ser. **145:** 63-75.

Magalhaes, C. M., A. A. Bordalo, and W. J. Wiebe. 2002. Temporal and spatial patterns of intertidal sediment-water nutrient and oxygen fluxes in the Douro River estuary, Portugal. Mar. Ecol.-Prog. Ser. **233:** 55-71.

Precht, E., U. Franke, L. Polerecky, and M. Huettel. 2004. Oxygen dynamics in permeable sediments with wave-driven pore water exchange. Limnol. Oceanogr. **49:** 693-705.

Rasheed, M., C. Wild, U. Franke, and M. Huettel. 2004. Benthic photosynthesis and oxygen consumption in permeable carbonate sediments at Heron Island, Great Barrier Reef, Australia. Est. Coast. Shelf Sci. **59:** 139-150.

Revsbech, N. P., B. B. Jørgensen, and T. H. Blackburn. 1980. Oxygen in the sea bottom measured with a microelectrode. Science **207:** 1355-1356.

Rusch, A., S. Forster, and M. Huettel. 2001. Bacteria, diatoms and detritus in an intertidal sandflat subject to advective transport across the water-sediment interface. Biogeochemistry **55:** 1-27.

Shum, K. T. 1992. Wave-iInduced advective transport below a rippled water-sediment interface. J. Geophys. Res.-Oceans **97:** 789-808.

Webb, J. E., and J. Theodor. 1968. Irrigation of submerged marine sands through wave action. Nature **220:** 682-&.

Wild, C., M. Rasheed, U. Werner, U. Franke, R. Johnstone, and M. Huettel. 2004. Degradation and mineralization of coral mucus in reef environments. Mar. Ecol.-Prog. Ser. **267:** 159-171.

## Abstracts of manuscripts not included in this thesis

**Microbial community structure of North Sea sandy intertidal sediments, Sylt-Rømø Basin, Wadden Sea**

by Niculina Musat, Ursula Werner, Steffen Kolb, Tanja Dodenhof, Katrin Knittel, Justus van Beusekom, Nicole Dubilier, and Rudolf Amann

**Abstract**: Molecular biological methods were used to investigate the microbial diversity and community structure in intertidal sandy sediments of the island of Sylt (Wadden Sea) at a site which was in a parallel study characterized for transport and mineralization rates (de Beer *et al*., 2005, Limnology & Oceanography 50:113-127). Comparative 16S rRNA sequence analysis revealed a high bacterial diversity. Most sequences retrieved by PCR with a general bacterial primer set were affiliated to *Bacteroidetes*, *Gammaproteobacteria*, *Deltaproteobacteria* and the *Pirellula* cluster of *Planctomycetales*. Fluorescence *in situ* hybridization (FISH) and slot blot hybridization with group specific rRNA-targeted oligonucleotide probes were used to characterize the microbial community structure over depth (0 to 12 cm) and seasons (March, July, October). We found high abundance of bacteria with total cell numbers up to 3 X $10^9$ cells $ml^{-1}$ and a clear seasonal variation, with higher values in July and October versus March. The microbial community was dominated by members of the *Planctomycetales*, the *Cytophaga/Flavobacterium* group, *Gammaproteobacteria*, and bacteria of the *Desulfosarcina/Desulfococcus* group. Conflicting data were obtained for the *Alphaproteobacteria* for which no sequences were retrieved although probing supported their presence. The high abundance (1.5 x $10^7$ – 1.8 x $10^8$ cells $ml^{-1}$ accounting for 3 – 19% of all cells) of likely aerobic heterotrophic polymer-degrading planctomycetes is in line with the high permeability, deep oxygen penetration and the high rates of aerobic mineralization of algal biomass measured in the sandy sediments by de Beer *et al*. (2005). The high and stable – both over depth and throughout the seasonal samples examined – abundance of members of the *Desulfosarcina/Desulfococcus* group suggests a higher importance of sulphate reduction as revealed by parallel rate measurements.

**Nutrient release from an exposed intertidal sand flat**

by Markus Billerbeck , Ursula Werner, Katja Bosselmann, Eva Walpersdorf, Markus Huettel

**Abstract**: We studied pore water seepage and associated nutrient release in the intertidal sand flat "Janssand" (North Sea) during exposure at low tide. The hydraulic gradient developing at ebb tide between the pore water level in the elevated sand flat and the water level in the tidal gully generated interstitial water flows towards the seepage zone with velocities ranging from 0.54 (March) to 0.86 cm $h^{-1}$ (July). Pore water was discharged from a 20 m wide release zone near the seaward margin of the flat at rates of 2.4 (March) and 4.2 L $m^{-2}$ $d^{-1}$ (July). Nutrient and DIC concentrations of the seepage water exceeded those measured in the pore water of the upper section of the flat by 10- and 5-fold, respectively. Nutrient effluxes through seepage reached 1074 and 5078 µmol $m^{-2}$ $d^{-1}$ for $NH_4$, 280 and 1668 µmol $m^{-2}$ $d^{-1}$ for $PO_4$ and 141 and 1142 µmol $m^{-2}$ $d^{-1}$ for $Si(OH)_4$ in March and July, respectively. Benthic flux chambers revealed that nutrients and DIC were released from the still submerged sediment as soon as the ebb tide exposed the upper section of the elevated flat. A conservative estimate based on our measurements suggests that 84,000 (March) to 147,000 (July) L pore water are discharged each tidal cycle from the sandy northeast margin of the Janssand (3.5 km length). Nutrients contained in this water corresponded to 6 – 25 kg $d^{-1}$ carbon mineralized during March and 42 – 223 kg $d^{-1}$ during July. Our study indicates that the Janssand intertidal flat does not accumulate organic matter but releases mineralization products that can account for all if not more than the organic matter that is potentially filtered through the permeable beds. Nutrient fluxes associated with seepage exceeded 5 to 8-fold those fluxes caused by the combined effects of diffusion, advection and bioirrigation during inundation, emphasizing the importance of sand flat drainage for the nutrient cycles in the Wadden Sea.

**Degradation and mineralization of coral mucus in reef environments**
by Christian Wild, Mohammed Rasheed, Ursula Werner, Ulrich Franke, Ron Johnstone and Markus Huettel

**Abstract**: With in-situ and laboratory chamber incubations we demonstrate that coral mucus, an important component of particulate organic matter in reef ecosystems, is a valuable substrate for microbial communities in water column and sandy sediments of coral reefs. The addition of coral mucus to the water of benthic chambers placed on lagoon sands in the coral cay Heron Island, Australia resulted in a fast and significant increase in both $O_2$ consumption and dissolved inorganic carbon (DIC) production in the chambers. The permeable coral sands permitted the transport of mucus into the sediment with interfacial water flows, resulting in the mucus being mainly (> 90%) degraded in the sediment and not in the water column of the chambers. A low ratio of 0.48 (in-situ) to 0.64 (laboratory) for $O_2$ consumption/DIC production after the addition of coral mucus and high sulfate reduction rates (SRR) in natural sediments, which were exposed to coral mucus, suggest a large contribution of anaerobic processes to the degradation of coral mucus. Oxygen penetrated less than 5 mm deep into these sediments. The microbial reaction to the mucus addition was rapid, with a calculated in-situ C turnover rate ranging from 7 to 18% $h^{-1}$. The degradation of coral mucus showed a dependency on the permeability of the carbonate sediments, with faster degradation and remineralization in coarse sands. This indicates the importance of permeable reef sediments for the trapping and degradation of organic matter. We suggest that coral mucus may have a function as a carrier of energy to the benthic microbial consumers.

**Sediment surface topographies and bottom water flow: an in situ case-study on the fundamentals of porewater advection**
by Felix Janssen, Hans Røy, Ursula Werner & Ursula Witte

**Abstract**: Advective porewater exchange along horizontal pressure gradients substantially affects benthic solute and particle fluxes in permeable sands and has strong implications for biogeochemical zonation and organic matter mineralization. The pressure gradients, and hence the rates of porewater exchange, scale with the size of the current exposed topographical features at the sediment surface. This study presents small-scale surface topographies that were obtained at a fine-, medium-, and coarse sand site by means of laser-based surface scanning and acoustic altimetry. Seafloor topographies are highly variable with a more than 6 fold range in average roughness element height between the respective stations and cruises (3.1 to 20.1 mm). Ripples generally provide the most prominent roughness elements. Highest ripples are observed at the medium sand station while ripples are smaller and less common at the coarse sand site. Here, bioroughness prevails, indicating that ripple formation may be hampered due to the large grain size. Based on ripple dimensions and measurements of near-bottom flow advection at the medium sand station is expected to result in porewater exchange at a rate of 45.4 L $m^{-2}$ $d^{-1}$. The presence of porewater advection at that site is confirmed by a time series of in situ oxygen microprofiles. These measurements clearly indicate an intensive advective oxygen supply which is expected to substantially affect oxygen uptake and sediment biogeochemistry. This may be even more pronounced at the coarse sand site where similar pressure gradients would result in 2.8 times higher rates of porewater advection. However, an assessment of the effect of advection at that site is limited by the lack of appropriate modeling approaches that allow a quantification of porewater exchange as it is induced by irregularly spaced biogenic roughness elements.

**Many thanks!**

I would like to thank Prof. B.B. Jørgensen and Prof. G. Kirst for accepting me as a PhD student and for the support during the entire time. I would like to thank Prof. B.B. Jørgensen and Prof. G. Kirst also for the examination of my thesis. Prof. Jørgensen , Prof. G. Kirst , Dr. D. de Beer and Prof. M. Wolff, Susanne Hinck and Angela Scharfbillig are acknowledged for participating as committee members in the thesis defence.

The biggest thanks are for you, Dirk de Beer, for the great support, inspiration and supervision during all stages of my PhD.

Markus Billerbeck, you were a great, great co-worker in the field, the lab, for discussion and for cheering me up in stressful times, thank you so much for your support.

The fieldtrips I shared with some wonderful people: Markus Billerbeck, Eva Walpersdorf, Lubos Polerecky, Katja Bosselmann, Uli Franke, Martina Alisch, Ingrid Dohrmann, Christiane Hüerkamp and Kyriakos Vamvakopoulos, Alex Theune, you all helped me very much.
I had some very nice and helpful collaborations. Markus, Uli and Lubos were always available for discussion and support. Christian Wild, thank you, you were always there to help and discuss. Anna Blazejak, Niculina Mussat, it was a pleasure working with you.
Michael Böttcher thank you for your support and discussion on many subjects (not only science). Felix Janssen, Hans Røy, Tim Ferdelman, Perran Cook, Raid Abed, Henk Jonkers, Andrew Bisset and Stefan Jansen were always helpful and always open for discussions.
Gabrielle Eickert, Ines Schröder, Karin Hohmann, Cäcilia Wiegand, Ingrid Dohrmann, Vera Hübner and Anja Eggers you were always a great support not only by providing wonderful microsensors.
Volker Meyer, Paul Färber, Harald Osmers, Jens Langreder, Axel Nordhausen, Alfred Kutsche and Georg Herz are thanked for their great technical support. Bernd Stickfort is thanked for getting weird, hidden manuscripts.
Some exceptional great and helpful people were those who shared the office with me: Felix, Rebecca, Alex, Dörte and Andrew thanks for all, I will miss these times!
In the last days (the hot phase) I got such great support, I am still very delighted and grateful: Markus, Felix, Alex, Rebecca, Andrew, Susanne H., Marie-Liese Schläpy and Dirk!
My friends and my family thank you for being with me and simply being there in these busy times.
Markus, thank you so much for all!!!!